

ASTRONOMICAL INSTITUTE
SLOVAK ACADEMY OF SCIENCES

PROCEEDINGS OF THE WORKSHOP
OBSERVING TECHNIQUES,
INSTRUMENTATION AND SCIENCE
FOR METRE-CLASS TELESCOPES

III

September 11 – 15, 2023, Tatranská Lomnica, Slovakia

CONTRIBUTIONS
OF THE ASTRONOMICAL OBSERVATORY
SKALNATÉ PLESO

• VOLUME LIV •

Number 2



February 2024

Editorial Board

Editor-in-Chief

Augustín Skopal, *Tatranská Lomnica, The Slovak Republic*

Managing Editor

Richard Komžík, *Tatranská Lomnica, The Slovak Republic*

Editors

Július Koza, *Tatranská Lomnica, The Slovak Republic*

Aleš Kučera, *Tatranská Lomnica, The Slovak Republic*

Luboš Neslušan, *Tatranská Lomnica, The Slovak Republic*

Vladimír Porubčan, *Bratislava, The Slovak Republic*

Theodor Pribulla, *Tatranská Lomnica, The Slovak Republic*

Advisory Board

Bernhard Fleck, *Greenbelt, USA*

Arnold Hanslmeier, *Graz, Austria*

Marian Karlický, *Ondřejov, The Czech Republic*

Jan Vondrák, *Prague, The Czech Republic*

©

Astronomical Institute of the Slovak Academy of Sciences

2024

ISSN: 1336-0337 (on-line version)

CODEN: CAOPF8

Editorial Office: Astronomical Institute of the Slovak Academy of Sciences
SK-059 60 Tatranská Lomnica, The Slovak Republic

CONTENTS

| | |
|--------------------------------|----|
| List of participants | 9 |
| Preface | 13 |

Session A: OBSERVING TECHNIQUES AND INSTRUMENTATION FOR METRE-CLASS TELESCOPES

| | |
|---|----|
| A04: M. Minev, N. Petrov, E. Semkov: Technical performance and first light of the new 1.5-meter telescope at the National Astronomical Observatory Rozhen | 15 |
| A05: S. Yalçınkaya, E.M. Esmer, Ö. Baştürk: ObsMap: Preparing observing maps with the best comparison stars for photometry | 22 |
| A09: L. Zampieri, M. Fiori, G. Naletto, A. Spolon, C. Barbieri, A. Burtovoi, U. Munari, G. Umbricco, B. Gaiani, L. Lessio, P. Ochner: Fast photon-counting optical astronomy | 29 |
| AP01: T. Pribulla, M. Vaňko, R. Komžík, P. Sivanič: High-resolution échelle spectrograph at Skalnaté Pleso Observatory | 43 |

Session B: SCIENCE WITH SMALL TELESCOPES

| | |
|--|-----|
| B02: A.S. Miroshnichenko, S. Danford, S. Zharikov, A. Aarnio, P. Prendergast, S.A. Khokhlov, I.A. Gabitova, A. Amantayeva, N.L. Vaidman, S.S. Baktybayev, I.L. Andronov, L.L. Chinarova, I.A. Usenko: A variety of binary targets for small telescopes | 47 |
| B05: K. Gazeas: Low-mass contact binaries as probes of stellar merging events | 58 |
| B07: C.I. Eze, G. Handler: Photometric sample of early B-type pulsators in eclipsing binaries observed with TESS | 70 |
| B09: M. Perko: Accreting-only symbiotic stars in the era of large Galactic Archeology spectroscopic surveys | 75 |
| B10: A. Skopal: Exploring outbursts of accreting white dwarfs in symbiotic binaries – basic concept | 85 |
| B14: A. Maliuk, J. Budaj, D. Mkrtichian, Z. Garai, S. Zharikov, T. Pribulla, R. Komžík, A. Kusakin, L. Shestakova, R. Kokumbaeva, I. Reva, S. Joshi, A. Valeev, D. Gadelshin, G. Valyavin, N. A-thano, R. Mennickent, A. Serebryanskiy, T.G. Kaye: Studying of exoasteroids orbiting around WD 1145+017 | 98 |
| B15: F. Teyssier, F. Sims: ARAS eruptive stars monitoring | 107 |

| | |
|---|-----|
| B17: E. Pavlenko, S. Shugarov, T. Kato, O. Antonyuk, A. Sosnovskij, Ju. Babina, A. Shchurova, K. Isogai, A. Sklyanov, A. Gutaev, R. Zhuchkov, P. Dubovsky, K. Petrik, J. Hamsch: V1006 Cyg: SU UMa-type dwarf nova in the period gap that wobbles between subclasses | 117 |
| B19: P.A. Dubovský, K. Petřík, V. Breus: Nova Herculi 2021 as an intermediate polar | 128 |
| B20: E. Semkov, S. Ibryamov, S. Peneva, A. Mutafov: Photometric monitoring of PMS stars with the telescopes at Rozhen Observatory | 135 |
| B23: H.J. Deeg, R. Alonso: Ground-based photometric follow-up for exoplanet detections with the PLATO mission | 142 |
| B24: Z. Garai, H.P. Osborn, A. Tuson, S. Ulmer-Moll, The CHEOPS Consortium: Confirming long-period transiting exoplanets with TESS and CHEOPS. The case of HD 22946 d | 150 |
| B25: E.W. Guenther, L. Fossati, P. Kabáth: The evaporation of planetary atmospheres | 157 |
| BP01: B. Dębski, L. Kulczycka, W. Skrobacz, J. Pęgiel, M. Jacak: First determination of the system parameters in five contact binaries | 164 |
| BP02: Š. Parimucha, P. Gajdoš, Y. Markus, V. Kudak: Deep-learning classification of eclipsing binaries | 167 |
| BP05: M. Vaňko, T. Pribulla, N. Shagatova, R. Komžík, P. Dubovský: FM CMa: hot and massive eclipsing binary with a pulsating component | 171 |
| BP06: Ľ. Hambálek, T. Pribulla: The uniqueness of determination of the photometric mass ratio of contact binary stars with applications to selected binaries | 175 |
| BP08: M. Skarka, J. Lipták, D. Stoklásek, P. Cagaš, P. Kabáth: TYC 1083-12-1 – an SB2 binary mimicking an exoplanetary candidate | 182 |
| BP09: M. Tomova, K. Stoyanov, Y. Nikolov, P. Kaygorodov: Optical observations of RS Oph after its 2021 outburst | 186 |
| BP10: M. Leitzinger, P. Kabáth, M. Vaňko, T. Pribulla, R. Komžík, Z. Garai, R. Karjalainen, P. Odert, J. Lipták, P. Heinzel, J. Wollmann, R. Greimel, E.W. Guenther: Spectroscopic characterization of superflares on solar-type stars – a joint observing campaign | 190 |
| BP11: P. Gajdoš, Š. Parimucha, M. Kamenec: Spotted eclipsing binary KIC 7023917 with δ-Scuti pulsations | 194 |
| BP13: A. Maliuk, V. Krushevskaya, S. Shugarov, Z. Garai, Ya. Romanyuk, Yu. Kuznyetsova, M. Andreev: Photometric study of the Delta Scuti variable 2MASS J13122513+5443409 in UMa | 198 |

| | |
|--|-----|
| BP19: V.G. Godunova, A.O. Simon, Y.S. Markus, S.Yu. Shugarov, V.V. Troianskyi, V.M. Reshetnyk, I.O. Izviakova, B.E. Zhilyaev, A.V. Shchurova, M. Husárik, S. Geier, D. Oszkiewicz, D. Tomko: Photometric and colorimetric studies of target objects using small and medium-size telescopes | 205 |
| BP20: V. Marsakova, S. Shugarov, I. Andronov: Multiwavelength research of the cyclic variability of symbiotic nova RT Ser | 213 |

**Session C: GROUND-BASED SUPPORT
OF COSMIC MISSIONS AND TELESCOPE NETWORKS**

| | |
|--|-----|
| C04: M. Mesarč, L. Hambálek: Validation of selected TESS exoplan- etary candidates | 219 |
| C05: E.M. Esmer, Ö. Baştürk, S.O. Selam, F. Akar, E. Sertkan, B. Güler, S. Yalçinkaya: Eclipse timing variations of evolved eclipsing binaries: potential targets for meter-sized telescopes in the light of TESS observations | 228 |
| C06: I. Soszyński: Three decades of the OGLE survey | 234 |
| C07: P.-E. Christopoulou, E. Lalounta, A. Papageorgiou, C.E. Ferreira Lopes, M. Catelan, A.J. Drake: Discovery of star systems at the merger limit by large astronomical surveys | 249 |

The Contributions of the Astronomical Observatory Skalnaté Pleso
are available in the full version
in the frame of ADS Abstract Service
and can be downloaded in a usual way from the URL address:

<https://ui.adsabs.harvard.edu/>

as well as from the website of
the Astronomical Institute of the Slovak Academy of Sciences
on the URL address:

<https://www.astro.sk/caosp/caosp.php>

The journal is covered/indexed by:

Web of Science (WoS)

WoS Core Collection: Science Citation Index Expanded

SCOPUS

Index Copernicus International

PROCEEDINGS OF THE WORKSHOP

Edited by

Theodor Pribulla, Ján Budaj,
Augustín Skopal, Martin Vaňko

OBSERVING TECHNIQUES, INSTRUMENTATION AND SCIENCE FOR METRE-CLASS TELESCOPES III

September 11 – 15, 2023, Tatranská Lomnica, Slovakia

The Astronomical Institute of the Slovak Academy of Sciences

<https://www.ta3.sk/conferences/80AI2023/>

Scientific Organizing Committee Local Organizing Committee

Theodor Pribulla, chair (Slovakia)

Henri Boffin (ESO, Germany)

Ján Budaj (Slovakia)

Hans Deeg (Spain)

Eric Gaidos (USA)

Eike Guenther (Germany)

Raine Karjalainen (Czech Republic)

Anatoly Miroshnichenko (USA)

Ulisse Munari (Italy)

Augustín Skopal (Slovakia)

Gyula Szabó (Hungary)

Martin Vaňko (Slovakia)

Staszek Zola (Poland)

Lubomír Hambálek, chair

Ján Adamčák

Richard Komžík

Emil Kundra

Andrii Maliuk

Natalia Shagatova



LIST OF PARTICIPANTS

Regular participants:

| | |
|-------------------------------------|---|
| Adamčák, Ján | Astronomical Institute, Slovak Academy of Sciences, Tatranská Lomnica, Slovakia |
| Borkovits, Tamás | Baja Astronomical Observatory of Szeged University & ELKH-SZTE Stellar Astrophysics Research Group, Hungary |
| Brož, Miroslav | Astronomical Institute, Faculty of Mathematics and Physics, Charles University, Czech Republic |
| Budaj, Ján | Astronomical Institute, Slovak Academy of Sciences, Tatranská Lomnica, Slovakia |
| Cehula, Jakub | Institute of Theoretical Physics, Faculty of Mathematics and Physics, Charles University, Czech Republic |
| Christopoulou, Eleftheria Panagiota | Dept of Physics University of Patras, Greece |
| Dębski, Bartłomiej | Astronomical Observatory of the Jagiellonian University, Poland |
| Deeg, Hans | Instituto de Astrofísica de Canarias, Spain |
| Demir, Eylül | Ankara University, Turkey |
| Dubovský, Pavol | Vihorlat Observatory in Humenné, Slovakia |
| Esmer, Ekrem | Ankara University, Faculty of Science, Dept. of Astronomy and Space Sciences, Turkey |
| Eze, Christian | Nicolaus Copernicus Astronomical Center of the Polish Academy of Sciences, Warsaw, Poland |
| Garai, Zoltán | HUN-REN-ELTE Exoplanet Research Group, Szombathely, Hungary |
| Gazeas, Kosmas | Section of Astrophysics, Astronomy and Mechanics, Department of Physics, National and Kapodistrian University of Athens, Greece |
| Guenther, Eike | Thüringer Landessternwarte Tautenburg, Germany |
| Hambálek, Ľubomír | Astronomical Institute, Slovak Academy of Sciences, Tatranská Lomnica, Slovakia |
| Hrobár, Tomáš | Faculty of Mathematics, Physics and Informatics, Comenius University in Bratislava, Slovakia |
| Ivanova, Oleksandra | Astronomical Institute, Slovak Academy of Sciences, Tatranská Lomnica, Slovakia |
| Jeon, Young-Beom | Korea Astronomy and Space Science Institute, Republic of Korea |
| Kabáth, Petr | Astronomical Institute of the Czech Academy of Sciences, Ondřejov, Czech Republic |

| | |
|-------------------------|--|
| Kálmán, Szilárd | ELTE Eötvös Loránd University, Doctoral School of Physics, Budapest, Hungary |
| Kiss, Csaba | Konkoly Observatory, Research Centre for Astronomy and Earth Sciences, Budapest, Hungary |
| Kolář, Jakub | Masaryk University, Brno, Czech Republic |
| Komžík, Richard | Astronomical Institute, Slovak Academy of Sciences, Tatranská Lomnica, Slovakia |
| Krushevskaja, Viktoriia | Astronomical Institute, Slovak Academy of Sciences, Tatranská Lomnica, Slovakia |
| Kučáková, Hana | Institute of Physics, Silesian University in Opava, Czech Republic |
| Kundra, Emil | Astronomical Institute, Slovak Academy of Sciences, Tatranská Lomnica, Slovakia |
| Kurowski, Sebastian | Astronomical Observatory of the Jagiellonian University, Poland |
| Kuznyetsova, Yuliana | Main Astronomical Observatory of NAS of Ukraine |
| Maliuk, Andrii | Astronomical Institute, Slovak Academy of Sciences, Tatranská Lomnica, Slovakia |
| Markus, Yana | Institute of Physics, University of P.J.Šafárik in Košice, Slovakia |
| Marsakova, Vladyslava | Richelieu Scientific Lyceum, Odesa, Ukraine |
| Mártonfi, Pavol | Institute of Physics, University of P.J.Šafárik in Košice, Slovakia |
| Minev, Milen | Institute of Astronomy and National Astronomical Observatory, Bulgarian Academy of Sciences, Sofia, Bulgaria |
| Miroshnichenko, Anatoly | University of North Carolina Greensboro, USA |
| Parimucha, Štefan | Institute of Physics, University of P.J.Šafárik in Košice, Slovakia |
| Park, Yoon-Ho | Korea Astronomy and Space Science Institute, Republic of Korea |
| Perko, Manica | Faculty of Mathematics and Physics, University of Ljubljana, Slovenia |
| Plávalová, Eva | Mathematical Institute, Slovak Academy of Sciences, Slovakia |
| Pomazan, Anton | Shanghai Astronomical Observatory, Chinese Academy of Science, China |
| Pribulla, Theodor | Astronomical Institute, Slovak Academy of Sciences, Tatranská Lomnica, Slovakia |
| Raskin, Gert | Institute of Astronomy, KU Leuven, Belgium |
| Romanyuk, Yaroslav | Main Astronomical Observatory of National Academy of Sciences of Ukraine |

| | |
|---------------------|--|
| Semkov, Evgeni | Institute of Astronomy and NAO, Bulgarian Academy of Sciences, Bulgaria |
| Shagatova, Natalia | Astronomical Institute, Slovak Academy of Sciences, Tatranská Lomnica, Slovakia |
| Shakun, Leonid | RI "Astronomical Observatory" of the Odessa I.I. Mechnikov National University, Ukraine |
| Shugarov, Sergey | Astronomical Institute, Slovak Academy of Sciences, Tatranská Lomnica, Slovakia |
| Sims, Forrest | Desert Celestial Observatory, USA |
| Skarka, Marek | Astronomical Institute of the Czech Academy of Sciences, Ondřejov, Czech Republic |
| Skopal, Augustin | Astronomical Institute, Slovak Academy of Sciences, Tatranská Lomnica, Slovakia |
| Soszyński, Igor | Astronomical Observatory, University of Warsaw, Poland |
| Stefanov, Stefan | Institute of Astronomy with NAO, Bulgarian Academy of Sciences, Sofia University, Bulgaria |
| Sung, Hyun-II | Korea Astronomy and Space Science Institute, Republic of Korea |
| Szabó, Gyula | ELTE Gothard Astrophysical Observatory MTA-ELTE Exoplanet Research Group Szombathely, Hungary |
| Tala Pinto, Marcelo | Universidad Adolfo Ibañez, Chile |
| Teyssier, Francois | South Rouen Observatory, France |
| Uppal, Namita | Physical Research Laboratory, Ahmedabad, India |
| Vaňko, Martin | Astronomical Institute, Slovak Academy of Sciences, Tatranská Lomnica, Slovakia |
| Voitko, Anhelina | Astronomical Institute, Slovak Academy of Sciences, Tatranská Lomnica, Slovakia |
| Vrašťák, Martin | Private observatory Liptovská Štiavnica, Slovakia |
| Yalçinkaya, Selçuk | Ankara University, Faculty of Science, Astronomy & Space Sciences Department, Turkey |
| Zampieri, Luca | INAF-Astronomical Observatory of Padova, Italy |
| Zejda, Miloslav | Department of Theoretical Physics and Astrophysics, Faculty of Science, Masaryk University, Brno, Czech Republic |
| Zocłońska, Elżbieta | Nicolaus Copernicus Astronomical Centre of the Polish Academy of Sciences, Poland |
| Zoła, Staszek | Astronomical Observatory of the Jagiellonian University, Poland |

On-line participants:

| | |
|------------------------|---|
| Bernhard, Klaus | Bundesdeutsche Arbeitsgemeinschaft für veränderliche Sterne, Germany |
| Mitrokhina, Veronika | University of Tartu, Tartu Observatory, Estonia |
| Pavlenko, Elena | Crimean astrophysical observatory, Crimea |
| Saleh, Ghaleh | Saleh Research Center, The Netherlands |
| Simon, Andrii | Astronomy and Space Physics Department, Taras Shevchenko National University of Kyiv, Ukraine |
| Slowikowska, Agnieszka | Joint Institute for VLBI ERIC, The Netherlands; Nicolaus Copernicus University, Toruń, Poland |
| Sosnovskij, Aleksej | Crimean astrophysical observatory, Crimea |
| Syniavskiy, Ivan | Main Astronomical Observatory NAS of Ukraine, Ukraine |
| Szücs-Csillik, Iharka | Astronomical Institute of Romanian Academy of Sciences, Astronomical Observatory Cluj-Napoca, Romania |
| Tomova, Mima | Institute of Astronomy and National Astronomical Observatory, Bulgarian Academy of Sciences, Bulgaria |

PREFACE

The metre-class telescopes are still vital for current astrophysics. Although large telescopes excel in the studies of faint objects at the edge of the observable Universe and provide high-angular and spectral resolution of astrophysically important objects, small telescopes (diameter < 2 m) are valuable in long-term monitoring, continuous observations, or large-scale surveys. A large flotilla of small telescopes can often provide observations which would be cost-prohibitive for large telescopes. Most of astrophysically crucial objects/events are still being discovered through extensive all-sky surveys run by robotic telescopes, or by very small telescopes of well-organized amateur astronomers. Apart from that, small telescopes continue to play a vital role in recruiting and training the next generation of astronomers and instrumentalists and serve as test beds for development of novel instruments and experimental methods for larger telescopes. Moreover, a metre-class telescope is available at almost any historical observatory and, after some effort, can be turned into a powerful instrument. This requires better focal instrumentation and modern telescope control.

This book contains proceedings of the 3rd international conference on the role of small telescopes in astrophysics. *Observing techniques, instrumentation, and science for metre-class telescopes III*. It took place in the Congress Center Academia near a village called Tatranská Lomnica at the foothill of the scenic High Tatra mountains in northern Slovakia from September 11 to September 15, 2024. Its program was divided into three sessions: *A: Observing techniques and instrumentation for metre-class telescopes*, *B: Science with small telescopes*, and *C: Ground-based support of cosmic missions and telescope networks*. The first conference of this series was held at the same place in 2013. The conference commemorates the 80th anniversary of the very first observation performed at the Skalnaté Pleso Observatory. Currently, its bigger dome houses a 1.3m Nasmyth-Cassegrain telescope equipped with several advanced focal instruments.

The SOC thanks all the participants for their high-level contributions. Seventy-five participants from 18 countries took part in the meeting. The organizers are indebted to the Astronomical Institute of the Slovak Academy of Sciences for general support and also to the Congress Center Academia for smooth cooperation during the conference. We thank the members of the LOC: Ján Adamčák, Ľubomír Hambálek (chair), Richard Komžík, Emil Kundra, Andrii Maliuk, and Natalia Shagatova for their help in preparing and running this workshop. We also thank all the referees for their hard work in peer-reviewing all contributions. The conference was supported mainly by project APVV-20-0148 of the Slovak Development and Research Agency and VEGA grant 2/0031/22 from the Slovak Academy of Sciences.

T. Pribulla, J. Budaj, A. Skopal, M. Vaňko
the editors

Technical performance and first light of the new 1.5-meter telescope at the National Astronomical Observatory Rozhen

M. Minev, N. Petrov and E. Semkov

*Institute of Astronomy and National Astronomical Observatory, Bulgarian
Academy of Science, 72 Tsarigradsko Chaussee Blvd., 1784 Sofia, Bulgaria
(E-mail: msminev13@gmail.com)*

Received: October 29, 2023; Accepted: January 22, 2024

Abstract. A new 1.5-meter Ritchey-Chretien telescope has been inaugurated as part of the observational equipment of the Institute of Astronomy and the National Astronomical Observatory Rozhen (IANAO) at the Bulgarian Academy of Science (BAS). The telescope, designed with advanced optical and mechanical components, aims to enhance observational capabilities from NAO Rozhen. Here, we present the initial tests and setup procedures conducted for the new telescope and we describe the assembly process, alignment procedures, and calibration techniques implemented to ensure optimal performance. The tests involved nighttime observations and preliminary results highlight the successful alignment of the telescope's optics, the stability of its tracking mechanism, and the establishment of an efficient data acquisition workflow. The findings from these initial tests provide valuable insights into the telescope's capabilities and help us to set up a fully robotic telescope for observational campaigns and scientific research. This new observational instrument will primarily perform photometric and astrometric tasks. However, there is also the possibility of conducting low-dispersion spectral observations.

Key words: telescopes – instrumentation: miscellaneous – site testing

1. Introduction

In the middle of the last century, there was significant global interest in astronomy, both among scientists and the general population. Bulgaria was no exception to this trend, and there was a growing appreciation for this scientific discipline in the country. This led to the construction of numerous public observatories with planetariums throughout Bulgaria. Additionally, important decisions were made in the country that laid the groundwork for the development of modern astronomical observatories. On March 13, 1981, the Bulgarian National Astronomical Observatory (NAO) Rozhen was officially opened. It was the final result in the long sequence of dreams, ideas, projects, decisions, and actions of many people and institutions which placed Bulgaria among the modern nations possessing their own resources to investigate the Cosmos (Petrov et al.,

2018). NAO Rozhen is the main observatory of the Institute of Astronomy, BAS. From the beginning, the observatory has featured several optical telescopes for photometric and spectral observations in the visible part of the electromagnetic spectrum. The primary instrument is the 2-meter RCC telescope, complemented by the 50/70 cm Schmidt telescope and the 60 cm Cassegrain telescope, all produced by the Carl Zeiss factories in Jena. Since 2005 NAO Rozhen has also had a 15 cm Lyot coronagraph with Ha filter, designed for observations of prominences on the solar limb. In 2021, this telescope was replaced by a 30 cm chromospheric telescope for observing and researching active formations on the solar disk (Tsvetkov & Petrov, 2020).

In addition to its strictly scientific observational and research activities, the National Astronomical Observatory Rozhen has, in the past decade, provided opportunities for collaborative work with amateur astronomers from both Bulgaria and abroad. The observatory grounds smaller optical telescopes with remote access capabilities for observations. An excellent example of such collaborative work is the IRIDA observatory, which includes two separate telescopes for night observations (<https://www.irida-observatory.org/>). The results of this joint effort have led to numerous scientific publications in reputable journals (Popov & Petrov (2022) and Kjurkchieva et al. (2018)).

NAO Rozhen is continually evolving, striving for improvement by incorporating new light detectors and technologies. This commitment to progress led to the realization and operation of a new telescope for observations. In the summer of 2023, the observatory achieved first light with its new 1.5-meter Alt-Azimuth telescope. This telescope allows remote control access or can execute fully robotic observational programs. All the tests and adjustments described in this work are made in remote control mode but our goal is to use fully robotic mode when everything adjusted.

2. Specifications and science programs of the new telescope

The AZ1500 is a 1.5 m f/6 Ritchey-Chrétien Alt-Az telescope equipped with quartz optics from ASA (Astro Systeme Austria) GmbH that guarantees diffraction-limited performance and best micro-roughness values with higher contrast and less obstruction¹. The optical system is designed with two Nasmyth focus positions (configurable up to four) with an image field of 200 mm or 1.27°. This design results in a more compact system with a weight of only 5.5 tons that fits perfectly in a 6 m diameter dome. All drives are direct drives and they are equipped with high-resolution absolute encoders. To improve the accuracy of a telescope's pointing and tracking capabilities first we had to create and refine a T-Point model (Wallace, 1994). The best model with 60 points brings us good results with a pointing accuracy of less than 5" RMS (<60 pixels) and a tracking accuracy of 0.07" RMS/min.

¹<https://www.astrosysteme.com/products/asa-az1500/>

The telescope is equipped with a Moravian C3-61000 Pro camera with a back-illuminated Sony IMX455 CMOS sensor, offering very low dark current, full-well capacity over 50 ke^- and quantum efficiency of about 90%. The sensor format is 9576×6388 pixels (36×24 mm) with a square pixel size of $3.76 \mu\text{m}$. With a corresponding optical system that results in an image scale of $0.086''/\text{pixel}$ and a field of view $13.75' \times 9.17'$.

The telescopes at NAO Rozhen conduct a wide range of astronomical observations (photometric and spectral) on various celestial objects from the night sky, as well as research in the field of heliophysics and space weather (Tsvetkov (2020); Myshyakov & Tsvetkov (2020) and Bogomolov et al. (2018)). Objects observed from the night sky include small bodies from the Solar System, primarily asteroids and comets (Borisov et al. (2023) and Bebekovska et al. (2023)). Objects from our galaxy include young stars and star-forming regions (Ibryamov et al., 2023), binary and symbiotic stars (Zamanov et al. (2022) and Stoyanov et al. (2020)), supernovae remnants (SNR) (Vučetić et al. (2023) and Vučetić et al. (2019)); star clusters and exoplanets. Additionally, extragalactic objects such as galaxies and quasars are observed (Bachev et al. (2023) and Agarwal et al. (2021)). The new telescope will complement these observations and enhance efficiency in terms of observational time. This undoubtedly provides greater opportunities for new collaborative observations by astronomers in Bulgaria and the potential for new projects with international participation. In addition, due to the fast pointing and robotic mode, the telescope can join international networks for transient observations, such as supernova explosions, gravitational microlensing events, gamma-ray burst (GRB) afterglows, and gravitational wave events follow-ups. Currently, only photometric observations will be conducted, but we plan to install a low-dispersion spectrograph in a few years to significantly expand the scientific capabilities.

3. Photometry tests

We performed the first photometry tests on globular cluster M92 (NGC6341). It is one of the Stetson targets with standard stars². During a good photometric night with seeing $\sim 0.7''$, we obtained 3×3 min exposures in Johnson-Cousinns photometric BVR filters. For data reduction (dark current subtraction and flat fielding normalization) and aperture photometry, we used standard procedures in IRAF³ (Image Reduction and Analysis Facility). Images in each filter were combined median. The results of photometry in the R filter show a perfect linear

²This research used the Canadian Advanced Network For Astronomy Research (CANFAR) operated in partnership with the Canadian Astronomy Data Centre and The Digital Research Alliance of Canada with support from the National Research Council of Canada the Canadian Space Agency, CANARIE and the Canadian Foundation for Innovation.

³IRAF is distributed by the National Optical Astronomy Observatory, which is operated by the Association of Universities for Research in Astronomy under a cooperative agreement with the National Science Foundation.

trend between instrumental and Stetson standard magnitudes for the whole range of magnitudes with constant value $R_{\text{Stetson}} - R_{\text{inst}} = 3.994 \pm 0.004$ mag (Fig.1, left). The photometric error for $R < 17$ mag is about $R_{\text{err}} \approx 3$ mmag, shown on the right panel of Fig.1. Radial flux variation in the field of view was not found. We also construct a color-magnitude diagram for M92 to compare the results with others in the literature and the results are indistinguishable down to 22 mag (Fig.2).

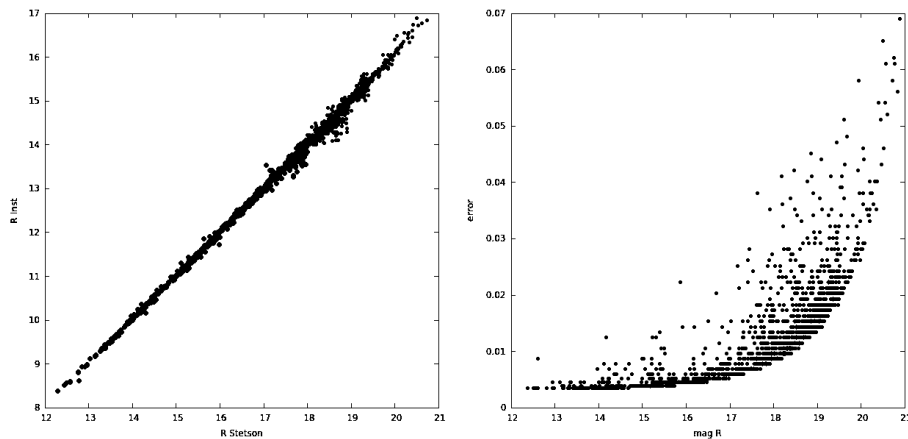


Figure 1. Photometry of a few thousand stars in the field of M92 cluster. On the left panel are shown instrumental versus Stetson standard magnitudes and photometric error on the right panel.

4. Conclusion

Nearly half a century after opening the doors of our NAO Rozhen, we now have another new, modern optical telescope for night observations. The initial observations and results demonstrate the telescope's precise performance. The AZ1500 has a fast pointing speed (up to $6^\circ/\text{sec}$). After creating a pointing model, we achieved a pointing deviation of less than $5''$, which is up to 60 pixels of the currently used digital camera. Under favorable meteorological conditions, our new telescope achieved a resolution of $0.4''$.

Photometric evaluations were conducted on star clusters (such as M92 presented here), galaxies, variable stars, and exoplanet transits. The results are entirely consistent with our expectations for accuracy and are scientifically justified. The initial results from the new telescope serve as the basis for presentation at scientific forums and as publications in scientific journals.

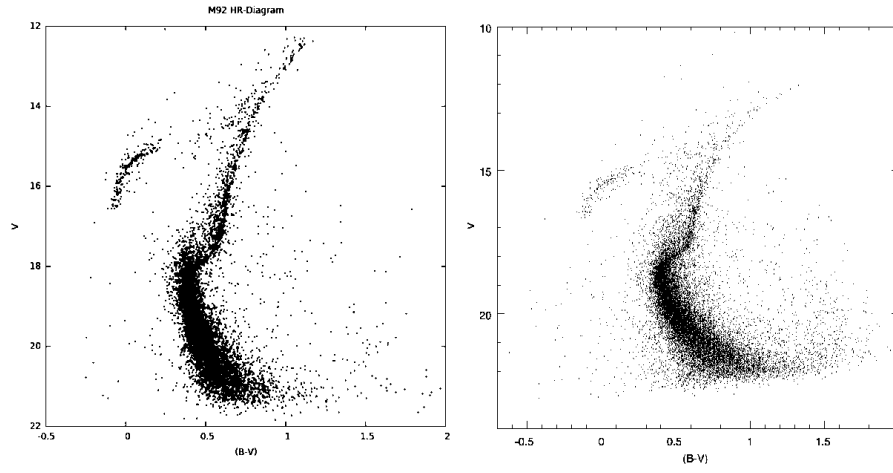


Figure 2. Colour-magnitude diagram for M92 – comparison between our photometry (left) and photometry from [Ruelas-Mayorga & Sánchez \(2008\)](#) (right).



Figure 3. M16 – Pillars of Creation in Ha filter. Stack of 15 images with 5 min exposure.

Automated observing programs with the new telescope are in progress. We believe that this can enhance our observational efficiency.

One of the first images taken with the AZ1500 telescope is shown in Fig.3.

Acknowledgements. The presented research infrastructure (AZ1500) was done with is funded by the Ministry of Education and Science of Bulgaria (support for the Bulgarian National Roadmap for Research Infrastructure). The authors thank the ASA Astrosysteme GmbH for the correct cooperation in the process of building and installing the AZ1500. We express our gratitude to E. Ivanov and V. Popov (IRIDA Observatory) for the processing and presentation of images in true colors obtained with the presented telescope.

References

- Agarwal, A., Mihov, B., Andruchow, I., et al., Multi-band behaviour of the TeV blazar PG 1553+113 in optical range on diverse timescales. Flux and spectral variations. 2021, *Astronomy and Astrophysics*, **645**, A137, DOI: 10.1051/0004-6361/202039301
- Bachev, R., Tripathi, T., Gupta, A. C., et al., Intra-night optical flux and polarization variability of BL Lacertae during its 2020-2021 high state. 2023, *Monthly Notices of the RAS*, **522**, 3018, DOI: 10.1093/mnras/stad1063
- Bebekovska, E. V., Apostolovska, G., Boeva, S., et al., Lightcurve analysis of asteroid 15691 Maslov using NAO Rozhen observations and sparse data. 2023, *Bulgarian Astronomical Journal*, **39**, 65
- Bogomolov, A., Myagkova, I., Myshyakov, I., et al., Comparative analysis of the proton generation efficiency during 17 March 2003 and 11 April 2004 solar flares. 2018, *Journal of Atmospheric and Solar-Terrestrial Physics*, **179**, 517–526, DOI: 10.1016/j.jastp.2018.08.010
- Borisov, G. B., Christou, A. A., & Apostolovska, G., Physical and dynamical properties of selected Earth co-orbital asteroids. 2023, *Planetary Space Science*, **225**, 105619, DOI: 10.1016/j.pss.2022.105619
- Ibryamov, S., Zidarova, G., Semkov, E., & Peneva, S., Study of the Long-term BVR_cI_c Photometric Variability of Eight PMS Stars in the Young Open Cluster Trumpler 37. 2023, *Research in Astronomy and Astrophysics*, **23**, 085006, DOI: 10.1088/1674-4527/acd8a0
- Kjurkchieva, D. P., Popov, V. A., & Petrov, N. I., USNO-B1.0 1452-0049820 and ASAS J102556+2049.3: Two W UMa Binaries Close to the Lower Mass-ratio Limit. 2018, *Astronomical Journal*, **156**, 77, DOI: 10.3847/1538-3881/aace5e
- Myshyakov, I. & Tsvetkov, T., Comparison of Kinematics of Solar Eruptive Prominences and Spatial Distribution of the Magnetic Decay Index. 2020, *Astrophysical Journal*, **889**, DOI: 10.3847/1538-4357/ab6334
- Petrov, N., Kjurkchieva, D., & Tsvetkov, T., Modern history of astronomy in Bulgaria. 2018, *Astronomical and Astrophysical Transactions*, **30**, 441

- Popov, V. A. & Petrov, N. I., Absolute parameters of four W UMa stars with extreme low mass ratios. 2022, *New Astronomy*, **97**, 101862, DOI: 10.1016/j.newast.2022.101862
- Ruelas-Mayorga, A. & Sánchez, L. J., CCD Photometry of M92. 2008, in *Revista Mexicana de Astronomia y Astrofisica Conference Series*, Vol. **34**, *Revista Mexicana de Astronomia y Astrofisica Conference Series*, 137–138
- Stoyanov, K. A., Hkiewicz, K., Luna, G. J. M., et al., Optical spectroscopy and X-ray observations of the D-type symbiotic star EF Aql. 2020, *Monthly Notices of the RAS*, **495**, 1461, DOI: 10.1093/mnras/staa1310
- Tsvetkov, T., Research on the destabilization and eruption of prominences/filaments in solar active regions. 2020, *Bulgarian Astronomical Journal*, **33**, 117–118
- Tsvetkov, T. & Petrov, N., New 30-cm Solar Telescope at National Astronomical Observatory Rozhen. 2020, in *Twelfth Workshop on Solar Influences on the Magnetosphere, Ionosphere and Atmosphere*, ed. K. Georgieva, B. Kirov, & D. Danov, 36–39
- Vučetić, M., Milanović, N., Urošević, D., et al., Proper Motion of Cygnus Loop Shock Filaments. 2023, *Serbian Astronomical Journal*, **207**, 9, DOI: 10.2298/SAJ2307009V
- Vučetić, M. M., Onić, D., Petrov, N., Ćiprijanović, A., & Pavlović, M. Z., Optical Observations of the Nearby Galaxy NGC 2366 Through Narrowband H_α and [SII] Filters. Supernova Remnants Status. 2019, *Serbian Astronomical Journal*, **198**, 13, DOI: 10.2298/SAJ190131003V
- Wallace, P. T., TPOINT – Telescope Pointing Analysis System. 1994, *Starlink User Note*, **100**
- Zamanov, R. K., Stoyanov, K. A., Marchev, D., et al., Optical spectroscopy of the Be/black hole binary MWC 656 - interaction of a black hole with a circumstellar disc. 2022, *Astronomische Nachrichten*, **343**, e24019, DOI: 10.1002/asna.20224019

ObsMap: Preparing observing maps with the best comparison stars for photometry

S. Yalçınkaya¹, E.M. Esmer¹ and Ö. Baştürk¹

Department of Astronomy & Space Sciences, Faculty of Science, Ankara University, TR-06100, Ankara, Türkiye (E-mail: yalcinkayas@ankara.edu.tr)

Received: November 7, 2023; Accepted: December 4, 2023

Abstract. We present ObsMap, a Python framework that allows for the interactive creation of various alternative observation maps to maximize the potential of each observing night. The code requires the user to input the star’s name or equatorial coordinates, the passband of observation, field of view (FoV), and desired count level together with the minimum and maximum count limits in ADUs for the detector. ObsMap queries the stars in the Gaia DR3 archive within an area four times the size of the FoV, as the target star could be located anywhere within the FoV. It then generates a list of stars in that area, along with additional information about each star. Variable stars are eliminated from the list using Gaia’s variability flag. The total incoming light in the specified filter is calculated with the blackbody approach for the remaining stars, utilizing Gaia’s effective temperature, stellar radius, and parallax data. Using the filter-specific fluxes, the count levels of the stars are determined relative to that input by the user for the target. As a result, ObsMap creates three maps: a) A large map that is four times the size of the FoV, where the effective temperature and count levels of the stars are annotated. The user can manually select the appropriate FoV, based on this map. b) A suggested map that minimizes photon noise (scatter). c) A suggested map to maximize the number of comparison stars. In some cases, a single comparison star with a high count level could outperform a combination of dim comparison stars. However, if that bright comparison star is variable and not flagged as such in the Gaia archive, choosing dimmer comparison stars could be a better option.

Key words: observation maps

1. Introduction

Accurate and precise light curves are always desired in photometry, regardless of the observed object. These two elements depend not only on the brightness of the target object but also on the properties of comparison stars within the field of view (FoV). An ideal comparison star should not be a variable star, should be bright enough to increase the precision while staying within the limits of linear response of the detector and also its color should be as close as possible to that of the target star.

In order to minimize atmospheric effects such as airmass on the final light curve, the relative flux of the target is acquired using the differential photometry method. The relative flux can be measured using one or a combination of comparison stars (Collins et al., 2017). According to equation (9) in Collins et al. (2017), precision increases with the total integrated count of comparison stars. For the cases where only a single comparison star is used, this is limited by the saturation level or the linearity limit of the detector. In other cases where the combination of comparison stars is used, precision is limited by the total number of comparison stars.

As the target star can be placed anywhere on the detector, the observable sky region varies depending on the location of the target star. For rectangular-shaped FoV, the target star can be placed in close proximity to one of the four corners, making the potentially observable region including the target four times bigger than the FoV. This raises a problem: determining the optimal location of the target star on the detector to maximize the total count of comparison stars, and assessing whether they are suitable for use as comparison stars, for instance, checking if they are variable stars.

In the selection of suitable comparison stars, the data provided by Gaia can be very helpful. Gaia is a multi-purpose space telescope that can measure parallaxes, atmospheric parameters, radial velocities, positions of stars on the sky plane, and even perform photometry (Gaia Collaboration et al., 2016, 2018, 2023; Riello et al., 2021). Employing these measurements from Gaia, an observational map optimized for the best possible precision can be created.

2. Predetermination of comparison stars

2.1. Noise types

Final light curves have basically two types of noise sources, which are the so-called random scatter and correlated noise. Random scatter is also called photon noise, Poisson noise or white noise (e.g. Southworth et al. 2009), and is generally parameterized by the Photon Noise Rate (PNR, Fulton et al. 2011). White noise is dependent on the amount of light acquired in unit time by the detector. Since the light from the target and comparison stars is recorded by the same telescope and camera setup in the same exposure time, white noise will be dependent on the brightness of these stars. If a dim star is used as a comparison, then the relative fluxes will have a high scatter. It is possible to use a combination of dimmer stars to achieve better precision. Nevertheless, a better comparison star could be constituted with a combination of bright stars to reduce the white noise. The other noise type, correlated noise is due to the light variation correlated with astrophysical and/or observational variables, generally parameterized with β -factor (Winn et al., 2008). If a variable star is used as a comparison star, then the relative fluxes of the target will vary in the reverse direction as a result of the differential photometry technique. Consequently, one should have prior

knowledge of the variability, color and brightness of the stars within the specified passband to select them for comparison in differential photometry.

2.2. Predetermination of relative fluxes

An estimation of precision in photometric measurements requires predetermination of relative fluxes. In order to have an estimate on the relative fluxes of a target star prior to photometric measurements, we make use of the following equation inspired by Wong et al. (2021) based on blackbody radiation (B_λ):

$$Relative\ flux = \left(\frac{d_{comparison}}{d_{target}}\right)^2 \left(\frac{R_{target}}{R_{comparison}}\right)^2 \frac{\int B_\lambda(T_{target})t(\lambda)d(\lambda)}{\int B_\lambda(T_{comparison})t(\lambda)d(\lambda)} \quad (1)$$

where d is the distance, R is the radius, and T is the effective temperature of the stars, which can be assumed to be equal to Gaia values, while the transmission curve of the passband can be obtained from the Spanish Virtual Observatory's (SVO) filter profile service¹.

2.3. Creating observing maps

Assuming the FoV of the detector is a rectangle, the target star can be located on any of the four corners of the FoV, which makes the potential observable area four times bigger than the FoV. We have developed an open source code² in PYTHON that generates three maps. a) A large map that is four times the area of the FoV, where the effective temperature and count levels of the stars are annotated, allowing the user to adjust their real FoV with a visual inspection. b) a map that has the same size as the FoV and maximizes the total count of comparison stars to achieve optimum precision. c) a map that has the same size as the FoV and maximizes the number of acceptable comparison stars. This map can be useful in the case of a single bright star, which can induce more counts than a combination of dim comparison stars does on the detector. However, a single bright star can be an undetected variable. In that case, it should be ideal to choose the map that maximizes the number of comparison stars.

To create such maps, the code requires the target name (or its equatorial coordinates), detector's FoV in both axes in units of arcminutes, filter name, target's desired count level in units of Analog-to-Digital Units (ADU), maximum and minimum count levels for the comparison stars to be input. Then the code converts the FoV of the detector to the World Coordinate System (WCS) using ASTROPY's (Astropy Collaboration et al., 2013, 2018, 2022) WCS tool³ and queries the stars in a field four times bigger than the FoV around

¹<http://svo2.cab.inta-csic.es/theory/fps/>

²<https://github.com/selcukyalcinkaya>

³<https://docs.astropy.org/en/stable/wcs>

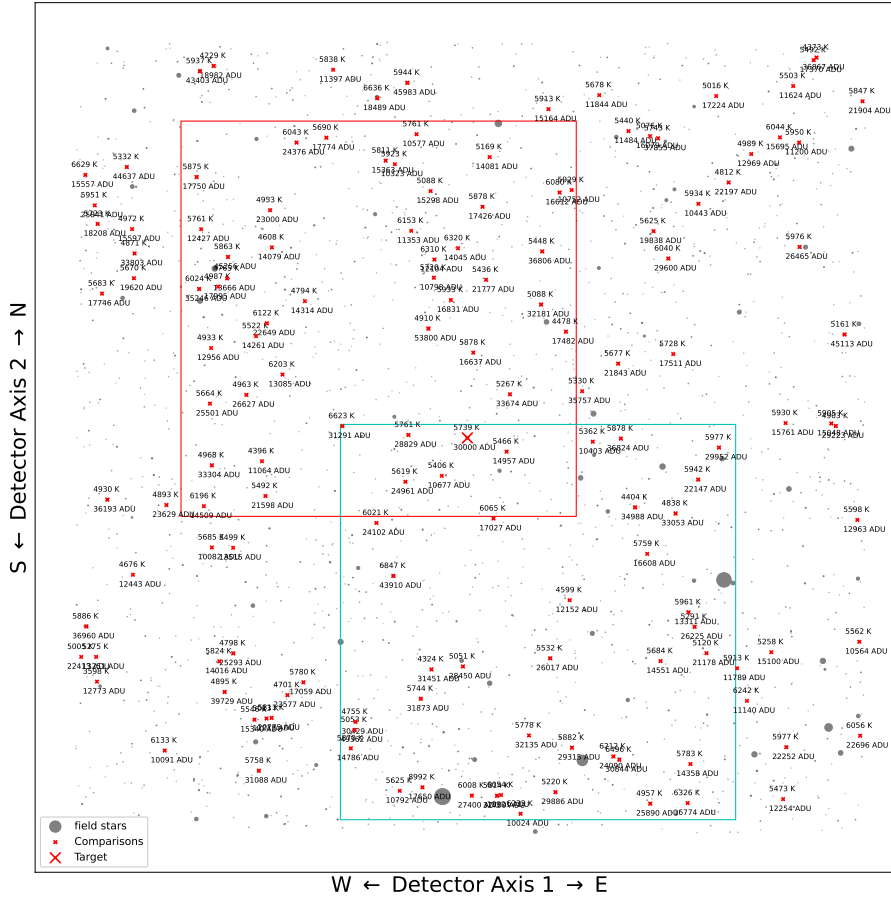


Figure 1. Example of the large map for Kepler-111. The red frame indicates the map that provides the maximum number of comparison stars, while the cyan frame offers the best comparisons in terms of maximum comparison counts. FoV is set at $12' \times 12'$, target adu is 30000 ADU, linearity limits are between 10000 and 55000 ADU, scan-step is $3''$, and edge threshold is 5%. Declination increases upwards along the Y-axis, while right ascension decreases towards the right on the X-axis. The unused field stars are represented by gray circles, while comparison stars are depicted with a red cross. The target star is situated in the center of the large map and is marked with a prominent red cross.

the target star. We use ASTROQUERY's (Ginsburg et al., 2019) Gaia function⁴ for this purpose. Querying is performed by an SQL code that discards variable stars detected by Gaia and it is possible to put a magnitude offset between the target and the field stars to avoid very dim stars. The parallax, radius, equatorial coordinates, magnitudes in the g -band, and the T_{eff} parameters are retrieved. Then the transmission function of the filter is retrieved from SVO using the ASTROQUERY's relevant function⁵. The relative fluxes of the field stars are calculated using Eq-1 and the desired counts for the target as provided by the user. If the stars are out of the user-defined count limits (out of linearity limit or saturation), they are eliminated from the list. The code creates a "large map", centered on the target star by marking potential comparison stars and other stars (fig-1 as an example). The real observed area (FoV) is scanned with an arbitrary value of arcsecond-steps through the large map in each of which the number of comparison stars and the total counts from them are determined. Step size can be determined by the user depending on the proximity of the stars in the large map. We suggest small values such as seeing value for populated fields (e.g. galactic plane). When the scanning is complete, the maximum average distance of the target and comparison stars to the edges of the detector are selected for both optimum precision and a maximum number of comparisons stars maps because there can be more than one way to fit the stars inside FoV. The minimum distance of a star to the any edge of the detector is also an input parameter between 0 and 1, in units of related axis of detector. If the value is 0, then the target or comparison star can be placed on the edges and a value of 0.1 means the target or comparison star can be placed as close as 10% of the length of each axes from the edge.

3. Discussion

ObsMap interactively allows observers to prepare observing maps with an optimal set of available comparison stars to obtain high-quality light curves in terms of precision and accuracy. Knowing the exact location of comparison stars allows the user to observe Regions of Interest (RoI) by cutting out unused pixels, which significantly reduces the readout time and reduces the size of CCD images. OBSMAP is also very useful to avoid bad/hot pixel regions.

We would like to note that OBSMAP uses blackbody approximation for the estimation of relative fluxes. Therefore, photometric measurements in narrow-band filters around specific strong lines may not be accurate. In addition, interstellar extinction is not taken into account. Gaia is also not sensitive to short-period, low amplitude variations due to its poor timing resolution, which makes it difficult to detect every observed variable star, especially those that have such variations. In the presence of only a couple of good comparison stars, we

⁴<https://astroquery.readthedocs.io/en/latest/gaia/gaia.html>

⁵https://astroquery.readthedocs.io/en/latest/svo_fps/svo_fps.html

suggest checking these stars in other databases for variability. The light curves from Transiting Exoplanet Survey Satellite (TESS) (Ricker et al., 2015) can be employed to check variability.

OBSMAP is an open-source code, allowing the user to edit it at will. Users can upload a variable star database, specify a photometric filter by importing its transmission function, or improve the code further by using observed spectra from Gaia instead of the blackbody approach to eliminate stellar extinction.

Acknowledgements. We thank the scientific organizing committee and the local organizing committee for the organization and their support for the conference on Observing techniques, instrumentation, and science for metre-class telescopes III. We thank the attendees for their useful discussions and suggestions.

References

- Astropy Collaboration, Price-Whelan, A. M., Lim, P. L., et al., The Astropy Project: Sustaining and Growing a Community-oriented Open-source Project and the Latest Major Release (v5.0) of the Core Package. 2022, *Astrophysical Journal*, **935**, 167, DOI: 10.3847/1538-4357/ac7c74
- Astropy Collaboration, Price-Whelan, A. M., Sipőcz, B. M., et al., The Astropy Project: Building an Open-science Project and Status of the v2.0 Core Package. 2018, *Astronomical Journal*, **156**, 123, DOI: 10.3847/1538-3881/aabc4f
- Astropy Collaboration, Robitaille, T. P., Tollerud, E. J., et al., Astropy: A community Python package for astronomy. 2013, *Astronomy and Astrophysics*, **558**, A33, DOI: 10.1051/0004-6361/201322068
- Collins, K. A., Kielkopf, J. F., Stassun, K. G., & Hessman, F. V., AstroImageJ: Image Processing and Photometric Extraction for Ultra-precise Astronomical Light Curves. 2017, *Astronomical Journal*, **153**, 77, DOI: 10.3847/1538-3881/153/2/77
- Fulton, B. J., Shporer, A., Winn, J. N., et al., Long-term Transit Timing Monitoring and Refined Light Curve Parameters of HAT-P-13b. 2011, *Astronomical Journal*, **142**, 84, DOI: 10.1088/0004-6256/142/3/84
- Gaia Collaboration, Brown, A. G. A., Vallenari, A., et al., Gaia Data Release 2. Summary of the contents and survey properties. 2018, *Astronomy and Astrophysics*, **616**, A1, DOI: 10.1051/0004-6361/201833051
- Gaia Collaboration, Prusti, T., de Bruijne, J. H. J., et al., The Gaia mission. 2016, *Astronomy and Astrophysics*, **595**, A1, DOI: 10.1051/0004-6361/201629272
- Gaia Collaboration, Vallenari, A., Brown, A. G. A., et al., Gaia Data Release 3. Summary of the content and survey properties. 2023, *Astronomy and Astrophysics*, **674**, A1, DOI: 10.1051/0004-6361/202243940
- Ginsburg, A., Sipőcz, B. M., Basseur, C. E., et al., astroquery: An Astronomical Web-querying Package in Python. 2019, *Astronomical Journal*, **157**, 98, DOI: 10.3847/1538-3881/aafc33

- Ricker, G. R., Winn, J. N., Vanderspek, R., et al., Transiting Exoplanet Survey Satellite (TESS). 2015, *Journal of Astronomical Telescopes, Instruments, and Systems*, **1**, 014003, DOI: 10.1117/1.JATIS.1.1.014003
- Riello, M., De Angeli, F., Evans, D. W., et al., Gaia Early Data Release 3. Photometric content and validation. 2021, *Astronomy and Astrophysics*, **649**, A3, DOI: 10.1051/0004-6361/202039587
- Southworth, J., Hinse, T. C., Jørgensen, U. G., et al., High-precision photometry by telescope defocusing - I. The transiting planetary system WASP-5. 2009, *Monthly Notices of the RAS*, **396**, 1023, DOI: 10.1111/j.1365-2966.2009.14767.x
- Winn, J. N., Holman, M. J., Torres, G., et al., The Transit Light Curve Project. IX. Evidence for a Smaller Radius of the Exoplanet XO-3b. 2008, *Astrophysical Journal*, **683**, 1076, DOI: 10.1086/589737
- Wong, I., Kitzmann, D., Shporer, A., et al., Visible-light Phase Curves from the Second Year of the TESS Primary Mission. 2021, *Astronomical Journal*, **162**, 127, DOI: 10.3847/1538-3881/ac0c7d

Fast photon-counting optical astronomy

L. Zampieri¹ , M. Fiori¹, G. Naletto^{2,1}, A. Spolon¹, C. Barbieri^{2,1},
A. Burtovoi^{3,4}, U. Munari¹, G. Umbriaco⁵, B. Gaiani⁶, L. Lessio¹ and
P. Ochner²

¹ *INAF-Astronomical Observatory of Padova, Italy (E-mail: luca.zampieri@inaf.it)*

² *Department of Physics and Astronomy, University of Padova, Italy*

³ *Physics and Astronomy Department, University of Florence, Italy*

⁴ *INAF-Astrophysical Observatory of Arcetri, Italy*

⁵ *Department of Physics and Astronomy, University of Bologna, Italy*

⁶ *Marelli Automotive Lighting, Italy*

Received: November 15, 2023; Accepted: December 22, 2023

Abstract. Fast sub-second optical variability exists in some important classes of astrophysical sources, in particular pulsars and X-ray binaries. We regularly perform ultra-fast optical photometric campaigns on some of the most interesting targets and transient events. At the same time, we are tackling new campaigns searching for fast optical variability in other types of sources (Fast Radio Bursts, magnetars). To this end we use and develop dedicated fast photon counting instrumentation in the visible band, an area in which our team is the leader. Observations are carried out within the framework of multiwavelength campaigns and in synergy with facilities operating at other wavelengths. Here we report on some of the most recent observing campaigns and technological developments, and on the outcome of a km-baseline experiment of stellar intensity interferometry carried out in photon counting mode.

Key words: Astronomical instrumentation, methods and techniques – Instrumentation: photometers – Techniques: interferometric – stars: magnetars – pulsars: general – pulsars: individual: PSR J1023+0038 – pulsars: individual: SGR J1935+2154 – radio continuum: transients – fast radio bursts – FRB 20180916B

1. Introduction

The project of Fast Photon Counting Optical Astronomy (FPC-OA) in Padova is focused on the study of sub-second optical variability in various types of astrophysical sources, and on experimental applications of Quantum Optics concepts to astronomical observations. We also design and develop optical fast photon counting instrumentation for these observations and applications.

The two main instruments that we realized and operate are AQuEye+ (Asiago Quantum Eye+; Barbieri et al. 2009; Naletto et al. 2013; Zampieri et al.

2015, 2019b), mounted at the Copernicus telescope in Asiago, and IQuEye (Italian Quantum Eye; Naletto *et al.* 2009), that was mounted at several telescopes around the world and is now attached at the Galileo telescope in Asiago. Other technological activities involve the low-impact fiber-feeding of FPC-OA instrumentation to telescopes (Iqueye Fiber Interface, IFI; Zampieri *et al.* 2019b). With the goal of carrying out further technological activities within the framework of this project, we recently realized a dedicated laboratory at Cima Ekar, in Asiago, where the Copernicus telescope is located. This ASTRI-AQUEYE laboratory serves jointly for the assembly, test, and verification activities of the FPC-OA project and for those of the ASTRI Mini-Array Stellar Intensity Interferometry Instrument (Zampieri *et al.*, 2022a).

Several observing FPC-OA programs are currently undertaken, such as the simultaneous multicolor observations of optical pulsars, the timing of optical transients and X-ray binaries, the searches for optical flashes from Fast Radio Bursts (FRBs) and magnetars, the monitoring of the intra-night variability of Blazars, Lunar and asteroidal occultations, and Stellar Intensity Interferometry experiments. Time at the telescopes is granted through two approved proposals for visitor instruments, for a total of 28 nights/year at the Copernicus telescope (cycles 22-24) and 2-3 nights/month at the 1.2-m Galileo telescope.¹ Observations are often carried out within the framework of simultaneous or coordinated multiwavelength (MWL) campaigns with other facilities from the radio to the gamma-ray bands (e.g. SRT, NC, GMRT, TNG, NICER, HXMT, MAGIC).

This paper reports a summary of the results and activities in FPC-OA that we carried out in the last few years.

2. Aqueye+ and Iqueye

Aqueye+ and Iqueye² are non-imaging instruments with a field of view of a few arcseconds tailored to performing very fast photon counting observations in the optical band (Barbieri *et al.* 2009; Naletto *et al.* 2009, 2013; Zampieri *et al.* 2015, 2019b). Their distinctive features are: an optical design with an entrance pupil split, four on-source Single Photon Avalanche Detectors (SPADs), one on-sky SPAD detector (offset by 10 arcmin), an acquisition system capable of sub-nanosecond time tagging accuracy with respect to UTC.

Both instruments adopt the same concept of splitting the telescope entrance pupil proposed for QuantEYE (Dravins *et al.*, 2005). The pupil is divided into four parts, each of them focused on a single SPAD detector. SPADs have < 50 ps time resolution, ~ 100 cts/s dark count rate, ~ 8 MHz maximum count rate, and $\sim 50\%$ photon detection efficiency. The acquisition electronics time tags and stores the arrival time of each detected photon with < 100 ps relative time accuracy and < 500 ps absolute time accuracy with respect to UTC. All times

¹For requests of observations, contact our team at: aqueye.iqueye@gmail.com

²<http://web.oapd.inaf.it/zampieri/aqueye-iqueye/index.html>

are stored in event lists that can be analyzed in post-processing. The maximum data rate in the linear regime is a few MHz.

Aqueye+ is regularly mounted at the 1.8-m Copernicus telescope in Asiago, while Iqueye was mounted at the New Technology Telescope at La Silla, the William Herschel Telescope in La Palma, and the Telescopio Nazionale Galileo in La Palma. Since 2015, it is fiber-fed at the 1.2-m Galileo telescope in Asiago through a dedicated instrument (the Iqueye Fiber Interface, IFI).

3. PSR J1023+0038: The first ms optical and UV pulsar

Since the beginning, one of the main goals of the project was to study optical pulsars at the highest time resolution and to search for new optical pulsators. In 2017, millisecond optical pulsations were indeed discovered in PSR J1023+0038 by [Ambrosino et al. \(2017\)](#). Soon after, we succeeded in detecting them with Aqueye+@Copernicus, for the first time with a 2-m class telescope ([Zampieri et al., 2019a](#)). Other detections both in the optical ([Karpov et al., 2019](#)) and UV bands ([Jaodand et al., 2021](#)) were also reported since then.

PSR J1023+0038 is a pulsar in a binary system ([Papitto & Martino, 2022](#)). The neutron star is rotating with an amazingly small spin period of 1.69 milliseconds, and is weakly magnetized ($10^8 - 10^9$ G), while the companion is a low mass ($< 1M_{\odot}$) star. Old millisecond radio pulsars in binary systems are ‘recycled’ and spun up by deposition of angular momentum from the companion in an accreting Low Mass X-ray Binary phase ([Wijnands & van der Klis, 1998](#)). PSR J1023+0038 was discovered as a radio pulsar in 2009 ([Archibald et al., 2009](#)) and later observed to switch from a rotation-powered ms pulsar to an accretion (subluminous) X-ray binary phase. It is probably crossing an unstable evolutionary phase, swinging between the two states and, for this reason, it is called a transitional Millisecond Pulsar (tMP). Besides PSR J1023+0038, two similar systems are known at present: XSS J1227-4853 ([de Martino et al., 2010](#)) and IGR J1824-2452 ([Papitto et al., 2013](#)). They are clearly instrumental to understanding the formation of ms pulsars and the accretion physics in low magnetic field neutron stars.

3.1. Optical versus X-ray pulse

From 2017 through 2023 we have extensively monitored PSR J1023+0038 with Aqueye+. Nearly simultaneous observations were carried out in the optical band with the fast photometer SiFAP2 at Telescopio Nazionale Galileo, and in the X band with the satellites *XMM-Newton* and *NICER*.

We found that the optical pulse lags that in the X-rays by $\sim 150\mu\text{s}$ ([Figure 1](#); [Illiano et al. 2023](#)), with Aqueye+ and NICER providing the best absolute temporal uncertainty with respect to UTC. We note, in passing, that measurements are performed after correcting for the orbital motion, with the parameters (in particular the time of passage at the ascending node) estimated

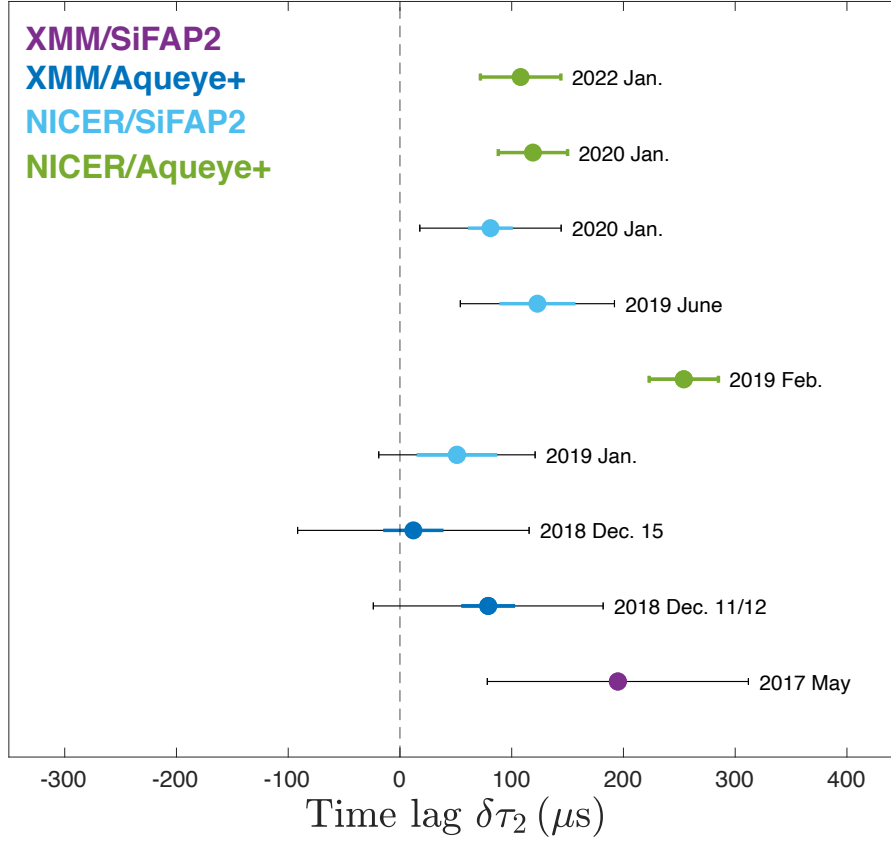


Figure 1. Optical - X-ray delay of the second harmonic component of the pulse profile of PSR J1023+0038. The dashed line indicates a zero time lag. Measurements indicate that the optical pulse lags that in the X-rays by $\sim 150\mu\text{s}$. Colored error bars represent 1σ statistical uncertainties, while the black error bars indicate the total error (including systematics). The best timing accuracy is provided by the Aqueye+ and *NICER* measurements (from [Illiano et al. 2023](#)).

as described in [Illiano et al. \(2023\)](#). In principle, if the optical observations are not exactly simultaneous with those of the satellite in orbit, the timing of the orbital ephemeris could affect the lags. For this reason, in the future, we plan to repeat this measurement using only strictly simultaneous observations.

This result indicates that both the optical and X-ray pulsations come from the same region, confirming a common emission mechanism. Both pulsations could originate from synchrotron emission in the shocked region that forms within a few light cylinder radii away (~ 100 km) from the pulsar, where its

striped wind encounters the accretion disc inflow (Papitto et al., 2019).

This result is also consistent with the spin-down rate measured from Aqu-eye+ data, which is only $\sim 5\%$ faster than that measured in the radio band during the radio pulsar phase (Burtovoi et al., 2020), suggesting that the pulsar engine is still active during the subluminescent X-ray binary phase.

4. Fast Radio Bursts and magnetars

In the last three years we started a new observing program aiming at searching for prompt/delayed optical emission from Fast Radio Bursts (FRB 20180916B; Pilia et al. 2020; Trudu et al. 2023) and magnetars during outburst/flare activity phases (SGR J1935+2154; Zampieri et al. 2022b).

Fast Radio Bursts (FRBs) are transient radio pulses lasting from a millisecond to a few seconds. They have luminosity between 10^{38} erg s $^{-1}$ and 10^{46} erg s $^{-1}$, large dispersion measure and isotropic sky distribution. FRBs are detected in the range 150 MHz-8 GHz and their radio emission is likely to be coherent emission from relativistic particles. The first FRB was discovered by Lorimer & Narkevic in 2007, looking through archival pulsar survey data (Lorimer et al., 2007). Many FRBs have since been recorded (> 500), including several that have been detected to repeat ($\sim 4\%$; e.g. Petroff et al. 2022).

The origin of FRBs is still not understood, but several of them are associated to normal galaxies (at $z < 0.5$). A number of models predict the existence of multiwavelength (MWL) counterparts of FRBs in the form of an afterglow or an impulsive event (e.g. Nicastro et al. 2021). A MWL and/or optical detection would provide critical information on the nature of the progenitor and would greatly enhance our understanding of the FRB phenomenon.

4.1. Searching for prompt/delayed optical flashes in FRB 20180916B

FRB 20180916B shows repeating burst activity (CHIME/FRB Collaboration et al., 2019), detected from 150 MHz (Pastor-Marazuela et al. 2021; Pleunis et al. 2021) up to 6 GHz (Bethapudi et al., 2023). It is localized with high accuracy and associated to a star-forming region in a nearby (redshift $z = 0.0337 \pm 0.0002$) massive spiral galaxy (Marcote et al., 2020). A 16.33 days periodicity in the arrival times of the radio bursts (with an activity window of ± 2.6 days) has been reported (Chime/Frb Collaboration et al. 2020; Pleunis et al. 2021). Clearly, such a periodicity allows for dedicated searches for bursts at other wavelengths during time intervals of possible radio activity.

Between 2020 and 2021 we carried out simultaneous multi-instrument/MWL campaigns on FRB 20180916B (Pilia et al. 2020; Trudu et al. 2023). Within the framework of this collaboration, we performed a fast photometric campaign in the optical band with our instruments in Asiago. In the observations carried out between Oct 2020 and Aug 2021, the net on-target observing time was 122 ks for Aqu-eye+@Copernicus and 62 ks for IFI+Iquye@Galileo. The count rate,

averaged over all acquisitions, was ~ 3000 c/s for Aqueye+ and ~ 1300 c/s for IFI+Iqueye (Trudu *et al.*, 2023).

A total of 14 radio bursts were detected during optical observing windows, 9 of which in Nov 2020 with the Sardinia Radio Telescope (SRT) and another 5 between Feb and Aug 2021 with the Giant Metrewave Radio Telescope (GMRT) (Trudu *et al.*, 2023). No prompt emission has been detected in any of the observations. For Aqueye+, the upper limit in an interval of ± 100 ms around the detection of the radio bursts with a sampling time 1 ms is $V_{min} = 14.25 - 14.64$ mag per ms, corresponding to a fluence $F_{max} = 4.6 \times 10^{-15}$ erg cm $^{-2}$ (fluence density 0.005 Jy ms) and a luminosity $L_{max} = 1.2 \times 10^{43}$ erg s $^{-1}$ at 150 Mpc.

In fact, a 1 ms-long Fast Optical Burst (FOB) was detected (at the 90% confidence level) 13.971 s before the arrival time of the second SRT radio burst (barycentric time of arrival at infinity frequency MJD 59162.8343320911; see Figure 2). The FOB has $V = 14.4$ mag per ms, corresponding to a fluence $F_{max} = 6.4 \times 10^{-15}$ erg cm $^{-2}$ (0.007 Jy ms) and a luminosity $L_{max} = 1.6 \times 10^{43}$ erg s $^{-1}$ at 150 Mpc. We calculate a detection threshold n_t corresponding to a chance probability of $0.0027/N_{trials}$ to exceed a Poissonian distribution at the average rate in any of the bins, where N_{trials} is the total number of bins in the time interval considered. The peak is statistically above the threshold ($n_t = 15$ counts/bin) for a window of ± 15 s centered around the time of arrival of the radio burst, but it is below the threshold obtained considering the bins of the entire observation ($n_t = 19$ counts/bin). We then can not robustly tag it as the optical counterpart of the radio burst.

The nature of this event is under investigation. It could be a faint foreground event produced by a field meteor. The rate of this type of events at this magnitude level (14.5) is completely unknown. Extrapolations from measurements made with fast photomultipliers in the '80s (Cook *et al.*, 1980) could be roughly consistent with our observations. However, this conclusion is highly uncertain and needs further investigation in the future.

5. Stellar Intensity Interferometry: The pilot Asiago km-baseline experiment on Vega

One of the most innovative activities that we have undertaken within the framework of the FPC-OA project is certainly the photon counting, the km-baseline experiment of Stellar Intensity Interferometry (SII) in Asiago (Zampieri *et al.*, 2021). It consists in a measurement of the (2nd order) spatial correlation of the intensity of the light from a star with two Asiago telescopes (Copernicus and Galileo), equipped with Aqueye+ and IFI+Iqueye. A pioneering astronomical experiment devoted to measuring stellar radii with SII was performed by Hanbury Brown and Twiss from 1964 through 1972 (see, e.g., Hanbury Brown 1974).

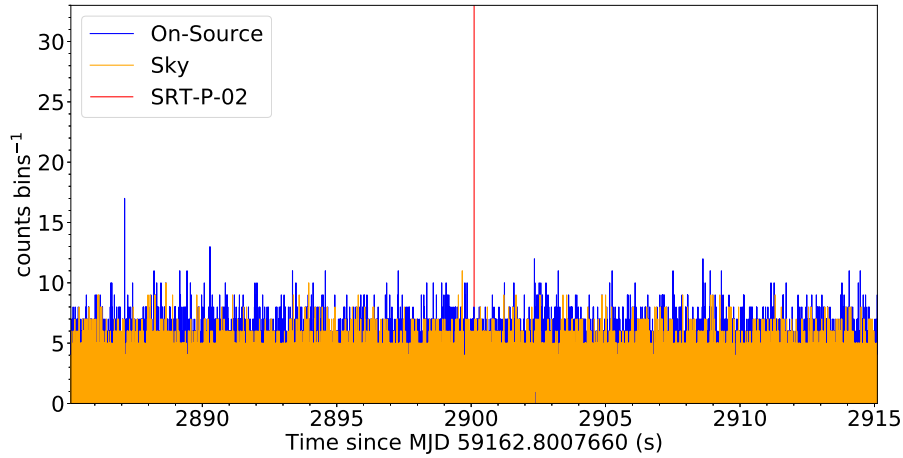


Figure 2. Light curves (binned at 1 ms) of the on-source (blue) and sky (orange) detectors of the Aqueye+ observation corresponding to the detection of an SRT radio burst (Obs ID 20201109-200635, on 2020/11/09; the Aqueye+ starting time has been barycentred). An interval of ± 15 s around the time of arrival of the burst (red vertical line) is shown (from [Trudu et al. 2023](#)).

This pilot Asiago experiment turned out to be successful. We performed for the first time measurements of the correlation of the star Vega counting photon coincidences with sub-nanosecond time resolution in post-processing by means of a single photon software correlator and exploiting entirely the quantum properties of the light emitted from the star. We successfully detected the temporal correlation of Vega at zero baseline (discrete degree of coherence $\langle g^{(2)} \rangle = 1.0034 \pm 0.0008$) and also performed a measurement of the correlation on a projected baseline of ~ 2 km.

Measurements are consistent with the expected degree of coherence for a source with the 3.3 mas diameter of Vega. We can also place a constraint on the size of any potential bright feature on the star surface, that has to be $> 30 \mu\text{as}$ (3×10^9 cm) to be consistent with the absence of correlation on ~ 2 km.

This experiment represented a crucial for addressing the feasibility of potential future implementations of SII in photon counting mode on arrays of Cherenkov telescopes (like the INAF ASTRI Mini-Array; [Zampieri et al. 2022a](#)).

6. Technological Developments

6.1. Iqueye Fiber Interface+ (IFI+)

The Iqueye Fiber Interface (IFI) is the instrument that allows to fiber-feed Iqueye at the 1.2-m Galileo telescope. It was designed and realized during 2014-

2016 to perform the Asiago SII experiment. It consists of a focal reducer with a demagnification 1:2, that injects light in an optical fiber, and a field camera for pointing and guiding, fed by an 8-92% beam splitter (Zampieri *et al.*, 2019b). The specifications of the optical fiber are carefully chosen so as to match the telescope Point Spread Function (PSF) and minimize the beam aperture. The overall efficiency of IFI tested in the laboratory is $\sim 80\%$.

At the beginning of 2023, IFI was completely re-aligned with the telescope optical axis and refurbished. New more robust supports for the lenses and the field camera have been installed. Two optical fiber patches with core diameters $365\ \mu\text{m}$ and $200\ \mu\text{m}$ (that can work alternately) were included to couple IFI directly with the Extended Fiber Interface (see below). An additional optical fiber with a core diameter of $365\ \mu\text{m}$ can be positioned directly on the telescope focal plane with a movable arm. We refer to this upgraded version of the instrument as IFI+ (see Figure 3).

6.2. Fiber-fed Aqueye+

During the last few years, a parallel technological activity for the implementation of an optical fiber interface for Aqueye+@Copernicus was also performed, with the main purpose to trigger a prompt use of Aqueye+ in Target of Opportunity mode for observing transients. The main requirement is coupling the large field of view ($400\ \mu\text{m}$) at the focal plane with the small instrument detector area ($100\ \mu\text{m}$). To this end, we positioned a dedicated tapered optical fiber with a low numerical aperture directly off-axis at the Cassegrain focus (exploiting the mechanical support provided by the spectrograph AFOSC). The taper has inner and outer diameters of $400\ \mu\text{m}$ and $200\ \mu\text{m}$, respectively, and a numerical aperture 0.12. For pointing and guiding we use the telescope field camera. Light from the optical fiber is then injected into Aqueye+ through a separate module positioned in front of Aqueye+. The system is still in the testing phase and can reach at present an overall efficiency of $\sim 20\%$ (compared to Aqueye+ directly mounted).

6.3. Extended Fiber Interface (EFI)

To improve the optical efficiency in fiber-fed mode at the Copernicus telescope, we decided to realize an additional module (Extended Fiber Interface, EFI; see Figure 4) with an on-board SPAD detector fed directly through the optical taper positioned at the Cassegrain focus. EFI consists essentially of a focal reducer with a demagnification 1:2.5. The incoming beam is collimated through an achromatic lens doublet and then focused on the SPAD detector with a second achromatic doublet. The focal lengths of the two doublets are 75 mm and 30 mm, respectively. The second doublet is centered and focussed on the detector through a xyz translation stage. Filters can be inserted in the collimated portion of the beam. At the polychromatic autofocus, the spot radius is $31\ \mu\text{m}$, while

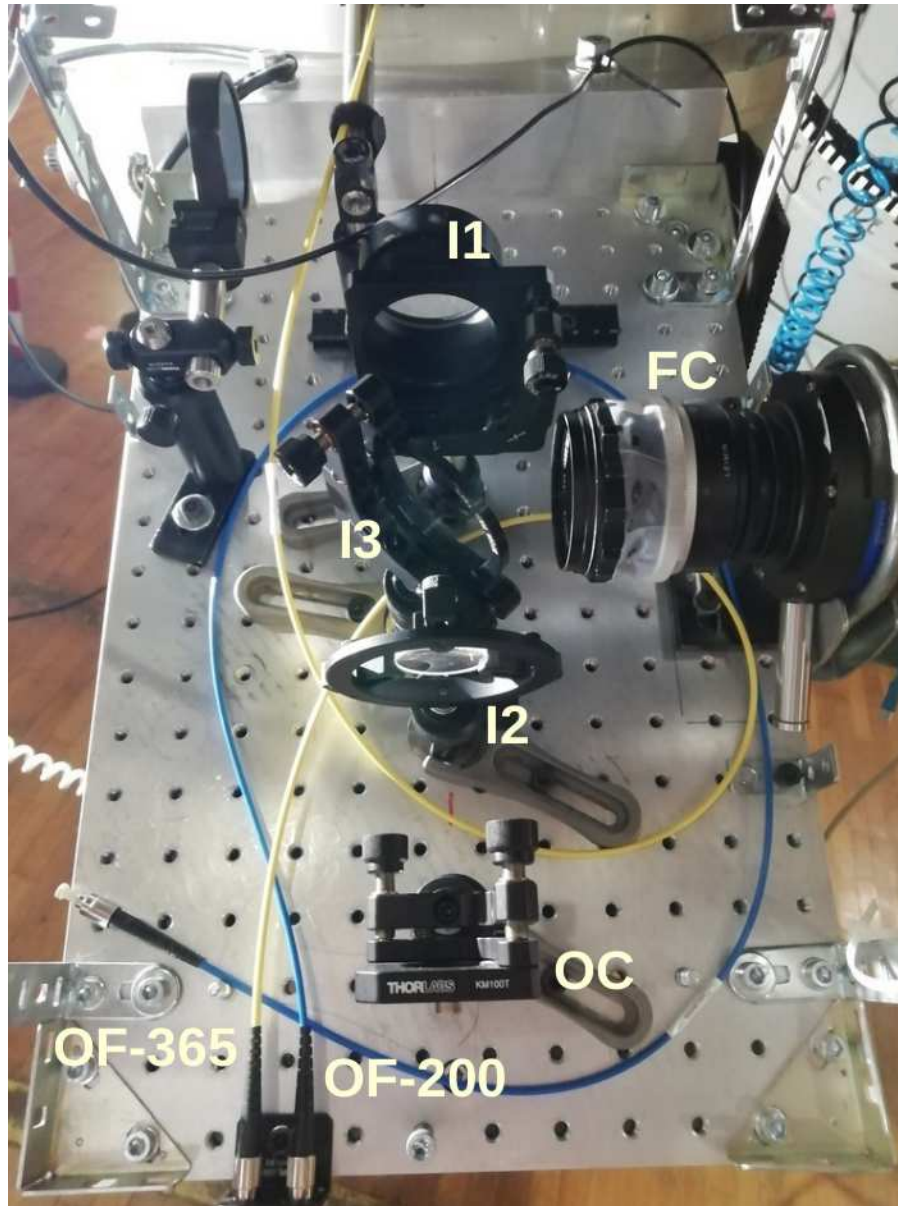


Figure 3. Iqueye Fiber Interface+ (IFI+) mounted at the Nasmyth focus of the 1.2-m Galileo telescope in Asiago. The optical components indicated on the image are: Achromatic lens doublet with focal length 200 mm (I1), achromatic lens doublet with focal length 100 mm (I2), 8-92% reflecting mirror (I3), field camera (FC), optical fiber with 365 μm core (OF-365), optical fiber with 200 μm core (OF-200), optical fiber connector (OC).

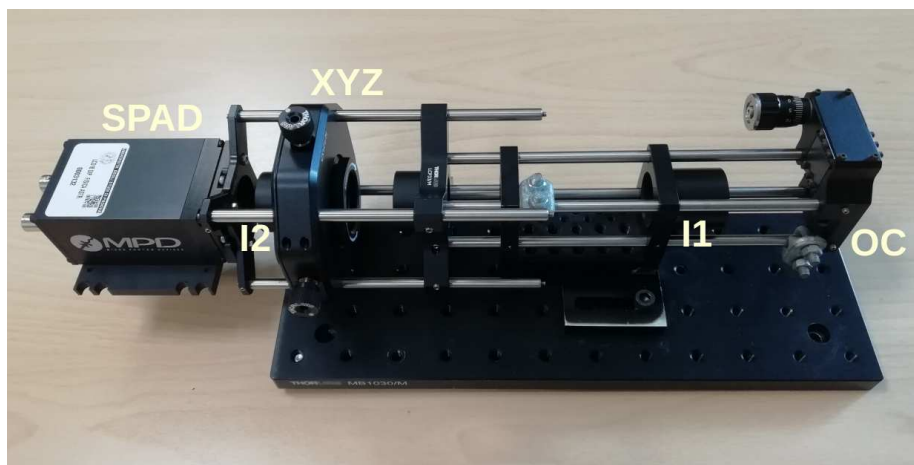


Figure 4. Extended Fiber Interface (EFI). The components indicated on the image are: Achromatic lens doublet with focal length 75 mm (I1), achromatic lens doublet with focal length 30 mm (I2), *xyz* translation stage (XYZ), SPAD detector (SPAD), optical fiber connector (OC).

the ensquared energy distributions is 98%. The overall transmission efficiency of the focal reducer in the *V* band, measured in the laboratory, is 80%.

The module can host a second SPAD detector fed with an additional optical fiber also positioned at the telescope focus for monitoring the sky. Both SPADs are connected to the Aqueye+ acquisition electronics so that the entire system can work as a stand-alone instrument. EFI can, in fact, also work together with IFI+ and be fed through it at the Galileo telescope. The entire system is still under test and development.

7. Conclusions

From 2017 through 2023 we have extensively monitored the optical ms pulsar PSR J1023+0038 with Aqueye+. Nearly simultaneous observations were carried out in the optical and X-ray bands. We found that the optical pulse lags in the X-rays by $\sim 150 \mu\text{s}$, with Aqueye+ and NICER providing the best absolute temporal uncertainty with respect to UTC. This result indicates that both the optical and X-ray pulsations come from the same region, confirming a common emission mechanism and supporting the model of a mini pulsar wind nebula fueled by the shock between the pulsar wind and the accretion disk.

We also perform regular observations and participate to multiwavelength campaigns of repeating Fast Radio Bursts and magnetars in outbursts. The main goal is searching for prompt/delayed optical flashes in these sources. We pre-

sented the results of the most recent campaign carried out on FRB 20180916B, which, together with a similar campaign on the magnetar SGR J1935+2154, provide the deepest upper limits for optical emission coincident with bursts for these sources to date. A 1 ms-long Fast Optical Burst was detected (at the 90% confidence level) 13.971 s before the arrival time of a radio burst in FRB 20180916B, but we can not robustly tag it as the optical counterpart of the radio burst.

One of the most innovative activities that we have undertaken within the framework of the FPC-OA project is certainly the photon counting, km-baseline experiment of Stellar Intensity Interferometry in Asiago. We successfully detected the temporal correlation of the star Vega at zero baseline and also performed a measurement of the correlation on a projected baseline of ~ 2 km. This experiment represented a crucial step for addressing the feasibility of potential future implementations of SII in photon counting mode on arrays of Cherenkov telescopes (like the INAF ASTRI Mini-Array).

Finally, we reported on new technological developments in our work on efficient fiber coupling and our photon counting instrumentation on meter-class telescopes. In particular, we presented the new design and prototype realization of the Extended Fiber Interface.

Acknowledgements. Based on observations collected at the Copernicus telescope (Asiago, Italy) of the INAF-Osservatorio Astronomico di Padova and at the Galileo telescope (Asiago, Italy) of the University of Padova. Presently funded by INAF (Research Grant “Uncovering the optical beat of the fastest magnetized neutron stars (FANS)”) and the University of Padova (DOR grant).

References

- Ambrosino, F., Papitto, A., Stella, L., et al., Optical pulsations from a transitional millisecond pulsar. 2017, *Nature Astronomy*, **1**, 854, DOI: 10.1038/s41550-017-0266-2
- Archibald, A. M., Stairs, I. H., Ransom, S. M., et al., A Radio Pulsar/X-ray Binary Link. 2009, *Science*, **324**, 1411, DOI: 10.1126/science.1172740
- Barbieri, C., Naletto, G., Occhipinti, T., et al., AquEYE, a single photon counting photometer for astronomy. 2009, *Journal of Modern Optics*, **56**, 261, DOI: 10.1080/09500340802450565
- Bethapudi, S., Spitler, L. G., Main, R. A., Li, D. Z., & Wharton, R. S., High frequency study of FRB 20180916B using the 100-m Effelsberg radio telescope. 2023, *Monthly Notices of the RAS*, **524**, 3303, DOI: 10.1093/mnras/stad2009
- Burtovoi, A., Zampieri, L., Fiori, M., et al., Spin-down rate of the transitional millisecond pulsar PSR J1023+0038 in the optical band with Aqueye+. 2020, *Monthly Notices of the RAS*, **498**, L98, DOI: 10.1093/mnrasl/slaa133
- Chime/Frb Collaboration, Amiri, M., Andersen, B. C., et al., Periodic activity from a fast radio burst source. 2020, *Nature*, **582**, 351, DOI: 10.1038/s41586-020-2398-2

- CHIME/FRB Collaboration, Andersen, B. C., Bandura, K., et al., CHIME/FRB Discovery of Eight New Repeating Fast Radio Burst Sources. 2019, *Astrophysical Journal, Letters*, **885**, L24, DOI: 10.3847/2041-8213/ab4a80
- Cook, A. F., Weekes, T. C., Williams, J. T., & Omongain, E., Flux of optical meteors down to $M_{PG} = +12$. 1980, *Monthly Notices of the RAS*, **193**, 645, DOI: 10.1093/mnras/193.3.645
- de Martino, D., Falanga, M., Bonnet-Bidaud, J. M., et al., The intriguing nature of the high-energy gamma ray source XSS J12270-4859. 2010, *Astronomy and Astrophysics*, **515**, A25, DOI: 10.1051/0004-6361/200913802
- Dravins, D., Barbieri, C., Fosbury, R. A. E., et al., QuantEYE: The Quantum Optics Instrument for OWL. 2005, *arXiv e-prints*, astro, DOI: 10.48550/arXiv.astro-ph/0511027
- Hanbury Brown, R. 1974, *The intensity interferometer. Its applications to astronomy*
- Illiano, G., Papitto, A., Ambrosino, F., et al., Investigating the origin of optical and X-ray pulsations of the transitional millisecond pulsar PSR J1023+0038. 2023, *Astronomy and Astrophysics*, **669**, A26, DOI: 10.1051/0004-6361/202244637
- Jaodand, A. D., Hernández Santisteban, J. V., Archibald, A. M., et al., Discovery of UV millisecond pulsations and moding in the low mass X-ray binary state of transitional millisecond pulsar J1023+0038. 2021, *arXiv e-prints*, arXiv:2102.13145, DOI: 10.48550/arXiv.2102.13145
- Karpov, S., Beskin, G., Plokhotnichenko, V., Shibanov, Y., & Zyuzin, D., The study of coherent optical pulsations of the millisecond pulsar PSR J1023+0038 on Russian 6m telescope. 2019, *Astronomische Nachrichten*, **340**, 607, DOI: 10.1002/asna.201913663
- Lorimer, D. R., Bailes, M., McLaughlin, M. A., Narkevic, D. J., & Crawford, F., A Bright Millisecond Radio Burst of Extragalactic Origin. 2007, *Science*, **318**, 777, DOI: 10.1126/science.1147532
- Marcote, B., Nimmo, K., Hessels, J. W. T., et al., A repeating fast radio burst source localized to a nearby spiral galaxy. 2020, *Nature*, **577**, 190, DOI: 10.1038/s41586-019-1866-z
- Naletto, G., Barbieri, C., Occhipinti, T., et al., Iqueye, a single photon-counting photometer applied to the ESO new technology telescope. 2009, *Astronomy and Astrophysics*, **508**, 531, DOI: 10.1051/0004-6361/200912862
- Naletto, G., Barbieri, C., Verroi, E., et al., Aqueye Plus: a very fast single photon counter for astronomical photometry to quantum limits equipped with an Optical Vortex coronagraph. 2013, in Society of Photo-Optical Instrumentation Engineers (SPIE) Conference Series, Vol. **8875**, *Quantum Communications and Quantum Imaging XI*, ed. R. E. Meyers, Y. Shih, & K. S. Deacon, 88750D
- Nicastro, L., Guidorzi, C., Palazzi, E., et al., Multiwavelength Observations of Fast Radio Bursts. 2021, *Universe*, **7**, 76, DOI: 10.3390/universe7030076
- Papitto, A., Ambrosino, F., Stella, L., et al., Pulsating in Unison at Optical and X-Ray Energies: Simultaneous High Time Resolution Observations of the Transitional

- Millisecond Pulsar PSR J1023+0038. 2019, *Astrophysical Journal*, **882**, 104, DOI: 10.3847/1538-4357/ab2fdf
- Papitto, A., Ferrigno, C., Bozzo, E., et al., Swings between rotation and accretion power in a binary millisecond pulsar. 2013, *Nature*, **501**, 517, DOI: 10.1038/nature12470
- Papitto, A. & Martino, D. d. 2022, *Transitional Millisecond Pulsars*, ed. S. Bhattacharyya, A. Papitto, & D. Bhattacharya (Cham: Springer International Publishing), 157–200
- Pastor-Marazuela, I., Connor, L., van Leeuwen, J., et al., Chromatic periodic activity down to 120 megahertz in a fast radio burst. 2021, *Nature*, **596**, 505, DOI: 10.1038/s41586-021-03724-8
- Petroff, E., Hessels, J. W. T., & Lorimer, D. R., Fast radio bursts at the dawn of the 2020s. 2022, *Astronomy and Astrophysics Reviews*, **30**, 2, DOI: 10.1007/s00159-022-00139-w
- Pilia, M., Burgay, M., Possenti, A., et al., The Lowest-frequency Fast Radio Bursts: Sardinia Radio Telescope Detection of the Periodic FRB 180916 at 328 MHz. 2020, *Astrophysical Journal, Letters*, **896**, L40, DOI: 10.3847/2041-8213/ab96c0
- Pleunis, Z., Michilli, D., Bassa, C. G., et al., LOFAR Detection of 110-188 MHz Emission and Frequency-dependent Activity from FRB 20180916B. 2021, *Astrophysical Journal, Letters*, **911**, L3, DOI: 10.3847/2041-8213/abec72
- Trudu, M., Pilia, M., Nicastro, L., et al., Simultaneous and panchromatic observations of the fast radio burst FRB 20180916B. 2023, *Astronomy and Astrophysics*, **676**, A17, DOI: 10.1051/0004-6361/202245303
- Wijnands, R. & van der Klis, M., A millisecond pulsar in an X-ray binary system. 1998, *Nature*, **394**, 344, DOI: 10.1038/28557
- Zampieri, L., Bonanno, G., Bruno, P., et al., A stellar intensity interferometry instrument for the ASTRI Mini-Array telescopes. 2022a, in Society of Photo-Optical Instrumentation Engineers (SPIE) Conference Series, Vol. **12183**, *Optical and Infrared Interferometry and Imaging VIII*, ed. A. Mérand, S. Sallum, & J. Sanchez-Bermudez, 121830F
- Zampieri, L., Burtovoi, A., Fiori, M., et al., Precise optical timing of PSR J1023+0038, the first millisecond pulsar detected with Aqueye+ in Asiago. 2019a, *Monthly Notices of the RAS*, **485**, L109, DOI: 10.1093/mnras/slz043
- Zampieri, L., Mereghetti, S., Turolla, R., et al., Deep Upper Limit on the Optical Emission during a Hard X-Ray Burst from the Magnetar SGR J1935+2154. 2022b, *Astrophysical Journal, Letters*, **925**, L16, DOI: 10.3847/2041-8213/ac4b60
- Zampieri, L., Naletto, G., Barbieri, C., et al., (Very) Fast astronomical photometry for meter-class telescopes. 2019b, *Contributions of the Astronomical Observatory Skalnaté Pleso*, **49**, 85, DOI: 10.48550/arXiv.1908.03396
- Zampieri, L., Naletto, G., Barbieri, C., et al., Aqueye+: a new ultrafast single photon counter for optical high time resolution astrophysics. 2015, in Society of Photo-Optical Instrumentation Engineers (SPIE) Conference Series, Vol. **9504**, *Pho-*

ton Counting Applications 2015, ed. I. Prochazka, R. Sobolewski, & R. B. James, 95040C

Zampieri, L., Naletto, G., Burtovoi, A., Fiori, M., & Barbieri, C., Stellar intensity interferometry of Vega in photon counting mode. 2021, *Monthly Notices of the RAS*, **506**, 1585, DOI: 10.1093/mnras/stab1387

High-resolution échelle spectrograph at Skalnaté Pleso Observatory

T. Pribulla , M. Vaňko , R. Komžík  and P. Sivanič 

*Astronomical Institute of the Slovak Academy of Sciences
059 60 Tatranská Lomnica, The Slovak Republic (E-mail: pribulla@astro.sk)*

Received: November 2, 2023; Accepted: December 14, 2023

Abstract. A clone of échelle spectrograph MUSICOS (Multi-Site COntinuous Spectroscopy) is mounted in the Nasmyth-Cassegrain focus of the 1.3m telescope at Skalnaté Pleso Observatory. The spectrograph is a cross-dispersed, bench-mounted, fiber-fed instrument giving a resolving power in the range of 25 000 to 38 500 (FWHM). Fifty-six orders cover the spectral range between 4250 and 7375 Å. The spectrograph is primarily used to observe novae, symbiotic stars, pulsating variables, binaries, and multiple stellar systems. The radial-velocity stability ($100 - 200 \text{ m s}^{-1}$) is sufficient to detect easily the orbital motion of hot Jupiters orbiting bright stars. In order to improve the spectrograph throughput and radial-velocity stability, several technical changes are planned in the near future.

Key words: instrument – spectrograph

1. Introduction

Skalnaté Pleso Observatory ($20^\circ 14' 02''$ E, $49^\circ 11' 22''$ N, 1786 m a.s.l.) is one of the three observatories of the Astronomical Institute of the Slovak Academy of Sciences. Its bigger, 8 m dome shelters a 1.3 m ($f/8.36$) Nasmyth-Cassegrain telescope (Astelco GmbH, Germany). This is a fully automated instrument with an active optics system on a fast-slewing alt-azimuth fork mount. The first observations were performed in November 2016. The telescope is equipped with a fiber-fed échelle spectrograph following the MUSICOS design (Baudrand & Bohm, 1992). Its Fiber Injection and Guiding Unit (FIGU) is mounted in one of the Nasmyth foci of the telescope using a simple focal reducer to meet the focal ratio of the telescope ($f/8.36$) and collimator ($f/4$). The fiber fore-optics is telecentric. A simple video camera WATEC 120N is used to guide the telescope on the entrance of the $50 \mu\text{m}$ hole. The spectrograph throughput is mainly limited by strongly variable seeing at the site ($1.5 - 4''$). During times when seeing is $<1.5''$, part of the light is lost due to the point-spread-function imperfections.

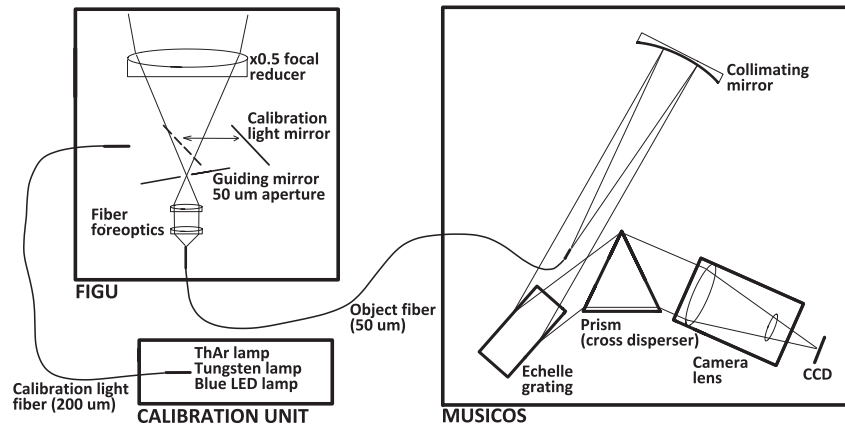


Figure 1. Schematic layout of the MUSICOS spectrograph.

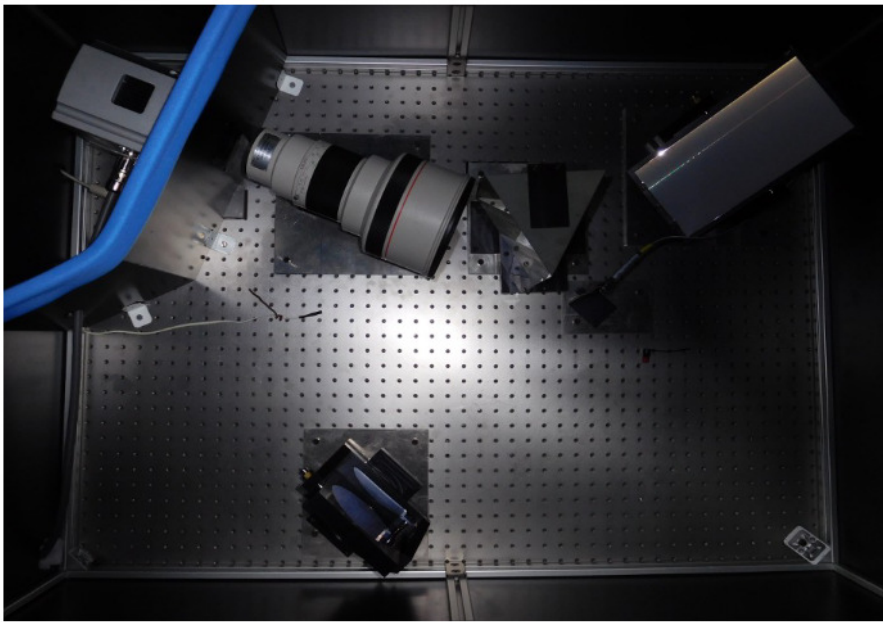


Figure 2. MUSICOS on the optical bench.

2. Components of the MUSICOS spectrograph

Fiber injection and guiding unit, fibers: Made by Shelyak, 200 μm calibration fiber, 50 μm object fiber (UV grade) – both multimode;

Calibration lamps: Thorium-Argon (ThAr), halogen lamp, and blue diodes in a unit made by Shelyak;

Collimator: $f/4$ (480 mm focal length) on-axis dielectrically multi-coated parabolic mirror;

Grating: 31.6 lines/mm, R2 échelle, 128 \times 254 mm;

Crossdisperser: SF5 glass prism with 57° apex angle; optimized antireflection coatings on both sides;

Camera: Canon lens FD 2.8/400L;

Detector: Andor iKon-L DZ936N-BV CCD, 2048 \times 2048 array, 13.5 μm pixels, read-out noise 2.9 e^- , with water assist -95 °C;

Spectral range: 4250-7375 Å in 56 échelle orders;

Spectral resolution: $R = 25\,000$ to 38 500 (FWHM), depending on the focusing

RV stability: 100-200 m.s^{-1}

3. Data reduction

The raw spectroscopic data are being reduced using IRAF package tasks, LINUX shell scripts, and FORTRAN programs. In the first step, master dark and flat-field frames are produced, based on the spectra from the tungsten lamp and blue LED. In the second step, the photometric calibration of the frames is performed using dark and flat-field frames. Bad pixels are cleaned using a bad-pixel mask, and cosmic ray hits are removed using the program of Pych (2004). Order positions are defined by fitting sixth-order Chebyshev polynomials to tungsten-lamp and blue LED spectra on the frames. The resulting two-dimensional (2D) spectra are then extracted and dispersion-solved using ThAr line positions. In the final step, 2D spectra are normalised to the continuum and combined to one-dimensional spectra.

4. Future prospects

It is planned to improve the capabilities of the spectrograph by (i) increasing its throughput, and (ii) improving its radial-velocity (RV) stability. Currently,

the optical throughput of the spectrograph and telescope system is only around 3%. The typical signal-to-noise ratio (per pixel) for a $V = 11$ star is about 15 in a 900-second exposure. The largest light losses are due to seeing and fiber injection. The seeing losses are planned to be mitigated by using two-times thicker fiber ($100\ \mu\text{m}$) and a $50\ \mu\text{m}$ slit (on the spectrograph fiber end) and later using an image slicer to preserve the original spectrograph resolution. A direct injection of light to the fiber is also considered. This would exclude complicated aligning and light losses in the fiber foreoptics. The RV stability is planned to be improved using a bifurcated fiber enabling simultaneous ThAr calibration.

Acknowledgements. This work was supported by the Slovak Research and Development Agency under contract No. APVV-20-0148 and by grant VEGA No. 2/0031/22.

References

- Baudrand, J. & Bohm, T., MUSICOS : a fiber-fed spectrograph for multi-site observations. 1992, *Astronomy and Astrophysics*, **259**, 711
- Pych, W., A Fast Algorithm for Cosmic-Ray Removal from Single Images. 2004, *Publications of the ASP*, **116**, 148, DOI: 10.1086/381786

A variety of binary targets for small telescopes

A.S. Miroshnichenko^{1,2,3} , S. Danford¹ , S. Zharikov^{3,4} ,
A. Aarnio¹ , P. Prendergast⁵, S.A. Khokhlov³ , I.A. Gabitova³ ,
A. Amantayeva³ , N.L. Vaidman³ , S.S. Baktybayev³ ,
I.L. Andronov⁶ , L.L. Chinarova⁶  and I.A. Usenko^{7,8} 

¹ *Department of Physics and Astronomy, University of North Carolina at Greensboro, P.O. Box 26170, Greensboro, NC 27402-6170, USA (E-mail: a_mirosh@uncg.edu)*

² *Fesenkov Astrophysical Institute, Observatory, 23, Almaty, 050020, Kazakhstan*

³ *Al-Farabi Kazakh National University, Al-Farabi Ave., 71, 050040, Almaty, Kazakhstan*

⁴ *Universidad Nacional Autónoma de México, Instituto de Astronomía, AP 106, Ensenada 22800, BC, México*

⁵ *Kernersville Observatory, Winston-Salem, NC 27285, USA*

⁶ *Department of Mathematics, Physics and Astronomy, Odesa National Maritime University, Mechnikova St. 34, 65029 Odesa, Ukraine*

⁷ *Astronomical Observatory, Odesa National University, Shevchenko Park, Odesa 65014, Ukraine*

⁸ *Mykolaiv Astronomical Observatory, Obsevatorna 1, Mykolaiv 54030, Ukraine*

Received: November 8, 2023; Accepted: December 4, 2023

Abstract. Results are reviewed of a long-term program of binary systems observing since 2013 at the 0.81 m telescope of the Three College Observatory in North Carolina, USA, with an échelle spectrograph at a medium spectral resolution. The target list includes recognized and suspected binary systems with normal stars (no spectral lines in emission), classical Be stars, and objects with the B[e] phenomenon. The results include refinement of the orbital elements of bright binaries previously observed with photographic plates, further evidence for phased-locked peak intensity variations of double-peaked line profiles in Be binaries, and recent discoveries of binaries among objects with the B[e] phenomenon.

Key words: spectroscopy – emission-line stars – binary systems

1. Introduction

Many Galactic stars exist in binary systems, whose studies allow us to measure stellar masses and study the process and consequences of the mass exchange between the system components. It turns out that a noticeable fraction of bright (naked-eye or somewhat fainter) binaries have been observed during the epoch before the appearance of CCD detectors that resulted in determination of their orbital and physical properties with a relatively low accuracy. Revisiting these objects with higher quality detectors is necessary to better constrain their properties. This task is doable today with telescopes that are meter-class or smaller.

Binary systems that contain normal (not emission-line) stars can show spectral lines of either one (single-lined) or both (double-lined) components. Determining orbital properties, such as periods, radial velocity (RV) amplitudes, and eccentricities, from spectroscopic data of double-lined systems allows us to measure masses of the components directly. Dealing with single-lined binaries is more complicated, because in addition to the inclination angle of the system's orbital axis other orbital parameters need to be known for both components in order to determine their masses. If the inclination angle in a double-lined spectroscopic binary is unknown, one may determine the mass ratio of the pair from the inverse ratio of the RV amplitudes but it may not be possible to determine each individual mass. The latter is possible with the knowledge of the stellar fundamental parameters (temperature and luminosity).

Stars and stellar systems of all masses go through periods of being surrounded by large amounts of gaseous and dusty circumstellar (CS) material. The duration of these periods mostly depends on the objects' masses and orbital separations. Some reasons for the presence of the CS matter include formation of stars in molecular clouds, stellar winds, and mass transfer between components in binary systems. The CS matter processes starlight and becomes partially ionized; that results in the formation of emission lines, while CS dust can form in more distant and mostly neutral areas of the CS matter.

Although many phenomena due to the CS matter have been successfully explained by the theory of stellar evolution, some remain puzzling even with the currently available wealth of data and sophisticated modeling methods. Two of them, the Be and B[e] phenomenon, are still under investigation aimed at revealing their causes. The Be phenomenon is defined as the presence of permitted emission lines in the spectra of mostly B-type dwarf stars (effective temperatures, $T_{\text{eff}} = 9,000\text{--}30,000$ K), while the B[e] phenomenon also includes the presence of both forbidden emission lines and infrared (IR) excesses due to the radiation of CS dust. Explanations of both the phenomena went through periods of alternatively favoring or mostly ignoring the binary nature of the underlying stars. However, recent evidence that comes from traditional observing techniques (photometry and spectroscopy) and more advanced ones (e.g., interferometry, spectro-astrometry) shows that binary systems play an important role in formation of these objects.

Our observations are described in Sect. 2, examples of our results are shown in Sect. 3, and conclusions and future plans are presented in Sect. 4.

2. Observations

Our team uses the 0.81 m telescope of the Three College Observatory (TCO) located in the central North Carolina, USA, to monitor various binary systems in nearly the entire optical region with a fiber-fed échelle spectrograph. The Observatory was open in the early 1980's, and was used for public viewing and photometric observations until 2011, when the spectrograph eShel from Shelyk Instruments¹ was installed on the telescope. A focal reducer changes the original focal ratio of F/13.6 to F/9 that matches the input focal ratio of the fiber optics.

The spectrograph with an ATIK-460EX detector (2749×2199 pixels, pixel size 4.54 μm × 4.54 μm) provides a spectral resolving power of $R \sim 12,000$ in a spectral range from 3,800 Å to 7,900 Å without gaps between the spectral orders. The location latitude (35°56' N) allow observations of the entire northern sky and a big portion of the southern sky (down to a declination of about -40°).

The signal gets low near the blue and red boundaries of the above spectral range due to a decreasing sensitivity of the detector. The maximum signal is achieved at wavelengths of $\sim 5800\text{--}6200$ Å. The spectrograph is stored in a refrigerator at a stable temperature $\sim 10\text{--}15^\circ\text{C}$, one floor below the telescope and connected to it with a 10-meter long fiber. The one-stage Peltier cooler allows achieving working temperatures of -2°C to -20°C at the detector, which fortunately has a low temperature dependence of the quantum efficiency.

Final spectra typically consist of several individual exposures, which are summed up during the data reduction process. The latter uses the IRAF package *echelle* and includes bias subtraction, spectral order separation, and wavelength calibration using spectra from a ThAr lamp. The number of comparison lines identified in the calibration spectra range from ~ 800 to over 1,000. A typical scatter of the comparison line positions from a polynomial solution is ~ 0.03 Å which results in a potential RV accuracy of ~ 300 m s^{-1} .

Flat field images are not taken, because the detector has a pixel sensitivity difference of $\leq 1.5\%$ and the flat field lamp does not cover the entire extracted spectral range. The spectra contained 24 orders between 4200 Å to 7900 Å during the first 7 years of observations. In the Fall of 2018 the number of orders increased to 31 after the installation of an optical fiber with better UV transmission. Since 2022 we also extract two additional spectral orders that extend the spectra to ~ 8450 Å.

The location of TCO at a low elevation of ~ 180 meters above the sea level has both advantages and disadvantages. The main advantage is that most cosmic rays get absorbed in the Earth's atmosphere before reaching the telescope. Another advantage is that the place has a relatively low humidity, which rarely

¹<https://www.shelyak.com>

reaches 80–85% on clear nights. Typically there are ~ 150 clear and semi-clear nights a year. One of the main disadvantages is that an average seeing is 2–3 arcseconds, but it can be better during nights with a high humidity. Another problem is high temperatures during summer time reaching 35°C.

The ATIK-460EX detector was installed in January 2013, while a Watec 120N TV camera has been used to view the observed targets since the very beginning of the spectroscopic program in October 2011. Observers (A.M. and S.D. and later A.A., who joined the team in 2018) were taking spectra on-site until 2020. TCO was automated in the Fall of 2019. Remote observations began in April 2020 and allowed us to increase the number of used nights from ~ 80 –85 to ~ 150 –160.

3. Results

Our observing projects target a variety of objects that include nearly 140 dwarfs and roughly the same number of supergiants of the spectral types B, A, and F for the purpose of calibration of fundamental parameters and studying spectral variations; ~ 30 classical Be stars, ~ 10 objects with the B[e] phenomenon, ~ 10 pre-main-sequence Herbig Ae/Be stars, 5 horizontal branch stars, 5 post-AGB dusty binaries, and some other peculiar objects. In particular, we have been monitoring ~ 20 binary systems of different kinds (with and without emission lines) and some stars suspected of binarity.

The total number of spectra taken since the beginning of spectroscopic observations during $\sim 1,150$ nights approaches 12,000. Radial velocity (RV) standard stars of early and late spectral types from such lists as [Stefanik et al. \(1999\)](#) and [Soubiran et al. \(2018\)](#) are being observed every night. The fraction of RV standard observations in our entire set of data is nearly 12%. The latter allows us to constantly keep track of the wavelength calibration quality.

In this paper, we will present several results from our observing program mostly concerning very bright known binary systems undergoing different evolutionary stages. However, we first go over the observed features of binaries and difficulties of different kinds of object. The features include but are not limited to the following: the presence of two systems of spectral lines in the spectrum, periodic RV variations of spectral lines, periodic intensity variations in double-peaked line profiles (e.g., orbital phase-locked, found in Be stars), differing positions of the continuum and spectral lines on detectors (spectro-astrometry), and direct detection of secondary components by imaging or interferometry. The difficulties include the presence of broad spectral lines due to fast rotation of the underlying star (e.g., in Be stars), distortion of absorption lines by CS emission or replacement some absorption lines with emission lines (most often of hydrogen lines), and much fainter secondary components (≥ 2 mag in the visual part of the spectrum found in Be and B[e] stars) that hampers spectroscopic detection

of the secondaries. The methods used for the data approximation, when periodic processes were found, are described in [Andronov \(2020\)](#).

A selection of recently published results on binary systems with a significant fraction of observations taken at TCO includes the following.

1. Refining orbital parameters of bright “normal” binaries Mizar B, 2 Lac, ϕ Aql ([Miroshnichenko et al., 2023b](#))
2. A systematic study of the peak intensity variations of double-peaked line profiles in Be stars to detect faint secondary companion ([Miroshnichenko et al., 2023a](#))
3. First reliable detection of the secondary companion in the brightest B[e] binary 3 Pup ([Miroshnichenko et al., 2020](#))
4. Monitoring the pulsational period and surface temperature variations of Polaris A and refining its binary orbit ([Usenko et al., 2020](#))

Examples of the results from some of the mentioned papers are given below.

3.1. Mizar B

Mizar B is the fainter among the two binary systems visible with the naked eye as one star, Mizar. Both systems are spectroscopic binaries easily resolved with a small telescope. Mizar B ($V = 3.9$ mag) is a single-lined binary. The RV variations in its spectrum were first announced by [Frost \(1908\)](#), while the first orbit determination attempt was made by [Abt \(1961\)](#) based on 24 photographic spectra taken in 1959 at the McDonald Observatory (Texas, USA) and found a wrong period of 361 days. [Gutmann \(1965\)](#) took 89 photographic spectra at the Dominion Astrophysical Observatory (DAO, Victoria, BC, Canada) between 1941 and 1963. These data covered several orbital cycles, but only 3 of them in detail. The latter is important due to a large orbital eccentricity. No new studies of Mizar B have been reported since that time to the best of our knowledge.

We took nearly 120 spectra of Mizar B in 2016–2021 and derived RVs by cross-correlation in a spectral region between ~ 5100 and ~ 5300 Å using the IRAF package *rvsao*. The cross-correlation template was obtained from averaging several exposures of the RV standard star $\delta 03$ Tau = HR 1389, heliocentric $RV = 39.0 \pm 0.1$ km s $^{-1}$ ([Stefanik et al., 1999](#); [Soubiran et al., 2018](#)).

Our data along with those from [Gutmann \(1965\)](#) are shown in [Fig. 1](#). Both data sets are folded with the best-fit orbital period 175.11 ± 0.10 days found from the TCO data, which exhibit a significantly lower scatter and a systemic RV of -14.34 ± 0.04 km s $^{-1}$ that is 5 km s $^{-1}$ more negative.

Based on the fundamental parameters of the primary component of Mizar B derived from published photometry and the Gaia distance (24.81 ± 0.17 pc, [Bailer-Jones et al., 2021](#)), its evolutionary mass is $1.8 M_{\odot}$. From the mass function calculated from our orbital parameters and the absence of signs of the

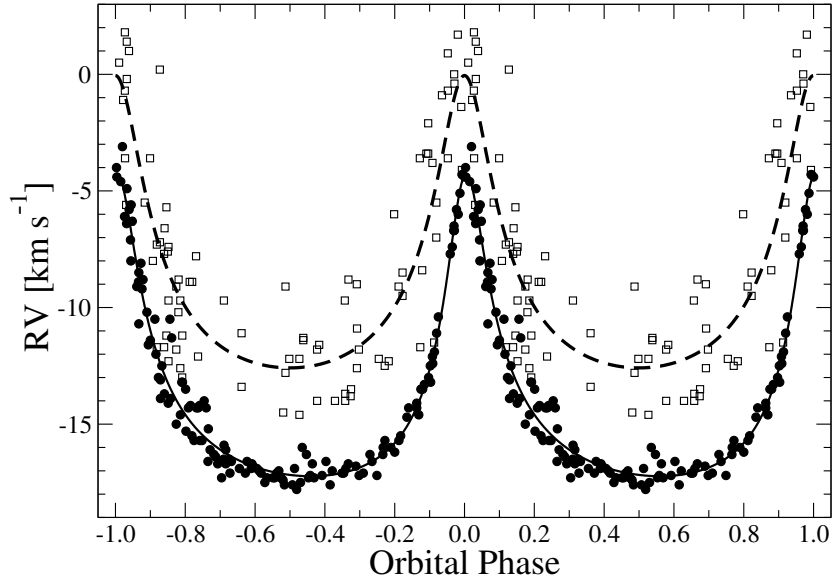


Figure 1. RV curves of Mizar B from [Gutmann \(1965\)](#) and from TCO data. The DAO data are shown by open squares, and the best fit to these data is shown by the dashed line. The TCO data are shown by filled circles, and the best fit is shown by the solid line. The RVs of both data sets are heliocentric.

secondary component, one can conclude that the secondary is a much lower mass star. It would be a K3 v star with a mass of $0.77 \pm 0.03 M_{\odot}$ at the orbital inclination angle of $i = 20^{\circ}$ or an M3 v star with a mass of $0.37 \pm 0.02 M_{\odot}$ at $i = 40^{\circ}$. The orbital parameters of the Mizar B binary system and more detailed conclusions from it are published in [Miroshnichenko et al. \(2023b\)](#).

3.2. Polaris A

Another bright interesting objects is Polaris A, a Cepheid that is the closest to our Solar system. A few facts about this object: it is a multiple system with three visual components (Polaris B = BD+88°9, C, and D) and a member of an anonymous open cluster; one of four Cepheids with a radius measured by optical interferometry ($46 \pm 3 R_{\odot}$, [Nordgren et al., 1999](#)). On top of that, it has the largest number of RV measurements among Cepheids for over 120 years.

The pulsation period of Polaris A was found gradually increasing by $4.45 \pm 0.03 \text{ yr}^{-1}$ from 3.9669 to 3.9707 days in 1896-2004 ([Turner et al., 2005](#)). The pulsation amplitude dropped from $\sim 5 \text{ km s}^{-1}$ before 1950 to $\sim 0.05 \text{ km s}^{-1}$ in the 1980s, then increased from $\sim 1.5 \text{ km s}^{-1}$ in 1987 to $\sim 2.4 \text{ km s}^{-1}$ in 2007.

We started observing it at TCO in 2015 and took over 500 spectra to-date. Some of our results include measuring changes in the pulsation period and refining the orbit of the Polaris A binary. In particular, TCO data covered the most recent periastron passage of Polaris B. Figure 2 shows our RV data taken in 2015–2020 along with those from [Anderson \(2019\)](#). This is the only periastron passage in this system that has been covered with modern high-quality spectroscopy, as the orbital period of this binary system is 29.3 years. We plan to keep monitoring Polaris A to further constrain its pulsational properties and orbit.

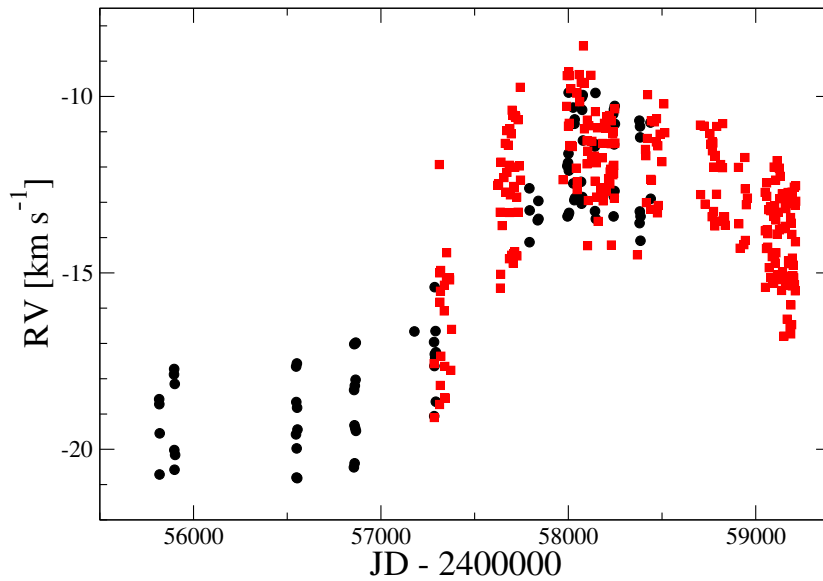


Figure 2. RV variations of Polaris over the last ten years. Red squares show TCO data, black circles show data from [Anderson \(2019\)](#).

3.3. Be stars

Our program studying classical Be stars includes ~ 40 objects with a V -band brightness from ~ 2.9 and ~ 8.0 mag. It aims at long-term monitoring of various features, such as emission lines appearance/disappearance, variations of the emission peak intensities in double-peaked spectral lines (“V/R” variations), and absorption-line positional variations. It covers known and suspected binaries as well as those currently considered single. One of our goals is to verify previously published results and improve our knowledge of binarity by using different spectroscopic diagnostics based on large sets of homogeneous data.

The objects for this program were selected based of the following criteria: 1) sufficiently bright ($V \leq 6$ mag) to achieve high signal-to-noise ratios with the TCO telescope in a wide spectral region, and 2) the presence of double-peaked Balmer emission lines that are not very strong to avoid possible longer-term periodicities observed in some objects of this class (e.g., 48 Lib). We intended to study the V/R behavior in more detail than previously, test the V/R variations as an indicator of binarity, and put more constraints on the applicability of this method. Our data on some of the program stars were supplemented by other data either published or taken from public data archives, such as the BeSS database (Neiner et al., 2011).

The results of our Be star program include include confirmation of the orbital periods in ν Geminorum, ϵ Capricorni, κ Draconis, 60 Cygni, and V2119 Cygni, refinement of the orbital period of o Puppis, and suggestions of binarity in o Aquarii, BK Camelopardalis, and 10 Cassiopeae. Monitoring of the $H\alpha$ line profile variations of β Canis Minoris for over the last 10 years gives further support to the existence of a 182.5-day period found earlier in a smaller set of data. A similar but still preliminary period (179.6 days) was found the $H\alpha$ line profile variations of ψ Persei.

Perhaps the most important result of the TCO program concerns the 4th magnitude star ν Geminorum. History of studies of this multiple system was recently reviewed in Klement et al. (2021) and focused on the inner binary and the distant tertiary component. Following the first measurement of the inner binary orbital period (53.73 days) and the conclusion on the absence of phase-locked V/R variations of the double-peaked $H\alpha$ line profile Rivinius et al. (2006), it was assumed that the Be star is the tertiary component, while the inner pair consists of two B-type stars of nearly equal masses. However, the latest long-baseline interferometry results (Gardner et al., 2021) revealed an inconsistency between the astrometric and the mentioned spectroscopic orbital solutions.

We have been monitoring ν Gem since 2014 at TCO, and our data always showed double-peaked $H\alpha$ line profiles with small V/R variations. However, earlier observations published in Rivinius et al. (2006) as well as some others found in public archives showed a much larger range of the V/R ratios and a more complex structure the $H\alpha$ line profile with three and even four emission peaks around the year 2000. The line profile returned back to a double-peaked in the beginning of 2003, but large V/R variations remained until mid-2006 matching the time period reported in Rivinius et al. (2006), when no regular V/R variations were detected.

Our spectra showed a V/R amplitude of ~ 0.2 and a temporal trend toward smaller V/R. Also, the V/R ratio exhibited a strictly periodic phase-locked behavior, which became especially obvious after subtracting a linear trend. Therefore, the Be star takes part in the 53.78-day orbital period and cannot be identified with the tertiary component of the ν Gem system. The RVs derived by cross-correlation with in a spectral region near 4500 Å and a detrended V/R data are shown in Fig. 3.

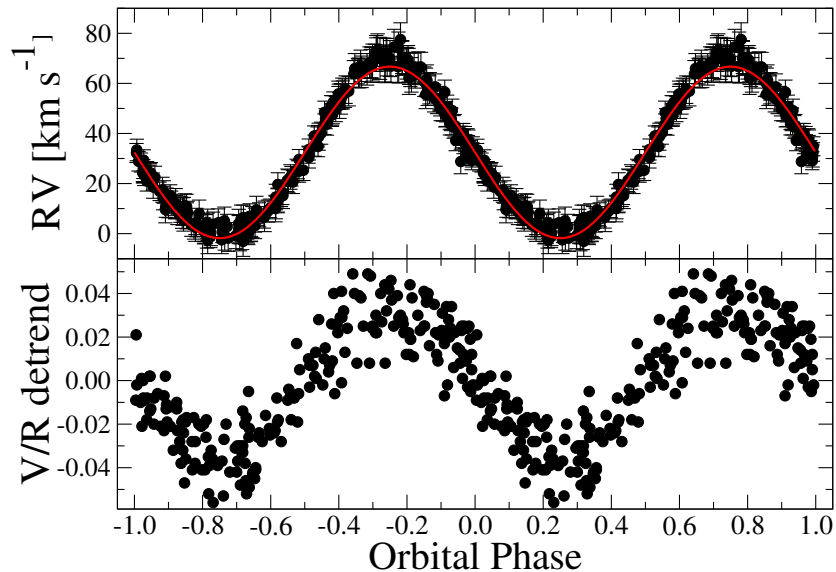


Figure 3. Top panel: RV variations of the absorption lines in the spectrum of ν Geminorum in a region 4450–4555 Å folded with the orbital period (53.73 days). Red line shows our circular solution. Bottom panel: V/R variations of the H α line profile de-trended with a quadratic function and folded with the same period.

We also found the phase-locked V/R variations in ϵ Capricorni, κ Draconis, 60 Cygni, and V2119 Cygni, and o Puppis. Our results show that such variations are observed in more Be binary systems than previously known and can be used to search for binarity of Be stars when application of other methods is inconclusive. A detailed description of the results of our Be star program has been recently published in [Miroshnichenko et al. \(2023a\)](#).

4. Conclusions

Spectroscopy of binary systems is still important, because even very bright objects may not have well-constrained orbital and hence physical parameters. Spectral resolving powers of $R \geq 5,000$ are needed to reliably search for RV and intensity variations. Observations need to be taken as frequently as possible and for a period of at least several years. The V/R variation method successfully complements other methods of discovering binarity of Be stars.

These projects can be successfully performed with meter-class telescopes equipped with inexpensive échelle and long-slit spectrographs. Sensitivities of modern CCD detectors allow taking high-quality data of many stars and stel-

lar systems down to $V \sim 11$ mag. at intermediate $R \sim 10,000\text{--}20,000$. Overall, performing these observations not only helps refining older results on binary systems but also discover new phenomena and contribute to a better understanding of stellar evolution.

5. Acknowledgments

This research has made use of the SIMBAD database, operated at CDS, Strasbourg, France; SAO/NASA ADS; BeSS database, operated at LESIA, Observatoire de Meudon, France: <http://basebe.obspm.fr>, data provided by the Ritter Observatory Data Archives of the Ritter Astrophysical Research Center, University of Toledo. We thank Daniela Korčáková for sharing spectra of ν Geminorum taken at the 2 m telescope of the Ondřejov Observatory (Czech Republic). The UNCG team acknowledges technical support from Dan Gray (Sidereal Technology company), Joshua Haislip (University of North Carolina Chapel Hill), and Mike Shelton (University of North Carolina Greensboro) as well as TCO funding by the College of Arts and Sciences and the Department of Physics and Astronomy of the University of North Carolina Greensboro.

References

- Abt, H. A., The Frequency of Binaries among Metallic-Line Stars. 1961, *Astrophysical Journal, Supplement*, **6**, 37, DOI: 10.1086/190060
- Anderson, R. I., Probing Polaris' puzzling radial velocity signals. Pulsational (in-)stability, orbital motion, and bisector variations. 2019, *Astronomy and Astrophysics*, **623**, A146, DOI: 10.1051/0004-6361/201834703
- Andronov, I. L., Advanced Time Series Analysis of Generally Irregularly Spaced Signals: Beyond the Oversimplified Methods. 2020, in *Knowledge Discovery in Big Data from Astronomy and Earth Observation*, ed. P. Škoda & F. Adam, DOI: 10.1016/B978-0-12-819154-5.00022-9, 191–224
- Bailer-Jones, C. A. L., Rybizki, J., Fouesneau, M., Demleitner, M., & Andrae, R., Estimating Distances from Parallaxes. V. Geometric and Photogeometric Distances to 1.47 Billion Stars in Gaia Early Data Release 3. 2021, *Astronomical Journal*, **161**, 147, DOI: 10.3847/1538-3881/abd806
- Frost, E. B., On certain spectroscopic binaries. 1908, *Astronomische Nachrichten*, **177**, 171, DOI: 10.1002/asna.19081771103
- Gardner, T., Monnier, J. D., Fekel, F. C., et al., ARMADA. I. Triple Companions Detected in B-type Binaries α Del and ν Gem. 2021, *Astronomical Journal*, **161**, 40, DOI: 10.3847/1538-3881/abcf4e
- Gutmann, F., The spectroscopic orbit of zeta1 Ursae Majoris (Mizar B). 1965, *Publications of the Dominion Astrophysical Observatory Victoria*, **12**, 361

- Klement, R., Hadrava, P., Rivinius, T., et al., ν Gem: A Hierarchical Triple System with an Outer Be Star. 2021, *Astrophysical Journal*, **916**, 24, DOI: 10.3847/1538-4357/ac062c
- Miroshnichenko, A. S., Chari, R., Danford, S., et al., Searching for Phase-Locked Variations of the Emission-Line Profiles in Binary Be Stars. 2023a, *Galaxies*, **11**, 83, DOI: 10.3390/galaxies11040083
- Miroshnichenko, A. S., Danford, S., Andronov, I. L., et al., Refining Orbits of Bright Binary Systems. 2023b, *Galaxies*, **11**, 8, DOI: 10.3390/galaxies11010008
- Miroshnichenko, A. S., Danford, S., Zharikov, S. V., et al., Properties of Galactic B[e] Supergiants. V. 3 Pup-Constraining the Orbital Parameters and Modeling the Circumstellar Environments. 2020, *Astrophysical Journal*, **897**, 48, DOI: 10.3847/1538-4357/ab93d9
- Neiner, C., de Batz, B., Cochard, F., et al., The Be Star Spectra (BeSS) Database. 2011, *Astronomical Journal*, **142**, 149, DOI: 10.1088/0004-6256/142/5/149
- Nordgren, T. E., Germain, M. E., Benson, J. A., et al., Stellar Angular Diameters of Late-Type Giants and Supergiants Measured with the Navy Prototype Optical Interferometer. 1999, *Astronomical Journal*, **118**, 3032, DOI: 10.1086/301114
- Rivinius, T., Štefl, S., & Baade, D., Bright Be-shell stars. 2006, *Astronomy and Astrophysics*, **459**, 137, DOI: 10.1051/0004-6361:20053008
- Soubiran, C., Jasniewicz, G., Chemin, L., et al., Gaia Data Release 2. The catalogue of radial velocity standard stars. 2018, *Astronomy and Astrophysics*, **616**, A7, DOI: 10.1051/0004-6361/201832795
- Stefanik, R. P., Latham, D. W., & Torres, G., Radial-Velocity Standard Stars. 1999, in *Astronomical Society of the Pacific Conference Series*, Vol. **185**, *IAU Colloq. 170: Precise Stellar Radial Velocities*, ed. J. B. Hearnshaw & C. D. Scarfe, 354
- Turner, D. G., Savoy, J., Derrah, J., Abdel-Sabour Abdel-Latif, M., & Berdnikov, L. N., The Period Changes of Polaris. 2005, *Publications of the ASP*, **117**, 207, DOI: 10.1086/427838
- Usenko, I. A., Miroshnichenko, A. S., Danford, S., Kovtyukh, V. V., & Turner, D. G., Spectroscopic Investigations of the Polaris (α UMi) System: Radial Velocity Measurements, New Orbit, and Companion Influence for the Cepheid Polaris Aa Pulsation Activity. 2020, *Odessa Astronomical Publications*, **33**, 65, DOI: 10.18524/1810-4215.2020.33.216289

Low-mass contact binaries as probes of stellar merging events

K. Gazeas

*Section of Astrophysics, Astronomy and Mechanics, Department of Physics,
National and Kapodistrian University of Athens, GR-15784 Zografos, Athens,
Greece*

Received: November 13, 2023; Accepted: January 8, 2023

Abstract. Gravitational interaction is important for nearly every aspect of Astrophysics. Theoretical models are tough tested in cases where strong, stellar winds, angular momentum loss, and mass transfer take place in the course of stellar evolution within a common envelope. Stellar interaction impacts the formation and evolution of diverse types of binary and multiple stellar systems. Therefore, evolution in a binary (and a multiple) stellar environment is still an open question in Astrophysics while contact binaries are challenging the well-established and solid theories that concern thermal equilibrium and orbital stability. There is a vast number of such systems observed in the Milky Way and the Magellanic Clouds. Systematic (independent or combined) observations, all-sky surveys, ground-based and space telescopes have offered very detailed photometric and spectroscopic information about these systems. Special attention is given when extreme cases are observed, such as ultra-short orbital period contact binaries or extremely low mass ratio systems. These cases can give insights into the physical and orbital parameters of low-mass contact binaries and their temporal variations. For example, one can investigate the orbital period modulation, the spot activity, and the possibility of contact binaries to host planets, as well as predict a stellar merger, red nova events, and a possible connection with exotic stellar populations such as blue stragglers. The purpose of this work is to present the recent developments in observations of low-mass contact binaries, highlighting the most important findings, in combination with existing theories. The research of such systems, at an international level, is constantly challenging our current knowledge of stellar interactions and advances our understanding of stellar dynamics in common envelope and contact phases.

Key words: Stars: low-mass – Stars: evolution – (Stars:) binaries (including multiple): close – (Stars:) binaries: eclipsing

1. Introduction

Binarity in nature is something very common, expressed in a wide range of scales, from binary asteroids and dwarf planets to binary stars, clusters, and

galaxies. Kepler’s law and the two-body theory can be simply applied to understand the orbital behavior of the involved objects, assuming that there is no intrinsic variability or evolution that alters their physical properties. Consequently, the binary system behavior is dominated by the stellar interaction between the two components. This process is the dominant mechanism that leads the individual components and the system itself through the paths of binary evolution. Although most of the eclipsing binaries are observed to be members of triple, quadruple, or multiple systems in general, they are formed in a hierarchical configuration. Stellar evolution in a contact binary system is different than a single-star evolution in many aspects. Evolution alters the physical parameters of single (solar-type) stars in a timescale of 5–10 Gyr. On the contrary, the current theoretical models support that evolution within a binary environment can be even slower, exceeding the timescale of 10–15 Gyr (Gazeas & Stepień, 2008). Therefore, what we see today as a contact binary stellar system is just a snapshot of this long-lasting process.

Stellar evolution theories indicate that we should be able to observe stellar merging events (Webbink, 1976; Stepień, 2006) due to the gradual coalescence of contact binaries. However, this has not been the case until the detection of the merging event of V1309 Sco in 2008 (Tylanda et al., 2011). Even in this case, the contact binary nature of the progenitor was discovered only after the red nova event (Nova Sco 2008). Numerous observations of V1309 Sco are available in the OGLE-III and IV surveys (Udalski, 2003) before the red nova event and they helped to identify the nova progenitor as a low mass ratio contact binary in deep contact configuration with an orbital period of about 1.4 days.

A merging event is presumed to be driven by the instability of the two involved stellar components. A contact binary system can experience mass and angular momentum loss via mass outflow from the Lagrange point L_2 or via stellar wind and magnetic activity (e.g. flares). The system can be also unstable if the orbital angular momentum is less than three times the total spin angular momentum (Hut, 1980), also known as ”Darwin instability”. Systematic studies of such systems started to appear only very recently, suggesting that low mass ratio contact binary systems are promising merger candidates (Li et al., 2022; Wadhwa et al., 2023b,a; Liu et al., 2023).

2. Challenging theoretical models

From the observational aspect, there are efforts to increase the sample of well-studied systems, derive their physical and orbital parameters with high accuracy, and eventually understand the nature of the contact binary configuration. Fortunately, there is a vast number of contact binary systems in the Milky Way and the Magellanic Clouds, and the majority of them (over 60%) are accompanied by tertiary members, as shown in past and recent studies (D’Angelo et al., 2006), (Loukaidou et al., 2022). Low-mass and low-temperature contact bina-

ries are the most frequently observed types of eclipsing binary systems. Their components have smaller sizes in comparison with other main-sequence stars, and they belong to the old stellar population group (Rucinski, 2000).

In parallel to the observations, there are several attempts to understand the evolution processes within a binary environment. We have more than a century of knowledge of the existence of contact binary systems. In the early 50's and 60's, we had the first attempts to understand the physics within a common envelope environment. It was only after the 80's that the first statistical studies showed that low-mass contact binaries share common orbital and physical characteristics. It was also found that the members in such systems are surrounded by a common convective envelope that lies between the inner and outer critical Roche surfaces.

In most of cases, low-mass contact binaries are low-temperature Main Sequence (MS) stars of F, G, and K spectral type. They have solar-type characteristics and they belong to the old population group of our Galaxy, confirming that they are old stars that did not evolve towards the Red Giant Branch (RGB), remaining at the MS together with the rest of the young dwarf (single) stars. According to (Bilir et al., 2005) contact binaries have a kinematic age of 5–12 Gyr. Observations also show that there are several low-mass contact binaries with their total mass close to 1–1.4 M_{\odot} (Gazeas & Niarchos, 2006; Gazeas & Stepień, 2008). Magnetic activity (expressed by cool photospheric spots or even hot chromospheric flares) is something expected in cool stars with convection zone. Low-mass contact binaries are among the binary systems with the highest level of chromospheric activity. Therefore, they lose angular momentum and mass by the magnetized wind, as is observed in single, highly active stars. Cool spots can explain the observed asymmetries in light curves sufficiently. In addition, the heavily covered surface of the components by cool spots is the most likely explanation of the so-called 'W-phenomenon' (Stepien, 1980; Eaton et al., 1980; Zola et al., 2010).

Their contact configuration puts several constraints on their physical properties due to the Roche geometry. In addition, there is a link between the orbital and the physical properties, i.e. the mass, radius, temperature, and luminosity. This is how the first empirical relations started to appear in literature, correlating the physical parameters with quantities that are directly derived from observations, such as the orbital period or the mass ratio, as shown in Fig. 1.

3. Why contact binaries are so interesting?

A low-mass contact binary is formed when a short orbital period system undergoes stable mass transfer between its components. Angular momentum is lost due to stellar wind and magnetic braking phenomena, while both stars overflow their Roche lobes. This process eventually leads towards a contact configuration. The components of low-mass and low-temperature contact binaries follow

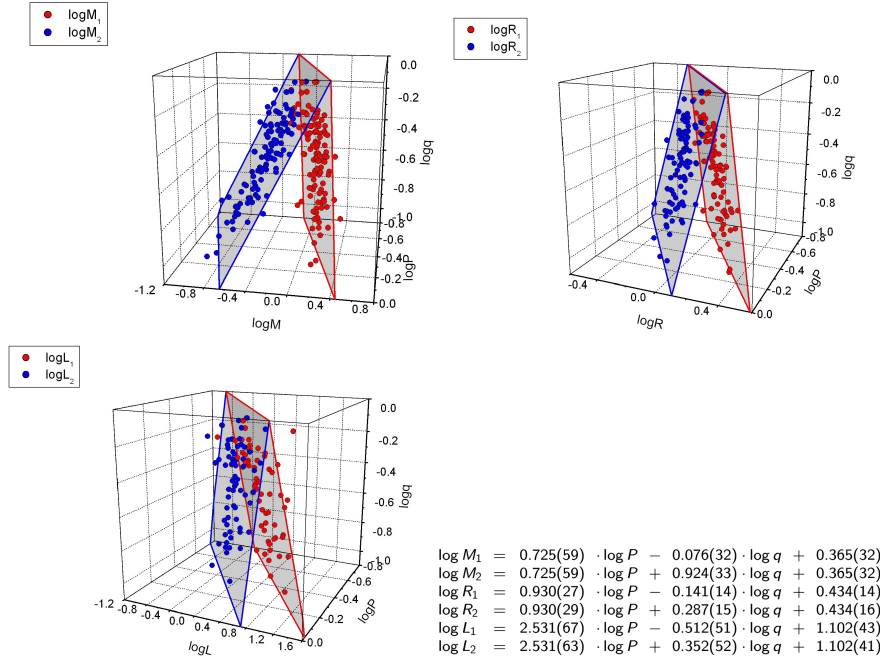


Figure 1. The above 3D diagrams show that there is a direct correlation of the absolute physical parameters (M, R, L) with the directly observed parameters (orbital period P and mass ratio q) of low mass contact binary systems. The extracted empirical relations express the equations of the shaded flat surfaces (Gazeas, 2009).

certain empirical relationships, which closely correlate physical parameters with each other, due to the Roche geometry. As a result, contact binaries are excellent astrophysical tools for the determination of the fundamental physical parameters (mass, radius, luminosity) of low-temperature stellar components, that can be used to trace their evolutionary paths. They are of great interest to the study of stellar populations since they provide an excellent opportunity to investigate stellar merging scenarios. They can be very successfully used as distance indicators, a fact that was proposed and tested in several studies in the past (Rucinski, 1997; Rubenstein & Bailyn, 1996; Edmonds et al., 1996; Yan & Mateo, 1994). They provide an excellent opportunity to investigate evolution paths such as stellar merging, while their parameters can be measured or derived in a highly accurate way. This leads to the close monitoring of the orbital (and physical) parameter modulations, which can provide evidence of evolution toward merging.

Following careful methodology in data treatment, negligible modulation of parameters can be traced and therefore their temporal variation can be mon-

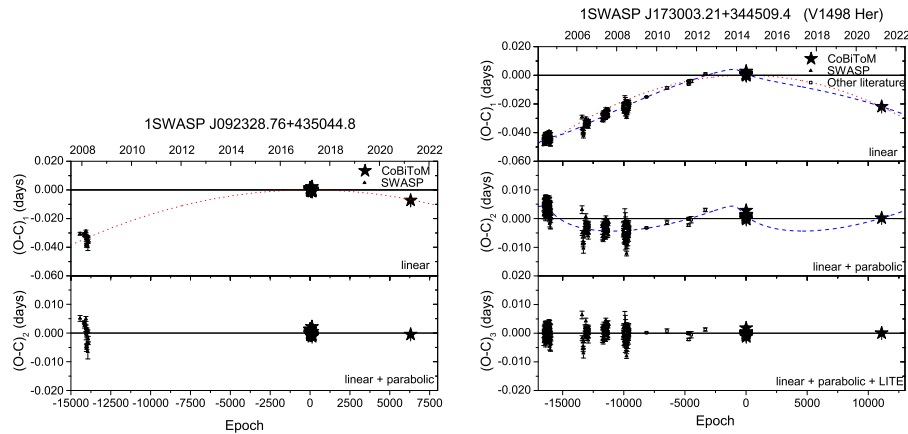


Figure 2. The diagrams present the observed (O) minus the calculated (C) value of orbital period in two low mass contact binaries with ultra-short orbital period (Loukaidou et al., 2022). Both systems show an orbital period decrease (expressed as a negative parabolic trend), while the second one additionally shows the existence of a tertiary component orbiting the close binary.

itored. For example, Fig. 2 shows the O-C diagrams of two selected contact binaries with ultra-short orbital period (Loukaidou et al., 2022). Both systems exhibit a negative parabolic trend on their orbital period modulation, which is translated as an orbital shrinkage. On top of that, 1SWASP J173003.21+344509.4 shows an additional periodic modulation, as a consequence of a tertiary component orbiting the contact binary. The diagrams are so sensitive, that even tiny fluctuations of the orbital parameters can be detected. The overall trend, as derived from the diagrams, can quantify the orbital shrinkage, and therefore the merging timescale. Angular momentum and mass loss of the system via stellar wind may be the dominating mechanism, that explains the observed orbital period modulation. In addition, mass transfer between the components may alter the orbital period, and it can reverse the mass ratio between the two components (Stepień & Gazeas, 2008).

4. Physical and orbital properties of contact binaries

An alternative model of stellar evolution in a binary environment was proposed by Stepień & Gazeas (2012). The model is based on the idea that a detached binary system with an orbital period of ~ 1.5 -2 days loses angular momentum through stellar wind. Such a process can be dramatically accelerated through Kozai-Lindov cycles (Kozai, 1962), by the existence of a tertiary component that

pumps angular momentum out of the close binary. The angular momentum loss shrinks the orbit and the two components come in contact, sharing a common photosphere, and therefore sharing thermal energy. However, such a process requires an exceptional amount of time, of about 10-12 Gyr. To have a good agreement of the model with the observed parameters in low mass contact binary systems as we observe them today, the angular momentum loss rate, as well as the mass loss rate, should be constrained within narrow limits (Fig. 3).

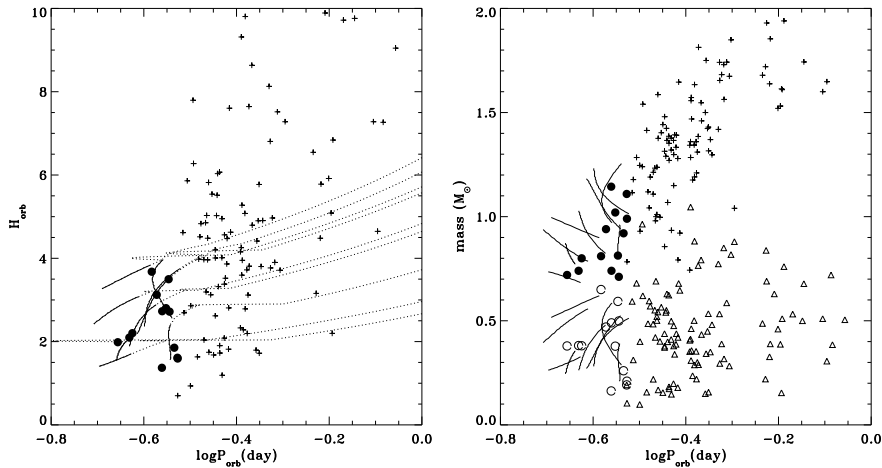


Figure 3. Left panel: The distribution of angular momentum of 112 contact binaries in cgs units ($\times 10^{51}$). Evolutionary tracks of models given by [Stępień & Gazeas \(2012\)](#) are also shown. Parts of the tracks plotted with dotted lines correspond to pre-contact phases and those plotted with solid lines describe binary evolution while in contact configuration. Right panel: The components of low-mass contact binaries (open and filled circles) and of other contact binary systems ('plus' signs and triangles). These values are compared with parameters derived after direct observations of contact binaries ([Gazeas & Stępień, 2008](#)).

5. Observations of low mass contact binaries

Information about the properties of contact binaries comes almost explicitly from photometric and spectroscopic observations. Dedicated observing campaigns collect high-resolution data, to provide analytical solutions to match theoretical models with the observations.

Space telescopes provide ultra-high precision photometric data for a long uninterrupted period of time, which is essential for the orbital period determi-

nation and its modulation. However, in most cases, space-borne spectroscopic data are still limited to low-resolution data, which are adequate for temperature determination, but not for radial velocity measurements.

On the other hand, ground-based sky surveys can also contribute to the long-term monitoring of the contact binaries with several photometric data and (again) limited spectroscopic observations. Large telescope facilities are needed for high-resolution spectra, which is not always easy, since long-term photometric observations are almost impossible, due to the limited observing time and availability in large aperture telescopes.

Small telescope networks can contribute significantly to this field. Some examples are AAVSO (Watson et al., 2006), ASAS (Pojmanski, 2002), ASAS-SN (Jayasinghe et al., 2019), CoRoT (Deleuil et al., 2018), CSS (Drake et al., 2014), GCVS (Samus et al., 2018), Kepler (Kirk et al., 2016), LAMOST (Qian et al., 2020), OGLE (Szymański et al., 2001), SWASP (Norton et al., 2011), WISE (Petrosky et al., 2021), and ZTF (Chen et al., 2020). Survey observations can provide a uniform data set for the long-term monitoring of such systems and their study can trace the orbital and physical parameter modulations for decades.

6. CoBiToM Project

The Contact Binaries Towards Merging (*CoBiToM* Project, Gazeas et al. (2021)) was initiated in 2012 under the idea of the long-term monitoring of low mass contact binaries and the modulations of their physical parameters. The ultimate goal is to investigate stellar coalescence and merging processes towards red nova events, as the final state of stellar evolution of low-mass contact binary systems. The program aspires to give insights into their physical and orbital parameters and their temporal variations, e.g. the orbital period modulation, spot activity, etc. The innovation of *CoBiToM* Project is based on a multi-method approach and a detailed investigation, that will shed light on the origin of stellar mergers and rapidly rotating stars for the first time. *CoBiToM* Project is closely connected with the *WUMa* program (Kreiner et al., 2003), which was initiated in 2002 and resulted in a list of 160 contact binary systems with high-resolution spectroscopy and mass ratio determination.

Fig. 4 shows the mass distribution over the orbital period of 118 well-studied contact binaries with combined photometric and spectroscopic techniques. The current investigation, in the frame of *CoBiToM* Project, focuses on the study of ultra-short orbital period systems (extreme left part of the plot), and investigates the systems with an extremely small secondary component, and therefore ultra-low mass ratio (systems with the smallest mass at the lower part of the plot). The preliminary results show that the ultra-short orbital period contact binaries are very stable systems, while over 60% of them are hosted within triple or multiple systems. In addition, half of them present orbital period modulation.

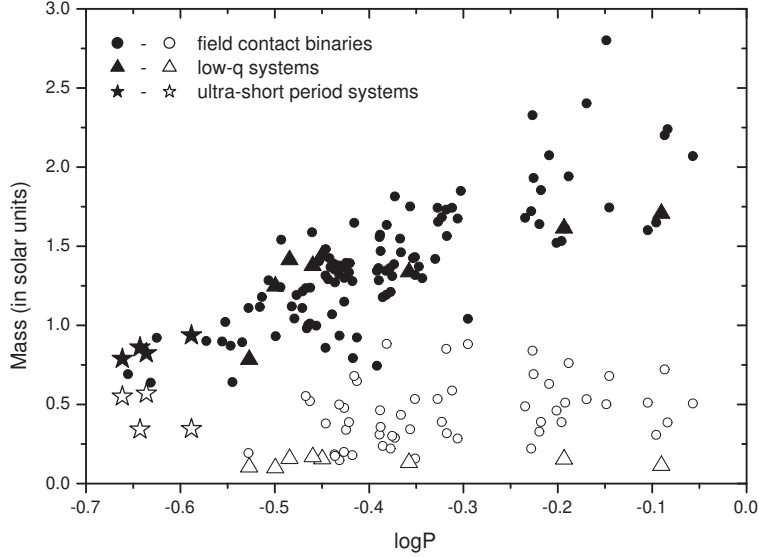


Figure 4. The mass distribution for the two components of all 118 contact binaries in our sample. The mass of the primary components is plotted with full circles, while the mass of the secondary ones is plotted with open circles. Triangles represent the low- q systems with secondary components of very small mass. Note that the mass of the secondaries lies within the range of $0\text{--}1 M_{\odot}$, while the mass of the primaries gradually increases proportionally to $\log P$ (Gazeas & Niarchos, 2006).

7. Observing challenges and future goals

The current and future trend of the research on low mass contact binaries is to further study the ultra-short orbital period systems and the prominent cut-off limit, detect systems with significant orbital period modulation via the O-C diagrams, investigate the ultra-low mass ratio systems, and search for possible unstable orbits among them. Furthermore, the study of contact binaries as common envelope systems investigates the possibility of discovering exoplanets hidden within the circumbinary material and the stellar ejecta from the stellar wind and the mass loss processes. Dedicated observing programs seek for red nova progenitors and future merger candidates and aspire to connect the merger results with fast rotating stars, such as the population of Blue Stragglers.

8. Summary

The evolution of low-mass contact binaries is mostly driven by mass transfer and angular momentum loss via the magnetized wind, which shrinks the orbit and makes both components overflow their outer Roche lobes. It is known that all low-mass contact binaries are old, with a typical age of 7–8 Gyr, although their contact phase lasts less than 1 Gyr, leading into coalescence (Stępień & Gazeas, 2012). There is an obvious need for dedicated sky surveys focusing on high-resolution spectroscopy on such systems. Ground-based surveys and telescope networking, play an important role in time-domain Astrophysics and this is a key aspect for future research in this field. Long-term observing campaigns and active Pro-Am collaborations in data acquisition are essential for monitoring temporal modulations of physical and orbital parameters.

References

- Bilir, S., Karataş, Y., Demircan, O., & Eker, Z., Kinematics of W Ursae Majoris type binaries and evidence of the two types of formation. 2005, *Monthly Notices of the RAS*, **357**, 497, DOI: 10.1111/j.1365-2966.2005.08609.x
- Chen, X., Wang, S., Deng, L., et al., The Zwicky Transient Facility Catalog of Periodic Variable Stars. 2020, *Astrophysical Journal, Supplement*, **249**, 18, DOI: 10.3847/1538-4365/ab9cae
- D’Angelo, C., van Kerkwijk, M. H., & Rucinski, S. M., Contact Binaries with Additional Components. II. A Spectroscopic Search for Faint Tertiaries. 2006, *Astronomical Journal*, **132**, 650, DOI: 10.1086/505265
- Deleuil, M., Aigrain, S., Moutou, C., et al., Planets, candidates, and binaries from the CoRoT/Exoplanet programme. The CoRoT transit catalogue. 2018, *Astronomy and Astrophysics*, **619**, A97, DOI: 10.1051/0004-6361/201731068
- Drake, A. J., Djorgovski, S. G., García-Álvarez, D., et al., Ultra-short Period Binaries from the Catalina Surveys. 2014, *Astrophysical Journal*, **790**, 157, DOI: 10.1088/0004-637X/790/2/157
- Eaton, J. A., Wu, C. C., & Rucinski, S. M., Ultraviolet colors of W UMa : gravity darkening, temperature differences and the cause of W-type light curves. 1980, *Astrophysical Journal*, **239**, 919, DOI: 10.1086/158179
- Edmonds, P. D., Gilliland, R. L., Guhathakurta, P., et al., Stellar Variability in the Central Populations of 47 Tucanae from WF/PC Observations with the Hubble Space Telescope. II. Binary Systems. 1996, *Astrophysical Journal*, **468**, 241, DOI: 10.1086/177687
- Gazeas, K. & Stępień, K., Angular momentum and mass evolution of contact binaries. 2008, *Monthly Notices of the RAS*, **390**, 1577, DOI: 10.1111/j.1365-2966.2008.13844.x

- Gazeas, K. D., Physical parameters of contact binaries through 2-D and 3-D correlation diagrams. 2009, *Communications in Asteroseismology*, **159**, 129
- Gazeas, K. D., Loukaidou, G. A., Niarchos, P. G., et al., CoBiToM project - I. Contact binaries towards merging. 2021, *Monthly Notices of the RAS*, **502**, 2879, DOI: 10.1093/mnras/stab234
- Gazeas, K. D. & Niarchos, P. G., Erratum: Masses and angular momenta of contact binary stars. 2006, *Monthly Notices of the RAS*, **372**, L83, DOI: 10.1111/j.1745-3933.2006.00229.x
- Hut, P., Stability of tidal equilibrium. 1980, *Astronomy and Astrophysics*, **92**, 167
- Jayasinghe, T., Stanek, K. Z., Kochanek, C. S., et al., The ASAS-SN catalogue of variable stars - II. Uniform classification of 412 000 known variables. 2019, *Monthly Notices of the RAS*, **486**, 1907, DOI: 10.1093/mnras/stz844
- Kirk, B., Conroy, K., Prša, A., et al., Kepler Eclipsing Binary Stars. VII. The Catalog of Eclipsing Binaries Found in the Entire Kepler Data Set. 2016, *Astronomical Journal*, **151**, 68, DOI: 10.3847/0004-6256/151/3/68
- Kozai, Y., Secular perturbations of asteroids with high inclination and eccentricity. 1962, *Astronomical Journal*, **67**, 591, DOI: 10.1086/108790
- Kreiner, J. M., Rucinski, S. M., Zola, S., et al., Physical parameters of components in close binary systems. I. 2003, *Astronomy and Astrophysics*, **412**, 465, DOI: 10.1051/0004-6361:20031456
- Li, K., Gao, X., Liu, X.-Y., et al., Extremely Low Mass Ratio Contact Binaries. I. The First Photometric and Spectroscopic Investigations of Ten Systems. 2022, *Astronomical Journal*, **164**, 202, DOI: 10.3847/1538-3881/ac8ff2
- Liu, X.-Y., Li, K., Michel, R., et al., The study of 11 contact binaries with mass ratios less than 0.1. 2023, *Monthly Notices of the RAS*, **519**, 5760, DOI: 10.1093/mnras/stad026
- Loukaidou, G. A., Gazeas, K. D., Palafouta, S., et al., CoBiToM Project - II. Evolution of contact binary systems close to the orbital period cut-off. 2022, *Monthly Notices of the RAS*, **514**, 5528, DOI: 10.1093/mnras/stab3424
- Norton, A. J., Payne, S. G., Evans, T., et al., Short period eclipsing binary candidates identified using SuperWASP. 2011, *Astronomy and Astrophysics*, **528**, A90, DOI: 10.1051/0004-6361/201116448
- Petrosky, E., Hwang, H.-C., Zakamska, N. L., Chandra, V., & Hill, M. J., Variability, periodicity, and contact binaries in WISE. 2021, *Monthly Notices of the RAS*, **503**, 3975, DOI: 10.1093/mnras/stab592
- Pojmanski, G., The All Sky Automated Survey. Catalog of Variable Stars. I. 0 h - 6 h Quarter of the Southern Hemisphere. 2002, *Acta Astronomica*, **52**, 397, DOI: 10.48550/arXiv.astro-ph/0210283

- Qian, S., Zhu, L., Liu, L., et al., Contact binaries at different evolutionary stages. 2020, *Research in Astronomy and Astrophysics*, **20**, 163, DOI: 10.1088/1674-4527/20/10/163
- Rubenstein, E. P. & Bailyn, C. D., A W UMa Contact Binary in the Globular Cluster NGC 6397. 1996, *Astronomical Journal*, **111**, 260, DOI: 10.1086/117778
- Rucinski, S. M., Eclipsing Binaries in the OGLE Variable Star Catalog.II.Light Curves of the W UMa-Type Systems in Baade's Window. 1997, *Astronomical Journal*, **113**, 1112, DOI: 10.1086/118329
- Rucinski, S. M., W UMa-Type Binary Stars in Globular Clusters. 2000, *Astronomical Journal*, **120**, 319, DOI: 10.1086/301417
- Samus, N. N., Durlevich, O. V., Kazarovets, E. V., Kireeva, N. N., & Pastukhova, E. N., Version 5.1 of the General Catalogue of Variable Stars for the Constellation Cepheus. 2018, *Astronomy Reports*, **62**, 1050, DOI: 10.1134/S1063772918140019
- Stepień, K., The Low-Mass Limit for Total Mass of W UMa-type Binaries. 2006, *Acta Astronomica*, **56**, 347
- Stepień, K. & Gazeas, K., Evolutionary scenario for W UMa-type stars. 2008, in IAU Symposium, Vol. **252**, *The Art of Modeling Stars in the 21st Century*, ed. L. Deng & K. L. Chan, 427–428
- Stepień, K. & Gazeas, K., Evolution of Low Mass Contact Binaries. 2012, *Acta Astronomica*, **62**, 153
- Stepien, K., SW Lac and the SPOT activity on W UMa stars. 1980, *Acta Astronomica*, **30**, 315
- Szymański, M., Udalski, A., Kubiak, M., et al., OGLE Survey - Microlensing in the Milky Way. 2001, in Astronomical Society of the Pacific Conference Series, Vol. **228**, *Dynamics of Star Clusters and the Milky Way*, ed. S. Deiters, B. Fuchs, A. Just, R. Spurzem, & R. Wielen, 277
- Tylenda, R., Hajduk, M., Kamiński, T., et al., V1309 Scorpii: merger of a contact binary. 2011, *Astronomy and Astrophysics*, **528**, A114, DOI: 10.1051/0004-6361/201016221
- Udalski, A., The Optical Gravitational Lensing Experiment. Real Time Data Analysis Systems in the OGLE-III Survey. 2003, *Acta Astronomica*, **53**, 291
- Wadhwa, S. S., Arbutina, B., Petrović, J., et al., A Study of Six Extreme Low Mass Ratio Contact Binary Systems. 2023a, *Publications of the ASP*, **135**, 094201, DOI: 10.1088/1538-3873/acf40d
- Wadhwa, S. S., Arbutina, B., Tothill, N. F. H., et al., A Study of Twelve Potential Merger Candidate Contact Binary Systems. 2023b, *Publications of the ASP*, **135**, 074202, DOI: 10.1088/1538-3873/ace3f5

- Watson, C. L., Henden, A. A., & Price, A., The International Variable Star Index (VSX). 2006, *Society for Astronomical Sciences Annual Symposium*, **25**, 47
- Webbink, R. F., The evolution of low-mass close binary systems. I. The evolutionary fate of contact binaries. 1976, *Astrophysical Journal*, **209**, 829, DOI: 10.1086/154781
- Yan, L. & Mateo, M., Primordial Main sequence Binary Stars in the Globular Cluster M71. 1994, *Astronomical Journal*, **108**, 1810, DOI: 10.1086/117194
- Zola, S., Gazeas, K., Kreiner, J. M., et al., Physical parameters of components in close binary systems - VII. 2010, *Monthly Notices of the RAS*, **408**, 464, DOI: 10.1111/j.1365-2966.2010.17129.x

Photometric sample of early B-type pulsators in eclipsing binaries observed with *TESS*

C.I. Eze^{1,2}  and G. Handler¹ 

¹ *Nicolaus Copernicus Astronomical Center of the Polish Academy of Sciences, Warsaw, Poland (E-mail: cheze@camk.edu.pl)*

² *Department of Physics and Astronomy, University of Nigeria, Nsukka, Nigeria*

Received: November 1, 2023; Accepted: November 28, 2023

Abstract. Asteroseismology coupled with eclipsing binary modelling shows great potential in improving the efficiency of measurements or calibrations of the interior mixing profile in massive stars. This helps, for instance in treating the challenging and mysterious discrepancies between observations and models of its stellar structure and evolution. This paper discusses the findings in our work titled *β Cephei pulsators in eclipsing binaries observed with *TESS**, which aimed to compile a comprehensive catalogue of β Cep pulsators in eclipsing binaries. Seventy-eight (78) pulsators of the β Cep type in eclipsing binaries among which 59 new discoveries were reported. Here, we also report a fresh analysis of eight additional stars that were outside the scope of the earlier-mentioned work. Six β Cep pulsators in eclipsing binaries are reported, among which 5 are new discoveries and 1 is a confirmation of a candidate earlier suggested in the literature. Our sample allows for future ensemble asteroseismic modelling of massive pulsators in eclipsing binaries to treat the discrepancy between observations and models.

Key words: asteroseismology - binaries: general - stars: evolution - massive stars: oscillations (including pulsations) - stars: rotation

1. Introduction

Asteroseismology is the study of the interior structure of stars via their pulsations (e.g., Gough, 1985). Massive stars also show pulsations and offer unique opportunities to constrain their properties via asteroseismology (Aerts et al., 2010). Three classes of massive pulsators exist, among which are β Cephei stars. Beta Cephei stars are main sequence stars with masses of approximately 9 – 17 M_{\odot} (e.g., Stankov & Handler, 2005). They have low radial order pressure (p), gravity (g), and mixed modes, pulsation amplitudes up to a few tenths of magnitudes, and pulsation periods of several hours (approximately 2 to 6 hours) (e.g., Stankov & Handler, 2005). Studying massive pulsators in eclipsing binaries proves to be very beneficial as it combines the strengths of asteroseismology

and eclipsing binary modelling to probe the stars. Unfortunately, the number of such reported systems is much smaller compared to that of their low-mass counterparts (Kirk et al., 2016; Pedersen et al., 2019). This, however, impedes a more holistic asteroseismic study of massive stars.

The present paper discusses the findings in the work titled *β Cephei pulsators in eclipsing binaries observed with *TESS** by Eze & Handler (ApJS, submitted), which aimed to compile a comprehensive catalogue of early B-type (B0 – B3) pulsators in eclipsing binaries observed by *TESS* with a particular focus on β Cep pulsators, to probe the evolution and properties of massive stars by harnessing the combined potentials of eclipsing binary stars and asteroseismology. In this paper, we also conduct a fresh analysis of eight additional stars which were outside the scope of our earlier-mentioned work. Here, we briefly describe the analysis in Sect. 2, discuss the results in Sect. 3 and conclude in Sect. 4.

2. Analysis

A total of 8055 stars of spectral types B0 – B3 were analyzed in our referenced paper (see the paper for the details of the analysis and results). Here, as already pointed out, we also analyzed eight additional stars of spectral types O8 – B0 and B3 – B5. The analysis was done using the methods described in detail in the referenced work. The result is shown in Table 1.

We examined the *TESS* light curves (Ricker et al., 2015) of the targets for independent pulsations via successive prewhitening of their Fourier spectra using the *Period04* software (Lenz & Breger, 2005) and accounted for blends in their *TESS* pixels using Eleanor (Feinstein et al., 2019) and *TESS*-Localize (Higgins & Bell, 2022). In each case, we removed the effect of binarity by subtracting the harmonic binary model from the light curves before the pulsation analysis. The orbital periods of the stars with their analytical uncertainties are also determined using the *Period04* program (Lenz & Breger, 2005). The binned phase diagrams and Fourier spectra of the stars' *TESS* light curves are shown in Figures 1 and 2 respectively.

3. Results and discussion

Eze & Handler (ApJS, submitted) reported 78 pulsators of the β Cephei type in eclipsing binaries, 59 of which are new discoveries. Ten ellipsoidal variables with β Cep pulsating components are also reported in the paper. Here, we report three definite and three candidate β Cep pulsators in eclipsing binaries as shown in Table 1. The stars adjudged candidates have nearby contaminators and signals that are too weak to be localized. They are denoted with '?' in their variability in Table 1. The binarity and β Cep variability are reported for the first time here for the stars TIC 2323229 (HD 330666; Sp. type: B8), TIC 155286121 (HD 319702; Sp. type: O8III), TIC 237173297 (HD 329034; Sp. type:

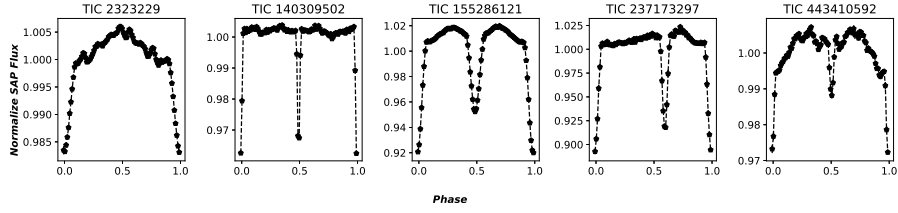


Figure 1. Binned Phase diagrams of light curves of the additional new definite and candidate β Cep pulsators in eclipsing binaries after prewhitening the strongest pulsations. TIC 336660284 is not included in Figure 1 as it has insufficient data (an incomplete orbital cycle) to be accurately phased but showed the first primary eclipse at 1606.35(30) BTJD. TIC 2323229, TIC 140309502, and TIC 443410592 are definite β Cep pulsators in eclipsing binaries whereas TIC 155286121, TIC 237173297, and TIC 336660284 are candidate β Cep pulsators in eclipsing binaries.

B3V) and TIC 336660284 (HD 125206; Sp. type: O9.7IVn). TIC 237173297 has an eccentric orbit and shows a likely reflection effect in its light curves. The binarity of TIC 443410592 (HD 115282; Sp. type: B2III) was first identified by [IJspeert et al. \(2021\)](#), but the β Cep pulsations are reported here for the first time. [Labadie-Bartz et al. \(2020\)](#) first reported the β variability of TIC 140309502 (CD-44 4484; Sp. type: B5) and also observed shallow eclipses in its light curves, for which they recommended further photometric confirmation. Using *TESS* photometry, this work confirms TIC 140309502 to be a definite β Cep pulsator in an eclipsing binary as both the eclipses and the β Cep pulsations are localized to the position of this target. However, contrary to the orbital period of 13.721(7) d reported by [Labadie-Bartz et al. \(2020\)](#), an orbital period of 4.649(5) or twice as much is obtained with the *TESS* photometry. Two stars TIC 72211082 and TIC 141903541 with no eclipses are rejected here. They, however, show β Cep pulsations with dominant pulsational frequencies 12.48585 c/d and 7.14297 c/d respectively. TIC 72211082 appears more like a rotational or ellipsoidal variable with pulsating component(s).

4. Conclusion

In this paper, we report the findings from our work which analyzed 8055 stars for β Cep pulsations in eclipsing binaries and that resulted in 78 pulsators of the β Cephei type in eclipsing binaries, among which 59 are new discoveries. Here, six β Cep pulsators in eclipsing binaries are also reported, five of which are new additional discoveries and one is a confirmation of a candidate earlier mentioned in the literature. The present paper adds a few stars to the sample of β Cep pulsators, reported to date, for a more general and homogeneous in-depth asteroseismic analysis of massive stars. We have already started follow-up

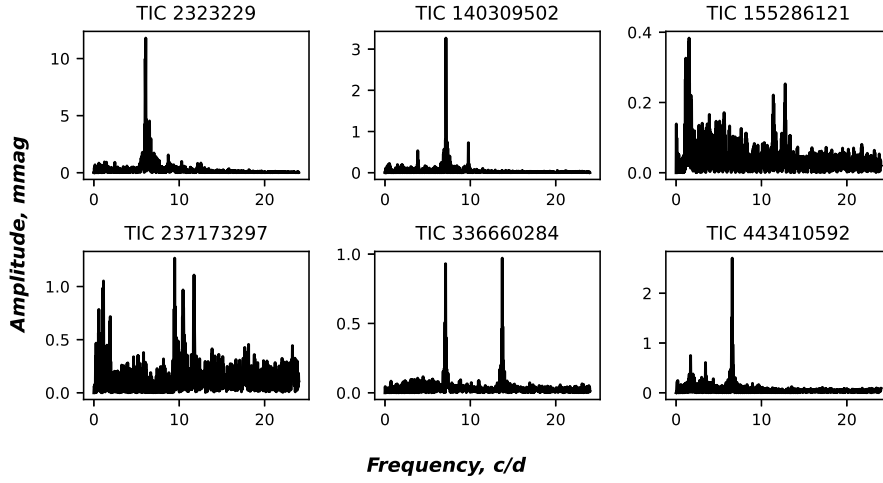


Figure 2. Fourier spectra of the additional new definite and candidate β Cep pulsators in eclipsing binaries after removing the orbital light variations. Whereas TIC 2323229, TIC 140309502, and TIC 443410592 are definite β Cep pulsators in eclipsing binaries, TIC 155286121, TIC 237173297, and TIC 336660284 are candidates.

Table 1. The lists of the additional new definite and candidate β Cep pulsators in eclipsing binaries not reported in the earlier work. F_d is the dominant β Cep pulsational frequency in c/d, A is the amplitude of the dominant pulsational frequency in mmag and S/N is the signal-to-noise ratio of the dominant frequency

| TIC ID | Variability | P (d) | F_d (c/d) | A (mmag) | S/N |
|---------------|--------------|-------------|-------------|----------|------|
| TIC 2323229 | EB+bCep | 1.0170(1) | 6.0782 | 13.55 | 81.5 |
| TIC 140309502 | EB+bCep | 9.298(5) | 7.1382 | 3.51 | 78.6 |
| TIC 155286121 | EB+bCep+SPB? | 2.01443(9) | 11.4033 | 0.34 | 8.6 |
| TIC 237173297 | EB+bCep+SPB? | 2.9907(2) | 11.7226 | 1.4 | 10.2 |
| TIC 336660284 | EB+bCep? | 13.35781(3) | 13.7379 | 0.98 | 48.6 |
| TIC 443410592 | EB+bCep | 4.2311(3) | 6.5731 | 2.99 | 59.1 |

of some of the most interesting candidates. The spectroscopic observations of some of the candidates have been conducted using four different instruments among which is Skalná Pleso Observatory (SPO). Four β Cep pulsators in eclipsing binaries listed in the referenced work were observed using the echelle spectrograph at SPO and are currently under analysis.

Acknowledgements. This work was supported by the Polish National Science Foundation (NCN) under grant nr. 2021/43/B/ST9/02972 and used the *TESS* data

obtained from the Mikulski Archive for Space Telescopes (MAST). This paper also made use of the SIMBAD database and the VizieR catalogue access tool operated at CDS, Strasbourg, France; and the SAO/NASA Astrophysics Data System. It also made use of data from the European Space Agency (ESA) mission *Gaia*¹, processed by the *Gaia* Data Processing and Analysis Consortium (DPAC²). Funding for the DPAC has been provided by national institutions, in particular, the institutions participating in the *Gaia* Multilateral Agreement.

References

- Aerts, C., Christensen-Dalsgaard, J., & Kurtz, D. W. 2010, *Asteroseismology*
- Feinstein, A. D., Montet, B. T., Foreman-Mackey, D., et al., eleanor: An Open-source Tool for Extracting Light Curves from the TESS Full-frame Images. 2019, *Publications of the ASP*, **131**, 094502, DOI: 10.1088/1538-3873/ab291c
- Gough, D., Inverting Helioseismic Data. 1985, *Solar Physics*, **100**, 65, DOI: 10.1007/BF00158422
- Higgins, M. E. & Bell, K. J., Localizing Sources of Variability in Crowded TESS Photometry. 2022, *arXiv e-prints*, arXiv:2204.06020, DOI: 10.48550/arXiv.2204.06020
- Ijspeert, L. W., Tkachenko, A., Johnston, C., et al., An all-sky sample of intermediate-to high-mass OBA-type eclipsing binaries observed by TESS. 2021, *Astronomy and Astrophysics*, **652**, A120, DOI: 10.1051/0004-6361/202141489
- Kirk, B., Conroy, K., Prša, A., et al., Kepler Eclipsing Binary Stars. VII. The Catalog of Eclipsing Binaries Found in the Entire Kepler Data Set. 2016, *Astronomical Journal*, **151**, 68, DOI: 10.3847/0004-6256/151/3/68
- Labadie-Bartz, J., Handler, G., Pepper, J., et al., New Beta Cephei Stars from the KELT Project. 2020, *Astronomical Journal*, **160**, 32, DOI: 10.3847/1538-3881/ab952c
- Lenz, P. & Breger, M., Period04 User Guide. 2005, *Communications in Asteroseismology*, **146**, 53, DOI: 10.1553/cia146s53
- Pedersen, M. G., Chowdhury, S., Johnston, C., et al., Diverse Variability of O and B Stars Revealed from 2-minute Cadence Light Curves in Sectors 1 and 2 of the TESS Mission: Selection of an Asteroseismic Sample. 2019, *Astrophysical Journal, Letters*, **872**, L9, DOI: 10.3847/2041-8213/ab01e1
- Ricker, G. R., Winn, J. N., Vanderspek, R., et al., Transiting Exoplanet Survey Satellite (TESS). 2015, *Journal of Astronomical Telescopes, Instruments, and Systems*, **1**, 014003, DOI: 10.1117/1.JATIS.1.1.014003
- Stankov, A. & Handler, G., Catalog of Galactic β Cephei Stars. 2005, *Astrophysical Journal, Supplement*, **158**, 193, DOI: 10.1086/429408

¹<https://www.cosmos.esa.int/gaia>

²<https://www.cosmos.esa.int/web/gaia/dpac/consortium>

Accreting-only symbiotic stars in the era of large Galactic Archeology spectroscopic surveys

M. Perko 

Faculty of Mathematics and Physics, University of Ljubljana, Jadranska ulica 19, 1000 Ljubljana, Slovenia (E-mail: manica.perko@fmf.uni-lj.si)

Received: October 18, 2023; Accepted: January 3, 2024

Abstract. Symbiotic stars are interacting binary systems consisting of a primary star, usually a red giant, and a companion star, usually a white dwarf. In general, there are two phases of symbiotic stars: a burning phase characterized by a rich emission line spectrum and an accreting-only phase in which the optical spectrum is dominated by the red giant, making them difficult to detect as a symbiotic star. The characterization and quantification of the entire population of symbiotic stars can provide crucial insights into the evolution and properties of our Galaxy. Our research is based on the GALAH spectroscopic survey, where we aim to identify symbiotic stars with the lowest accretion rates through spectral emission lines such as $H\alpha$ and $H\beta$. In the search for new accreting-only symbiotic star candidates, we focus on spectroscopic and photometric properties that distinguish these systems from single giants.

Key words: symbiotic stars – outbursts – photometry – spectroscopy

1. Symbiotic stars

Symbiotic stars are close binary systems consisting of a cool giant (either a red giant branch, RGB, or an asymptotic giant branch, AGB giant) and a degenerate companion, typically a white dwarf (see [Munari \(2019\)](#)). In symbiotic binary systems, the separation between two stars is relatively large, and the mass is transferred from red giant onto the surface of the white dwarf mostly in the form of a stellar wind emitted by the giant ([Mürset & Schmid, 1999](#)). The accretion leads to a buildup of material on the white dwarf, eventually resulting in the nuclear burning of the accreted shell. This process can happen either explosively, which can be observed as a nova eruption, or in thermal equilibrium, depending on the degree of degeneracy and mixing ([Shen & Bildsten, 2007](#)). Symbiotic stars have been known to have long orbital periods ranging from a few hundred days to more than a few hundred years ([Zamanov et al., 2021](#)).

In symbiotic systems, the white dwarf is accreting material onto its surface. When it accretes enough material, the nuclear burning of accreted material begins. If the accreted matter is electron degenerate, the burning process can be explosive. However, if the accreted matter is not electron degenerate, the

nuclear burning is slow and in thermal equilibrium. It can take a few years to reach maximum brightness and a few decades to burn the accreted envelope and return to the quiet phase. Therefore, symbiotic stars can be broadly divided into two distinct phases: an accreting-only and a burning-type star. There are several hundred known symbiotic systems (see recent catalogs by [Merc et al. \(2019a\)](#) and [Akras et al. \(2019a\)](#)), most of which are the burning-type stars, but we believe that this is due to an observational bias ([Munari et al., 2021a](#)). In the burning-type case, we observe a strong nebular continuum and a rich emission line spectrum, so systems in this phase can be easily detected at the optical part of the spectrum throughout the Galaxy and beyond, with about 400 systems known so far ([Zamanov et al., 2021](#); [Mukai et al., 2016](#)). In the case of accreting-only symbiotic systems, the optical part of the spectrum is dominated by the red giant. There are generally none or only very weak emission lines present in the spectrum, and only a few tens of systems were discovered until recently ([Merc et al., 2019b](#); [Munari et al., 2021a](#)).

In accreting-only symbiotic star systems, the accreted material from the red giant slowly accumulates on the surface of the white dwarf. This is a very slow process in comparison with the nuclear burning of the material. The latter can last several decades or even centuries, as also observed thus far ([Munari et al., 2021a](#)), while the accretion time is supposedly several orders of magnitude longer, which is why we assume that most of the symbiotic stars belong to the accreting-only type. This is in stark contrast to previously stated numbers of observed systems where the burning-type symbiotic stars dominate, and we aim to statistically evaluate this observational bias. This can further lead to determining the significance of symbiotic stars in the Galaxy, for which we need to characterize and quantify the entire population, not just the easily observed burning-type systems ([Munari et al., 2021a](#)).

Symbiotic stars are important for a better understanding of the evolution and properties of our Galaxy. They are considered one of the candidates responsible for the enrichment of the interstellar medium with lithium and other elements due to their nova outbursts. Furthermore, in the case of a white dwarf reaching critical mass, the subsequent accretion process may result in an explosion, making them promising Type Ia supernova progenitors, as initially proposed by [Munari & Renzini \(1992\)](#) (see also [Hachisu et al. \(1999\)](#)). For these reasons, obtaining better knowledge about the properties of accreting-only symbiotic stars and quantifying their total number in the Galaxy is essential.

This research aims to uncover the hidden population of symbiotic stars by examining their spectral and photometric characteristics and quantifying their total number in the Galaxy, ultimately shedding light on their significance in the evolution of our Galaxy.

In this contribution are presented two (and three additional) of the validation criteria for confirming the symbiotic star candidates by analysing their spectral and photometric properties using primarily spectroscopic data from the GALAH survey, complemented with follow-up spectroscopic and photomet-

ric observations from Asiago, and archival data from large photometric surveys, such as Gaia, 2MASS and ASAS-SN.

2. Properties of symbiotic stars

Symbiotic stars have unique properties that allow us to distinguish them from single red giants and can be broadly divided into two categories: the ones related to their stellar spectrum and the ones related to their photometric nature.

The optical spectrum of accreting-only symbiotic stars is dominated by a red giant, where we can observe distinct absorption features, including molecular absorption bands, and generally weak emission lines forming presumably in the accretion disk and showing both irregular and periodic variability (Chen et al., 2019).

In symbiotic systems, we can detect excess light, which serves as another indication of the presence of a white dwarf in these systems, and such excess light can be observed across different wavelengths:

- *Ultraviolet excess*

The UV excess is a direct manifestation of the presence of an accretion disk, with direct emission from the central white dwarf (Luna et al., 2013). A higher accretion rate causes a brightening of the accretion disk around the white dwarf, manifesting as an excess in near-UV luminosity and detectable emission lines.

- *X-ray excess*

The X-rays are emitted from regions of the accretion disk positioned closer to the white dwarf than the UV-dominated regions. The hardness of the X-ray spectrum also depends on the strength of the gravitational potential well, signifying that more massive white dwarfs yield harder X-ray spectra. In the case of white dwarfs with a mass exceeding $0.6M_{\odot}$, these systems may experience recurrent nova outbursts or produce strong X-ray emission. The X-ray production also depends on the accretion rate (Luna et al., 2013),

- *Infrared excess*

The IR radiation of symbiotic stars is caused by either stellar photosphere of the giant, free-free/free-bound emission from the ionized portion of the wind and from the outer portions of the accretion disk (Chen et al., 2019).

Two spectra of a symbiotic star SU Lyn taken with the Asiago telescope are shown in Figure 1, illustrating the differences between very low (black) and moderately high (red) accretion rates (Munari et al., 2021a). At low rates, the spectrum is dominated by a red giant and resembles a typical spectrum of a single giant. This presents a difficulty in the search for symbiotic stars with the lowest accretion rates. A higher rate causes a brightening of the accretion disk

around the white dwarf, which manifests as an excess near-UV brightness and detectable emission lines.

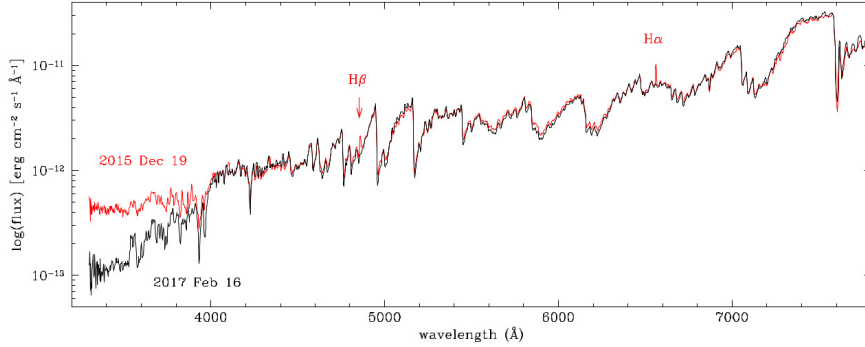


Figure 1. There are two spectra of an accreting-only symbiotic star SU Lyn presented: one at low (black) and one at high (red) accretion rates, the latter showing an excess in the near-UV regions and detectable emission lines (Munari et al., 2021a).

Among the most important photometric properties of symbiotic stars is the presence of flickering. Flickering is a rapid, non-periodic change in magnitude resulting from chaotic processes, such as density fluctuations within the accretion stream flowing from the primary to the accreting star. It develops on timescales of a few minutes, significantly shorter than the timescales associated with other sources of variability (Zamanov et al., 2022), typical for active accretion disks (Zamanov et al., 2021). Moreover, the photometric data provides information on the detection of excess light in the UV and X-ray regions.

Photometric data analysis also allows the opportunity to explore the presence of IR excess caused by either the stellar photosphere of the giant, free-free/bound-free emission emanating from the wind of the giant, or by the thermal dust emission surrounding the binary system (Chen et al., 2019; Akras et al., 2019c).

3. Observational data and sample selection

Our research includes the analysis of both spectroscopic and photometric datasets. In addition to the publicly available data from the spectroscopic and photometric surveys, we are conducting follow-up observations of a selected sample of symbiotic star candidates using the Copernico 1.82m telescope with a high-resolution Echelle spectrograph in Asiago. Simultaneously, we are executing photometric observations using the Schmidt 67/92cm telescope in Asiago.

3.1. Spectroscopic data

The selection of our large primary sample of red giant stars was based on spectroscopic observations from the GALactic Archaeology with HERMES (GALAH) survey (Buder et al., 2021) using the HERMES instrument with the Anglo-Australian 4m telescope. The focus of our research is giants of spectral type M, which appear to be the most common among the known symbiotic stars (Akraś et al., 2019b), selected and described in detail in the paper of Munari et al. (2021a). The identification of potential symbiotic star candidates within the sample was achieved by examining characteristic features that can be used to distinguish a symbiotic star from a single giant; more specifically, we were looking for emission in the $H\alpha$ and $H\beta$ spectral lines. For these selected candidates, the data set is complemented by high-resolution spectra obtained with the Copernico telescope and the Echelle spectrograph in Asiago. The repeated observations enable us to monitor any temporal changes in emission lines.

3.2. Photometric data

To isolate the cool giants from the other objects in our primary sample, we first apply selection criteria based on their color. The photometric data was used from the Gaia and the Two Micron All-Sky (2MASS) surveys. In addition, the light curves of the selected candidates were obtained from the All Sky Automated Survey for SuperNovae (ASAS-SN) and used to exclude false positives due to pulsating stars. Photometric follow-up observations of our symbiotic star candidates are carried out with the Schmidt telescope in Asiago.

4. Validation criteria for symbiotic star candidates

The search for symbiotic stars has only recently begun. The theoretical models predict that many more accreting-only symbiotic stars can be found. Now, through the confirmation of the accreting-only symbiotic stars, we continue the search for the hidden population. Among the selected candidates, we are focusing on the variability in $H\alpha$ and $H\beta$ emission lines and searching for the presence of flickering.

4.1. Emission line variability

Our research involves the search for characteristic signatures that indicate the presence of the accretion process within the binary star system. The main focus is on the study of emission lines present in the spectrum, such as $H\alpha$ and $H\beta$, both originating from the area of the accretion disk or from the wind of the giant in the vicinity of the disk and ionized by it. The presence of strong emission lines can serve as a potential indicator of a symbiotic nature. However, it is crucial to investigate other properties of symbiotic stars, as such emission lines may also be the result of other processes.

In the spectra of our symbiotic star candidates, we are searching for the variability in emission lines. An example of such variability in the $H\alpha$ emission line is shown in Figure 2. The figure shows eight low-resolution spectra of the symbiotic star 2SXPS taken with the 0.84m telescope in Varese, Italy, under the direction of the collaboration. Over a four-month period, an apparent change in the profile and intensity of the $H\alpha$ emission line can be seen, indicating the degree of accretion and the state of the accretion disk around a white dwarf (Munari et al., 2021b).

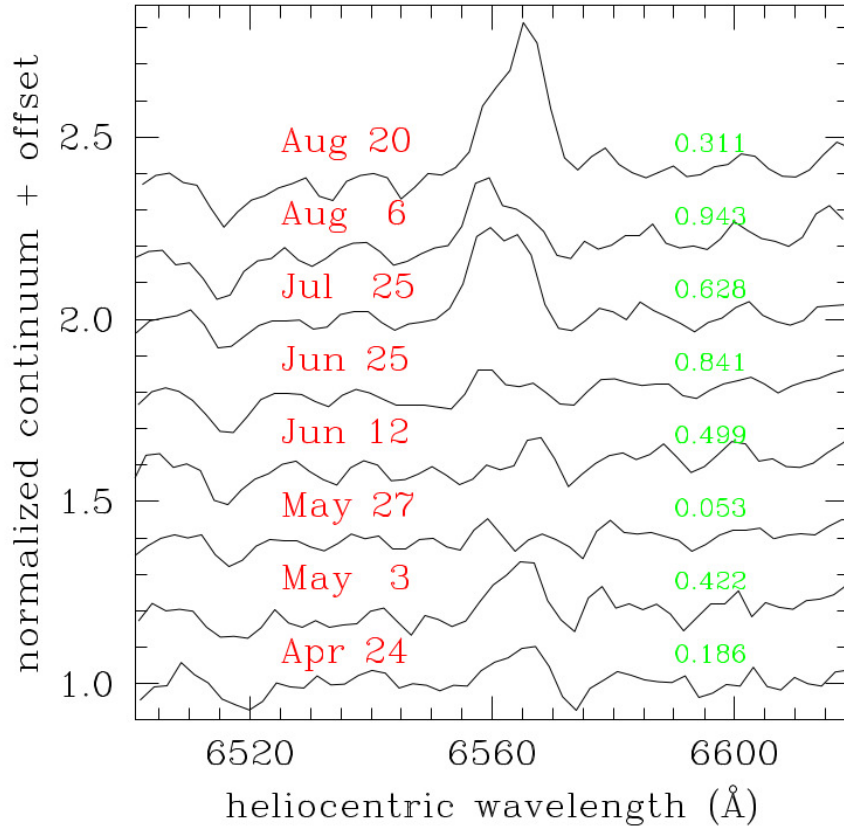


Figure 2. Low-resolution spectra of a symbiotic star 2SXPS were obtained on eight separate nights in 2020. They illustrate the temporal evolution of the $H\alpha$ emission line over a four-month interval, indicating the presence of the accretion disk. The observational dates (red) and equivalent width of $H\alpha$ line (green) are provided above each spectrum (Munari et al., 2021b).

4.2. Optical flickering

Symbiotic stars exhibit a significant photometric feature known as flickering. Detecting this rapid change in magnitude could confirm the presence and nature of a compact object.

The left panels of Figure 3 show two examples of the B-band time series for two distinct symbiotic star candidates in the search for evidence of flickering emanating from the accretion disk. The measurements of each symbiotic star are presented in blue dots, along with the nearby field stars of similar brightness and photometric color shown in different colors. Beneath the measurements for each object is provided the dispersion around the median of the B-band data. The accompanying plots in the right panels of Figure 3 show the relationship between dispersion and B-band magnitude, with the symbiotic star indicated by a red star and the nearby field stars represented as black circles. As evident in the visual representation, the top panels demonstrate that the symbiotic star candidate exhibits flickering well over the noise levels observed in the comparison stars, despite it being less apparent in the left panels. On the other hand, the symbiotic star candidate in the bottom panel remains stable, showing a noise level equivalent to that of the field stars.

4.3. Additional validation criteria

Establishing validation criteria describes a fundamental aspect of confirming the symbiotic nature within binary systems, and the criteria described above only serve as two of the indicators. Beyond the initial confirmation of $H\alpha$ variability and the presence of flickering, candidates must satisfy additional criteria, some of them being:

- *Long-term photometric variability*

The observation of long-term photometric variability can be helpful in separating the radial pulsators, such as Mira variables, from symbiotic stars. The lightcurves are usually reconstructed from multi-band photometric campaigns such as ASAS-SN. Radial pulsators can be identified by the characteristics of their lightcurves, which typically exhibit regular, long periods and sinusoid-like variations with large amplitudes, often exceeding ten magnitudes. Symbiotic stars also show significant variability in magnitude, but their lightcurves lack a large amplitude and regular period (Munari et al., 2021a).

- *Radial velocity variability*

Monitoring the radial velocity variability is another feature that provides insights into the nature of the variable object. Symbiotic stars exhibit irregular and complex velocity changes resulting from dynamic interactions within the binary system, such as accretion and mass transfer, which can often obscure clearly defined orbital periods, making it difficult to decipher the underlying

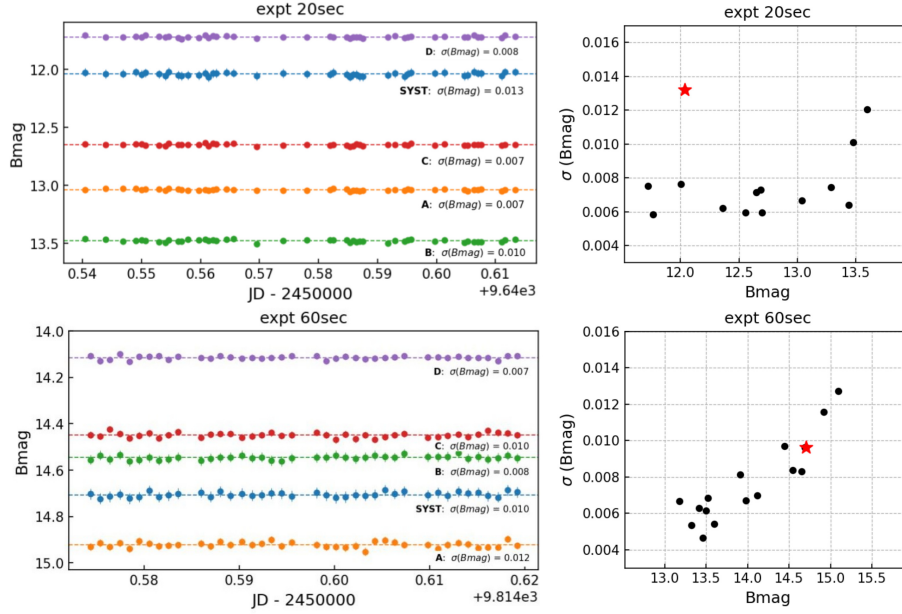


Figure 3. Examples of two symbiotic star candidates, one showing flickering (top panels) and one not showing flickering (bottom panels). Left panels display B-band time series data, aiming to detect flickering from the accretion disk. Periodic gaps represent V-band frame acquisitions for data transformation to the Landolt system. The measurements of the symbiotic star candidate (in blue) and field stars (in various colors) are accompanied by dispersion values around the median written beneath, denoted as "SYST" for the symbiotic star and "A, B, C, and D" for comparison stars. The right panels illustrate the relationship between the dispersion and B-band magnitude, contrasting the symbiotic star (marked by a red star) and the nearby field stars (represented as black circles). As evident from the right panels, the symbiotic star clearly shows the presence (upper panels) and the absence of flickering (bottom panels).

orbital dynamics. In contrast, when we examine the orbital motion in other long-period variables, e.g. Mira pulsators, they show regular and sinusoidal-like radial velocity variations driven by their intrinsic pulsation mechanisms, leading to well-defined orbital periods (Munari et al., 2021a).

– *Detectable emission excess in UV and X-ray part of the spectrum*

Yet another criterion for confirming symbiotic stars is the detection of excess light at wavelengths shorter than 4000 \AA . This excess emission, particularly in the UV and X-ray regions, indicates a higher accretion rate, which causes the brightening of an accretion disk around a white dwarf (Luna et al., 2014).

5. Conclusion

Symbiotic stars provide important insights into the evolution and properties of our Galaxy. The accretion of stellar wind from the red giant onto the surface of the white dwarf makes symbiotic stars a promising Type Ia supernova progenitor. They are also considered to be one of the candidates responsible for the enrichment of the interstellar medium with lithium and other elements because of their novae outbursts.

The spectroscopic analysis of symbiotic stars offers valuable insights into their physical properties, enabling the determination of mass accretion rates and providing an indication of the origin of the mechanism governing mass transfer, shedding light on their evolutionary state. On the other hand, photometric analysis can reveal the variability behavior of symbiotic stars, focusing on the search for flickering and looking for the presence of UV, X-ray, and IR excess.

Examining these characteristics will contribute to a better understanding of symbiotic stars, allowing us to identify and characterize accreting-only symbiotic stars within large-scale spectroscopic surveys such as GALAH, Gaia-ESO, and in the future 4MOST and WEAVE.

References

- Akras, S., Guzman-Ramirez, L., Leal-Ferreira, M. L., & Ramos-Larios, G., A Census of Symbiotic Stars in the 2MASS, WISE, and Gaia Surveys. 2019a, *Astrophysical Journal, Supplement*, **240**, 21, DOI: 10.3847/1538-4365/aaf88c
- Akras, S., Guzman-Ramirez, L., Leal-Ferreira, M. L., & Ramos-Larios, G., A Census of Symbiotic Stars in the 2MASS, WISE, and Gaia Surveys. 2019b, *Astrophysical Journal, Supplement*, **240**, 21, DOI: 10.3847/1538-4365/aaf88c
- Akras, S., Leal-Ferreira, M. L., Guzman-Ramirez, L., & Ramos-Larios, G., A machine learning approach for identification and classification of symbiotic stars using 2MASS and WISE. 2019c, *Monthly Notices of the RAS*, **483**, 5077, DOI: 10.1093/mnras/sty3359
- Buder, S., Sharma, S., Kos, J., et al., The GALAH+ survey: Third data release. 2021, *Monthly Notices of the RAS*, **506**, 150, DOI: 10.1093/mnras/stab1242
- Chen, P. S., Liu, J. Y., & Shan, H. G., Infrared photometric study of symbiotic stars. 2019, *Astrophysics and Space Science*, **364**, 132, DOI: 10.1007/s10509-019-3620-2
- Hachisu, I., Kato, M., & Nomoto, K., A Wide Symbiotic Channel to Type IA Supernovae. 1999, *Astrophysical Journal*, **522**, 487, DOI: 10.1086/307608

- Luna, G. J. M., Sokoloski, J. L., Mukai, K., & Nelson, T., Symbiotic stars in X-rays. 2013, *Astronomy and Astrophysics*, **559**, A6, DOI: 10.1051/0004-6361/201220792
- Luna, G. J. M., Sokoloski, J. L., Mukai, K., Nelson, T., & Nuñez, N. E., Symbiotic stars in X-rays and UV. 2014, in *Revista Mexicana de Astronomía y Astrofísica Conference Series*, Vol. **44**, *Revista Mexicana de Astronomía y Astrofísica Conference Series*, 158–159
- Merc, J., Gális, R., & Wolf, M., First Release of the New Online Database of Symbiotic Variables. 2019a, *Research Notes of the American Astronomical Society*, **3**, 28, DOI: 10.3847/2515-5172/ab0429
- Merc, J., Gális, R., & Wolf, M., New online database of symbiotic variables: Symbiotics in X-rays. 2019b, *Astronomische Nachrichten*, **340**, 598, DOI: 10.1002/asna.201913662
- Mukai, K., Luna, G. J. M., Cusumano, G., et al., SU Lynx, a hard X-ray bright M giant: clues point to a large hidden population of symbiotic stars. 2016, *Monthly Notices of the RAS*, **461**, L1, DOI: 10.1093/mnrasl/slw087
- Munari, U., The Symbiotic Stars. 2019, *arXiv e-prints*, arXiv:1909.01389, DOI: 10.48550/arXiv.1909.01389
- Munari, U. & Renzini, A., Are Symbiotic Stars the Precursors of Type IA Supernovae? 1992, *Astrophysical Journal, Letters*, **397**, L87, DOI: 10.1086/186551
- Munari, U., Traven, G., Masetti, N., et al., The GALAH survey and symbiotic stars - I. Discovery and follow-up of 33 candidate accreting-only systems. 2021a, *Monthly Notices of the RAS*, **505**, 6121, DOI: 10.1093/mnras/stab1620
- Munari, U., Valisa, P., Vagnozzi, A., et al., Photometry and spectroscopy of the new symbiotic star 2SXPS J173508.4-292958. 2021b, *Contributions of the Astronomical Observatory Skalnaté Pleso*, **51**, 103, DOI: 10.31577/caosp.2021.51.2.103
- Mürset, U. & Schmid, H. M., Spectral classification of the cool giants in symbiotic systems. 1999, *Astronomy and Astrophysics, Supplement*, **137**, 473, DOI: 10.1051/aas:1999105
- Shen, K. J. & Bildsten, L., Thermally Stable Nuclear Burning on Accreting White Dwarfs. 2007, *Astrophysical Journal*, **660**, 1444, DOI: 10.1086/513457
- Zamanov, R. K., Kostov, A., Moiseev, M., et al., The hidden symbiotic star SU Lyn – detection of flickering in U band. 2022, *arXiv e-prints*, arXiv:2206.10151, DOI: 10.48550/arXiv.2206.10151
- Zamanov, R. K., Stoyanov, K. A., Kostov, A., et al., The symbiotic binary ZZ CMi: Intranight variability and suggested outbursting nature. 2021, *Astronomische Nachrichten*, **342**, 952, DOI: 10.1002/asna.202113975

Exploring outbursts of accreting white dwarfs in symbiotic binaries – basic concept

A. Skopal 

*Astronomical Institute of the Slovak Academy of Sciences
059 60 Tatranská Lomnica, The Slovak Republic (E-mail: skopal@ta3.sk)*

Received: December 30, 2023; Accepted: January 26, 2024

Abstract. In this contribution I summarize the main characteristics and effects that are observed during outbursts of symbiotic stars: properties of the hot- and warm-type outbursts, enhanced mass outflow occasionally followed by ejection of bipolar jets, and the emergence of a neutral near-orbital-plane region. The results presented were largely obtained using small telescopes, supplemented by observations from the archives of terrestrial and space observatories.

Key words: Stars: binaries: symbiotic – Stars: jets – Stars: winds, outflows

1. Introduction

Symbiotic stars (SySts) are the widest interacting binaries with orbital periods typically of a few years. They consist of an evolved giant and, in vast majority, a white dwarf (WD) accreting from the giant’s wind (Boyarchuk, 1967; Kenyon, 1986; Mürset & Schmid, 1999; Belczyński et al., 2000). Only a few SySts have been detected to have a neutron star as an accretor (e.g., Chakrabarty & Roche, 1997; Masetti et al., 2007a,b; Yungelson et al., 2019).

The accretion process makes the WD very hot ($> 10^5$ K) and luminous ($\sim 10^1 - 10^4 L_{\odot}$) object, which ionizes a significant portion of the wind from the giant, giving rise to nebular emission (e.g. Seaquist et al., 1984). This configuration represents the so-called *quiescent phase*, during which SySt releases energy at an approximately constant rate. The most prominent feature of the optical light curves (LCs) of luminous SySts during quiescence is the wave-like orbital-related variation (see Figs. 1 and 2).

On the other hand, many SySts undergo unpredictable outbursts observed on a very different and variable timescale. The outbursts, resulting from the prolonged accretion by the WD until the ignition of a thermonuclear event on its surface, are analogous to classical novae in cataclysmic variables. They are called symbiotic novae or recurrent symbiotic novae, depending on the time scale of their recurrence. Due to the presence of the evolved giant in SySts, the brightness amplitude of symbiotic novae is as low as $\approx 4-9$ mag (e.g., Mürset & Nussbaumer, 1994; Bode & Evans, 2008). The typical and most frequently

observed outbursts of SySts are the so-called ‘Z And-type’ outbursts. They result from an increase in the accretion rate above the upper limit of the stable burning (see e.g. Fig. 2 of Shen & Bildsten, 2007), which can lead to expansion of the burning envelope simulating an A–F type pseudophotosphere (Tutukov & Yungelson, 1976; Paczynski & Rudak, 1980) and/or blowing optically thick wind from the WD (Kato & Hachisu, 1994; Hachisu et al., 1996). They are characterized by a few magnitude (multiple) brightening(s) in the optical observed on the timescale of a few months to years or even decades (see examples of historical LCs published by Brandi et al., 2005; Leibowitz & Formigini, 2008; Skopal et al., 2001) with signatures of a mass outflow (e.g., Fernandez-Castro et al., 1995; McKeever et al., 2011). Stages with Z And-type outbursts that interrupt quiescent phase are usually called *active phases* of a SySt (see Fig. 1). Analysing observations of Z And-type outbursts for non-eclipsing SySts AG Peg and V426 Sge, Skopal et al. (2017, 2020) confirmed the above-mentioned nature of this type of outbursts. The authors found that the optical brightening of these SySts is due to an increase of the nebular radiation from the very beginning of the outburst, while the contribution from the hot WD is negligible in the optical. The nebular continuum represents a fraction of the hot WD’s radiation (below 912 Å) converted by the enhanced wind from the WD at rates of a few times $10^{-6} M_{\odot} \text{ yr}^{-1}$ into the nebular emission. The corresponding emission measure and the temperature of the hot WD’s pseudophotosphere ($1.5 - 2 \times 10^5$ K) yield the WD luminosity of a few times $10^{37} \text{ erg s}^{-1}$ that is close to the Eddington limit. On the other hand, for eclipsing SySts the optical is usually dominated by a warm WD’s pseudophotosphere together with a strong nebular radiation (see Skopal, 2005, and Sect. 2.1 here).

The main goal of this contribution is to show the main common features of Z And-type outbursts. This work summarizes recent published results based on the optical multicolor photometry and, low- and medium-resolution spectroscopy obtained with small telescopes in part collected by amateur astronomers, supplemented by publicly available observations from archives.

2. Basic effects measured during outbursts

2.1. Warm and hot type outbursts¹

Using the method of multiwavelength modeling of combined spectra, Skopal (2005) found out that the spectrum of the hot component in eclipsing SySts during outbursts consists of two sources of radiation, differing significantly in their temperatures. He called it the two-temperature UV spectrum. This type of the spectrum consists of a relatively cool spectrum produced by a warm stellar pseudophotosphere radiating at $1 - 3 \times 10^4$ K, and the hot one represented

¹The sometimes used division of AG Dra outbursts into hot and cool (see González-Riestra et al., 1999) has nothing to do with the classification of SySts outbursts into warm and hot described in this section.

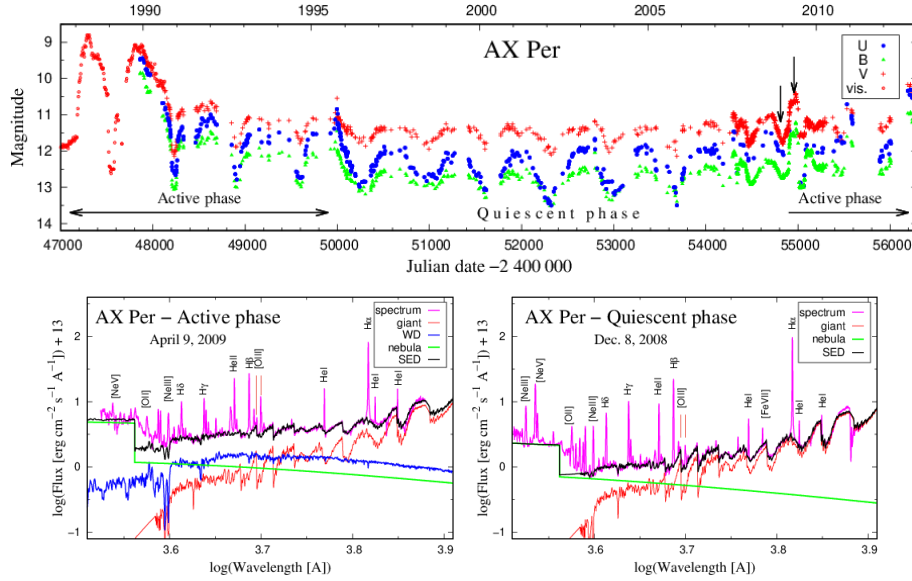


Figure 1. Example of the warm-type outburst observed for AX Per. The top panel shows evolution of multicolor LCs. The parts representing the active and quiescent phases are denoted. Bottom panels show the spectra (in magenta) and their SED models during active phase (left) and quiescence (right). Times of observations are marked by arrows in the top panel. Note the appearance of a strong warm WD’s pseudophotosphere (in blue) at simultaneous presence of a strong nebular spectrum (the continuum (in green) and emission lines) during outburst. Adapted according to Skopal et al. (2011).

by a strong nebular radiation. The warm stellar radiation is not capable of producing the measured nebular emission, which implies the presence of a strong ionizing source in the system. This discrepancy in the properties of the main components of radiation in the spectrum determines the disk-like structure of the hot component viewed under a high inclination angle. The outer optically thick flared rim of the disk (which is *the warm WD’s pseudophotosphere* with the effective radius of a few R_{\odot}), occults the central ionizing source in the line of sight, while the nebula above/below the disk is ionized by the central hot WD (see Fig. 27 of Skopal (2005) and Fig. 6 of Cariková & Skopal (2012)).

As a result, the disk-like structure of the hot component during outbursts is responsible for observing two different types of spectra depending on the orbital inclination (i). Outbursts in systems with a high i show the two-temperature type of the hot component spectrum. These outbursts are classified as the ‘warm-type’, because the stellar component of radiation is emitted by the warm WD’s pseudophotosphere, which usually dominates the optical (see Fig. 1). On the

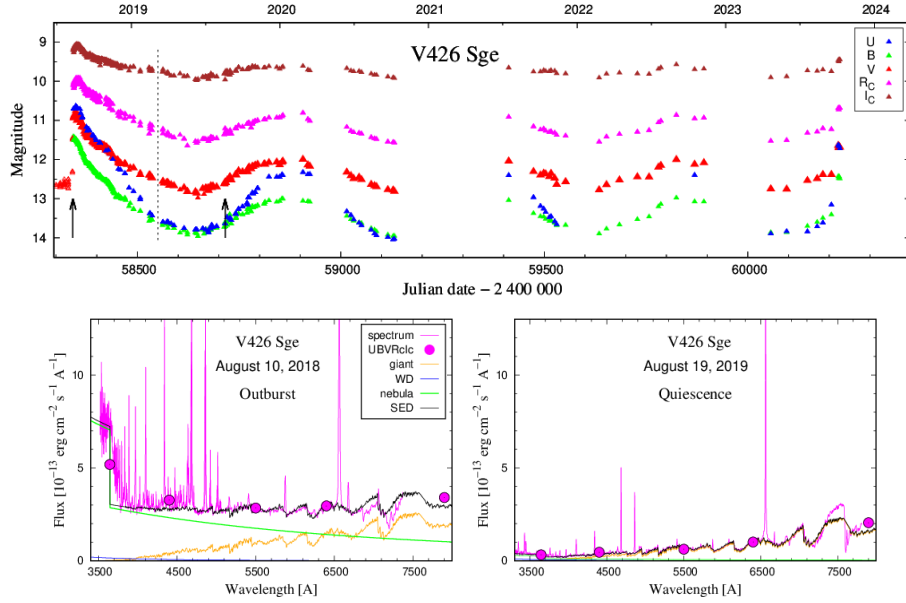


Figure 2. Example of the hot-type outburst observed for V426 Sge in 2018. The plots and their meaning as in Fig. 1. Note the appearance of a strong nebular radiation from the very beginning of the outburst, while the 2×10^5 K hot WD’s pseudophotosphere cannot be indicated in the optical. Adapted according to Skopal et al. (2020, 2023).

other hand, outbursts in systems with a low i are classified as ‘hot-type’, because the stellar component of radiation is emitted by *the hot WD’s pseudophotosphere* (i.e., the optically thick interface of the enhanced fast wind from the WD). Its temperature is $\approx 2 \times 10^5$ K and the effective radius $\approx 0.1 R_{\odot}$. As a result, the contribution of the hot WD’s pseudophotosphere is negligible in the optical, while the nebular continuum dominates the near-UV/optical from the very beginning of the outburst (see Fig. 2)².

2.2. Slow and high velocity mass-outflow during outbursts

A common feature of outbursts is a distinct increase of the mass-outflow from the burning WD, most often in the form of an enhanced stellar wind, indicated by the broadening of the emission line profiles, which in some cases are of the P Cygni type (e.g., Fernandez-Castro et al., 1995; Skopal, 2006; McKeever et al., 2011). Signs of mass outflow at moderate velocities (~ 100 – 500 km s $^{-1}$) are indicated by absorption components of P Cygni profiles in the spectrum of systems

²Originally, Skopal (2005) named these types of outbursts as 1st- and 2nd-type, later Skopal et al. (2020) renamed them to warm- and hot-type to express their physical nature.

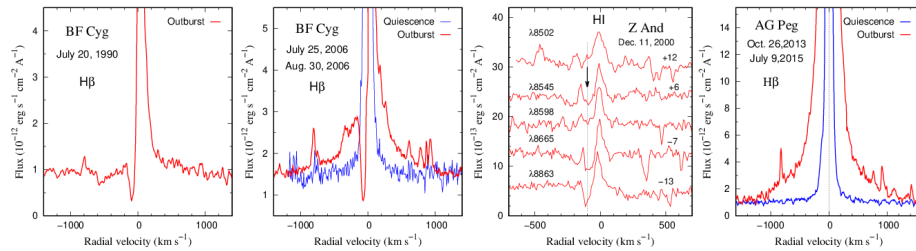


Figure 3. Example of the slow and high velocity mass-outflows indicated by P Cyg profiles and broad wings of emission lines for systems with high (BF Cyg and Z And) and low (AG Peg) i , respectively. Profiles from around the optical maxima and quiescence are in red and blue, respectively. From left to right: BF Cyg 1990 outburst (Skopal et al., 1997) and 2006 outburst (Skopal et al., 2013), Z And 2000 outburst (Skopal et al., 2006), and AG Peg 2015 outburst (Skopal et al., 2017).

with a high i , mostly at the beginning of the outburst, while high velocities ($\approx 1000\text{--}2000\text{ km s}^{-1}$) by broad emission wings of permitted lines, which are present in the spectra of all systems during the outburst. Examples are shown in Fig. 3.

Such the two-velocity type of mass-outflow during outbursts can be explained by the disk-like structure of the hot component (see Sect. 2.1), which expands at moderate velocities in the orbital plane, while at higher latitudes a fast optically thin wind escapes the central WD. Next, when viewing the system at a high i , the observer can see the slowly expanding warm WD’s pseudophotosphere, which allows the observation of P Cyg line profiles with broad emission wings, and features of the warm-type of outbursts in the spectrum. Conversely, for systems with a low i , we observe just the fast optically thin stellar wind down to the hot WD’s pseudophotosphere, which gives rise to the broadening of the profile of the emission lines, especially their wings, and spectral characteristics of the hot-type of outbursts.

Skopal (2006) showed that the broadening of the H α wings and the significant increase of the emission measure in the continuum during active phases are caused by the enhanced ionized wind from the hot component. Therefore, modeling the wing profiles and/or having the emission measure (EM) from the SED models, we can determine the corresponding mass-loss rate, \dot{M}_{WD} . Using a β -law, optically thin bipolar wind model from the hot components³ the author fitted the broad H α wings. In this way, he determined \dot{M}_{WD} to a few $\times 10^{-8} M_{\odot} \text{ yr}^{-1}$ and to a few $\times (10^{-7} - 10^{-6}) M_{\odot} \text{ yr}^{-1}$ during quiescent and active phases, respectively.

³In the model, the central torus blocks the wind in the orbital plane. The model is therefore only applicable for systems with a high i .

In the case of systems with a low i (i.e., for the hot-type outbursts), Skopal et al. (2017, 2020) expressed a relationship between EM and \dot{M}_{WD} for a spherically symmetric β -law wind around the WD. According to the theory of the optically thick wind in nova outbursts (e.g. Kato & Hachisu, 1994), the authors considered two limiting cases for the beginning of the wind – on the WD’s surface and on its pseudophotosphere. In both cases, the wind becomes optically thin at the WD’s pseudophotosphere. Applying this approach for EM from the SED models and the $\text{H}\alpha$ line luminosity, they obtained \dot{M}_{WD} of a few times $10^{-6} M_{\odot} \text{yr}^{-1}$ for both studied objects, AG Peg and V426 Sge, during their Z And-type outbursts.

2.3. Transient jets from a warped disk

The possibility of the formation of collimated bipolar outflows (jets) from the WD in symbiotic binaries seems to be related to the increase of accretion onto the WD during the Z And-type outbursts (Skopal et al., 2018). Usually, jets are observed at, but mainly, after the optical maximum (e.g., Tomov et al., 2007; Skopal et al., 2009). However, their detection is very rare, although a variety of methods from X-rays to the radio has been employed. Typical signatures of jets in the optical spectrum are satellite components to the main emission of the strongest hydrogen and helium lines. To date, such the indication of jets has only been recorded for five objects: Hen 3-1341, StH α 190, Z And, BF Cyg and St 2-22 (e.g., Tomov et al., 2000; Munari et al., 2001; Tomov et al., 2007; Skopal et al., 2013; Tomov et al., 2017).

Spectral properties of the satellite components to $\text{H}\alpha$ during the 2006 Z And outburst suggested an average opening angle of jets of $6^{\circ}.1$, the mass-outflow rate via jets of $\dot{M}_{\text{jet}} \sim 2 \times 10^{-6} (R_{\text{jet}}/1 \text{ AU})^{1/2} M_{\odot} \text{yr}^{-1}$, which corresponds to the emitting mass of $M_{\text{jet}}^{\text{em}} \sim 6 \times 10^{-10} (R_{\text{jet}}/1 \text{ AU})^{3/2} M_{\odot}$ and the emission measure of both jets of $1 - 2 \times 10^{58} \text{ cm}^{-3}$. During their lifetime (July – December, 2006), the jets released the total mass of $M_{\text{jet}}^{\text{total}} \approx 7.4 \times 10^{-7} M_{\odot}$ (Skopal et al., 2009).

The repeated ejection of jets during outbursts of Z And was always followed with the simultaneous emergence of the rapid photometric variability ($\Delta m \approx 0.06 \text{ mag}$) on the timescale of hours. According to models of SED, this type of variability is produced by the warm WD’s pseudophotosphere, i.e., the outer rim of the disk that develops during outbursts. Such the higher-amplitude photometric variability can represent observational response of the radiation-induced warping of the inner parts of the disk. According to theoretical modeling, the high luminosity of the central source can illuminate the disk, whose inner parts can become unstable to warping (Iping & Petterson, 1990; Pringle, 1996; Livio & Pringle, 1996). In agreement with the general view that the warped disk starts to wobble or precess (Livio & Pringle, 1997) we can thus observe wobbling of the outer parts of the disk, reflected by the $\sim 0.6 \text{ mag}$ photometric variability. Therefore, it was suggested that the jets ejection and the measured disk-jets

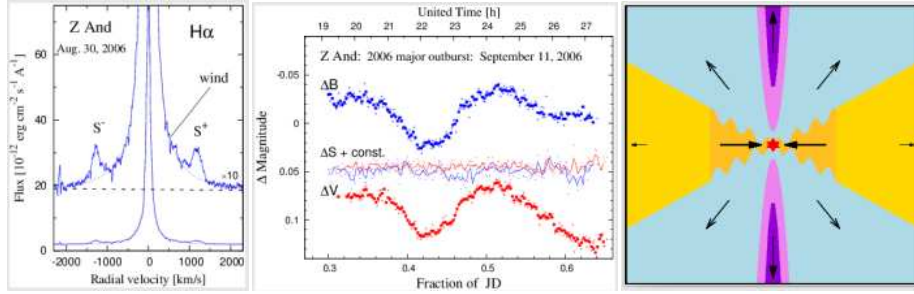


Figure 4. Example of the bipolar jets ejection from the symbiotic prototype Z And. Left: The bipolar jets are indicated by S $^-$ and S $^+$ satellite components to the H α line. Middle: Simultaneously, the photometric variation within $\Delta m \sim 0.06$ mag on the time-scale of hours develops. Right: Sketch of a disruption of the inner parts of the disk (dark yellow) due to the outburst of the central WD that can cause sudden increase in mass accretion and the ejection of bipolar jets (violet area) (see Skopal et al., 2018).

connection could be caused by the radiation-induced warping of the inner disk due to a significant increase of the burning WD luminosity during outbursts. In this way, the enhanced accretion through the disk warping, supplemented by the accretion from the wind of the giant, can keep a high luminosity of the WD for a long time, until depletion of the disk (see Skopal et al., 2018, in detail). Example of the relevant observations and a sketch of the disk warping effect are shown in Fig. 4.

2.4. Emergence of a neutral region in the orbital plane during Z And type outbursts

The formation of the disk-like structure of the hot component during outbursts of SySts (Sect. 2.1) represents the key effect for understanding the symbiotic phenomenon. For example, the two-temperature UV spectrum of the hot component, the two-velocity type of mass-outflow, and specific ionization structure that develop during outbursts (see Fig. 2 of Skopal, 2023, for an idea).

Its natural consequence is the simultaneous neutralization of the giant’s wind in the orbital plane during outbursts: The flared disk actually blocks ionizing photons from the central hot WD within its vertical extension, which causes the initially ionized wind before the outburst (i.e., during quiescence) to become neutral in the orbital plane during the outburst. Owing to the high densities of the giant’s wind in the orbital plane, the hydrogen recombination process occurs within minutes to days. As a result, a neutral wind region emerges in the orbital plane during outbursts of SySts (see Skopal, 2023).

This interesting effect is detectable by Rayleigh scattering on neutral atoms of hydrogen, best observable as a depression of the continuum around the Ly α

line (e.g., [Isliker et al., 1989](#); [Vogel, 1991](#)). In such the case, the strength of Rayleigh scattering is determined by the number of neutral H atoms on the path between the emitting source (here, it is the warm WD's pseudophotosphere) and the observer, i.e., on the hydrogen column density, N_{H} . Given the location of the presumed neutral region in the orbital plane, this effect is measurable for eclipsing systems at any orbital phase, because they are seen edge-on.

Therefore, to prove this effect, we selected eclipsing SySts for which a well-exposed ultraviolet spectrum from an outburst is available. By evaluating all candidates, we found that BF Cyg, CI Cyg, YY Her, AR Pav, AX Per and PU Vul fit best our objectives. Modeling the two-temperature UV spectra of these objects by the stellar continuum from the warm WD's pseudophotosphere and the nebular continuum from the ionized circumbinary matter above/below the disk (see Sect. 2.1), we determined N_{H} values from all suitable spectra (42) of our targets (the targets selection and the modeling are described by [Skopal, 2023](#), in detail).

Figure 5 shows the results. Top panels illustrate the continuum depression around the Ly α line due to Rayleigh scattering on H atoms at two different orbital phases. The bottom panel **c** depicts all N_{H} values as a function of the orbital phase, and panel **d** shows a schematic of the ionization structure of the symbiotic binary during the outburst. It is clear from the figure that the N_{H} measurements follow a common course along the orbit with a difference of more than two orders of magnitude between the values around the inferior and superior conjunction of the giant. High values of N_{H} at any orientation of the binary ($> 10^{22} \text{ cm}^{-2}$) prove the presence of a neutral region in the orbital plane because our targets are seen approximately edge-on.

The fact that this region consists of the neutral wind from the giant (see above) is confirmed by the significant difference in N_{H} values measured around the superior and the inferior conjunction of the giant. This is because of measuring N_{H} in the direction to the WD, while the source of neutral hydrogen is associated with the red giant (see [Skopal, 2023](#)). Also, the model of N_{H} values from Fig. 5c corresponds to the wind velocity profile of normal giants in SySts (see [Skopal & Shagatova, 2023](#), in detail).

The neutral near-orbital-plane region determines a biconical shape of the ionized region distributed above/below it, with the tops at the burning WD (see Fig. 5d). The nebular radiation is produced by the high-velocity mass-outflow in the form of an enhanced wind during outbursts (see Sect. 2.2). Accordingly, depending on the i , we observe the spectral characteristics of a hot or warm type of outburst (see Sect. 2.1).

3. Conclusion and future work

The key phenomenon for understanding the two-temperature UV spectrum of SySts that develops during outbursts is the formation of the disk-like structure

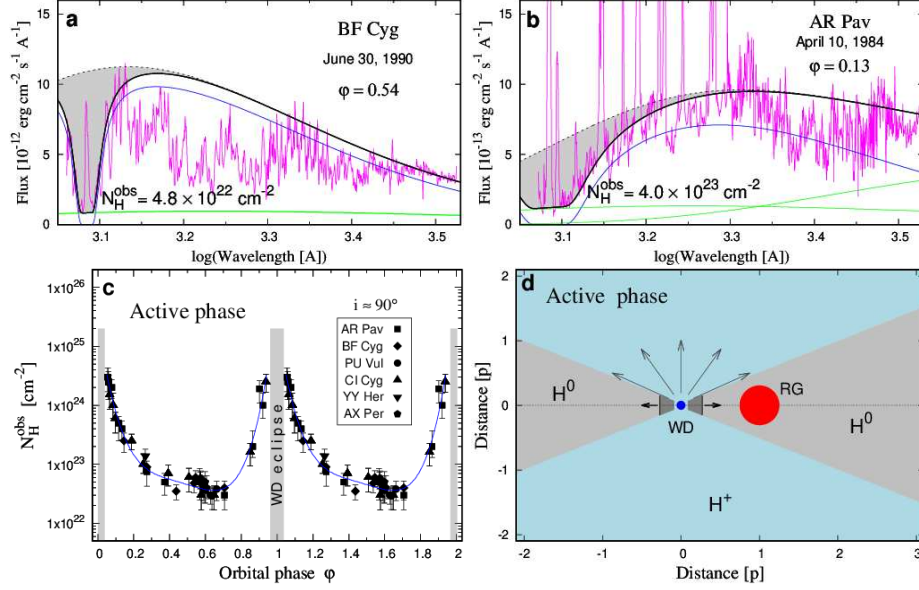


Figure 5. Top: Example of a strong depression of the continuum around the Ly α line due to Rayleigh scattering on H atoms (gray area) around the superior (panel **a**) and inferior (**b**) conjunction of the giant. Dotted line is the unattenuated continuum; meaning of other lines as in Fig. 1. Bottom: Column densities between the observer and the WD measured for our targets as a function of the orbital phase φ (**c**) and the corresponding ionization structure during outbursts is sketched on the right (**d**). The two-velocity type of mass outflow is denoted by arrows of different sizes. Adapted according to Skopal (2023).

around the WD. Such the non-spherical structure of the hot component is constrained by the contradictory properties of the radiation from the warm WD’s pseudophotosphere and the strong nebular radiation observed during outbursts in the spectrum of eclipsing systems. (see Sect. 2.1).

The disk-like structure is also responsible for observing the two-velocity type of mass-outflow indicated during outbursts. The slow component is due to the disk expansion in the orbital plane, while the fast component is due to the optically thin stellar wind that is driven by the burning WD through the rest of the sphere (see Sect. 2.2, Fig. 5d).

In rare cases, a significant increase in the luminosity of the burning WD during outbursts can induce warping of the inner disk with a subsequent sudden increase in mass accretion and the ejection of bipolar jets (see Sect. 2.3).

An interesting consequence of the disk-like structure of the hot component is the simultaneous emergence of a neutral near-orbital-plane region consisting

of the wind from the giant (see Sect. 2.4).

Based on the given basic characteristics of the SySts outbursts, two main tasks arise for future theoretical modeling directly related to the emergence of the neutral near-orbital-plane region:

- The N_{H} values measured around the orbit (Fig. 5c) represent a challenge for the theoretical modeling of the wind morphology of wide interacting binaries containing an evolved giant.
- During outbursts of non-eclipsing systems, the presence of the neutral wind region in the orbital plane is probably indicated by significant broadening and high fluxes of the Raman-scattered O VI 6825 Å line relative to the quiescent phase (e.g., Leedjäv et al., 2004; Skopal et al., 2017) because a significant amount of new scatterers appears in the orbital plane. Verification of this hypothesis, however, requires theoretical modeling.

Finally, the finding of the emergence of the neutral near-orbital-plane region can also be conducive to the explanation of more violent classical nova outbursts. Here, a similar structure of the nova ejecta containing a density enhanced equatorial region was directly inferred from radio imaging of the classical nova V959 Mon (see Chomiuk et al., 2014). Disk-like structure in the equatorial plane was also constrained by modeling the energy distribution in the spectrum of the classical nova V339 Del (see Skopal, 2019). Recently, Munari et al. (2022) needed an optically thick mass layer localized in the orbital plane (they called it "the density enhancement on the orbital plane") to interpret radio interferometric imaging of the recurrent symbiotic nova RS Oph after its explosions.

Acknowledgements. This research was supported by a grant of the Slovak Academy of Sciences, VEGA No. 2/0030/21, and the Slovak Research and Development Agency under the contract No. APVV-20-0148.

References

- Belczyński, K., Mikołajewska, J., Munari, U., Ivison, R. J., & Friedjung, M., A catalogue of symbiotic stars. 2000, *Astronomy and Astrophysics, Supplement*, **146**, 407, DOI: 10.1051/aas:2000280
- Bode, M. F. & Evans, A. 2008, *Classical Novae* (Cambridge: Cambridge University Press)
- Boyarchuk, A. A., The Nature of AG Pegasi. 1967, *Soviet Astronomy*, **11**, 8
- Brandi, E., Mikołajewska, J., Quiroga, C., et al., The spectroscopic orbits and other parameters of the symbiotic binary FN Sgr. 2005, *Astronomy and Astrophysics*, **440**, 239, DOI: 10.1051/0004-6361:20042552
- Cariková, Z. & Skopal, A., Ionization structure of hot components in symbiotic binaries during active phases. 2012, *Astronomy and Astrophysics*, **548**, A21, DOI: 10.1051/0004-6361/201219221

- Chakrabarty, D. & Roche, P., The Symbiotic Neutron Star Binary GX 1+4/V2116 Ophiuchi. 1997, *Astrophysical Journal*, **489**, 254, DOI: 10.1086/304779
- Chomiuk, L., Linford, J. D., Yang, J., et al., Binary orbits as the driver of γ -ray emission and mass ejection in classical novae. 2014, *Nature*, **514**, 339, DOI: 10.1038/nature13773
- Fernandez-Castro, T., Gonzalez-Riestra, R., Cassatella, A., Taylor, A. R., & Seaquist, E. R., The active phase of the hot component of Z Andromedae. 1995, *Astrophysical Journal*, **442**, 366, DOI: 10.1086/175446
- González-Riestra, R., Viotti, R., Iijima, T., & Greiner, J., IUE observations of the high-velocity symbiotic star AG Draconis. III. A compendium of 17 years of UV monitoring, and comparison with optical and X-ray observations. 1999, *Astronomy and Astrophysics*, **347**, 478
- Hachisu, I., Kato, M., & Nomoto, K., A New Model for Progenitor Systems of Type IA Supernovae. 1996, *Astrophysical Journal, Letters*, **470**, L97, DOI: 10.1086/310303
- Iping, R. C. & Petterson, J. A., Quasi-periodic precession of disks in X-ray binaries, with possible application to Centaurus X-3. 1990, *Astronomy and Astrophysics*, **239**, 221
- Islaker, H., Nussbaumer, H., & Vogel, M., Eclipse cross-sections of cool components in double star systems. 1989, *Astronomy and Astrophysics*, **219**, 271
- Kato, M. & Hachisu, I., Optically Thick Winds in Nova Outbursts. 1994, *Astrophys. J.*, **437**, 802, DOI: 10.1086/175041
- Kenyon, S. J. 1986, *The symbiotic stars* (Cambridge: Cambridge University Press)
- Leedjårv, L., Burmeister, M., Mikołajewski, M., et al., Emission lines in the spectrum of the symbiotic star AG Draconis from 1997 to 2003. 2004, *Astronomy and Astrophysics*, **415**, 273, DOI: 10.1051/0004-6361:20034224
- Leibowitz, E. M. & Formiggini, L., Activity cycle of the giant star of Z Andromedae and its spin period. 2008, *Monthly Notices of the RAS*, **385**, 445, DOI: 10.1111/j.1365-2966.2008.12847.x
- Livio, M. & Pringle, J. E., The Formation of Point-symmetric Nebulae. 1996, *Astrophysical Journal, Letters*, **465**, L55, DOI: 10.1086/310130
- Livio, M. & Pringle, J. E., Wobbling Accretion Disks, Jets, and Point-symmetric Nebulae. 1997, *Astrophysical Journal*, **486**, 835, DOI: 10.1086/304552
- Masetti, N., Landi, R., Pretorius, M. L., et al., IGR J16194-2810: a new symbiotic X-ray binary. 2007a, *Astronomy and Astrophysics*, **470**, 331, DOI: 10.1051/0004-6361:20077509
- Masetti, N., Rigon, E., Maiorano, E., et al., X-ray broad-band study of the symbiotic X-ray binary 4U 1954+31. 2007b, *Astronomy and Astrophysics*, **464**, 277, DOI: 10.1051/0004-6361:20066517
- McKeever, J., Lutz, J., Wallerstein, G., Munari, U., & Siviero, A., High-Dispersion Spectroscopy of BF Cygni at the Beginning of the 2006 Outburst. 2011, *Publications of the ASP*, **123**, 1062, DOI: 10.1086/662076

- Munari, U., Giroletti, M., Marcote, B., et al., Radio interferometric imaging of RS Oph bipolar ejecta for the 2021 nova outburst. 2022, *Astronomy and Astrophysics*, **666**, L6, DOI: 10.1051/0004-6361/202244821
- Munari, U., Tomov, T., Yudin, B. F., et al., Discovery of a bipolar and highly variable mass outflow from the symbiotic binary StH α 190. 2001, *Astronomy and Astrophysics*, **369**, L1, DOI: 10.1051/0004-6361:20010210
- Mürset, U. & Nussbaumer, H., Temperatures and luminosities of symbiotic novae. 1994, *Astronomy and Astrophysics*, **282**, 586
- Mürset, U. & Schmid, H. M., Spectral classification of the cool giants in symbiotic systems. 1999, *Astronomy and Astrophysics, Supplement*, **137**, 473, DOI: 10.1051/aas:1999105
- Paczynski, B. & Rudak, B., Symbiotic stars - Evolutionary considerations. 1980, *Astronomy and Astrophysics*, **82**, 349
- Pringle, J. E., Self-induced warping of accretion discs. 1996, *Monthly Notices of the RAS*, **281**, 357, DOI: 10.1093/mnras/281.1.357
- Seaquist, E. R., Taylor, A. R., & Button, S., A radio survey of symbiotic stars. 1984, *Astrophysical Journal*, **284**, 202, DOI: 10.1086/162399
- Shen, K. J. & Bildsten, L., Thermally Stable Nuclear Burning on Accreting White Dwarfs. 2007, *Astrophysical Journal*, **660**, 1444, DOI: 10.1086/513457
- Skopal, A., Disentangling the composite continuum of symbiotic binaries. I. S-type systems. 2005, *Astronomy and Astrophysics*, **440**, 995, DOI: 10.1051/0004-6361:20034262
- Skopal, A., Broad H α wings from the optically thin stellar wind of the hot components in symbiotic binaries. 2006, *Astronomy and Astrophysics*, **457**, 1003, DOI: 10.1051/0004-6361:20064935
- Skopal, A., Multiwavelength Modeling of the SED of Nova V339 Del: Stopping the Wind and Long-lasting Super-Eddington Luminosity with Dust Emission. 2019, *Astrophysical Journal*, **878**, 28, DOI: 10.3847/1538-4357/ab1f07
- Skopal, A., The Emergence of a Neutral Wind Region in the Orbital Plane of Symbiotic Binaries during Their Outbursts. 2023, *Astronomical Journal*, **165**, 258, DOI: 10.3847/1538-3881/acd193
- Skopal, A., Pribulla, T., Budaj, J., et al., Transient Jets in the Symbiotic Prototype Z Andromedae. 2009, *Astrophysical Journal*, **690**, 1222, DOI: 10.1088/0004-637X/690/2/1222
- Skopal, A. & Shagatova, N., Wind-mass transfer in S-type symbiotic binaries. IV. Indication of high wind-mass-transfer efficiency from active phases. 2023, *Astronomy and Astrophysics*, **680**, A60, DOI: 10.1051/0004-6361/202347396
- Skopal, A., Shugarov, S., Shagatova, N., et al., New burst of the symbiotic star V426 Sge (HBHA 1704-05). 2023, *The Astronomer's Telegram*, **16280**, 1
- Skopal, A., Shugarov, S. Y., Munari, U., et al., The path to Z And-type outbursts: The case of V426 Sagittae (HBHA 1704-05). 2020, *Astronomy and Astrophysics*, **636**, A77, DOI: 10.1051/0004-6361/201937199

- Skopal, A., Shugarov, S. Y., Sekeráš, M., et al., New outburst of the symbiotic nova AG Pegasi after 165 yr. 2017, *Astronomy and Astrophysics*, **604**, A48, DOI: 10.1051/0004-6361/201629593
- Skopal, A., Tarasova, T. N., Cariková, Z., et al., Formation of a disk structure in the symbiotic binary AX Persei during its 2007-10 precursor-type activity. 2011, *Astronomy and Astrophysics*, **536**, A27, DOI: 10.1051/0004-6361/201116969
- Skopal, A., Tarasova, T. N., Wolf, M., Dubovský, P. A., & Kudzej, I., Repeated Transient Jets from a Warped Disk in the Symbiotic Prototype Z And: A Link to the Long-lasting Active Phase. 2018, *Astrophysical Journal*, **858**, 120, DOI: 10.3847/1538-4357/aabc11
- Skopal, A., Teodorani, M., Errico, L., et al., A photometric and spectroscopic study of the eclipsing symbiotic binary AX Persei. 2001, *Astronomy and Astrophysics*, **367**, 199, DOI: 10.1051/0004-6361:20000413
- Skopal, A., Tomov, N. A., & Tomova, M. T., Discovery of collimated ejection from the symbiotic binary BF Cygni. 2013, *Astronomy and Astrophysics*, **551**, L10, DOI: 10.1051/0004-6361/201321030
- Skopal, A., Vittone, A., Errico, L., et al., A photometric and spectroscopic study of the symbiotic binary BF Cyg. 1997, *Monthly Notices of the RAS*, **292**, 703, DOI: 10.1093/mnras/292.3.703
- Skopal, A., Vittone, A. A., Errico, L., et al., Structure of the hot object in the symbiotic prototype Z Andromedae during its 2000-03 active phase. 2006, *Astronomy and Astrophysics*, **453**, 279, DOI: 10.1051/0004-6361:20052917
- Tomov, N. A., Tomova, M. T., & Bisikalo, D. V., Bipolar ejection by the symbiotic binary system Z And during its 2006 outburst. 2007, *Monthly Notices of the RAS*, **376**, L16, DOI: 10.1111/j.1745-3933.2007.00277.x
- Tomov, T., Munari, U., & Marrese, P. M., Bipolar jets from the symbiotic star Hen 3-1341 in outburst. 2000, *Astronomy and Astrophysics*, **354**, L25, DOI: 10.48550/arXiv.astro-ph/9912531
- Tomov, T., Zamanov, R., Gałan, C., & Pietrukowicz, P., St 2-22 - Another Symbiotic Star with High-Velocity Bipolar Jets. 2017, *Acta Astronomica*, **67**, 225, DOI: 10.32023/0001-5237/67.3.2
- Tutukov, A. V. & Yungelson, L. R., On the origin and evolutionary stage of symbiotic stars. 1976, *Astrofizika*, **12**, 521
- Vogel, M., Empirical velocity laws for cool giants. I. The symbiotic binary EG Andromedae. 1991, *Astronomy and Astrophysics*, **249**, 173
- Yungelson, L. R., Kuranov, A. G., & Postnov, K. A., Wind-accreting symbiotic X-ray binaries. 2019, *Monthly Notices of the RAS*, **485**, 851, DOI: 10.1093/mnras/stz467

Studying of exoasteroids orbiting around WD 1145+017

A. Maliuk¹, J. Budaj¹ , D. Mkrtychian², Z. Garai^{3,1,11}, S. Zharikov⁴,
T. Pribulla¹ , R. Komžík¹ , A. Kusakin⁵, L. Shestakova⁵,
R. Kokumbaeva⁵, I. Reva⁵, S. Joshi⁶, A. Valeev⁷, D. Gadelshin⁷,
G. Valyavin⁷, N. A-thano⁸, R. Mennickent⁹, A. Serebryanskiy⁵ and
T.G. Kaye¹⁰

¹ *Astronomical Institute of the Slovak Academy of Sciences,
059 60 Tatranská Lomnica, Slovakia*

² *National Astronomical Research Institute of Thailand, 50180 Chiang Mai,
Thailand*

³ *HUN-REN-ELTE Exoplanet Research Group, 9700 Szombathely, Szent
Imre h. u. 112, Hungary*

⁴ *Instituto de Astronomía, Universidad Nacional Autónoma de México,
Apdo. Postal 877, Ensenada, Baja California, México, 22800*

⁵ *Fesenkov Astrophysical Institute, Observatory 23, 050020 Almaty,
Kazakhstan*

⁶ *Aryabhata Research Institute of Observational Sciences, Manora Peak,
Nainital-263002, India*

⁷ *Special Astrophysical Observatory, Nizhniy Arkhyz 369167, Russia*

⁸ *Department of Physics and Institute of Astronomy, National Tsing-Hua
University, Hsinchu 30013, Taiwan*

⁹ *Universidad de Concepción, Departamento de Astronomía, Casilla 160-C,
Concepción, Chile*

¹⁰ *Raemore Vista Observatory, Sierra Vista Arizona*

¹¹ *ELTE Gothard Astrophysical Observatory, 9700 Szombathely, Szent Imre
h.u. 112, Hungary*

Received: November 13, 2023; Accepted: January 16, 2024

Abstract. WD 1145+017 is the first white dwarf known to be orbited by disintegrating exoasteroids. It is a helium-dominated white dwarf with lines of metals in spectra and variable asymmetric transits. The analysis of WD 1145 light curve allowed us to identify at least 8 bodies which periodically eclipse the star, showing periods ranging from 4.490 to 4.493 hours. Waterfall diagram shows that some of these periods are not stable. Estimating transit depths gave us possibility to assess the disintegration rate. We have estimated the lower limit of dust masses associated with these bodies, which exhibits time-varying characteristics, fluctuating within the range of approximately $2 - 3 \times 10^{14}$ kg.

Key words: exoplanets – circumstellar dust – exoasteroids

1. Introduction

The star known as WD 1145+017 (or WD 1145) is a white dwarf situated approximately 154 parsecs away from Earth. This object holds the distinction of being the first white dwarf ever observed with a planetary-mass entity in transit around it (Vanderburg et al., 2015). Vanderburg’s team documented their observations of a white dwarf undergoing transits by, at the very least, one disintegrating planetesimal, and quite likely, multiple such objects. These transits exhibited periods ranging from 4.5 hours to 4.9 hours, which translates to an approximate distance of $1R_{\odot}$ from the central star. The transit profiles displayed asymmetrical shapes and varying depths, with some transits reaching depths of up to 40% in flux. These observations strongly suggest the presence of small celestial bodies with cometary tails composed of dusty materials (Izquierdo et al., 2018).

The photosphere of WD 1145 is polluted by metals originating from disintegrating bodies, thus its spectra show strong lines of heavy elements like magnesium, aluminum, silicon, calcium, iron, and nickel (Xu et al., 2016). The star is surrounded by dusty debris disc which causes substantial infrared excess in the spectra. Hallakoun et al. (2017) and Xu et al. (2019) also revealed that UV transit depths are always shallower than those in the optical.

We aim to revise number of planetesimals and their orbital parameters.

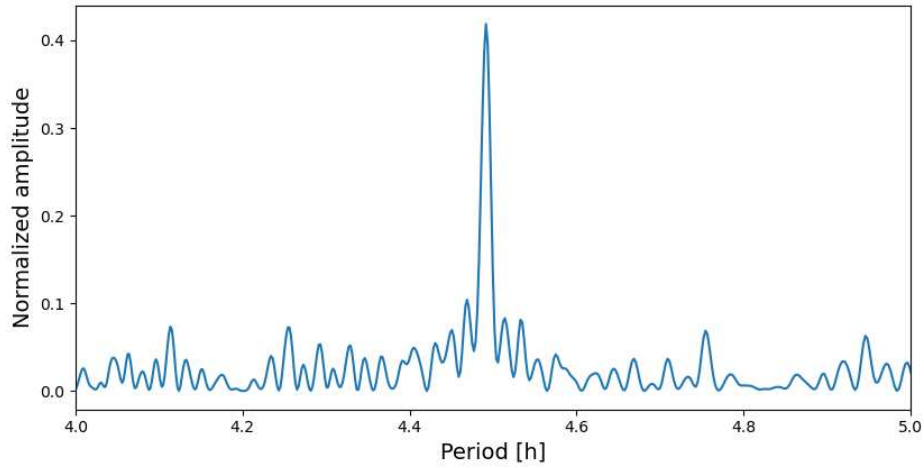
2. Observations

The task of revising the number of planetesimals is challenging because the light curve of white dwarf is constantly and rapidly evolving with time. Photometric observation we use in the analysis come from several observatories during 2016 - 2020 years. In our research we mostly focus on data obtained during 2017 because they are the most complete and precise. They were all obtained in the framework of a campaign organized by the Astronomical Institute of Slovak Academy of Sciences. Several medium and small size telescopes around the world participated with their observations. They are all listed in the Tab. 1. This data was complemented by observations obtained by Bruce Gary during 2016-2020 years with 14” telescope in Hereford, Arizona.

All the data were reduced in a uniform way using standard procedures and IRAF package. Observations from SAO had relatively short exposure times so they were binned in time to achieve about 60 second cadence. We follow Vanderbourg et al. (2015) and also use Lomb-Scargle periodogram(Scargle, 1982) to find periodicities in more recent data. Our periodogram is displayed on Fig. 1. It differs from one obtained by Vanderburg - some peaks are missing or shifted. This is an evidence of rapid evolution of the system. Preliminary results show that the strongest peak is at 4.48 hours.

Table 1. Telescopes participated in observation campaign of WD 1145

| Location | Aperture [m] |
|---|-----------------|
| Devastal, India | 3.6 |
| RATIR, Mexico | 1.5 |
| Skalnate Pleso, Slovakia | 1.3 |
| Nizhnij Arkhyz, Russia | 1 |
| TSAO, Kazakstan | 1 |
| Gaomeigu China | 0.7 |
| PROMPT-8, Cerro Tololo Inter-American Observatory | 0.6 |
| Stará Lesná, Slovakia | 0.6 |
| TNO, Narit, Thailand | 0.5 |
| Australia | 0.4 |
| Tenerife, Spain | 0.4 |

**Figure 1.** Periodogram of the data used in this work

3. Modelling lightcurve

To estimate orbital parameters of exoasteroids, we fit the light curve with combination of 8 asymmetric hyperbolic secants, following [Croll et al. \(2017\)](#):

$$M(t) = m_0 + \sum_{i=1}^N \frac{C_i}{e^{-\frac{(t-t'_i)}{\tau_{1i}}} + e^{-\frac{(t-t'_i)}{\tau_{2i}}}} \quad (1)$$

$M(t)$ is the total magnitude, $N = 8$ is the number of transiting bodies, m_0 is the out-of-transit magnitude, $C_i/2$ is approximately the transit depth of i -th body, t'_i is the closest transit midpoint for time t , and τ_{1i} and τ_{2i} are the characteristic durations of the ingress and egress, respectively. We have to take into account the fact that exoasteroids can lose their masses as well as dust clouds surrounding them. This means that the transit depth C depends on time. We approximate it with sixth degree polynomials:

$$C = \sum_{j=0}^6 a_j (t - t_0)^j \quad (2)$$

where t_0 is the first transit mid-point and a_j are independent parameters. To calculate t' we need to know the number of epochs passed from the start of observations:

$$n = \left[\frac{t - t_0}{P} \right] \quad (3)$$

where P is the orbital period and t_0 is the midpoint of first transit. Then we find

$$t' = t_0 + nP \quad (4)$$

Totally the equation describing the light curve has $N \times 11 + 1 = 89$ parameters (seven polynomial coefficients, time of ingress and egress, periods, transit midpoints (11 in total) of $N = 8$ bodies). To optimise them we use Powell's method (Powell, 1964). The observations overplotted with the best fit are displayed in Fig. 2. Periods vary around 4.48 hours and differ by 10 seconds. However, long-term stability of these periods is under question. We follow Rappaport et al. (2018) and use waterfall diagram as a reliable method of monitoring trends in optical activity over large timespan. Waterfall diagram (Fig. 3) displays the magnitude as a function of the orbital phase (x-axis) for different dates of observations (y-axis). Values of individual pixels correspond to brightness of the given object at given phase and date (darker ones correspond to higher magnitudes, lighter corresponds to lower magnitudes). Thus, periodic transits form clear traces in waterfall diagram. If the data is phase-folded with the correct orbital period, the trace is represented with straight vertical line. Other shape of trace may indicate changing or incorrect period. We construct our waterfall diagram as an image of 120120 pixels. The most challenging task is to take into account significant gaps in data. We followed Rappaport and handle missing observations as follows. The flux from each observation was placed into the appropriate $[x, y]$ bin according to the phase of the 4.5-h period and the date of the observation. For each point in the image, if there exists a data point, we leave it as it is. If a pixel is initially blank, we draw a circle around that point which is 5 pixels in radius, and take a distance weighted average of all the points within which there are data. The weighting was done according to d^{-2} , where

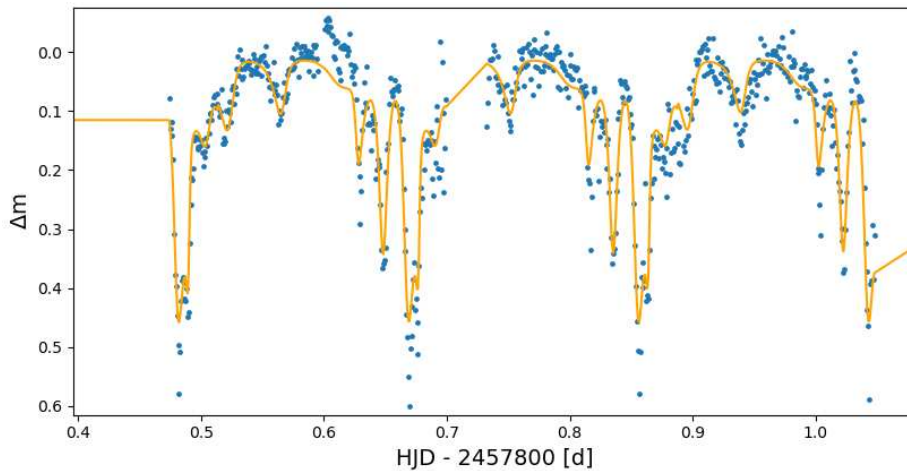


Figure 2. The observations overplotted with the best fit by Eq. 1.

d is the distance between the point being filled and the data points (in units of pixels). So the flux used to fill the blank bin is given by

$$F = \frac{\sum_{points} F_{point} d^{-2}}{\sum_{points} d^{-2}} \quad (5)$$

where we sum fluxes F_{point} within 5 pixels of blank bin, weighted with distance d from the center of blank bin to the point. The result is displayed in Fig. 3.

As one can notice, many objects have stable period, but at least two (number 3 and 5) show significant curvature. This may indicate that some periods change with time. An intriguing observation is that certain trajectories intersect. Our goal is to determine whether these intersections are indicative of genuine collisions between exoasteroids or simply the result of overlapping dusty tails.

4. Estimation of dust mass

Knowledge of the light curve helps us to estimate the dust mass. We operate on the following assumptions. First of all, we ignore the solid core of exoasteroid and suppose that the dust almost covers the whole disc of the star. Properties of the dust were determined by Budaj et al. (2022): it is composed mostly of silicates and mean grain size is about 5 microns. We also use dust opacities calculated by Budaj et al. (2015). We calculate the dust mass as follows.

$$I = I_0 e^{-\tau} \quad (6)$$

Here I_0 is constant out-of-transit intensity (we observe it when the disc is not covered by dust), I is total intensity, which varies with time, and τ is optical

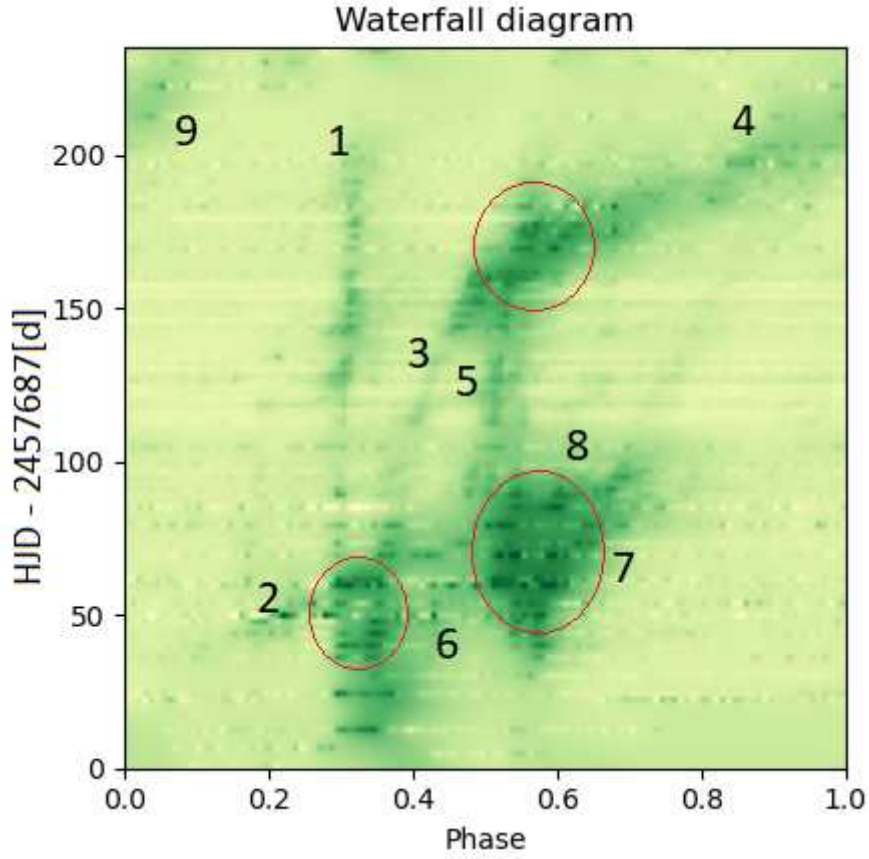


Figure 3. WD 1145 waterfall diagram for 2016 year. We can identify 8 or 9 objects. Intersections of trajectories are marked with red.

depth of the dust:

$$\tau = \kappa \rho z \quad (7)$$

where κ stands for opacity, ρ is dust density and z is geometric depth. Now we can calculate differential of mass

$$dM = \rho z dS, \quad dS = 2R_{\star} v dt \quad (8)$$

where R_{\star} is radius of white dwarf and v is orbital velocity. Thus, total mass of eclipsing dust is an integral over orbital period T :

$$M = -2 \int_0^T \ln \frac{I}{I_0} R_{WD} v \kappa^{-1} dt \quad (9)$$

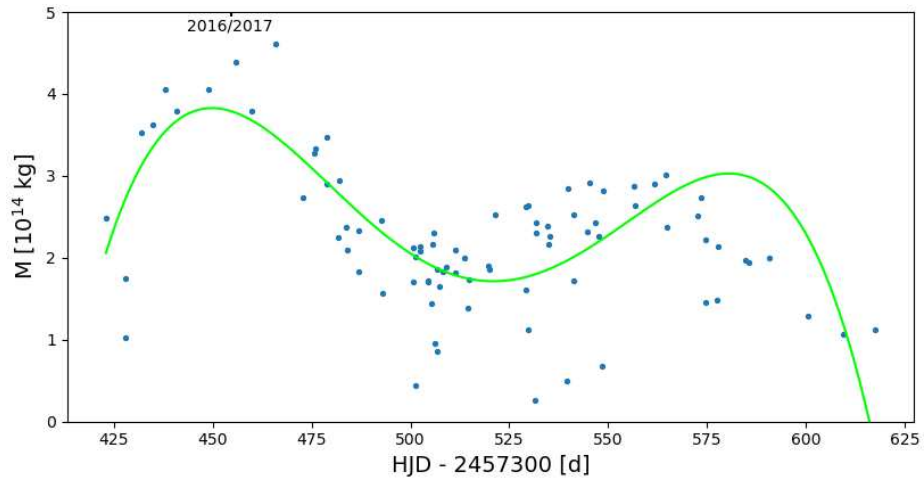


Figure 4. Variations of dust mass over 2017 year. One point corresponds to one epoch.

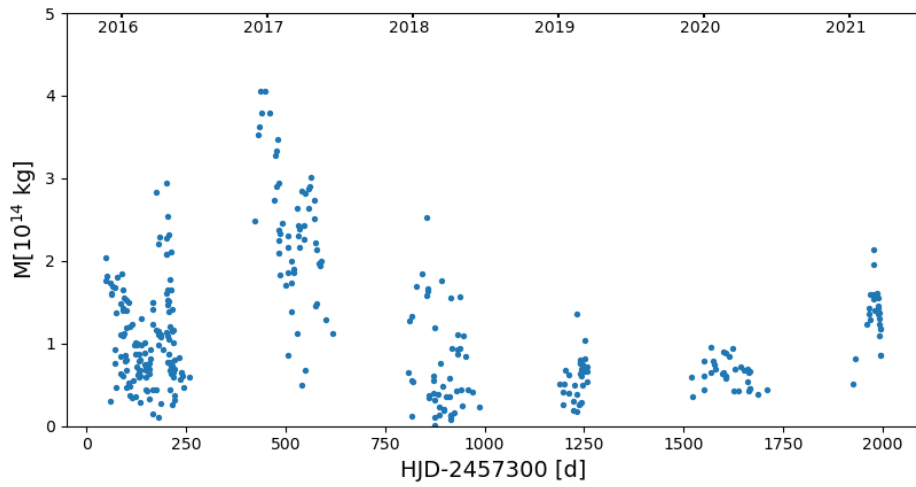


Figure 5. Variations of dust mass over 2016-2021 years. One point corresponds to one epoch.

Our results for year 2017 are displayed on Fig. 4. We can see that eclipsing dust mass does not remain stable during our observation campaign. Observed peaks at HJD = 2457750 and 2457850 correspond to intersections on waterfall diagram, marked with red circles (Fig. 3), which indicates that real collisions between exoasteroids occur. We also use unpublished data obtained by Bruce Gary to observe dust mass dynamics during 2016 - 2021 years. These results are displayed on Fig. 5. We observe significant variations every year.

5. Conclusions

In our study, we have detected a minimum of eight celestial bodies in orbit around WD 1145. These bodies exhibit orbital periods ranging from 4.4915 to 4.4932 hours. Our analysis, based on periodograms and waterfall diagrams, reveals that these orbital periods evolve over time. Furthermore, we have estimated the lower limit of dust masses associated with these bodies, which exhibits time-varying characteristics, fluctuating within the range of approximately $2\text{-}3 \times 10^{14}$ kg. Accordingly to Shestakova et al. (2019), estimated dust accretion rate is $3.2 \times 10^9 \text{ g s}^{-1}$, which means that the material of dust ring should be updated every 3 years.

Acknowledgements. This work is supported by project APVV-20-0148 and VEGA 02/0031/22. We would like to express our profound gratitude to B. Gary for his meticulous observations. ZG acknowledges the support of the Hungarian National Research, Development and Innovation Office (NKFIH) grant K-125015, the PRODEX Experiment Agreement No. 4000137122 between the ELTE University and the European Space Agency (ESA-D/SCI-LE-2021-0025) and the support of the city of Szombathely.

References

- Budaj, J., Kocifaj, M., Salmeron, R., & Hubeny, I., Tables of phase functions, opacities, albedos, equilibrium temperatures, and radiative accelerations of dust grains in exoplanets. 2015, *Monthly Notices of the RAS*, **454**, 2, DOI: 10.1093/mnras/stv1711
- Budaj, J., Maliuk, A., & Hubeny, I., WD 1145+017: Alternative models of the atmosphere, dust clouds, and gas rings. 2022, *Astronomy and Astrophysics*, **660**, A72, DOI: 10.1051/0004-6361/202141924
- Croll, B., Dalba, P. A., Vanderburg, A., et al., Multiwavelength Transit Observations of the Candidate Disintegrating Planetesimals Orbiting WD 1145+017. 2017, *Astrophysical Journal*, **836**, 82, DOI: 10.3847/1538-4357/836/1/82
- Hallakoun, N., Xu, S., Maoz, D., et al., Once in a blue moon: detection of ‘bluing’ during debris transits in the white dwarf WD 1145+017. 2017, *Monthly Notices of the RAS*, **469**, 3213, DOI: 10.1093/mnras/stx924

- Izquierdo, P., Rodríguez-Gil, P., Gänsicke, B. T., et al., Fast spectrophotometry of WD 1145+017. 2018, *Monthly Notices of the RAS*, **481**, 703, DOI: 10.1093/mnras/sty2315
- Powell, M. J. D., An efficient method for finding the minimum of a function of several variables without calculating derivatives. 1964, *Comput. J.*, **7**, 155
- Rappaport, S., Gary, B. L., Vanderburg, A., et al., WD 1145+017: optical activity during 2016-2017 and limits on the X-ray flux. 2018, *Monthly Notices of the RAS*, **474**, 933, DOI: 10.1093/mnras/stx2663
- Scargle, J. D., Studies in astronomical time series analysis. II. Statistical aspects of spectral analysis of unevenly spaced data. 1982, *Astrophysical Journal*, **263**, 835, DOI: 10.1086/160554
- Shestakova, L. I., Demchenko, B. I., & Serebryanskiy, A. V., On the orbital evolution of dust grains in the sublimation region around WD1145+017. 2019, *Monthly Notices of the RAS*, **487**, 3935, DOI: 10.1093/mnras/stz1598
- Vanderburg, A., Johnson, J. A., Rappaport, S., et al., A disintegrating minor planet transiting a white dwarf. 2015, *Nature*, **526**, 546, DOI: 10.1038/nature15527
- Xu, S., Hallakoun, N., Gary, B., et al., Shallow Ultraviolet Transits of WD 1145+017. 2019, *Astronomical Journal*, **157**, 255, DOI: 10.3847/1538-3881/ab1b36
- Xu, S., Jura, M., Dufour, P., & Zuckerman, B., Evidence for Gas from a Disintegrating Extrasolar Asteroid. 2016, *Astrophysical Journal, Letters*, **816**, L22, DOI: 10.3847/2041-8205/816/2/L22

ARAS eruptive stars monitoring

F. Teyssier¹  and F. Sims²

¹ *South Rouen Observatory 67, rue Jacques Daviel 76100 Rouen, France
(E-mail: francoismathieu.teyssier@gmail.com)*

² *Desert Celestial Observatory - 5900 E Bell St Apache Junction 85119*

Received: November 16, 2023; Accepted: February 13, 2024

Abstract.

The ARAS eruptive stars group monitors novae, symbiotic stars, and eventually dwarf novae ... with small telescopes (typically 20-60 cm) equipped with slit (R=600 to 15000) and echelle (R=10000) spectrographs. 4175 spectra of 65 novae and 8379 spectra of 104 symbiotics secured since 2013 are accessible for free access from the ASDB spectral database.

We present four examples to demonstrate the long-term monitoring, high cadence program, and the reactivity of the members to special events such as outbursts or eclipses.

1. The 2021 outburst of the recurrent nova RS Oph was carefully studied with daily echelle spectra and flux-calibrated low-resolution spectra for a period of one month. This monitoring allowed the construction of the evolution of the ionization state of the system during the outburst.
2. One of the main tasks of our program is the long-term monitoring of classical symbiotic stars over several orbital cycles following the suggestion of S. J. Kenyon (1986) and J. Mikolajewska. The complex behavior of the eclipsing system AX Persei is briefly summarized to illustrate our purpose.
3. An example of monitoring an eclipse in an accretion-powered symbiotic star BX Mon in April 2023.
4. The behavior of the recurrent symbiotic nova T CrB (1866, 1946) before its next nova event which is expected in the very next months or years. The cadency of the observations has enabled us to time precisely the end of the long high state detected in 2015.

Key words: novae – symbiotic stars – spectroscopy

1. Introduction

The ARAS eruptive stars group gathers worldwide amateurs observing with small telescopes ("decimeter class"). The typical diameter varies from 20 to 40 cm, exceptionally 50 and 60 cm, the full range is 8 cm to 1 m. The telescopes are equipped with various types of long slit and echelle spectrographs whose resolution varies from 600 to 15000, exceptionally 30000. Most of them are produced by Shelyak Company (Lhires III, LISA, ALPY600, eShel, ...).

Some are homemade spectrographs among them we can cite two peculiar projects: the UVEX¹ developed by "Nice People" (FR) with the support of Christian Buil, which is a 3D printing long slit spectrograph efficient in the near UV; NOU-T project, an echelle spectrograph with a resolution of 9000 mounted at the focus of a Schmidt-Cassegrain 14" telescope was developed by Joan Guarro Flo (SP) from an optical concept designed by Tim Lester (CA).

The spectra are archived in the ASDB², ARAS eruptive stars database (Teyssier, 2019). The first version was based on a Visual Basic macro applied to Excel spreadsheets and was launched in August 2013. The design and functionality based on Python codes were improved in 2022 by J. Merc (Charles University, Prague), producing the current version. The ARAS database is open to all observers who want to share their results. The resolution must be over 500. The spectra are reduced according to standards (bias, darks, flats, instrumental and atmospheric corrections applied). Most of them are reduced using ISIS³.

The observing program is firstly defined by observers themselves, individually or collectively. There are two main tasks: 1. monitoring of peculiar events such as outbursts, eclipses, and high states. 2. Long-term monitoring of symbiotic stars over several orbital cycles. We also respond to professional requests on peculiar programs.

The ASDB has been used by a number of publications⁴ (e.g. Skopal et al., 2017; Aydi et al., 2023; Iłkiewicz et al., 2022; Azzollini et al., 2023).

Table 1. ARAS Eruptive Stars Database

| Category | No. of Objects | No. of Spectra |
|-----------------|----------------|----------------|
| Novae | 65 | 4175 |
| Symbiotic stars | 104 | 8379 |
| Dwarf novae | 33 | 377 |

With four selected examples we demonstrate the value of long-term monitoring, a high cadency program, and the reactivity of the members to special events such as outbursts or eclipses.

2. Recurrent symbiotic nova RS Oph in 2021

Nova outbursts of the symbiotic system RS Oph were detected in 1898, 1933, 1958, 1967, 1985, 2006, and 2021 making it a recurrent nova. The 2021 outburst was detected on 2021-08-8.93 UT by K. Geary at a visual magnitude 6.0. The peak of luminosity was reached on 2023-08-09.55 (JD 2459436.30) which was

¹<https://spectro-uvex.tech/>

²<https://aras-database.github.io/database/index.html>

³<http://www.astrosurf.com/buil/isis-software.html>

⁴<https://ui.adsabs.harvard.edu/public-libraries/jd9bULL8SU-uBHbblit3Xw>

adopted as the start of the outburst T0. Our first spectra acquired around 2013-08-9.8 show broad emission lines of low ionized species (H I, Fe II, He I). The short recurrence time implies a massive white dwarf ($> 1.2 M_{\odot}$) explaining the high velocity of the ejecta ($> 4000 \text{ km.s}^{-1}$). The outburst occurs in the dense nebula of the symbiotic system which produces strong shocks (Azzollini et al., 2023) explaining the high degree (in comparison with classical novae) of ionization near the maximum luminosity ($\approx 25 \text{ eV}$) with the detection of recombination lines of He I or N II.

During the outburst, the degree of ionization of the ejecta increased as a consequence of the retraction of the remaining envelope, shocks, and changes in the opacity of the ejecta. The highest ionization potential observed in our spectra is 755 eV with the detection of Ar[XIV] 58.5 days after the peak luminosity.

The echelle (R = 10000) and flux calibrated (R=1000) spectra secured during the outburst allow a precise description of the phenomenon. From the extensive information obtained, we present the evolution of the degree of ionization.

Method: the epoch of the appearance of the species is determined by visual examination of the profiles (an example is shown in Fig. 1(c) with He II λ 4686 Å) and of the measures of the flux of each line: Fig. 1(b1) and 1(b2) show examples with He II and the scattered Raman OVI λ 6825 Å) on the sample of echelle spectra. The evolution of the level of ionization is shown in Fig. 1 (a).

Results: We detect three phases of the evolution of the ionization: A slow increase from 25 eV to $\approx 55 \text{ eV}$ during days 0 to 19 (± 1) with a slope of 2 eV/d.

Around day 20 the slope increases significantly (36 eV / day) until the appearance of [Ar X] (480 eV) on day 31 (± 1).

During the third phase, the slope remains positive with the lowest value.

The fluxes of He II and Raman OVI (Fig. 1) show strong variations during the rise of the lines and during the second phase. We detect the disappearance of He II λ 4686 Å two days after its rise and oscillations of the flux of Raman OVI λ 6825 Å between days 20 to 31.

3. Long-term monitoring of the nuclear burning symbiotic star AX Per

AX Per is an eclipsing (Skopal, 1991) classical symbiotic system consisting of an M4.5 III red giant (Mürset & Schmid, 1999) and a hot and luminous accreting white dwarf (for example $L = 710 L_{\odot}$, $T = 105000 \text{ K}$ on October 1984 in quiescence Muerset et al. (1991)) on a 680 days orbit.

AX Per is one of the bright symbiotic stars monitored in our program with 455 spectra acquired since 2011. Fig. 2 is an illustration of the monitoring: the equivalent widths of the two selected emission lines show a complex behavior over more than 5 orbital cycles. The dashed vertical lines mark the epoch of the eclipse according to ephemeris $\text{JD}_{\text{min}} = 2436667(3) + 680.8(0.2) * E$ (Mikolajewska & Kenyon, 1992).

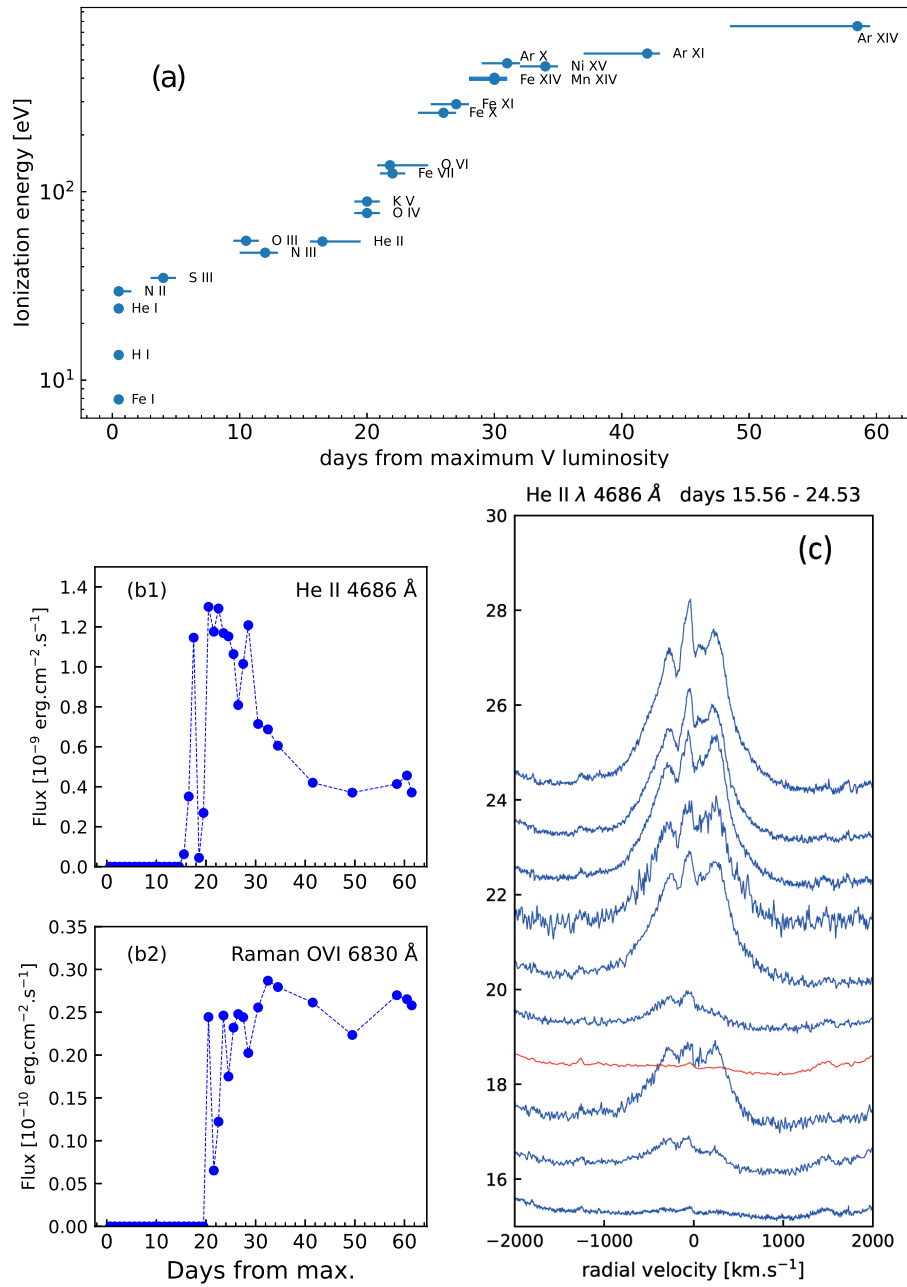


Figure 1. RS Oph, 2021 nova outburst. (a) level of ionization during the outburst; (b1,b2) flux in two lines He II $\lambda 4686 \text{ \AA}$ and Raman OVI $\lambda 6830 \text{ \AA}$; (c) evolution of He II $\lambda 4686 \text{ \AA}$ (days 15-24) in velocity space. The normalized continuum is shifted by the days since the peak of velocity.

In the 1950's, Merrill noted the complex variations of symbiotic systems and insisted on the necessity of long-term monitoring:

"Persistent observation, both spectroscopic and photometric, for 5 or 10 years of the brighter symbiotic stars would surely help us understand their mysterious behaviors and might develop ideas of considerable general interest." Merrill (1958).

This recommendation has been followed notably by S.J. Kenyon and J. Mikolajewska during the '80s and '90s producing monographic studies of these targets (e.g., Mikolajewska & Kenyon, 1992).

We continue this effort in the spirit of producing results that may constrain the models.

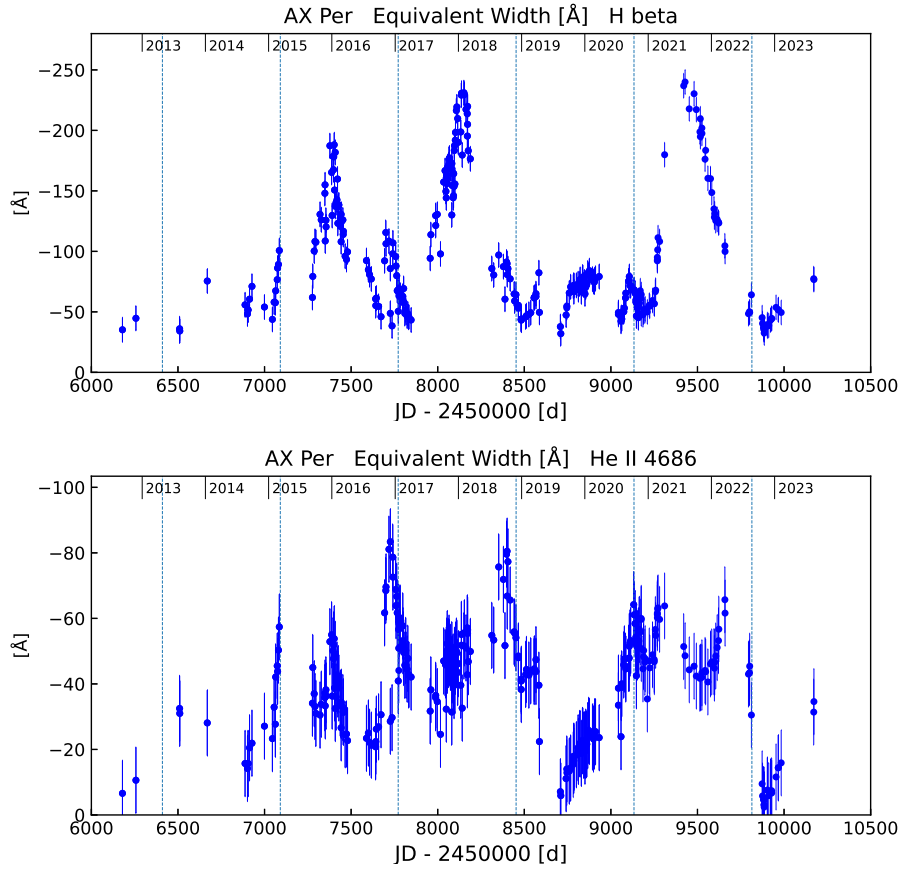


Figure 2. AX Per long term monitoring. Equivalent widths of $H\beta$ and He II 4686 Å emission lines during 10 years. The vertical dashed lines mark the epoch of the mid-eclipse of the hot component.

4. An eclipse in the symbiotic star BX Mon

BX Mon is an eclipsing symbiotic system. The orbital period of 1259 ± 16 days is long and the eccentricity (0.444 ± 0.067) is high for a classical symbiotic (Fekel et al., 2000). Moreover, historical photometric studies produced inconsistent values of the photometric period (Leibowitz & Formigini, 2011). In March-April of 2022, we obtained a series of spectra showing the egress of an eclipse.

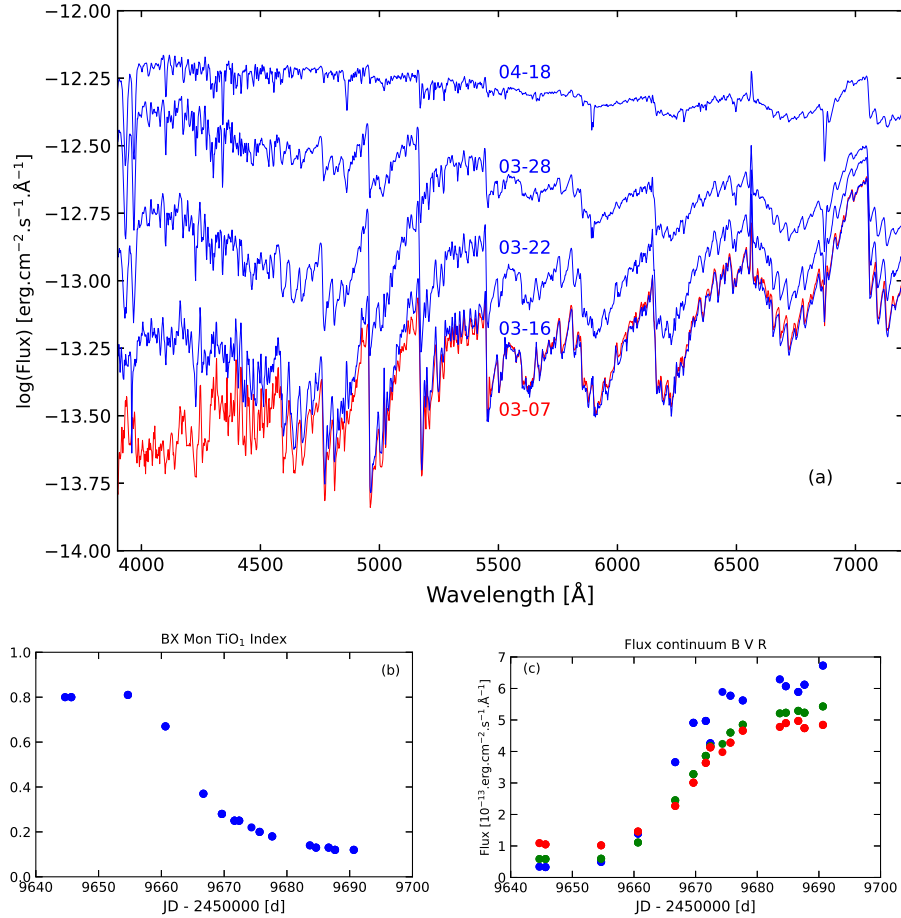


Figure 3. BX Mon spectral evolution during the egress of the eclipse (a). Variation of the TiO₁ index as the result of the overwhelming of the pseudo continuum of the red giant by the hot component (b). Evolution of the flux of the continuum in B, V, R (c).

Fig. 3 shows the spectral evolution of the egress with selected flux-calibrated spectra ($R=1000$) obtained by F. Sims and F. Boubault. The first spectra of our series are almost constant which we attribute to the fact that the hot component is fully eclipsed. The TiO_1 index described by Kenyon & Fernandez-Castro (1987) is 0.8 corresponding to a M5.8 III red giant. The change in the TiO_1 index describes the progressive overwhelming of the red giant spectrum by the hot component (Fig. 3b). This is also reflected in the evolution of the flux of the continuum measured at wavelengths $4361 \pm 10 \text{ \AA}$, $5448 \pm 10 \text{ \AA}$, $6407 \pm 10 \text{ \AA}$ (B, V, R in Fig. 3c) showing the strengthening of the blue part of the composite continuum.

5. Recurrent symbiotic nova T CrB before its next nova event

T CrB is an accretion-powered symbiotic which experienced two nova events in 1866 and 1946 making it a member of the small group of recurrent novae. The next nova event is expected in the next several years (Luna et al., 2020). Between the two nova-type outbursts, T CrB shows active phases during several years characterized by a brightening in B and V bands, an increase in the intensities of the emission lines, and the ionization level (He II). The last active phase began in 2014 (Ikiewicz et al., 2016; Munari et al., 2016). Ikiewicz et al. (2023) interpret the small and big active phases as an extreme case of dwarf nova outbursts and superoutbursts of SU UMa - type.

Our constant monitoring (850 spectra since 2012) allows tracing the evolution of the last superoutburst illustrated in Fig. 4 (a). The equivalent width of He II peaked ($\text{EW} \approx 18$) in 2015 then declined monotonically until 2020 followed by a plateau with a remarkable burst to $\text{EW} \approx 12$ in 2022 around JD 2459800. The high cadence coverage allowed us to detect precisely the end of the big active state in 2023 April on JD 2460046 ± 5 (Teyssier et al., 2023) with the sudden decrease of the equivalent widths of the emission lines (Balmer, He II, HeI) as shown in Fig. 4 (b) ($\text{H}\alpha$ equivalent width).

Since then, both the lightcurve and the spectrum continue to evolve as before the active state according to double waved orbital phase shown in Fig. 4 (c). Ephemeris: $\text{JD} = 2435687.6 (\pm 1.3) + 227.67 (\pm 0.02) \text{ E}$ (Lines et al., 1988).

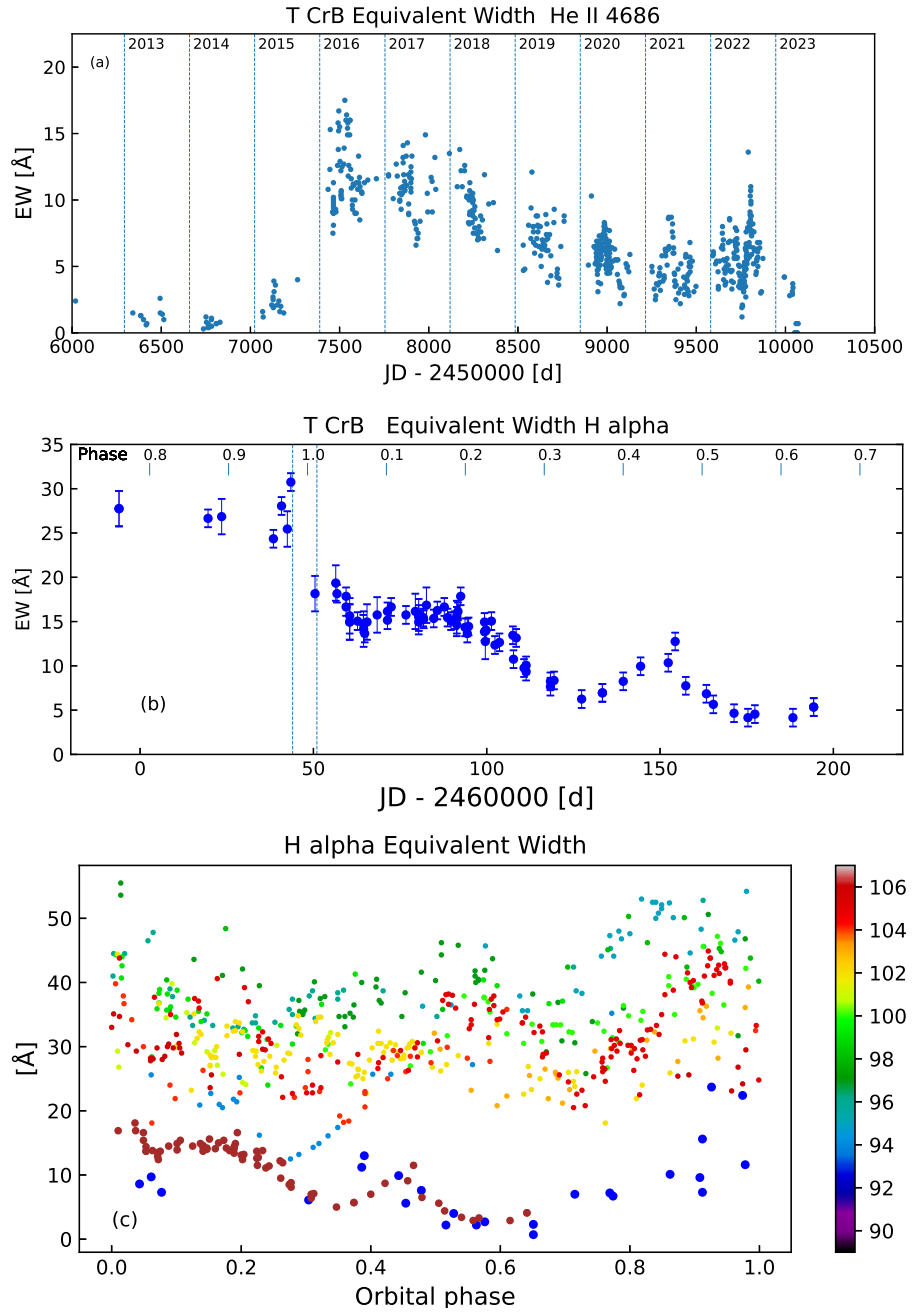


Figure 4. T CrB. Equivalent width of He II 4686 Å during the big active state 2015-2023. (a). The detection of the end of the active state in April 2023 (b). Variations of H α equivalent width according to the orbital phase. The current cycle (brown) matches with the last cycle before the active state (blue) (c)

Acknowledgements. We thank the organizers of the Conference for their invitation and the anonymous referee for his detailed proofreading of our manuscript. We are grateful to the many observers who contribute to this project⁵. We express our deep gratitude to Steven N. Shore (PISA-IT University) for his continued support of the project and to all professional teams who give us their confidence by using our spectra for their studies.

References

- Aydi, E., Chomiuk, L., Strader, J., et al., Revisiting the classics: On the evolutionary origin of the “Fe II” and “He/N” spectral classes of novae. 2023, *arXiv e-prints*, arXiv:2309.07097, DOI: 10.48550/arXiv.2309.07097
- Azzollini, A., Shore, S. N., Kuin, P., & Page, K. L., Multi-wavelength spectroscopic study of shock-driven phenomena in explosive outbursts in symbiotic-like recurrent novae with an emphasis on RS Ophiuchi. 2023, *Astronomy and Astrophysics*, **674**, A139, DOI: 10.1051/0004-6361/202245185
- Fekel, F. C., Joyce, R. R., Hinkle, K. H., & Skrutskie, M. F., Infrared Spectroscopy of Symbiotic Stars. I. Orbits for Well-Known S-Type Systems. 2000, *Astronomical Journal*, **119**, 1375, DOI: 10.1086/301260
- Ikiewicz, K., Mikołajewska, J., Scaringi, S., et al., SU Lyn - a transient symbiotic star. 2022, *Monthly Notices of the RAS*, **510**, 2707, DOI: 10.1093/mnras/stab3637
- Ikiewicz, K., Mikołajewska, J., Stoyanov, K., Manousakis, A., & Miszalski, B., Active phases and flickering of a symbiotic recurrent nova T CrB. 2016, *Monthly Notices of the RAS*, **462**, 2695, DOI: 10.1093/mnras/stw1837
- Ikiewicz, K., Mikołajewska, J., & Stoyanov, K. A., Symbiotic Star T CrB as an Extreme SU UMa-type Dwarf Nova. 2023, *Astrophysical Journal, Letters*, **953**, L7, DOI: 10.3847/2041-8213/ace9dc
- Kenyon, S. J. & Fernandez-Castro, T., The Cool Components of Symbiotic Stars. I. Optical Spectral Types. 1987, *Astronomical Journal*, **93**, 938, DOI: 10.1086/114379
- Leibowitz, E. M. & Formiggini, L., Period switching in the symbiotic star BX Mon. 2011, *Monthly Notices of the RAS*, **414**, 2406, DOI: 10.1111/j.1365-2966.2011.18558.x
- Lines, H. C., Lines, R. D., & McFaul, T. G., UBVRI Photometry of the Recurrent Nova T Coronae Borealis. 1988, *Astronomical Journal*, **95**, 1505, DOI: 10.1086/114746
- Luna, G. J. M., Sokoloski, J. L., Mukai, K., & M. Kuin, N. P., Increasing Activity in T CrB Suggests Nova Eruption Is Impending. 2020, *Astrophysical Journal, Letters*, **902**, L14, DOI: 10.3847/2041-8213/abbb2c
- Merrill, P. W., 51. Symbiosis in Astronomy: Introductory Report. 1958, in *Liege International Astrophysical Colloquia*, Vol. **8**, *Liege International Astrophysical Colloquia*, 436–448

⁵<https://aras-database.github.io/database/observers.html>

- Mikolajewska, J. & Kenyon, S. J., On the Nature of the Symbiotic Binary AX Persei. 1992, *Astronomical Journal*, **103**, 579, DOI: 10.1086/116085
- Muerset, U., Nussbaumer, H., Schmid, H. M., & Vogel, M., Temperature and luminosity of hot components in symbiotic stars. 1991, *Astronomy and Astrophysics*, **248**, 458
- Munari, U., Dallaporta, S., & Cherini, G., The 2015 super-active state of recurrent nova T CrB and the long term evolution after the 1946 outburst. 2016, *New Astronomy*, **47**, 7, DOI: 10.1016/j.newast.2016.01.002
- Muerset, U. & Schmid, H. M., Spectral classification of the cool giants in symbiotic systems. 1999, *Astronomy and Astrophysics, Supplement*, **137**, 473, DOI: 10.1051/aas:1999105
- Skopal, A., New Ephemeris of the Eclipsing Symbiotic Star AX Per. 1991, *Information Bulletin on Variable Stars*, **3603**, 1
- Skopal, A., Shugarov, S. Y., Sekeráš, M., et al., New outburst of the symbiotic nova AG Pegasi after 165 yr. 2017, *Astronomy and Astrophysics*, **604**, A48, DOI: 10.1051/0004-6361/201629593
- Teyssier, F., Eruptive stars monitoring and the ARAS database. 2019, *Contributions of the Astronomical Observatory Skalnaté Pleso*, **49**, 217
- Teyssier, F., Hinnefeld, J. D., Boussin, C., et al., T CrB: the active spectroscopic state (2014-2023) is over. 2023, *The Astronomer's Telegram*, **16109**, 1

V1006 Cyg: SU UMa-type dwarf nova in the period gap that wobbles between subclasses

E. Pavlenko¹, S. Shugarov^{2,3}, T. Kato⁴, O. Antonyuk¹,
A. Sosnovskij¹, Ju. Babina¹, A. Shchurova², K. Isogai^{5,6}, A. Sklyanov⁷,
A. Gutaev⁷, R. Zhuchkov⁷, P. Dubovsky⁸, K. Petrik⁹ and
J. Hamsch¹⁰

¹ *Crimean Astrophysical Observatory of RAS Nauchny, Crimea 298409
(E-mail: eppavlenko@gmail.com)*

² *Astronomical Institute of the Slovak Academy of Sciences
059 60 Tatranská Lomnica, The Slovak Republic*

³ *Sternberg Astronomical Institute, Moscow State University, Universitetskij
pr., 13, Moscow, 119991, Russia*

⁴ *Department of Astronomy, Kyoto University, Kitashirakawa-Oiwake-cho,
Sakyo-ku, Kyoto, Kyoto 606-8502, Japan*

⁵ *Okayama Observatory, Kyoto University, 3037-5 Honjo, Kamogatacho,
Asakuchi, Okayama 719-0232, Japan*

⁶ *Department of Multi-Disciplinary Sciences, Graduate School of Arts and
Sciences, The University of Tokyo, 3-8-1 Komaba, Meguro, Tokyo
153-8902, Japan*

⁷ *Kazan Federal University, Kremlevskaya Street 18, 420008, Kazan, Russia*

⁸ *Vihorlat Observatory, Mierova 4, 06601 Humenne, Slovakia*

⁹ *M.R. Stefanik Observatory and Planetarium, Sladkovicova 41, 92001
Hlohovec, Slovakia*

¹⁰ *Vereniging voor Sterrenkunde, werkgroep veranderlijke sterren, Oostmeers
122 C, B-8000 Brugge, Belgium*

Received: November 3, 2023; Accepted: January 29, 2024

Abstract. We present a result of the multi-longitude campaign on a photometric investigation of the SU UMa-type dwarf nova in the period gap, V1006 Cyg in 2023. It displayed a long-lasting standstill (a feature of Z Cam-type stars) terminated by a long outburst (a feature of IW And stars). The long outburst did not have superhumps (a feature of SS Cyg-type stars) but showed orbital 0.09837(22) d periodicity instead. Color-color diagrams indicate that layers of the disk of different temperatures contribute to the total radiation of the system. In particular, a large contribution from the innermost hot layers is detected in quiescence.

Key words: accretion, accretion disks – cataclysmic variables – stars: dwarf novae – stars: individual: V1006 Cyg

1. Introduction

Non-magnetic cataclysmic variable stars (CVs) are close binary systems where a late-type component filling its Roche lobe loses matter on the white dwarf. CVs could be divided into three subclasses: SU UMa-type, Z Cam-type and U Gem-type (or SS Cyg-type). Originally this division was based on the morphology of the light curves (Warner, 1995). According to Warner, a distinctive feature of Z Cam-type stars is protracted standstills that are terminated by fading. There is a subgroup of "anomalous" Z Cam-type stars, IW And-type objects, displaying standstill terminated by brightening (Kato, 2019). SU UMa stars have two types of outbursts – superoutbursts lasting a couple of weeks and normal outbursts which are less bright and as short as 2-4 d; SS Cyg-type stars are neither Z Cam nor SU UMa stars. Osaki (2005) proposed that different outburst behaviour of non-magnetic CVs may be explained in a framework of disk instability model which uses two instabilities: thermal instability and tidal instability of accretion disk. There are two parameters characterizing accretion disks: mass transfer rate from the secondary component and the orbital period (or mass ratio). A period gap is a borderline region that determines the ability of CVs to undergo tidal instability (below the gap) or not (above the gap). Another borderline is a critical mass transfer rate \dot{M}_{crit} (Osaki, 1996). While CVs with mass-transfer rate higher than \dot{M}_{crit} are hot and exhibit "stable" disks, CVs with mass-transfer rate less than \dot{M}_{crit} , are in the region of thermal instability and show outbursts. Thus, accretion disks of U-Gem-type stars that have orbital periods longer than those in the "gap", are thermally unstable but tidally stable. SU UMa-type stars with orbital periods less than the gap have disks that are both thermally and tidally unstable. Z Cam-type stars are located close to the \dot{M}_{crit} and with periods above the gap. So the period gap is a region where these two instabilities intersect and therefore there is a possibility that some CVs in this region may have properties of neighboring subclasses.

As a dwarf nova V1006 Cyg is known since 1963 (Hoffmeister, 1963). Sheets *et al.* (2007) found that the orbital period of binary is 0.09903(9) d which classified it as a dwarf nova in the period gap. The 2006 outburst was suspected to be a superoutburst. Finally, V1006 Cyg was identified as the SU UMa-type dwarf nova in the period gap based on the results of studies during the 2015 superoutburst (Kato *et al.*, 2016). V1006 Cyg got attention not only by its localization in the period gap but also by detection in 2007, 2009 and 2017 of long outbursts without superhumps but with orbital-related brightness variations (Pavlenko *et al.*, 2014, 2018). It was also found that this star showed three types of outbursts – normal, long normal and superoutbursts (Kato *et al.*, 2016). A diversity of normal outbursts makes V1006 Cygnus look like the SS Cyg-type star.

2. Observations and data reduction

CCD photometry of V1006 Cyg has been carried out with eight telescopes at seven observatories during 72 nights in 2023. Most of the observations were made in unfiltered light corrected to R_C . In selected nights of outburst and quiescence, V1006 Cyg was observed in the Johnson-Cousins $UBVR_CI_C$ colour bands (see Tab.1). We used the $UBVR_CI_C$ values of comparison star No 140 as in the paper by Pavlenko et al. (2018) and $U = 15^m.58$ for this star obtained relatively to the stars with known magnitudes in the vicinity of CH Cyg (Henden & Munari, 2006). Standard data reduction included flat-fielding, bias and dark signal removal. The MAXIM DL and Goranskij (<http://www.vgoranskij.net/software/>) WinFit packages were used. A periodogram analysis was done with the help of the Stellingwerf method implemented in the Pelt (1992) package.

3. 2023 overall light curve

Our observations are shown in Fig 1. They start from JD 2460076 capturing the decline of outburst superposed on the quiescent state at mean brightness about $R_C \sim 16^m.4$ that turned out to be $1^m - 1^m.5$ magnitudes brighter compared to known previous observations in 2015-2017 (Pavlenko et al., 2018). This "bright" quiescence which lasted \sim three weeks, was terminated by the next long outburst with a duration of 10 d and amplitude of $\sim 2^m.5$. This behaviour resembles those in the IW And-type dwarf novae, where a quiescence terminates by outburst. After the end of the outburst, V1006 Cyg returned to its "usual" quiescent state, the return itself lasted about a couple of weeks. We did not detect any outburst during ~ 3.5 months after the long outburst. Note that during the 2015-2017 quiescence there was a brief episode of increased brightness around normal outburst No 3 (see Fig. 1 in Pavlenko et al. (2018)).

4. Brightness variations in outburst and quiescence

During the long outburst short-term periodical brightness variations were detected. The outburst and nightly light curves are shown in Fig 2. It is seen that these variations existed on the two nights at the top of the outburst and one night at the outburst decline (HJD 2460108-2460110). Variations at the JD 2460111 were not detected. A periodogram calculated for data of these three nights after the removal of the trend corresponding to the outburst profile, is shown in Fig 3, a. The most significant peak on the periodogram corresponds to the 0.09837(22) d period which, within the limits of error, coincides with known orbital period estimates. The phased light curve was calculated using the zero-epoch HJD=24060108.40317 and period 0.09837 d (Fig 3, b).

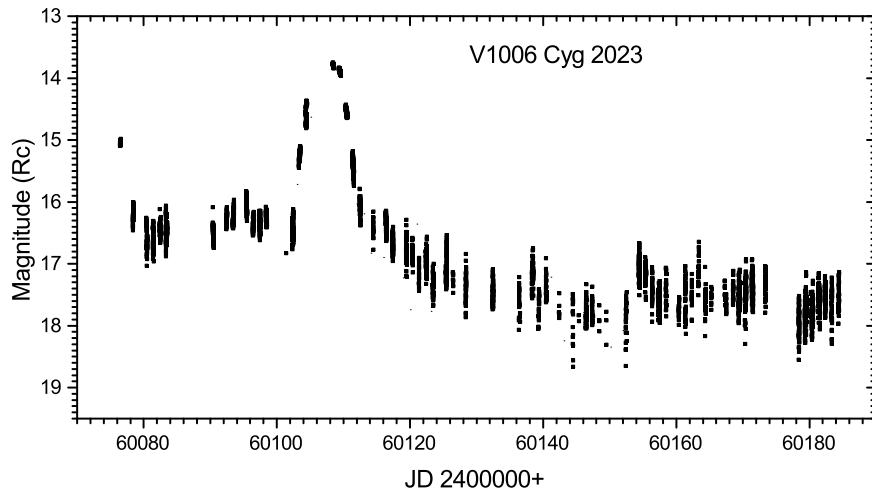


Figure 1. Long-term 2023 light curve.

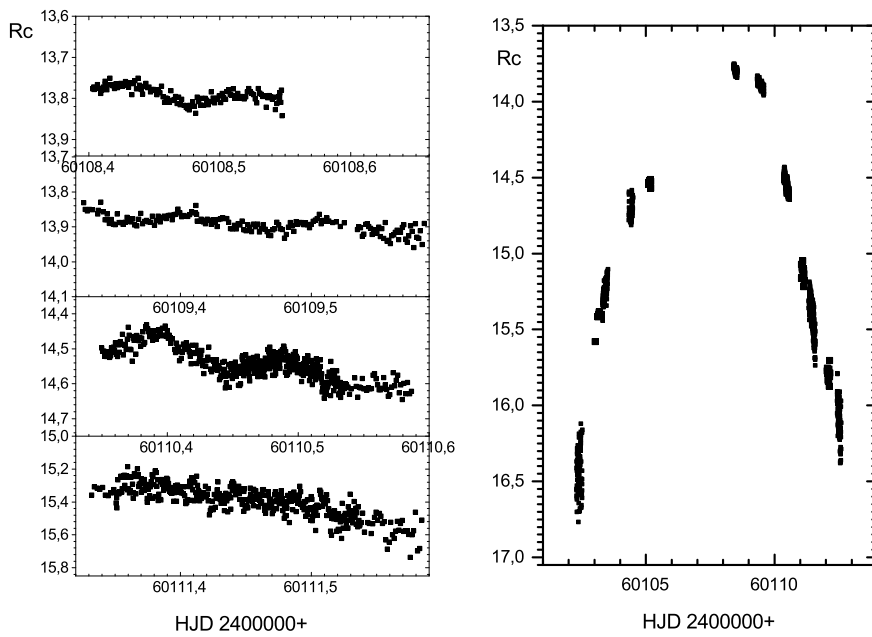


Figure 2. Short-term periodic variations in the R_C band (left) during the long outburst (right).

A mean R_C light curve has a symmetric profile and amplitude of $0^m.05$. Note that 2007 and 2009 orbital light curves displayed similar profiles (Pavlenko et al., 2014).

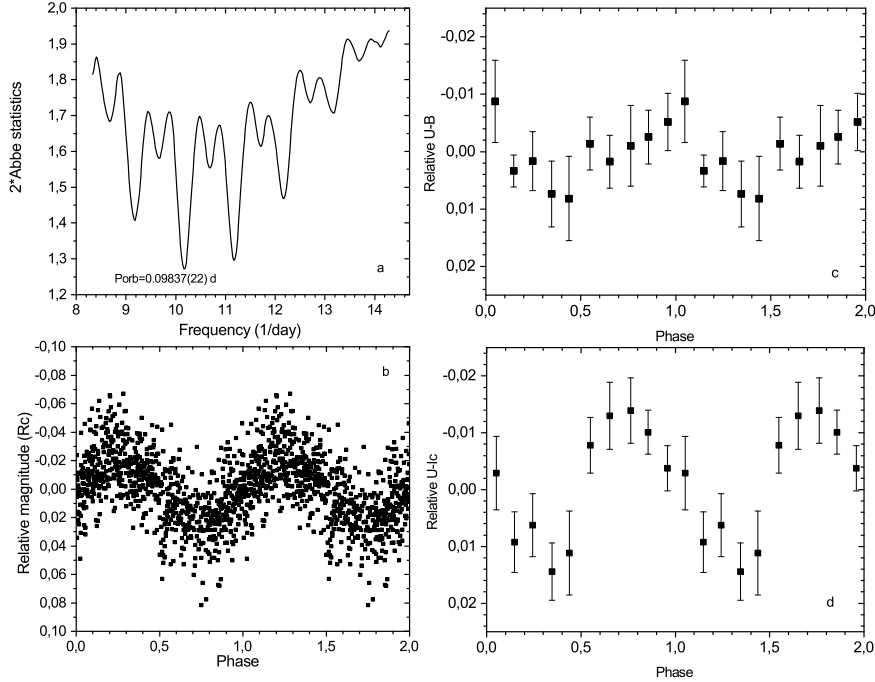


Figure 3. Orbital period of V1006 Cyg during the long outburst. Periodogram (a), R_C data from HJD 2460108, 2460109, 2460110, and mean $U - B$ and $U - I_C$ data from HJD 2460108, 2460109 folded on the orbital period 0.09837 d (b, c, d respectively).

For HJD 2460108 and 2460109 we calculated phase-resolved colour indices after removing the trend corresponding to the outburst profile. We have done this procedure for the closest colour bands $U - B$ and for the most distant wavelengths $U - I_C$ (see Fig 3, c and d, respectively). The mean amplitude in V is $0^m.016$. The $U - B$ and $U - I_C$ light curves displayed dependence on the phase of the orbital period with amplitudes $0^m.012$ in $U - B$ and $0^m.028$ in $U - I_C$. The blue peak of both $U - B$ and especially $U - I_C$ curves coincides with a minimum of the V light curve. We interpret these light curves as being caused by a hot spot on the disk. However, this behaviour is opposite to that observed in light curves, where the main contribution to the emission comes from the hot spot. We suppose that the ultraviolet excess at minimum is caused by a contribution from the innermost part of the accretion disk that is hotter

than the hot spot.

Characteristic of the quiescence is the presence of quasi-periodic oscillations (QPOs) in a range of minutes-hours. An example of short-term QPOs is shown in Fig 4,a. These QPOs were coherent on a scale of at least about an hour (see Fig 4, b). As during 2016 quiescence, no evidence of an orbital period was found in 2023 quiescence (Pavlenko *et al.*, 2018).

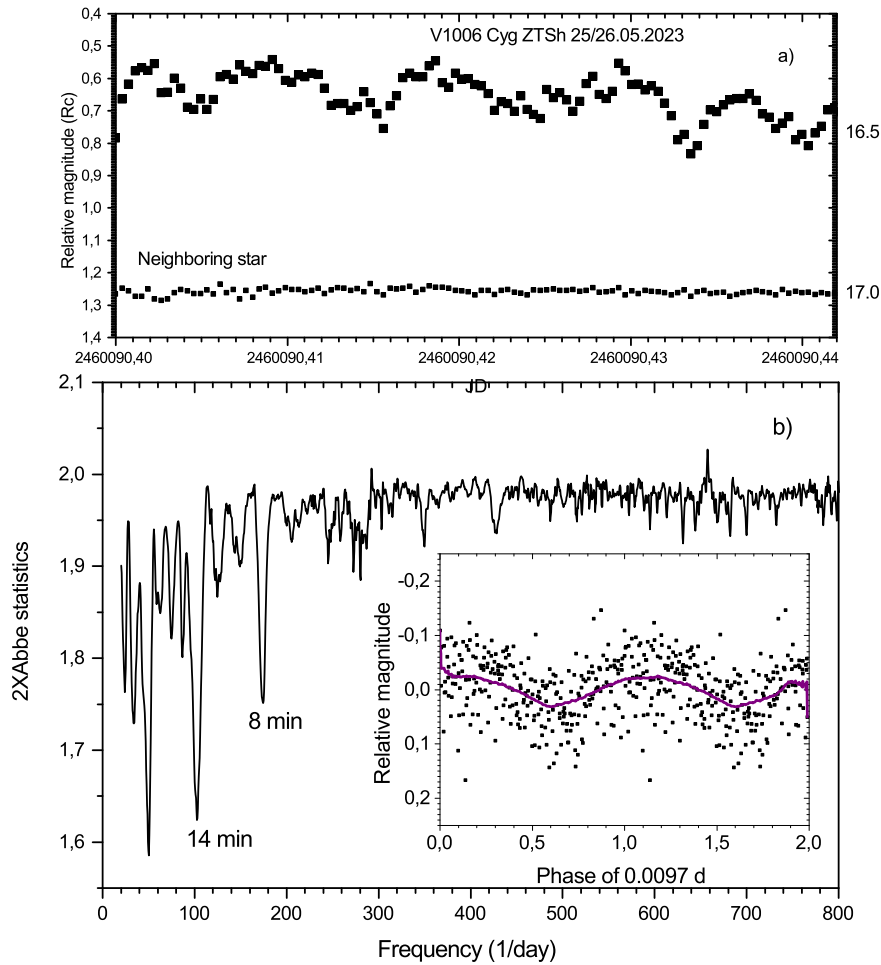


Figure 4. Example of nightly light curve in quiescence displaying short-term QPOs (a); periodogram and data folded on the 14-min period (b).

5. Colour variations

Colour-colour diagrams including changes in colour indices of V1006 Cyg during the transition from outburst to quiescence are shown in Fig 5. One could see that in U-B the object has a higher temperature at quiescence than at outburst. The opposite behaviour is observed in the region of longer wavelengths: radiation of the object is hotter at outburst compared to quiescence. This may mean that the radiation can come from the parts of the disk with different temperatures. In quiescence, the disk returns to a cold state, and its size decreases significantly. In this case, it is natural that the contribution to the total radiation of the hottest innermost layers of the disk increases. This can explain the ultraviolet excess in a quiet state in the $U - B, B - V$ diagram. Similar behaviour of colour indices was noted by Golysheva & Shugarov (2014) for the dwarf nova PNV J19150199+071947.

Table 1. Journal of observations

| HJD 2460000+ (start - end) | Observatory/telescope | CCD | N |
|-------------------------------|-----------------------|----------------|-----|
| 076.460 - 076.556 | SLO/0.60m | FLI ML3041 | 74 |
| 078.353 - 078.523 | SLO/0.60m | FLI ML3041 | 73 |
| 080.313 - 080.549 | CrAO/0.38m | Apogee E47 | 94 |
| 081.358 - 081.536 | CrAO/0.38m | Apogee E47 | 82 |
| 082.386 - 082.545 | CrAO/0.38m | Apogee E47 | 76 |
| 083.295 - 083.545 | CrAO/0.38m | Apogee E47 | 118 |
| 090.347 | SLO/0.60m | FLI ML3041 | 1 |
| 090.389 - 090.485 | CrAO/2.60m | Apogee E47 | 252 |
| 092.389 - 092.522 | SLO/0.60m | FLI ML3041 | 99 |
| 093.356 - 093.554 | SLO/0.60m | FLI ML3041 | 120 |
| 095.364 - 095.488 | SLO/0.60m | FLI ML3041 | 124 |
| 096.389 - 096.541 | SLO/0.60m | FLI ML3041 | 118 |
| 097.360 - 097.545 | SLO/0.60m | FLI ML3041 | 105 |
| 098.329 - 098.516 | KAZ/1.10m m | QSI 583wsg | 51 |
| 101.380 - 101.471 | CrAO/0.38m | Apogee E47 | 2 |
| 102.301 - 102.525 | CrAO/0.38m | Apogee E47 | 98 |
| 103.031 - 103.186 | JAP/0.50m | Apogee Alta F6 | 4 |
| 103.307 - 103.521 | CrAO/0.38m | Apogee E47 | 102 |
| 104.335 - 104.496 | CrAO/0.38m | Apogee E47 | 77 |
| 104.299 - 104.525 | KAZ/1.10m m | QSI 583wsg | 61 |
| 105.110 - 105.191 | JAP/0.50m | Apogee Alta F6 | 11 |
| 108.403 - 108.546 | SLO/0.60m | FLI ML3041 | 129 |
| 109.326 - 109.419 | SLO/0.60m | FLI ML3041 | 133 |
| 110.350 - 110.532 | SLO1/0.60m | Atik 383L | 237 |
| 111.041 - 111.148 | JAP/0.50m | Apogee Alta F6 | 14 |

Table 1. Journal of observations (continued)

| HJD 2460000+ (start - end) | Observatory/telescope | CCD | N |
|-------------------------------|-----------------------|----------------|-----|
| 111.350 - 111.537 | SLO1/0.60 | Atik 383L | 243 |
| 111.476 - 111.584 | Bel/0.40 | FLI 16803 | 84 |
| 111.332 - 111.466 | CrAO/0.38m | Apogee E47 | 51 |
| 112.046 - 112.151 | JAP/0.50mm | Apogee Alta F6 | 14 |
| 112.461 - 112.527 | CrAO/0.38m | Apogee E47 | 32 |
| 114.495 - 114.531 | CrAO/0.38m | Apogee E47 | 18 |
| 116.468 - 116.521 | CrAO/0.38m | Apogee E47 | 141 |
| 117.390 - 117.481 | CrAO/0.38m | Apogee E47 | 126 |
| 119.395 - 119.533 | CrAO/0.38m | Apogee E47 | 64 |
| 120.335 - 120.437 | CrAO/0.38m | Apogee E47 | 38 |
| 121.323 - 121.365 | CrAO/0.38m | Apogee E47 | 21 |
| 122.364 - 122.526 | SLO/0.60m | FLI ML3041 | 108 |
| 123.401 - 123.537 | SLO/0.60m | FLI ML3041 | 60 |
| 125.371 - 125.521 | SLO/0.60m | FLI ML3041 | 97 |
| 126.447 - 126.496 | CrAO/0.38m | Apogee E47 | 10 |
| 128.361 - 128.425 | SLO/0.60m | FLI ML3041 | 57 |
| 132.371 - 132.476 | SLO/0.60m | FLI ML3041 | 85 |
| 136.372 - 136.507 | CrAO/2.60m | Apogee E47 | 26 |
| 138.296 - 138.546 | CrAO/2.60m | Apogee E47 | 78 |
| 139.309 - 139.397 | CrAO/2.60m | Apogee E47 | 30 |
| 140.407 - 140.521 | KAZ/1.10m | QSI 583wsg | 24 |
| 140.443 - 140.492 | CrAO/0.38m | Apogee E47 | 3 |
| 142.391 - 142.410 | KAZ/1.10m | QSI 583wsg | 6 |
| 142.409 | CrAO/0.38m | Apogee E47 | 1 |
| 144.429 - 144.478 | KAZ/1.10m | QSI 583wsg | 13 |
| 144.507 | CrAO/0.38m | Apogee E47 | 1 |
| 145.336 - 145.358 | KAZ/1.10m | QSI 583wsg | 2 |
| 146.384 - 146.508 | SLO/0.60m | FLI ML3041 | 80 |
| 146.422 - 146.465 | KAZ/1.10m | QSI 583wsg | 7 |
| 147.352 - 147.477 | CrAO/0.38m | Apogee E47 | 25 |
| 148.428 - 148.464 | KAZ/1.10m | QSI 583wsg | 4 |
| 149.491 - 149.524 | CrAO/0.38m | Apogee E47 | 3 |
| 152.381 - 152.510 | SLO/0.60m | FLI ML3041 | 29 |
| 154.359 - 154.541 | CrAO/0.38m | Apogee E47 | 141 |
| 154.378 - 154.382 | SLO/0.60m | FLI ML3041 | 2 |
| 155.338 - 155.377 | SLO/0.60m | FLI ML3041 | 30 |
| 155.361 - 155.404 | CrAO/0.38m | Apogee E47 | 21 |
| 156.344 - 156.370 | CrAO/0.38m | Apogee E47 | 13 |
| 156.347 - 156.416 | SLO/0.60m | FLI ML3041 | 35 |
| 157.393 - 157.420 | SLO/0.60m | FLI ML3041 | 31 |

Table 1. Journal of observations (continued)

| HJD 2460000+ (start - end) | Observatory/telescope | CCD | N |
|-------------------------------|-----------------------|------------|-----|
| 160.344 - 160.425 | SLO/0.60m | FLI ML3041 | 29 |
| 161.326 - 161.428 | CrAO/0.38m | Apogee E47 | 49 |
| 162.308 - 162.344 | CrAO/0.38m | Apogee E47 | 18 |
| 163.317 - 163.377 | CrAO/0.38m | Apogee E47 | 29 |
| 164.314 - 164.386 | CrAO/0.38m | Apogee E47 | 35 |
| 165.272 - 165.305 | CrAO/2.60m | Apogee E47 | 11 |
| 167.269 - 167.320 | CrAO/2.60m | Apogee E47 | 14 |
| 169.331 - 169.413 | CrAO/0.38m | Apogee E47 | 40 |
| 170.311 - 170.397 | CrAO/0.38m | Apogee E47 | 42 |
| 173.341 - 173.430 | CrAO/0.38m | Apogee E47 | 43 |
| 178.348 - 178.494 | CrAO/0.38m | Apogee E47 | 67 |
| 179.295 - 179.543 | CrAO/0.38m | Apogee E47 | 129 |
| 180.275 - 180.542 | CrAO/0.38m | Apogee E47 | 126 |
| 181.312 - 181.410 | CrAO/0.38m | Apogee E47 | 47 |
| 183.288 - 183.387 | CrAO/0.38m | Apogee E47 | 48 |
| 184.351 - 184.440 | CrAO/0.38m | Apogee E47 | 41 |
| 202.346 - 202.490 | CrAO/0.38m | Apogee E47 | 69 |
| 205.301 - 205.388 | CrAO/0.38m | Apogee E47 | 42 |
| 206.342 - 206.435 | CrAO/0.38m | Apogee E47 | 42 |
| 209.340 - 209.397 | CrAO/0.38m | Apogee E47 | 28 |
| 212.323 - 212.391 | CrAO/0.38m | Apogee E47 | 33 |
| 222.251 - 222.474 | CrAO/0.38m | Apogee E47 | 111 |

Description of columns:

HJD 2460000+ (start-end): begin and end of observational run.

Observatory: SLO - Tatranska Lomnica, Slovakia; SLO1 - M.R. Stefanik Observatory and Planetarium, Slovakia; CrAO - Crimean astrophysical observatory, Republic of Crimea; KAZ - Kazan Federal University, Russia Federation; JAP - MITSuME telescope of Okayama Astrophysical Observatory, Japan; Bel - Association for Astronomy, Brugge, Belgium.

CCD: CCD camera type. N: number of observations.

6. Conclusion

We presented the results of multi-longitudinal 71-d photometric monitoring of the SU UMa-type dwarf nova in the period gap, V1006 Cyg in 2023. This dwarf nova showed that being a star of the SU UMa type, it can have properties of various subclasses – SS Cyg-type, Z Cam-type and IW And-type. Thus the dwarf nova V1006 Cyg shows that a division between CV subclasses may not be so sharp and deviations from standard behavior may not be so rare.

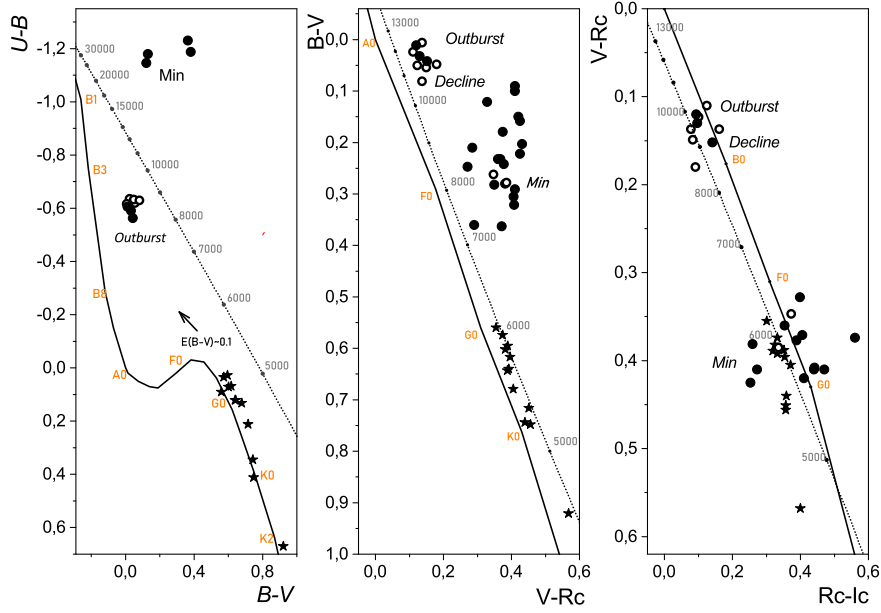


Figure 5. Two-colour diagrams. The dotted lines denote the black body sequence with a Kelvin scale marked along it. The Main sequence is designated by a solid line, the spectral classes are marked. The system state is indicated: outburst, fading or quiescence (Min). Data for the 2023 are indicated by filled circled and for the 2015 (Pavlenko et al., 2018) - by open circles. The positions of surrounding stars (shown by filled stars) are also plotted.

Acknowledgements. We thank the referee Augustín Skopal for useful comments and suggestions. The authors are grateful to N.Ikonnikova, A.Simon and V.Goranskij for help in observations. The work of Shugarov was financially supported by the Slovak Research and Development Agency under the contract No. APVV-20-0148 and by the Slovak Academy of Sciences grant VEGA 2/0030/21. The observations made by Isogai were partially supported by the Optical and Infrared Synergetic Telescopes for Education and Research (OISTER) program and Grants-in-Aid for Scientific Research 17H06362 funded by the MEXT of Japan. The work of Sklyanov was supported by the subsidy No FZSM-2023-0015 of the Ministry of Education and Science of the Russian Federation allocated to the Kazan Federal University for the State assignment in the sphere of scientific activities.

References

- Golysheva, P. & Shugarov, S., Multicolor photometric monitoring of a new WZ Sge-type star in Aquila. 2014, *Contributions of the Astronomical Observatory Skalnaté Pleso*, **43**, 312

- Henden, A. & Munari, U., UBVR(I)C photometric sequences for symbiotic stars. III. 2006, *Astronomy and Astrophysics*, **458**, 339, DOI: 10.1051/0004-6361:20065662
- Hoffmeister, C., Neue veränderliche Sterne. 1963, *Astronomische Nachrichten*, **287**, 169, DOI: 10.1002/asna.19632870403
- Kato, T., Three Z Camelopardalis-type dwarf novae exhibiting IW Andromedae-type phenomenon. 2019, *Publications of the ASJ*, **71**, 20, DOI: 10.1093/pasj/psy138
- Kato, T., Pavlenko, E. P., Shchurova, A. V., et al., V1006 Cygni: Dwarf nova showing three types of outbursts and simulating some features of the WZ Sge-type behavior. 2016, *Publications of the ASJ*, **68**, L4, DOI: 10.1093/pasj/psv138
- Osaki, Y., Dwarf-Nova Outbursts. 1996, *Publications of the ASP*, **108**, 39, DOI: 10.1086/133689
- Osaki, Y., The disk instability model for dwarf nova outbursts. 2005, *Proceedings of the Japan Academy, Series B*, **81**, 291, DOI: 10.2183/pjab.81.291
- Pavlenko, E. P., Kato, T., Antonyuk, O. I., et al., NY Serpentis: SU UMa-type nova in the period gap with diversity of normal outbursts. 2014, *Publications of the ASJ*, **66**, 111, DOI: 10.1093/pasj/psu099
- Pavlenko, E. P., Shugarov, S. Y., Simon, A. O., et al., Long-period SU UMa dwarf nova V1006 Cygni: outburst activity and variability at different brightness states in 2015 — 2017. 2018, *Contributions of the Astronomical Observatory Skalnaté Pleso*, **48**, 339, DOI: 10.48550/arXiv.1806.07638
- Pelt, J. 1992, *Irregularly Spaced Data Analysis User Manual*
- Sheets, H. A., Thorstensen, J. R., Peters, C. J., Kapusta, A. B., & Taylor, C. J., Spectroscopy of Nine Cataclysmic Variable Stars. 2007, *Publications of the ASP*, **119**, 494, DOI: 10.1086/518698
- Warner, B., Cataclysmic variable stars. 1995, *Cambridge Astrophysics Series*, **28**

Nova Herculi 2021 as an intermediate polar

P.A. Dubovský¹, K. Petrík² and V. Breus³

¹ *Vihorlat Observatory in Humenné, Slovakia*

² *Observatory and Planetarium M. R. Štefánik in Hlohovec, Slovakia*

³ *Department of Mathematics, Physics and Astronomy, Odessa National Maritime University, Odessa, Ukraine*

Received: November 7, 2023; Accepted: January 22, 2024

Abstract. We report the results of observations of Nova Herculi 2021 - V1674 Her. The object is characterized by several exceptional properties. The progenitor was identified as an intermediate polar. The speed of the outflow reached 10000 km s^{-1} . The brightness decline was exceptionally rapid: $t_2 \cong 1.2 d$, $t_3 \cong 3 d$. The pulse spin signal was detected in photometry soon after the nova eruption. Extremely fast spin-up of the white dwarf rotation was measured. Despite challenges in cycle counting, we successfully constructed the O-C diagram of spin pulse maxima based on three seasons of observations. The result suggests a stable spin acceleration, with an anticipated gradual decline over the next decades. Additionally, we investigated the evolution of the orbital period.

Key words: cataclysmic variables – novae

1. Introduction

In recent years, the northern hemisphere has witnessed an elevated occurrence of nova eruptions. One of them is V1674 Her = Nova Herculi 2021. The nova outburst was discovered on 2021 June 12.537 UT by Seiji Ueda. Chandra satellite observed a strong X-ray signal with a period of 503.9 s (Maccarone et al., 2021). A similar period of 501.42 s was found by Mroz et al. (2021) in the Zwicky Transient Facility (ZTF) data obtained before the nova outburst. Another modulation with a period $0.15302(2) \text{ days}$ was reported by Shugarov & Afonina (2021). A substantial set of fast photometry optical data collected within the Center for Backyard Astrophysics (CBA) network was analyzed by Patterson et al. (2022). They concluded that the progenitor of the nova is an intermediate polar. The short period was linked to the spin of the white dwarf, and the longer one with the orbital motion. They also reported the exceptionally rapid spin period change. We know several novae with intermediate polar as the progenitor. GK Per, V4745 Sgr, and V2487 Oph, among them. But this is the first case when we know the pre-outburst spin period.

We regularly make intermediate polar observations within the "Inter - Longitude Astronomy" project (Andronov et al., 2003). The primary objective is to

monitor the spin period changes. The theory predicts oscillations between spin-up and spin-down. Most intermediate polars are observed spinning up (Patterson et al., 2020), possibly due to a selection effect associated with higher accretion rates linked to higher brightness. Our observational approach involves fast photometry runs lasting 3-4 hours, with the typical cadence of 1 run per month per target. This way, we can construct an O-C diagram of spin pulse maxima. Following the report of the pre-outburst spin period, we added V1674 Her to our list of observation targets.

2. Observations

In this work, we analyze data from two sites. On the Astronomical Observatory on Kolonica Saddle, the Vihorlat National Telescope VNT 1000/9000 mm and FLI PL1001E camera were used. The second site was M.R. Štefánik Observatory in Hlohovec, where Csere Telescope 600/2500 mm equipped with Atik 383L CCD Camera was employed. Both instruments work with B, V, Rc, Ic filters. However, the focus of our observing program primarily involved integral light without filters. The reason is the higher importance of a good signal-to-noise ratio for period analysis rather than color information. To effectively capture variations in the ~ 8 min spin period, we set the maximum exposure time at 120 s. The fast period change in this particular object requires a higher cadence of observations than in regular intermediate polar. So we made observations every suitable night. We were trying to accumulate observations on several consecutive nights to provide data for orbital period investigation. Ensemble differential photometry was employed for data reduction using CoLiTecVS (Kudzej et al., 2019) and MCV (Kim et al., 2004; Andronov & Baklanov, 2004) software packages.

In addition to our self-consistent dataset, we have used observations from the database of The American Association of Variable Star Observers (AAVSO), particularly focusing on the beginning of the 3rd observing season. These observing runs were acquired just after the solar conjunction, resulting in short runs with a relatively large error in the mean time of spin maxima. Nonetheless, these data were crucial for correct cycle counting between 2nd and 3rd season of observations.

3. Analysis

We used the trigonometric polynomial approximation of the light curve implemented in MCV to determine spin maxima and orbital minima timings. We choose a 2-periodic model in the form:

$$m(t) = m_0 + r_1 \cos(\omega_1(t - T_{01})) + r_2 \cos(\omega_2(t - T_{02})), \quad (1)$$

where $m(t)$ is the smoothed value of brightness at time t , m_0 is the average brightness of theoretical curve, $\omega_j = 2\pi/P_j$, r_j is the semi-amplitude, and T_{0j}

is the epoch for maxima of brightness of photometric wave with number j and period P_j . In our case, $j = 1$ corresponds to the spin modulation and $j = 2$ to the orbital wave. This method has been previously widely used for approximation of observations of intermediate polars (see [Kim et al. \(2005\)](#); [Breus, Petrík, & Zola \(2019\)](#)).

4. Results

4.1. Spin period

The O - C diagram of mean spin maxima for each observing night was generated based on the following ephemeris:

$$T_{max}[HJD] = 59392.4526 + 0.00580320E. \quad (2)$$

We take special care to keep correct cycle counting. However, the period change between 1st (2021) and 2nd (2022) season was large. There are several possible solutions for how to deal with it. We prefer the solution depicted in [Fig. 1](#), as it can be reasonably approximated by a 3rd order polynomial. But we can not exclude abrupt period change, for instance, in the seasonal gap between 2021 and 2022. So we plot only 2nd order polynomial approximation for the data from 2nd and 3rd season. Such an approximation has a clear physical background. It is an acceleration of the white dwarf rotation, most likely due to the stable accretion of the mass with higher angular momentum. The following formula describes the approximation:

$$T_{max}[HJD] = 59392.447(2) + 0.00580349(5)E - 4.4(3) \times 10^{-12}E^2. \quad (3)$$

Equation (3) can be employed for future monitoring of the spin evolution.

O - C diagram is our main contribution to the investigation of V1674 Her. [Patterson et al. \(2022\)](#) analyzed a large dataset collected by CBA network citizen observers (our data from 2021 and 2022 included). But they didn't construct one O - C diagram for all data. Instead, they generated distinct plots for each season based on different spin periods. Using their method, we can list the mean spin period values in [Tab. 1](#). Looking at the 3rd column, one can compare it with other "normal" intermediate polars. The typical value of the spin-up period rate is 1 - 2 milliseconds per year.

4.2. Orbital period

To investigate orbital period evolution, we constructed O - C diagram of times of minima of the orbital wave. [Patterson et al. \(2022\)](#) previously established that the orbital modulation displays two minima. It was difficult to distinguish between primary and secondary minima, especially in noisy data during low brightness of the target. However, precise TESS observations ([Luna et al., 2023](#))

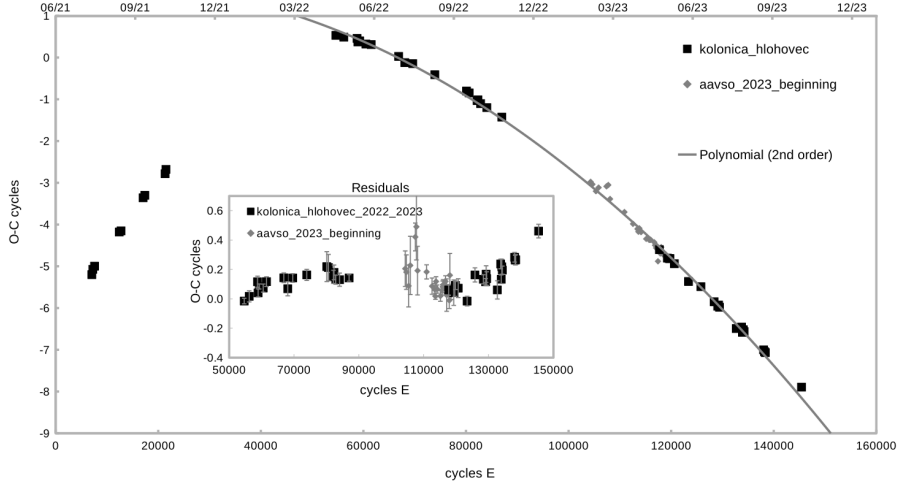


Figure 1. O-C diagram of spin pulse maxima.

Table 1. Mean spin period values for each observing season. Relative difference means the increase compared to the previous line. Absolute is the difference compared to the pre-outburst value.

| Season | Period | Difference (relative) | Difference (absolute) |
|------------------------------|---------------------------|--------------------------|--------------------------|
| WD spin before nova event | $P_{spin} = 0.00580356 d$ | | |
| WD spin in 2021 | $P_{spin} = 0.00580417 d$ | +53 ms | +53 ms |
| WD spin in 2022 | $P_{spin} = 0.00580315 d$ | -88 ms | -35 ms |
| WD spin in 2023 | $P_{spin} = 0.00580260 d$ | -47 ms | -82 ms |
| Orbital motion | $P_{orb} = 0.152921 d$ | | |

revealed that secondary minima are exactly distant at $\Delta\phi = 0.5$ from the primary minimum. Therefore, we used half of the orbital period to plot the O-C diagram, employing the following ephemeris:

$$T_{min}[HJD] = 59400.636 + 0.0764605E. \quad (4)$$

The approximation plotted in the Fig. 2 is described by the following formula:

$$T_{min}[HJD] = 59873.817(5) + 0.0764574(9)E - 1.5(3) \times 10^{-9}E^2. \quad (5)$$

The approximation is far from perfect. It is evident that between 2021 and 2022, the orbital period was on the rise, consistent with expectations for super-

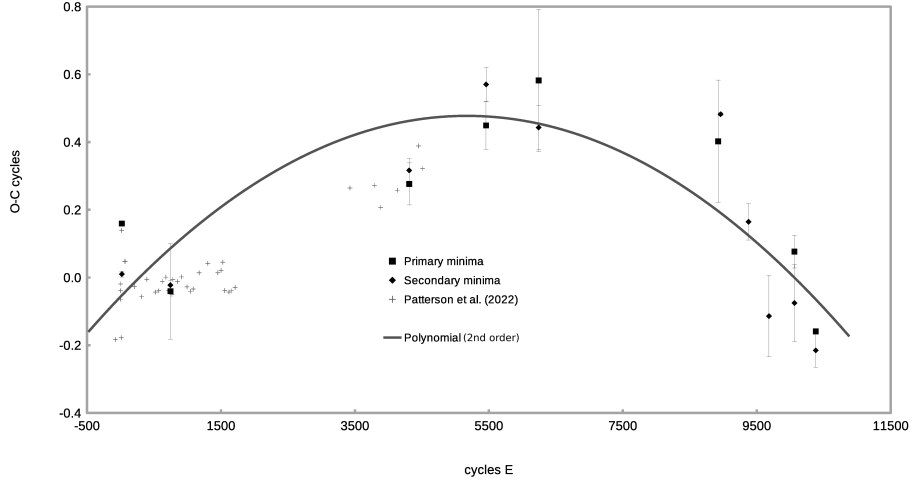


Figure 2. O-C diagram of orbital minima.

soft X-ray sources. The period shortening observed in 2023 is unexpected. It can be a short-term event or a long-term trend. In any case, if confirmed, it will require a theoretical explanation.

5. Conclusions

- We confirm an extremely fast spin-up after the nova eruption.
- Based on recent spin maxima measurements, we can conclude that following the turbulent period associated with the nova eruption, the system is now in a stable spin-up phase. The future evolution is expected to follow the provided ephemeris.
- The brightness is also stable, still 3 mag above the pre-eruption level. The difference could be attributed to the intermediate polar being in a low accretion, the spin-down phase just before the eruption.
- Evaluation of the orbital period evolution requires a more extended time baseline.
- For future research we provide calculated times of pulse maxima from our observations. They are listed in the Tab. 2. Orbital minima are provided in the Tab. 3.

Table 2. Spin pulse maxima timings in BJD - 2400000. BJD based on UTC.

| | | | |
|------------|------------|------------|------------|
| 59392.4526 | 59403.4640 | 59516.2187 | 59796.4009 |
| 59394.5963 | 59404.4282 | 59517.2523 | 59821.3880 |
| 59394.5787 | 59409.3899 | 59709.4903 | 59860.2959 |
| 59393.3941 | 59410.4580 | 59718.4792 | 59857.3133 |
| 59393.3892 | 59413.4425 | 59733.3991 | 59869.2898 |
| 59395.4433 | 59433.3640 | 59734.4200 | 59870.2706 |
| 59395.4436 | 59434.4267 | 59736.4570 | 59873.2646 |
| 59397.4402 | 59436.4351 | 59743.4669 | 59880.2801 |
| 59397.4407 | 59464.3474 | 59749.4731 | 59897.2125 |
| 59401.4382 | 59466.3671 | 59758.3849 | 60075.4916 |
| 59401.4385 | 59491.3081 | 59780.4547 | |
| 59402.4539 | 59493.2873 | 59787.4409 | |

Table 3. Orbital minima timings in BJD - 2400000. Values featuring a colon symbol represent what, in our opinion, are secondary minima.

| | | | |
|-------------|-------------|-------------|-------------|
| 59402.166 : | 59730.205 : | 60083.000 | 60170.052 : |
| 59402.177 | 59817.992 | 60085.759 : | 60194.356 : |
| 59457.597 : | 59818.077 : | 60117.619 : | 60194.360 |
| 59457.672 | 59878.013 : | 60140.994 : | |
| 59730.202 | 59878.100 | 60169.987 | |

Acknowledgements. This work was supported by Slovak Research and Development Agency under contract No. APVV-20-0148. We acknowledge the variable star observations from the AAVSO International Database (<https://www.aavso.org/>).

References

- Andronov, I. L., Antoniuk, K. A., Augusto, P., et al., Inter-longitude astronomy project: some results and perspectives. 2003, *Astronomical and Astrophysical Transactions*, **22**, 793, DOI: 10.1080/1055679031000124501
- Andronov, I. L. & Baklanov, A. V., Algorithm of the artificial comparison star for the CCD photometry. 2004, *Astronomical School's Report*, **5**, 264, DOI: 10.18372/2411-6602.05.1264
- Breus, V., Petřík, K., & Zola, S., Detection of white dwarf spin period variability in the intermediate polar V2306 Cygni. 2019, *Monthly Notices of the RAS*, **488**, 4526, DOI: 10.1093/mnras/stz2062
- Kim, Y., Andronov, I. L., & Jeon, Y.-B., CCD Photometry Using Multiple Comparison Stars. 2004, *Journal of Astronomy and Space Sciences*, **21**, 191, DOI:

10.5140/JASS.2004.21.3.191

- Kim, Y.-G., Andronov, I. L., Park, S.-S., et al., Two-Color VR CCD Photometry of the Intermediate Polar 1RXS J062518.2+733433. 2005, *Journal of Astronomy and Space Sciences*, **22**, 197, DOI: 10.5140/JASS.2005.22.3.197
- Kudzej, I., Savanevych, V. E., Briukhovetskyi, O. B., et al., CoLiTecVS – A new tool for the automated reduction of photometric observations. 2019, *Astronomische Nachrichten*, **340**, 68, DOI: 10.1002/asna.201913562
- Luna, G. J. M., Lima, I. J., & Orio, M., The orbital period of the nova V1674 Her as observed with TESS. 2023, *arXiv e-prints*, arXiv:2310.02220, DOI: 10.48550/arXiv.2310.02220
- Maccarone, T. J., Beardmore, A., Mukai, K., et al., X-ray Pulsations from Nova Her 2021. 2021, *The Astronomer's Telegram*, **14776**, 1
- Mroz, P., Burdge, K., Roestel, J. v., et al., An 8.4 min period in the archival ZTF light curve of Nova Herculis 2021. 2021, *The Astronomer's Telegram*, **14720**, 1
- Patterson, J., de Miguel, E., Kemp, J., et al., The Spin-period History of Intermediate Polars. 2020, *Astrophysical Journal*, **897**, 70, DOI: 10.3847/1538-4357/ab863d
- Patterson, J., Enenstein, J., de Miguel, E., et al., The Periodic Signals of Nova V1674 Herculis (2021). 2022, *Astrophysical Journal, Letters*, **940**, L56, DOI: 10.3847/2041-8213/ac9ebe
- Shugarov, S. & Afonina, M., Photometric Study of Classical Nova V1674 Her. 2021, *Peremennye Zvezdy*, **41**, 4, DOI: 10.24412/2221-0474-2021-41-14-18

Photometric monitoring of PMS stars with the telescopes at Rozhen Observatory

E. Semkov¹, S. Ibryamov², S. Peneva¹ and A. Mutafov¹

¹ *Institute of Astronomy and National Astronomical Observatory, Bulgarian Academy of Sciences, 72, Tsarigradsko Shose Blvd., 1784 Sofia, Bulgaria
(E-mail: esemkov@astro.bas.bg)*

² *Department of Physics and Astronomy, Faculty of Natural Sciences, University of Shumen, 115, Universitetska Str., 9712 Shumen, Bulgaria*

Received: October 31, 2023; Accepted: December 21, 2023

Abstract. For several decades we have been performing photometric monitoring of some of the star formation regions. Significant place in our program take observations of objects of the type FU Orionis, EX Lupi, UX Orionis and other similar but unclassified objects. These three types of young variable objects show changes in brightness with large amplitudes and attract the attention of star formation researchers. But it is not always possible to distinguish them from each other without the presence of long-term multicolor photometric data. For this reason, we collect data from current CCD observations and supplement them with data from the photographic plates archives. In this paper, we show the latest data from optical photometric studies of four PMS objects (V2493 Cyg, V582 Aur, V733 Cep and V1180 Tau) made at the Rozhen Observatory. Our monitoring is carried out in *BVRI* filters, which allows studying the variability in color indexes also. By analysis the historical light curves of these objects we are trying to obtain information about the processes associated with the early stages of stellar evolution.

Key words: stars: pre-main sequence; stars: variables: T Tauri, Herbig Ae/Be; stars: individual: V2493 Cyg, V582 Aur, V733 Cep, V1180 Tau

1. Introduction

A fundamental characteristic of pre-main sequence (PMS) stars is their photometric variability. The processes that took place during the formation of stars are manifested by changes in brightness with large amplitudes, which are accessible to observations with telescopes of medium and small size. Thus, for example the recorded outburst of stars from the type of FU Orionis (FUor) reach amplitudes of up to 6 magnitudes (Audard et al. 2014). These brightness changes are caused by an increase in the rate of accretion from the circumstellar disk onto the stellar surface (Hartmann & Kenyon 1996). Also the eclipses caused by clouds of dust, which are characteristic of stars of the UX Orionis

(UXor) type, have amplitudes of the order of 3-4 stellar magnitudes (Nata et al. 1997). On the other hand, the study of the processes taking place during star formation gives us valuable information about the evolution of stars and the accumulation of their mass.

2. Observations

National Astronomical Observatory Rozhen (Bulgaria) is situated in the Rhodope Mountains at 1750 m altitude and it is a leading astronomical center in the South-East Europe. Since its inception, the observatory has been equipped with three telescopes for optical observation: 2-m RCC telescope, 50/70 cm Schmidt telescope and 60-cm Cassegrain telescope. From mid-2023, the observatory already has a new 1.5-m RC robotic telescope, which will also be used for photometric observations. Mainly the 2-m RCC and the Schmidt telescope of the Rozhen Observatory were used for the photometric observations of PMS stars. Additional information on the procedure for obtaining and analyzing the photometric data, as well as on the technical parameters of the CCD cameras used, can be found in Mutafov et al. (2022). In order to construct the historical light curves of the studied objects, we have also used data from archival photographic observations where possible.

3. Results and Discussion

In this section we will present some of the most interesting results obtained from observations of PMS objects. We have selected four stars that exhibit large-amplitude variability and are readily accessible for observations with small and medium-sized telescopes.

3.1. V2493 Cyg

An outburst of a FUor-type star located in the region of the North America Nebula (NGC 7000) was registered at the Rozhen Observatory in 2010 (Semkov et al. 2010). The eruptive star received designation V2493 Cyg, but it has been known in previous studies as HBC 722 (Herbig et al. 1988). The star's brightness rises by over $R = 4^m$ within a few months, followed by an extended period of position at maximum light. (Semkov et al. 2021). Spectral observations of V2493 Cyg show significant changes in the profiles of the Balmer hydrogen lines and the sodium doublet, which are characteristic of FUor objects (Miller et al. (2011); Semkov et al. (2012)).

Data from our monitoring of V2493 Cyg show photometric behavior that is not typical of the other FUor objects. Usually, after the rapid increase in brightness, the FUor objects undergo a period of slow, gradual decrease in brightness over decades. But in the case of V2493 Cyg, we observe a prolonged photometric

plateau, with no indication of a significant decline in brightness. Photometric data we collected from archival photographic observations do not indicate the presence of other outbursts, but only small-amplitude variability that is characteristic of T Tauri stars.

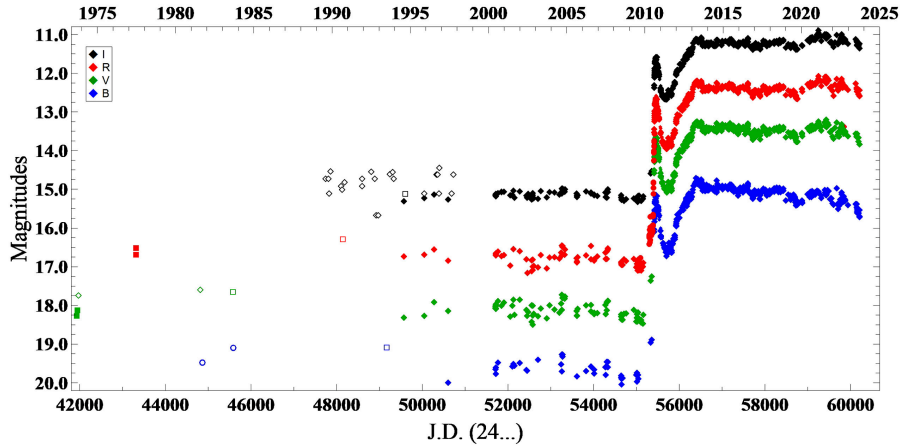


Figure 1. BVRI light curves of V2493 Cyg for the period September 1973 – September 2023. The symbols used are as in Semkov et al. (2012).

3.2. V582 Aur

The PMS star V582 Aur is located in a region of active star formation near Auriga OB2 association. The star was registered in 2009 by amateur astronomer Anton Khruslov, as an object with multiple increased brightness compared to the maps of the Palomar Sky Survey. Our data collected from photographic observations indicate that the outburst of V582 Aur began around 1986 (Semkov et al. 2013). The detailed photometric and spectral studies of V582 Aur indicate that it has all observational characteristics of FUor objects.

The results collected from our photometric monitoring of V582 Aur (2009–2023) show extremely strong photometric variability. Along with this, significant changes in the spectrum of the star are also observed. During the star’s maximum brightness, the spectrum is similar to a FUor object. And accordingly, at magnitude minima the spectrum of the V582 Aur is similar to the spectrum of a T Tauri star. The explanation for this spectral and photometric variability is a combination of variable accretion from the circumstellar disc and variable extinction from the circumstellar environment (Semkov et al. (2013); Zsidi et al. (2019)).

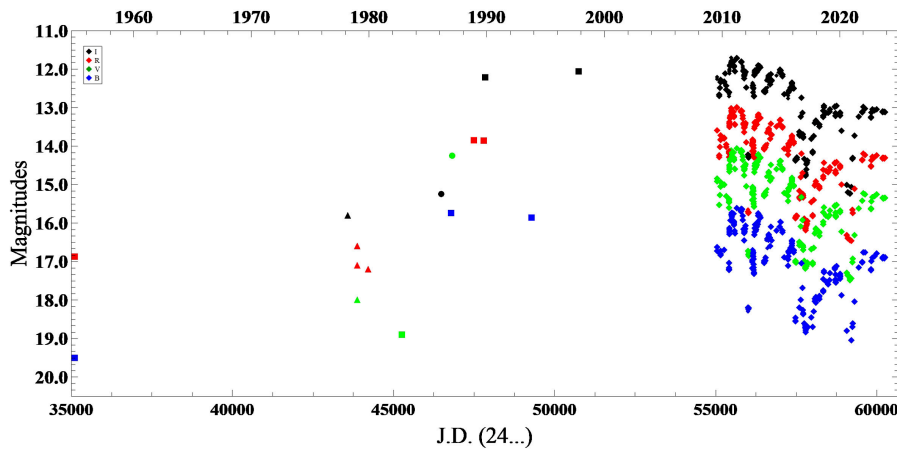


Figure 2. Historical BVRI light curves of V582 Aur for the period December 1954 – September 2023. The symbols used are as in Semkov et al. (2013).

3.3. V733 Cep

The variability of V733 Cep was discovered by Swedish amateur astronomer Roger Persson in 2004 after comparing the plate scans from the first and the second Palomar Sky Survey. The first detailed study of V733 Cep is presented by Reipurth et al. (2007) who suggested that the outburst occurred in the period 1953–1984. On the basis of spectral and photometric observations in the infrared region, Reipurth et al. (2007) show that this PMS star has all the main characteristics of FUor-type objects.

Our paper (Peneva et al. 2010) containing data on the star from photometric monitoring and archival observations also showed a large-amplitude outburst. The rise in brightness has continued over the period 1971–1993 after which the V733 Cep reached its maximum brightness. We register an increase in the brightness of the star by about $R = 4^m5$ compared to the measured value on the Red map of the Palomar Sky Survey (1953). Subsequent photometric observations of V733 Cep show a gradual decrease in brightness, and over a period of 16 years (2007–2023) it has decreased by about $R = 1^m5$. Thus, the star is a unique FUor object in which a nearly symmetric light curve is observed, the rate of increase in brightness being similar to the rate of decrease in brightness.

3.4. V1184 Tau

A variable PMS star of unclear classification was discovered by Yun et al. (1997) in the field of the Bok globule CB 34. Comparing the photometric observations obtained by the authors in 1991 with the plates from Palomar Sky Survey (1951)

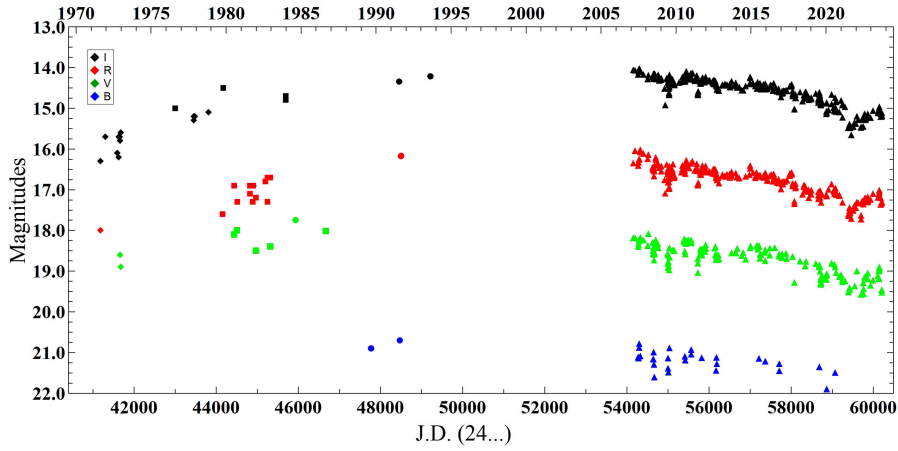


Figure 3. Historical BVRI light curves of V733 Cep for the period August 1971 – September 2023. The symbols used are as in Peneva et al. (2010).

shows a change in the brightness of this star of about $R = 3^m7$. The explanation proposed by Yun et al. (1997) for the change in the star’s brightness is that it is most likely a FUor object.

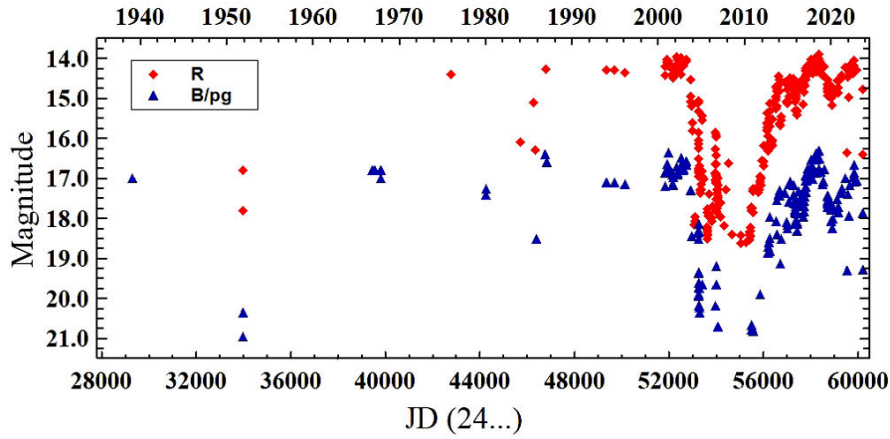


Figure 4. Historical R and B/pg light curves of V1184 Tau.

We began regular photometric observations of this object (designated V1184 Tau) in 2000, with the first results showing variability characteristic of Classical T Tauri stars (Semkov 2003). But in 2003, a deep eclipse of the star’s bright-

ness began, which lasted fourteen years (Semkov et al. 2015). The amplitude of the eclipse reached $\Delta I \approx 4^m 8$, and the changes in the color indices showed a color reversal (co-called “blueing”), characteristic of UX Orionis stars at brightness minima. This color-reversal effect is an evidence that the dimming was caused by dust clouds covering the star along the line of sight. In recent years, V1184 Tau has undergone several more short eclipses, which indicate a strong inhomogeneity of the material covering the star.

4. Conclusion

The results presented in this paper demonstrate the importance of continuous photometric observations of PMS stars. In many cases we register new types of variability in already studied objects. This shows the diversity of the processes taking place during star formation.

Acknowledgements. The research infrastructure this research was done with is funded by the Ministry of Education and Science of Bulgaria (support for the Bulgarian National Roadmap for Research Infrastructure).

References

- Audard, M., Ábrahám, P., Dunham, M. M., et al.: 2014, in Protostars and Planets VI, ed. H. Beuther et al. *Tucson, AZ: Univ. Arizona Press*, 387
- Hartmann, L., Kenyon, S. J.: 1996, *Ann. Rev. Astron. Astrophys.*, **34**, 207
- Herbig, G.H., Bell, K.R., Robbin, K.: 1988, *Lick Obs. Bull.*, 1111
- Miller, A.A., Hillenbrand, L.A., Covey, K.R. et al.: 2011, *Astrophysical Journal*, **730**, 80.
- Mutafov, A., Semkov, E., Peneva, S., Ibryamov, S.: 2022, *Research in Astron. and Astroph.*, **22**, id.125014
- Natta, A., Grinin, V. P., Mannings, V., Ungerechts, H.: 1997, *Astrophysical Journal*, **491**, 885
- Peneva, S. P., Semkov, E. H., Munari, U., Birkle, K.: 2010, *Astronomy and Astrophysics*, **515**, A24
- Reipurth, B., Aspin, C., Beck, T., et al.: 2007, *Astronomical Journal*, **133**, 1000
- Semkov, E. H.: 2003, *Astronomy and Astrophysics*, **404**, 655
- Semkov, E.H., Peneva, S.P., Munari, U., Milani, A., Valisa, P.: 2010, *Astronomy and Astrophysics*, **523**, L3
- Semkov, E. H., Peneva, S. P., Munari, U. et al.: 2012, *Astronomy and Astrophysics*, **542**, A43
- Semkov, E. H., Peneva, S. P., Munari, U. et al.: 2013, *Astronomy and Astrophysics*, **556**, A60

- Semkov, E. H., Peneva, S. P., Ibryamov, S. I.: 2015, *Astronomy and Astrophysics*, **582**, A113
- Semkov, E., Ibryamov, S., Peneva, S.: 2021, *Symmetry*, **13**, 2433
- Yun J. L., Moreira M. C., Alves J. F., Storm J.: 1997, *Astronomy and Astrophysics*, **320**, 167
- Zsidi, G., Ábrahám, P., Acosta-Pulido, J. A., et al.: 2019, *Astrophysical Journal*, **873**, 130

Ground-based photometric follow-up for exoplanet detections with the PLATO mission

H.J. Deeg^{1,2}  and R. Alonso^{1,2} 

¹ *Instituto de Astrofísica de Canarias, C. Vía Láctea S/N, E-38205 La Laguna, Tenerife, Spain (E-mail: hdeeg@iac.es)*

² *Universidad de La Laguna, Dept. de Astrofísica, E-38206 La Laguna, Tenerife, Spain*

Received: November 11, 2023; Accepted: December 21, 2023

Abstract. Detections of transiting planets from the upcoming PLATO mission are expected to face significant contamination from contaminating eclipsing binaries, resulting in false positives. To counter this, a ground-based programme to acquire time-critical photometry is pursued. Its principal aim is to obtain time-series observations of the planet candidate and its surrounding stars at the times of expected transits. This programme is part of the PLATO Ground-based Observations Programme, which also covers spectroscopic and imaging observations. The current photometric follow-up programme is assembling the required observational resources, executing benchmark observations, and defining strategies for the observations and their reporting. Post-launch, it will focus on coordinating photometric data collection and analysis, and will update candidate statuses in the PLATO follow-up database. Its work packages are outlined, covering specific tools, citizen contributions, standard and multi-colour observations, secondary eclipses, and reprocessing of archival photometry. Ground-based follow-up photometry will likely concentrate on longer-period candidates, given that false positives of short-period candidates will likely become identifiable in timeseries available from GAIA in the near future. Geographical considerations for follow-up observations from the first PLATO long-observation field LOPS2 are outlined, which lies in the southern hemisphere, with later fields expected to be more suitable for northern observers.

Key words: Exoplanet astronomy – Transits – Transit photometry – Space Probes: PLATO

1. Introduction

The succession of space missions dedicated to the detection of transiting exoplanet systems, starting in 2007 with CoRoT, followed by Kepler (and its derivative K2), the current TESS all-sky survey and the forthcoming PLATO mission, has marked an exciting trajectory in the quest for exoplanets. These missions have varied in their approach, with CoRoT and Kepler/K2 conducting deep surveys in relatively small fields, with most transit candidates in the 13th

to 15th magnitude range. TESS changed this paradigm with an all-sky survey devoted to stars brighter than 12th magnitudes. The PLATO (PLANetary Transits and Oscillations of stars) space mission, led by the European Space Agency, primarily aims to discover and study extrasolar planetary systems, with a focus on Earth-like planets in habitable zones around sun-like stars (Rauer et al., 2014; Rauer & Heras, 2018). It seeks to characterize the properties of these exoplanets and their host stars, including their mass, radius, age, and composition. Additionally, PLATO aims to understand stellar evolution and seismic activity by observing stellar oscillations. For these aims, PLATO is set to carry out a deep, wide-field survey focussing on stars brighter than 11th magnitude, with a second large sample of stars up to 13th mag.

For PLATO, a ground-based follow-up observing programme employing spectroscopy, time-critical photometry and imaging forms an integral part of the mission. The role of the ground-based photometric follow-up involves validating the plethora of planet candidates identified in space-based transit surveys, by differentiating genuine exoplanet transits from other astrophysical phenomena. This process usually employs the re-observation of known transit events from ground, but it may also involve multicolour photometric observations or the monitoring of Transit Timing Variations (TTVs) to verify a given candidate (and/or to detect the presence of additional planetary or stellar companions). In this contribution, we describe the current status of the preparation of this follow-up for the PLATO mission.

2. Identification of false positives from photometric follow-up

False positives pose a significant challenge in exoplanet transit detections, most often arising from configurations such as grazing and contaminating eclipsing binaries (EBs) within the photometric aperture, which can produce diluted eclipses that superficially resemble planetary transits; see Fig. 1. The community often employs the terms 'BEB' (blended or background eclipsing binary) or 'CEB' (contaminating eclipsing binary; the term used further in this contribution) to describe these misleading binaries. The problem of false positives from CEBs was known since the first ground-based transits surveys (Brown, 2003), but got more acute with the launch of the first space mission, CoRoT (Baglin et al., 2006; Auvergne et al., 2009). That mission's camera had fairly small pixels with an angular side-length of 2.32" when projected into the sky, but its point spread function (psf) was much larger, with a FWHM of about 6" x 20", with the larger value in one direction due to the placement of a prism that permitted the detection of three wavelength-bands. The Kepler mission (Borucki et al., 2010), launched in 2009, and the K2 successor mission (using the same satellite, Howell et al., 2014) had less issues with CEBs, for one because its image-resolution of 4" reduced the probability of nearby EBs to fall

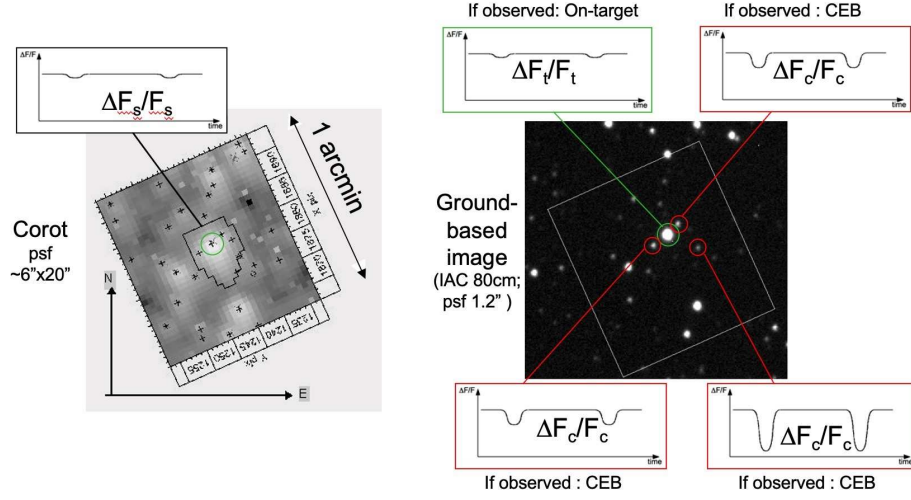


Figure 1. Left: Section of an image from the CoRoT mission around a target star (CoRoT target LRC01_E1_2376, marked with a circle). The irregular shape around it indicates the aperture from which photometry is extracted. The crosses indicate catalogued nearby stars. Right: the same field acquired with the IAC 80cm telescope in moderate ($1.5''$) seeing. If the ground observation shows a transit on the target of similar depth ($\Delta F_t/F_t$, in green box) as the transit from the space-based light-curve ($\Delta F_s/F_s$), the transit is classified as on-target. However, if ground-observations show a sufficiently deep eclipse ($\Delta F_c/F_c$, red boxes) on any of the stars that are close enough to 'contaminate' the target's flux in the aperture, that star is recognised as a CEB. The fact that the detection of a deep eclipse at a nearby star is sufficient to qualify it as a CEB, enables also the follow-up of space-based transits whose depth is too small to be observable as on-target transits from ground. Figure adapted from [Deeg et al. \(2009\)](#).

within the targets apertures, but also due to the direction of its target field away from the galactic plane, with a lower area density of faint EBs. The TESS mission ([Ricker et al., 2014, 2015](#)), launched in 2018, has four cameras observing a bright sample on adjacent fields, with a relatively low resolution of $21''$ per pixel. Consequently, it has suffered also a significant contamination by CEBs in its sample of transit detections. The PLATO mission is set to launch in late 2026 and features 24 cameras with 12 cm apertures (plus 2 fast cameras dedicated to bright stars). These cameras are arranged in four groups of six elements, with partially overlapping fields of view, leading to an area of 2232 deg^2 that is covered in each pointing. The PLATO cameras have a pixel size (and approximate resolution) of $15''$ and will observe fields that include low galactic latitudes, due to which a significant contamination of planet candidates by CEBs is expected.

The need for a ground-based photometric follow-up effort arose therefore initially with the CoRoT mission, and a dedicated follow-up programme was established for that purpose; its motivation, methodology and early results are described in [Deeg et al. \(2009\)](#). A similar effort is currently also under way for the TESS mission, as part of the TESS Follow-Up Observing Program (TFOP, [Collins, 2019](#)). The main observational technique for this follow-up has been the acquisition of single-colour photometric time-series of the planet candidate and nearby stars, at expected transit-times, with the primary aim to validate transit candidates. However, two further photometric techniques are occasionally also of use in the verification and characterisation of transiting planets: Multi-colour photometry, which may indicate false alarms from the typical colour-signatures of binary eclipses, or it may validate exoplanet transits from their colour signature ([Tingley, 2004](#); [Parviainen et al., 2019](#)). That validation technique is based on the colour dependence of transits due to stellar limb darkening, which generates specific transit shapes in different wavebands. Multi-colour photometry is mainly useful for the follow-up of deep transits, for which high signal-to-noise observations can be obtained with multi-channel imagers such as the MUSCAT-2 facility of Teide Observatory, Tenerife. Furthermore, observations geared towards the detection of Transit Timing Variations (TTVs) may be useful in refining the orbital parameters and masses of known planets (particularly in multi-planet systems) but also in detecting additional non-transiting planets from their gravitational influence on the transiting ones (e.g. [Agol & Fabrycky, 2018](#), and references therein).

3. The PLATO photometric follow-up programme

The PLATO time critical photometric follow-up programme is part of PLATO's Ground-based Observations Programme (GOP). During the current development /pre-launch phase of PLATO, its principal tasks are:

- Estimate the expected demand of observational resources.
- Assemble and organize the required observers
- Organize and execute benchmark observations to assess the performances of each facility.
- Define efficient and effective strategies for time critical follow-up photometry, including standards for the data to be provided and their reporting.

In the operational phase, after PLATO's launch, these tasks will change to:

- Coordinate the collection, analysis and interpretation of time critical photometric data, and the pertaining observing reports.
- Update the status of observed candidates in the PLATO Follow-Up database after a quality control of the data.

This follow-up programme consists of several lower level work packages (WP) under a coordination package (PLATO WP 143000, time-critical photometry from ground), led by R. Alonso at IAC. These lower-level WPs are:

- WP 143100, Photometric Specific Tools (chair H.J. Deeg, IAC) to define (and develop, if needed) the tools to be used by observers to analyse and report their observations, with reporting standards that are to be defined. Currently, software packages like AstroImageJ, HOPS, EXOTIC, Siril, MAXIM DL are being evaluated for their utility for the required task, including potential modifications to adapt them to our requirements. These tools might be used by both professional and non-professional contributors, albeit we are aware that professional observers often have their own pipelines in place. These might be used as well, provided that their reporting can be adapted to the required standards.
- WP 143200, Citizen Contribution (chair G. Wuchterl, Kuffner Sternwarte, Vienna). The PLATO team values the contribution by citizen scientists and amateurs astronomers, and this WP is preparing the interfacing with this community. This includes the development of specific procedures for the dissemination of the targets to be observed and the analysis and reporting of the data. This WP is already performing some test observations of transits with a group of amateurs, under the label PLATO-Mercury-Test (<https://mercurytest.plato-planets.at/>), with a participation open to the interested community.
- WP143300, Standard and Multi-colour Photometric Observations (chair E. Pallé, IAC) is the package which coordinates the observations of time-series of transit candidates by the professional community, both those performing standard observing procedures, and multicolour observations.
- WP143400, Secondary Eclipses (Chair R. Alonso, IAC) treats special observations for the detection of secondary eclipses (when a planet is occulted by the host star). Of particular interest are cases when these eclipses can be used to recognise false positive scenarios, and/or when the orbital parameters can be improved, as the timing the secondary eclipse provides constraints on the eccentricity.
- WP143500, Photometry Reprocessing and Homogenisation (chair P. Chote, Warwick Univ., UK) will provide tools and procedures to efficiently access archival time-series photometry acquired by previous surveys, such as TESS, WASP, ASAS, and potentially also photometric time-series from the upcoming GAIA DR4. As a first step, tools are being developed that permit the rapid finding of time-series photometry from a given target within these surveys; the implementation of efficient data-retrieval and eventual reprocessing will be the next development steps.

The current preparations of the PLATO follow-up are in defining ground photometry use cases and the procedures and information flows to be implemented, and in organising a collaborative network of observers and observatories. The definition of standards for the data-formats (e.g. meta-data to be provided in FITS headers) and for the reporting of observations is also a current task. A related task will be the development of converters for the ingestion of outputs from various software packages into the PLATO Follow-up Database. A pending issue is also a more detailed evaluation of the impact of photometric time-series from the GAIA DR4, which will be publicly released in late 2025. Using preliminary time-series from GAIA, Panahi et al. (2022) were able to identify CEBs within $\approx 5\%$ of a sample of TESS mission candidates. We therefore expect that GAIA timeseries may provide a significant contribution to the validation of PLATO candidates, with the caveat that PLATO candidates will typically be fainter, but also, that the temporal coverage of GAIA time-series is still increasing, which will improve the detection rates of both on-transit and CEB configurations in GAIA data. It may be expected that most CEBs near 'easy' short-periodic PLATO candidates will become identifiable from GAIA DR4 data, whereas longer-periodic candidates (e.g. periods longer than 20 d) will continue to need ground-based follow-up. As a consequence, the second version of the 'Mercury Test', mentioned above for WP 143200, focusses now on candidates with such longer periods.

For PLATO's first 'Long-duration Observation Phase (LOP)', an observing field in the southern hemisphere named LOPS2 has recently been defined, with a field center at a declination of -47.9° (Rauer et al., in prep)¹. Only about 10% of this field is north of declination -30° and its northernmost edge is at a declination of about -21° . This position implies that LOPS2 cannot be observed meaningfully from anywhere in continental Europe; and only marginally from some other observatories in the northern hemisphere. In the Canary Islands, for example, LOPS2's northernmost tip raises higher than 2 air masses for ≈ 4.5 h and reaches a lowest airmass of 1.55. Only from as far south as Hawaii, at a latitude near 20°N , will it however be possible to observe a substantial fraction ($\approx 1/4$) of LOPS2. This means that follow-up for LOPS2 will have to be done nearly exclusively from southern-hemisphere observatories, and efforts to recruit observers for the initial PLATO follow-up will have to concentrate on such locations. The fields for the remainder of the mission are not defined yet, with a strong contender for the second long pointing being one in the northern hemisphere, named LOPN1, at a declination of $+52.9^\circ$ (Nascimbeni et al., 2022). Further fields are not defined yet, but they will likely be widely distributed across both hemispheres and consist of shorter pointings, on the order of a few months. Interested observers, independent of their location, are therefore encouraged to sign up for a potential participation in <http://tiny.cc/participatePLATOphotFU>

¹<https://platomission.com/2023/07/11/first-plato-long-duration-observation-phase-lop-field-selected/>

or to get in contact with this contribution's authors for further information about the ground-followup for PLATO.

Acknowledgements. We thank the anonymous referee whose comments led to an improvement in the presentation of this work. The authors acknowledge support from the Spanish Research Agency of the Ministry of Science and Innovation (AEI-MICINN) under grant 'Contribution of the IAC to the PLATO Space Mission' with reference PID2019-107061GB-C66, DOI: 10.13039/501100011033.

References

- Agol, E. & Fabrycky, D. C., Transit-Timing and Duration Variations for the Discovery and Characterization of Exoplanets. 2018, in *Handbook of Exoplanets*, ed. H. J. Deeg & J. A. Belmonte, id. 7
- Auvergne, M., Bodin, P., Boissard, L., et al., The CoRoT satellite in flight: description and performance. 2009, *Astronomy and Astrophysics*, **506**, 411, DOI: 10.1051/0004-6361/200810860
- Baglin, A., Auvergne, M., Barge, P., et al., Scientific Objectives for a Minisat: CoRoT. 2006, in ESA Special Publication, Vol. **1306**, *The CoRoT Mission Pre-Launch Status - Stellar Seismology and Planet Finding*, ed. M. Fridlund, A. Baglin, J. Lochard, & L. Conroy, 33
- Borucki, W. J., Koch, D., Basri, G., et al., Kepler Planet-Detection Mission: Introduction and First Results. 2010, *Science*, **327**, 977, DOI: 10.1126/science.1185402
- Brown, T. M., Expected Detection and False Alarm Rates for Transiting Jovian Planets. 2003, *Astrophysical Journal, Letters*, **593**, L125, DOI: 10.1086/378310
- Collins, K., TESS Follow-up Observing Program Working Group (TFOP WG) Sub Group 1 (SG1): Ground-based Time-series Photometry. 2019, in American Astronomical Society Meeting Abstracts, Vol. **233**, *American Astronomical Society Meeting Abstracts #233*, 140.05
- Deeg, H. J., Gillon, M., Shporer, A., et al., Ground-based photometry of space-based transit detections: photometric follow-up of the CoRoT mission. 2009, *Astronomy and Astrophysics*, **506**, 343, DOI: 10.1051/0004-6361/200912011
- Howell, S. B., Sobeck, C., Haas, M., et al., The K2 Mission: Characterization and Early Results. 2014, *Publications of the ASP*, **126**, 398, DOI: 10.1086/676406
- Nascimbeni, V., Piotto, G., Börner, A., et al., The PLATO field selection process. I. Identification and content of the long-pointing fields. 2022, *Astronomy and Astrophysics*, **658**, A31, DOI: 10.1051/0004-6361/202142256
- Panahi, A., Mazeh, T., Zucker, S., et al., Gaia-TESS synergy: improving the identification of transit candidates. 2022, *Astronomy and Astrophysics*, **667**, A14, DOI: 10.1051/0004-6361/202244207
- Parviainen, H., Tingley, B., Deeg, H. J., et al., Multicolour photometry for exoplanet candidate validation. 2019, *Astronomy and Astrophysics*, **630**, A89, DOI: 10.1051/0004-6361/201935709

- Rauer, H., Catala, C., Aerts, C., et al., The PLATO 2.0 mission. 2014, *Experimental Astronomy*, **38**, 249, DOI: 10.1007/s10686-014-9383-4
- Rauer, H. & Heras, A. M., Space Missions for Exoplanet Science: PLATO. 2018, in *Handbook of Exoplanets*, ed. H. J. Deeg & J. A. Belmonte (Springer), id. 86
- Ricker, G. R., Winn, J. N., Vanderspek, R., et al., Transiting Exoplanet Survey Satellite (TESS). 2014, in Society of Photo-Optical Instrumentation Engineers (SPIE) Conference Series, Vol. **9143**, *Space Telescopes and Instrumentation 2014: Optical, Infrared, and Millimeter Wave*, ed. J. Oschmann, Jacobus M., M. Clampin, G. G. Fazio, & H. A. MacEwen, 914320
- Ricker, G. R., Winn, J. N., Vanderspek, R., et al., Transiting Exoplanet Survey Satellite (TESS). 2015, *Journal of Astronomical Telescopes, Instruments, and Systems*, **1**, 014003, DOI: 10.1117/1.JATIS.1.1.014003
- Tingley, B., Using color photometry to separate transiting exoplanets from false positives. 2004, *Astronomy and Astrophysics*, **425**, 1125, DOI: 10.1051/0004-6361:20035792

Confirming long-period transiting exoplanets with TESS and CHEOPS

The case of HD 22946 d

Z. Garai^{1,2,3}, H.P. Osborn^{4,5}, A. Tuson⁶, S. Ulmer-Moll^{4,7} and
The CHEOPS Consortium

¹ *HUN-REN-ELTE Exoplanet Research Group, 9700 Szombathely, Szent Imre h. u. 112, Hungary*

² *ELTE Gothard Astrophysical Observatory, 9700 Szombathely, Szent Imre h. u. 112, Hungary (E-mail: zgarai@gothard.hu)*

³ *Astronomical Institute of the Slovak Academy of Sciences, 059 60 Tatranská Lomnica, Slovakia (E-mail: zgarai@ta3.sk)*

⁴ *Space Research and Planetary Sciences, Physics Institute, University of Bern, Gesellschaftsstrasse 6, 3012 Bern, Switzerland*

⁵ *Department of Physics and Kavli Institute for Astrophysics and Space Research, Massachusetts Institute of Technology, Cambridge, MA 02139, USA*

⁶ *Astrophysics Group, Cavendish Laboratory, University of Cambridge, J.J. Thomson Avenue, Cambridge CB3 0HE, UK*

⁷ *Observatoire de Genève, Université de Genève, Chemin Pegasi, 51, 1290 Versoix, Switzerland*

Received: October 27, 2023; Accepted: December 15, 2023

Abstract. Due to the limited observing duration of the Transiting Exoplanet Survey Satellite (TESS) primary mission, which observed the majority of the near-ecliptic sectors for only 27 days, planets on long periods produce only single transits. However, thanks to its extended mission, TESS re-observed the same fields 2 years later, and in many cases was able to re-detect a second transit. These duotransit cases require follow-up in order to uncover the true orbital period due to the gap, which causes a set of aliases. The Characterising Exoplanet Satellite (CHEOPS) space observatory can be used to follow-up duotransit targets and to determine their true orbital periods and other characteristics. We investigated the HD 22946 planetary system with a similar aim. Based on the combined TESS and CHEOPS observations, we successfully determined the true orbital period of the planet d to be 47.42489 ± 0.00011 d, and derived precise radii of the planets in the system. Planet d, as a warm sub-Neptune, is very interesting because there are only a few similar confirmed exoplanets to date.

Key words: methods: observational – techniques: photometric – planets and satellites: fundamental parameters

1. Introduction

Nowadays the Transiting Exoplanet Survey Satellite (TESS) mission (Ricker et al., 2014) is the most active transiting-exoplanet searching program. However, due to the nature of its observing strategy, TESS is limited in its ability to discover long-period exoplanets. During its two-year primary mission, TESS observed the majority of the sky for about 27 consecutive days. This means that planets with periods longer than ~ 27 d would only have been observed to transit once, if at all. These single transit detections are known as monotransits and their orbital periods are unknown (Osborn et al., 2022).

Thanks to its extended mission, TESS re-observed the same fields two years later, and in many cases was able to detect a second transit. The result was a sample of duotransits, this means, long-period ($P_{\text{orb}} > 27$ d) planetary candidates with two observed transits separated by a large gap, typically two years. From the two non-consecutive transits, the orbital period of the planet remains unknown, but there now exists a discrete set of allowed period aliases. These aliases (P_n) can be calculated according to

$$P_n = \frac{T_{\text{diff}}}{n}, \quad (1)$$

where T_{diff} is the time between the two transit events and $n \in \{1, 2, 3, \dots, n_{\text{max}}\}$. The maximum value, n_{max} , is determined by the non-detection of a third transit in the TESS data. Follow-up photometric or spectroscopic observations are required to recover their true orbital periods. The follow-up of monotransits requires a blind survey approach, whereas the period aliases of a duotransit allow more targeted follow-up observations.

2. Photometric follow-up of TESS duotransits with CHEOPS

There is a dedicated Characterising Exoplanet Satellite (CHEOPS) Guaranteed Time Observing (GTO) program, called Duos, to recover the orbital periods of TESS duotransits, focusing on small planets that cannot be observed from the ground. Many duotransits produce transits on the order of 500–2500 ppm. These are also some of the most interesting objects, often being super-Earths or sub-Neptunes. CHEOPS is a European Space Agency (ESA) mission dedicated to the photometric follow-up of known exoplanets (Benz et al., 2021). The effective aperture diameter of CHEOPS (~ 30 cm) is about three times larger than that of TESS (~ 10 cm), allowing it to achieve a higher per-transit signal-to-noise ratio. Furthermore, CHEOPS performs targeted photometric observations. It is therefore very well-suited to the follow-up of small, long-period planets from TESS. Detecting long-period planets is important. For example, the increased distance from their host stars means that, when compared with close-in planets,

Table 1. Orbital period aliases of the planet HD 22946 d. Only the period aliases with a probability of $p > 1\%$ are listed here, as calculated by the `MonoTools` package from TESS data alone, i.e. before CHEOPS observations.

| Alias No. | Period alias (P_n) [d] | Probability (p) [%] |
|-----------|----------------------------|-------------------------|
| 1 | 39.5206 | 17.420 |
| 2 | 41.8454 | 20.078 |
| 3 | 44.4607 | 20.341 |
| 4 | 47.4248 | 18.113 |
| 5 | 50.8122 | 13.445 |
| 6 | 54.7209 | 7.061 |
| 7 | 59.2809 | 2.756 |
| 8 | 64.6701 | ~ 1.0 |

they may retain more of their primordial characteristics, such as unevaporated atmospheres (Owen, 2019).

We focus on a sample of targets, which are suitable for future characterisation observations, for example, with Ariel (Tinetti et al., 2021). In any of these cases, stellar magnitude is the most important parameter, and we use this as the key metric to rank targets, with an upper limit of $V = 11.5$ mag. In order to not compete with ground-based facilities performing similar programs, we also place an upper limit on the transit depth of our targets at 2500 ppm. There is a chance that this sample includes false positives (FPs). The best way to reduce such cases is to target unconfirmed long-period planets with a radius upper limit of $R_p = 10 R_{\oplus}$ that are in multi-planet systems, for which there is very low FP probability. This means that the investigation is performed mainly on a limited sample of multi-planet systems, for example on TOI-2076, HIP 9618 or HD 15906. We discovered 5 planet candidates in the TESS data using our specialised duotransit pipeline (Tuson, 2022). This pipeline was created to search for TESS duotransits suitable for CHEOPS follow-up. The pipeline concatenates the TESS Presearch Data Conditioning Simple Aperture Photometry (PDCSAP) light curves from the primary and extended mission, detrends the light curve using a mean sliding window, and then runs a box least squares (BLS) transit search (Kovács et al., 2002) on the detrended light curve with parameters optimized for duotransit detections.

3. Confirming HD 22946 d with TESS and CHEOPS

As an illustrative example, in this section we briefly summarise confirmation of the planet HD 22946 d, which was published in Garai et al. (2023). HD 22946 is a bright ($G = 8.13$ mag) late F-type star with three transiting planets. The planetary system was discovered and validated only recently by Cacciapuoti

et al. (2022). As TESS recorded several transits during observations in sector numbers 3, 4, 30, and 31, the discoverers easily derived the orbital periods of the two inner planets, b and c. The orbital period of planet d was not found by the discoverers. The authors determined its presence through a single transit found in sector number 4 and obtained its parameters from this single transit event. As Caciapuoti et al. (2022), we also initially recognised a transit-like feature in the sector number 4 data through visual inspection of the light curve. Given 65 – 80% of single transits from the TESS primary mission will re-transit in the extended mission sectors (Cooke et al., 2021), we subsequently visually inspected the light curve once the TESS year 3 data were available and found a second dip in the sector number 30 data with near-identical depth and duration. Given the high prior probability of finding a second transit, the close match in transit shape between events, and the high quality of the data, we concluded that this signal is a bona fide transit event and that the transits in sector numbers 4 and 30 are very likely caused by the same object, that is, by planet d.

In order to determine each possible period alias and to schedule CHEOPS observations of planet d, we first performed a period analysis of the available TESS data. For this purpose, we used the `MonoTools` package (Osborn et al., 2022). The package calculates probability distribution across all allowed aliases for a given transit model. The probabilities are estimated based on two major assumptions, namely that short-period orbits are highly favoured over long-period ones (Kipping, 2018), and that planets in multi-planet systems have low eccentricities (Van Eylen & Albrecht, 2015). The software `MonoTools` forecasted that a transit of planet d with the orbital period alias No. 2 (see Tab. 1) would take place on 25th October 2021. This forecasted event was observed with CHEOPS, but the expected transit of planet d did not happen; only the transit of planet b was recorded that time. After this observation, we were able to exclude the period alias No. 2 from the list of possible aliases. The next forecast predicted a transit of planet d on 28th October 2021, which means that, in this case, the alias No. 4 (see Tab. 1) was preferred as its true orbital period. This forecasted event was also observed with CHEOPS. This time, the transit of planet d was successfully detected together with a transit of planet c (see Fig. 1), confirming that the period alias No. 4 is the true orbital period of planet d.

With this gathered knowledge about the true orbital period of planet d, we were able to combine TESS and CHEOPS photometric observations and radial-velocity measurements in order to improve the orbital and planetary parameters of the HD 22946 system. Caciapuoti et al. (2022) expected an orbital period of $P_{\text{orb}} = 46 \pm 4$ d for planet d. We confirmed this prediction, finding an orbital period for planet d of $P_{\text{orb}} = 47.42489 \pm 0.00011$ d. According to the radius valley at $\sim 1.5 - 2.0 R_{\oplus}$ (Fulton et al., 2017), which separates super-Earths and sub-Neptunes and based on the refined planet radii ($R_{\text{p,b}} = 1.362 \pm 0.040 R_{\oplus}$, $R_{\text{p,c}} = 2.328 \pm 0.039 R_{\oplus}$, $R_{\text{p,d}} = 2.607 \pm 0.060 R_{\oplus}$), we find that planet b is a super-Earth, and planets c and d are similar in size and are sub-Neptunes, in agreement with the discoverers. For further details see Garai et al. (2023).

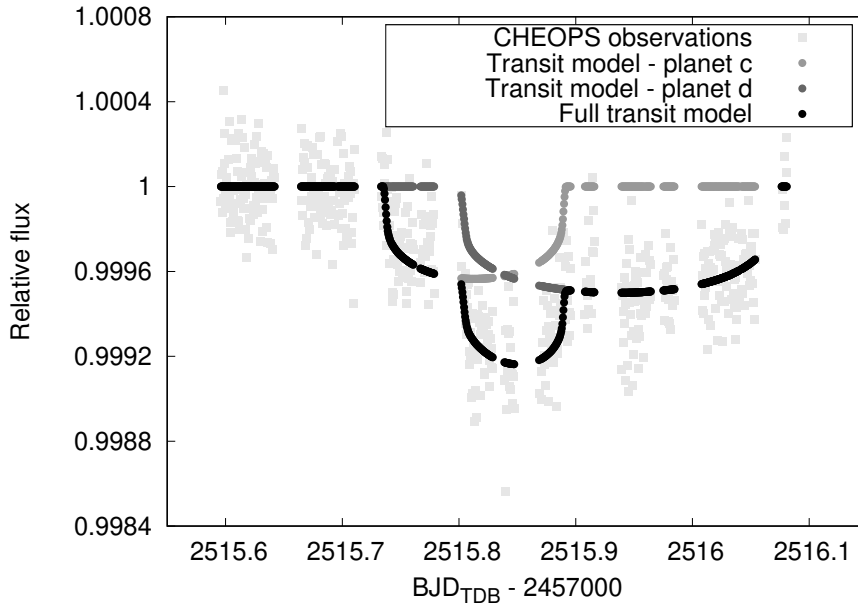


Figure 1. CHEOPS observations of HD 22946 on 28th October 2021. The observed light curve is overplotted with the best-fitting model. The individual transit models of planets c and d are also shown in addition to the summed model.

4. Conclusions

Due to the nature of its observing strategy, TESS is biased towards the discovery of short-period planets. We demonstrated how CHEOPS can be used to follow-up TESS duotransits to expand the sample of long-period planets. Through the CHEOPS GTO Duos program, we have contributed to the discovery of 6 planets with orbital periods longer than 20 d, radii smaller than $5 R_{\oplus}$, and host stars brighter than $G = 12$ mag (Osborn et al., 2022, 2023; Tuson et al., 2023; Ulmer-Moll et al., 2023; Garai et al., 2023). There are only ~ 18 other planets confirmed by TESS in this parameter space, illustrating the power of the TESS and CHEOPS synergy for the discovery of small, long-period planets transiting bright stars. Planet d as a warm sub-Neptune is very interesting, because there are only a few similar confirmed exoplanets to date. Thanks to the synergy of TESS and CHEOPS missions, there is a growing sample of planets, such as HD 22946 d. Such objects are worth investigating in the near future, for example in order to investigate their atmosphere, composition, and internal structure.

Acknowledgements. CHEOPS is an ESA mission in partnership with Switzerland

with important contributions to the payload and the ground segment from Austria, Belgium, France, Germany, Hungary, Italy, Portugal, Spain, Sweden, and the United Kingdom. The CHEOPS Consortium would like to gratefully acknowledge the support received by all the agencies, offices, universities, and industries involved. Their flexibility and willingness to explore new approaches were essential to the success of this mission. This paper includes data collected with the TESS mission, obtained from the MAST data archive at the Space Telescope Science Institute (STScI). Funding for the TESS mission is provided by the NASA Explorer Program. STScI is operated by the Association of Universities for Research in Astronomy, Inc., under NASA contract NAS 5-26555. This research has made use of the Exoplanet Follow-up Observation Program (ExoFOP; DOI: 10.26134/ExoFOP5) website, which is operated by the California Institute of Technology, under contract with the National Aeronautics and Space Administration under the Exoplanet Exploration Program. This work has made use of data from the European Space Agency (ESA) mission *Gaia* (<https://www.cosmos.esa.int/gaia>), processed by the *Gaia* Data Processing and Analysis Consortium (DPAC, <https://www.cosmos.esa.int/web/gaia/dpac/consortium>). Funding for the DPAC has been provided by national institutions, in particular the institutions participating in the *Gaia* Multilateral Agreement. ZG acknowledges the support of the Hungarian National Research, Development and Innovation Office (NKFIH) grant K-125015, the PRODEX Experiment Agreement No. 4000137122 between the ELTE Eötvös Loránd University and the European Space Agency (ESA-D/SCILE-2021-0025), the VEGA grant of the Slovak Academy of Sciences No. 2/0031/22, the Slovak Research and Development Agency contract No. APVV-20-0148, and the support of the city of Szombathely. This work has been carried out within the framework of the NCCR PlanetS supported by the Swiss National Science Foundation under grants 51NF40_182901 and 51NF40_205606.

References

- Benz, W., Broeg, C., Fortier, A., et al., The CHEOPS mission. 2021, *Experimental Astronomy*, **51**, 109, DOI: 10.1007/s10686-020-09679-4
- Cacciapuoti, L., Inno, L., Covone, G., et al., TESS discovery of a super-Earth and two sub-Neptunes orbiting the bright, nearby, Sun-like star HD 22946. 2022, *Astronomy and Astrophysics*, **668**, A85, DOI: 10.1051/0004-6361/202243565
- Cooke, B. F., Pollacco, D., Anderson, D. R., et al., Resolving period aliases for TESS monotransits recovered during the extended mission. 2021, *Monthly Notices of the RAS*, **500**, 5088, DOI: 10.1093/mnras/staa3569
- Fulton, B. J., Petigura, E. A., Howard, A. W., et al., The California-Kepler Survey. III. A Gap in the Radius Distribution of Small Planets. 2017, *Astronomical Journal*, **154**, 109, DOI: 10.3847/1538-3881/aa80eb
- Garai, Z., Osborn, H. P., Gandolfi, D., et al., Refined parameters of the HD 22946 planetary system and the true orbital period of planet d. 2023, *Astronomy and Astrophysics*, **674**, A44, DOI: 10.1051/0004-6361/202345943
- Kipping, D., The Orbital Period Prior for Single Transits. 2018, *Research Notes of the American Astronomical Society*, **2**, 223, DOI: 10.3847/2515-5172/aaf50c

- Kovács, G., Zucker, S., & Mazeh, T., A box-fitting algorithm in the search for periodic transits. 2002, *Astronomy and Astrophysics*, **391**, 369, DOI: 10.1051/0004-6361:20020802
- Osborn, H. P., Bonfanti, A., Gandolfi, D., et al., Uncovering the true periods of the young sub-Neptunes orbiting TOI-2076. 2022, *Astronomy and Astrophysics*, **664**, A156, DOI: 10.1051/0004-6361/202243065
- Osborn, H. P., Nowak, G., Hébrard, G., et al., Two warm Neptunes transiting HIP 9618 revealed by TESS and Cheops. 2023, *Monthly Notices of the RAS*, **523**, 3069, DOI: 10.1093/mnras/stad1319
- Owen, J. E., Atmospheric Escape and the Evolution of Close-In Exoplanets. 2019, *Annual Review of Earth and Planetary Sciences*, **47**, 67, DOI: 10.1146/annurev-earth-053018-060246
- Ricker, G. R., Winn, J. N., Vanderspek, R., et al., Transiting Exoplanet Survey Satellite (TESS). 2014, in Society of Photo-Optical Instrumentation Engineers (SPIE) Conference Series, Vol. **9143**, *Space Telescopes and Instrumentation 2014: Optical, Infrared, and Millimeter Wave*, ed. J. Oschmann, Jacobus M., M. Clampin, G. G. Fazio, & H. A. MacEwen, 914320
- Tinetti, G., Eccleston, P., Haswell, C., et al., Ariel: Enabling planetary science across light-years. 2021, *arXiv e-prints*, arXiv:2104.04824, DOI: 10.48550/arXiv.2104.04824
- Tuson, A., A Search for Long-Period Transiting Exoplanets with TESS and CHEOPS. 2022, in *European Planetary Science Congress*, EPSC2022–499
- Tuson, A., Queloz, D., Osborn, H. P., et al., TESS and CHEOPS discover two warm sub-Neptunes transiting the bright K-dwarf HD 15906. 2023, *Monthly Notices of the RAS*, **523**, 3090, DOI: 10.1093/mnras/stad1369
- Ulmer-Moll, S., Osborn, H. P., Tuson, A., et al., TOI-5678b: A 48-day transiting Neptune-mass planet characterized with CHEOPS and HARPS. 2023, *Astronomy and Astrophysics*, **674**, A43, DOI: 10.1051/0004-6361/202245478
- Van Eylen, V. & Albrecht, S., Eccentricity from Transit Photometry: Small Planets in Kepler Multi-planet Systems Have Low Eccentricities. 2015, *Astrophysical Journal*, **808**, 126, DOI: 10.1088/0004-637X/808/2/126

The evaporation of planetary atmospheres

E. W. Guenther¹, L. Fossati² and P. Kabáth³

¹ *Thüringer Landessternwarte Tautenburg, 07778 Tautenburg, Sternwarte 5, Germany (E-mail: guenther@tls-tautenburg.de)*

² *Space Research Institute, Austrian Academy of Sciences, Schmiedl-strasse 6, 8042 Graz, Austria*

³ *Astronomical Institute of the Czech Academy of Sciences, 251 65 Ondřejov, The Czech Republic*

Received: November 1, 2023; Accepted: January 8, 2024

Abstract. In recent years the focus of exoplanet research has shifted from the mere detection to detailed characterization. Precise measurements of the masses and radii of transiting planets have shown that some low-mass planets have extended atmospheres while others are bare rocks. Hybrid atmospheres consisting of a mixture of Hydrogen and large amount of heavy elements have also been detected. A key factor in explaining this diversity of planetary atmospheres is the erosion by the X-ray and EUV-radiation (XUV) from the host-star. The evaporation through XUV-radiation has already been measured for a few exoplanets. The apparent weakness of the Ca II HK and the Mg II h&k emission cores has been interpreted as evidence for the evaporation of planetary atmospheres. The interpretation is that the evaporating material from the planet forms a thick torus which absorbs the Ca II HK and the Mg II h&k lines from the host star. In this contribution a new way how to prove, or disprove this hypothesis by observations is proposed. It is furthermore shown that there are enough bright targets already known that can be observed, and more will be found with the PLATO mission.

Key words: planet – atmosphere – star – activity

1. The evolution of the atmospheres of low-mass planets

Before exoplanets were discovered, it was generally thought that they would resemble the planets in our solar system, but research in the past years have shown that exoplanets are much more diverse. Precise measurements of the masses and radii of transiting planets allowed us to gain more insight into what these planets are. Virtually all Neptunes, Jupiters and super-Jupiters turned out to have extended hydrogen-dominated atmospheres. Indeed, it appears that seemingly all planets larger than $1.8 R_{\text{Earth}}$ host extended, hydrogen-dominated atmospheres, but there are significant differences between Jupiter-mass planets and planets close to the border of the super-Earth class.

While Jupiter-mass planets are gas-giants for which much of the mass is contained inside the Hydrogen/Helium dominated envelope, for the so-called mini-Neptunes, instead, the Hydrogen/Helium dominated envelope contains just 1-2% of the total mass of the planet. Mini-Neptunes are thus not gaseous planets, but rocky planets with extended envelopes. In a few cases it was shown that the atmospheres of mini-Neptunes are hybrid atmosphere containing hydrogen and a substantial amount of elements heavier than Hydrogen and Helium (García Muñoz et al. 2021). The density measurements of low-mass planets imply that there are three populations: rocky, water-rich, and gas-rich planets (Luque & Pallé 2022).

Close-in planets ($a < 0.1$ AU) with radii smaller than $1.4 R_{\text{Earth}}$ are rocky without an extended atmosphere and close-in planets with radii larger than $1.8 R_{\text{Earth}}$ are mini-Neptunes. Close-in planets with radii between 1.4 and $1.8 R_{\text{Earth}}$ are rare (Fulton & Petigura 2018; Owen & Wu, 2013; Jin et al., 2014; Lopez & Fortney, 2014; Fridlund et al. 2020). Surprisingly, the masses of super-Earths are almost the same as for mini-Neptunes. These results are very surprising. Why do some low-mass planets have extended hydrogen atmospheres, and others not? Furthermore mini-Neptunes and super-Earths are the most common type of planet, but we do not have any such planet in the solar-system.

The fact that some of these planets have extended atmospheres, while others do not, must be related to their formation and evolution history. Several possible mechanisms have been proposed. One process is atmospheric erosion (e.g. Lammer et al. in 2014). Another possibility is gas-poor formation (e.g. Owen & Wu, 2013; Lee et al. 2022). More recently, Venturini et al. (2020) presented a model in which a planet grows from a moon-mass embryo by either silicate or icy pebble accretion, followed by type I-II migration, and photoevaporation driven mass-loss. Atmospheric erosion could either be caused by photoevaporation due to the X-ray and EUV (together XUV) irradiation from the host-star, or by atmospheric escape due to formation heating (i.e. core powered mass-loss; e.g. Izidoro et al. 2022). However, even if gas-poor formation or formation heating were the dominant processes, atmospheric erosion due to the XUV irradiation from the host star would still play an important role. Tian & Heng (2023) have shown that hybrid atmospheres are a natural outcome of the evolution in atmospheres of close-in, low-mass planets.

2. Evidence for mass-loss

Arguably, the best studied cases for atmospheric erosion are the hot Jupiters HD 209458 b and HD 189733 b. The detection of atomic hydrogen beyond the Roche lobe first established that atmospheric material was escaping from HD 209458 b. Estimated escape rates for HD 209458 b are of the order of 10^{10} - 10^{11} g s^{-1} (e.g. Vidal-Madjar et al. 2003, García Muñoz 2007) and 10^9 - 10^{11} g s^{-1} for HD189733b (e.g. Lecavelier Des Etangs et al. 2010). Therefore, both hot

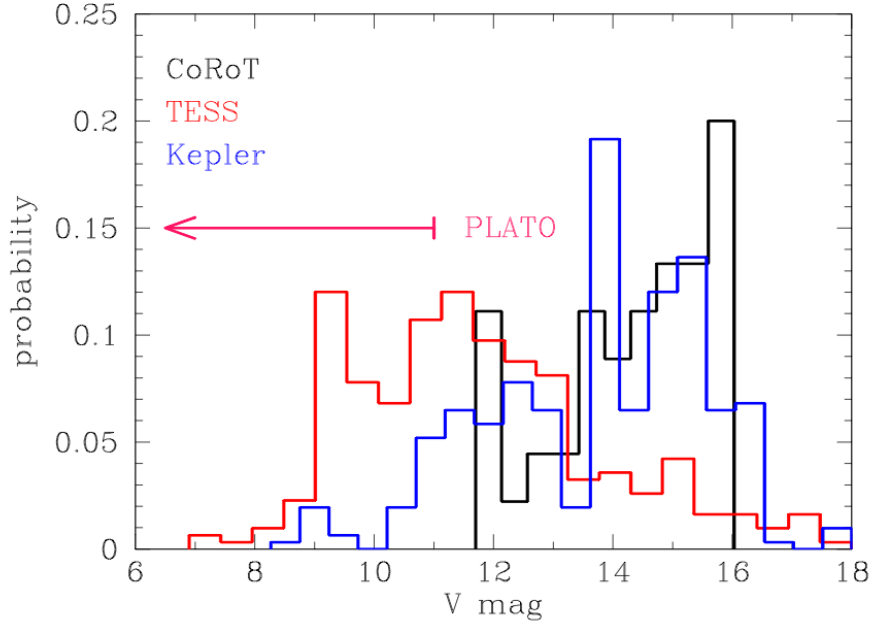


Figure 1. Brightness in V of the planet host stars discovered by CoRoT, Kepler and TESS. The P1 sample of PLATO contains host stars between $V=4$ and $V=11$.

Jupiters loose about 0.1 to 0.2% of their mass per Gyr. Thus, the observed atmospheric escape of the gas-giants is not large enough to fully erode these planets to their rocky cores.

Since the Hydrogen/Helium atmosphere of a mini-Neptune contains only 1-2% of the total mass of the planet, mass loss becomes critically important for low-mass planets. Since the amount of XUV radiation of a solar-like star with an age of 10 Myrs is 300 to 1500 times higher than that of the current Sun, the main erosion phase occurs when the star is young (e.g. Ketzner & Poppenhaeger 2023). Therefore, it is possible that the Hydrogen/Helium atmosphere of a mini-Neptune is completely eroded in the first few Myrs. For example, V1298 Tau is a young star with four transiting exoplanets for which Poppenhaeger et al. (2021) showed that the innermost two planets may lose their hydrogen-dominated atmospheres to become rocky planets. Another interesting case is K2-33b, a young planet in Upper Sco, which may lose its entire hydrogen atmosphere if the planet has less than 7-10 M_{Earth} (Kubyshkina et al. 2018). HST observations of the Neptune-sized planet GJ3470b show an evaporation rate 10^{10}g s^{-1} . The planet may have already lost about 35% of its mass (Bourrier et al. 2018). Kepler-1520 b (=KIC 12557548 b) may have lost $\sim 70\%$ of its formation mass, today

we may be observing its naked iron core (Perez-Becker & Chiang 2013). However, the erosion rates of planets with hybrid atmospheres are lower than those of pure Hydrogen-dominated atmospheres (Tian & Heng 2023).

3. The observing strategy

Mass loss certainly is a key factor in the evolution of a planet. In the case of WASP-12 b Haswell et al. (2012) detected the gas escaping from this heavily irradiated planet. They observed the planet in the UV and found that the transit is three times deeper than in the optical, indicating the presence of diffuse gas, extending well beyond the Roche lobe. They also found that surprisingly the MgII h&k line cores have zero flux indicating that the inner portions of these strong resonance lines are likely affected by extrinsic absorption due to the material escaping from the planet (Fossati et al. 2013). There is thus strong evidence for mass loss for WASP-12b.

Mass loss from a close-in planet can form a diffuse circumstellar gas cloud, which absorbs in the cores of strong resonance lines (e.g. CaII H&K and MgII h&k) seemingly suppressing the signatures of stellar activity below their true value (Haswell et al. 2012; Fossati et al. 2013). Simulations show that the density of the material in the torus is inhomogeneous (Bell et al. 2019; Dwivedi et al. 2019; Zhang et al. 2023). Observations of the Helium triplet line at 1083.3 nm during roughly a quarter of the orbit by Zhang et al. et al. (2023) indicate the material forms a torus.

Since the density of the material in torus varies along the orbit of the planet, the strength of the CaII H&K lines should also vary. By observing several orbits, it is then possible to reconstruct the density of material in the torus. However, if we observe only the CaII H&K lines, we would only constrain how much Ca has escaped from the planet. The strength of the absorption would depend on the amount of Ca that the envelope contains. Using not only the CaII H&K lines but also H α and NaD it would be possible to determine the physical properties of the torus, for example, how much mass it contains. In this way it would be possible to "see" the material that is escaping from the planet.

Shkolnik et al. (2003, 2005, 2008) have studied the chromospheric activity in the Ca II H and K lines with the aim to search for induced stellar activity. A spectralline that originates from the star has width that is of the order of the $v \sin i$ of the host star, depending on the location of the active region on the stellar surface. The RV-amplitude of a close-in planet is much larger than that. A ring of material the originates from material that has escaped from a close-in planet will have a width that corresponds to the RV-amplitude of the planet. Such a feature will thus be much broader than a stellar spectralline.

4. Preparing for PLATO and planned observations

The question is whether there are already good targets for such a project. Because the absolute mass-loss of gas-giants are larger than that of min-Neptunes, gas-giants are the preferred targets. Table 1 gives a list of nineteen known planets in the mass-range between $M_p = 0.5$ and $5.0 M_{Jup}$ with $R_p \geq 1.4 R_{Jup}$ orbiting stars with $V \leq 11$ mag that are observable from La Silla ¹. As can be seen, all of these targets are short-period planets. The large radii are thus most likely due to large heating by the host star. Thus, these planets are likely to have also a large mass-loss rate. For comparison WASP-12 b has $R_p = 1.47 M_{Jup}$, $M_p = 1.9 M_{Jup}$ (Collins et al. 2017).

While many bright stars hosting close-in gas-giant have already been identified it would be even more exciting if bright stars hosting close-in Neptunes were found. Absolutely thrilling would be the discovery of planets like those of V1298 Tau ($V=10.1$ mag), GJ3470b ($G=11.4$ mag), or K2-33b ($G=14.1$ mag), K2-240 ($V=13.4$ mag) but orbiting brighter stars.

What are the prospects to find planets like that but orbiting brighter stars? The key to find these is the PLATO mission. PLATO (PLANetary Transits and Oscillation of stars) will search for extrasolar planets by means of ultra-high-precision transit photometry. PLATO consists of 24 normal and 2 two high cadence cameras providing combined wide field of view (FoV) of 49×49 square degrees. The PLATO mission and the key-science goals are summarized in Rauer et al. (2014, 2021).

The first PLATO field has now been selected ². The center is at RA: 06:21:14.5 DE: -47:53:13. This field contains more than 9000 dwarf and subgiant stars of spectral types from F5 to K7 with $V < 11$ mag (P1 sample) that will be observed. The random noise of the P1-sample will be lower than 50 ppm in one hour. Fig. 1 shows the brightness of planet host stars discovered in the CoRoT, Kepler and TESS mission, respectively ³. As can be seen in the figure, one of the advantages of PLATO compared with previous missions is that planet host stars will be much brighter. The baseline observing strategy assumes that this field will be observed for at least two years. The PLATO spacecraft has been designed to perform scientific operations for at least 8.5 years. PLATO will also observe more than 159,000 dwarf and subgiant stars of spectral types from F5 to K7 with $m_V < 13$.

Ondrejov observatory, the Thüringer Landessternwarte Tautenburg and the Pontificia Universidad Católica de Chile as main partners have a unique access to the ESO1.5m telescope in La Silla (Chile). Minor partners are the IGAM of the university of Graz, Universidad Adolfo Ibanez and Masaryk University. The telescope has recently been refurbished. It is fully operational and currently

¹Objects selected using <https://exoplanet.eu>

²See <https://www.cosmos.esa.int/web/plato/first-sky-field>

³Figures produced using <https://exoplanet.eu>

equipped with the PUCHEROS Echelle spectrograph that has a resolution of $R=20,000$. By the end of 2024, we will install PLATOSpec, which is a state-of-the-art UV-optimised high-resolution Echelle spectrograph with a resolution of $R=68,000$ covering the 360-680 nm spectral range without gaps. The high UV throughput of the spectrograph, which is rather unique in the current instrumental landscape, enables one to collect high-quality spectra throughout the entire optical band, including the CaII H&K lines, the NaI D lines, and the $H\alpha$ line. The spectrograph will be fibre fed and will be placed in a temperature-stabilized room.

As the name of the instrument already suggest, its main purpose will be the follow-up observations of transiting planets discovered in the PLATO mission. Because of the relatively large amount of observing time required this instrument is ideal to carry the project.

Table 1. Inflated gas-giant planets observable from La Silla orbiting stars brighter than 11 mag in V.

| Star | RA ₂₀₀₀ (hh:mm:ss) | DE ₂₀₀₀ (dd:mm:ss) | V [mag] | Mass [M _{Jup}] | Radius [R _{Jup}] | Period [days] | K [m/s] |
|-----------|----------------------------------|----------------------------------|------------|-----------------------------|-------------------------------|------------------|------------|
| HIP65A | 00:00:45 | -54:49:51 | 11.1 | 3.213 ± 0.078 | $2.03^{+0.61}_{-0.49}$ | 0.98 | 754 |
| HD2685 | 00:29:19 | -76:18:15 | 9.6 | 1.18 ± 0.09 | 1.44 ± 0.01 | 4.13 | 118 |
| WASP-76 | 01:46:32 | +02:42:02 | 9.5 | 0.92 ± 0.03 | 1.83 ± 0.06 | 1.81 | 119 |
| WASP-79 | 04:25:29 | -30:36:02 | 10.1 | 0.9 ± -0.09 | 1.7 ± 0.11 | 3.66 | 88 |
| WASP-100 | 04:35:50 | -64:01:37 | 10.8 | 2.03 ± 0.12 | 1.69 ± -0.29 | 2.85 | 215 |
| WASP-82 | 04:50:39 | +01:53:38 | 10.1 | 1.24 ± 0.04 | $1.67^{+0.07}_{-0.05}$ | 2.71 | 130 |
| TOI-640 | 06:38:56 | -36:38:46 | 10.5 | 0.88 ± 0.16 | 1.771 ± 0.06 | 5.00 | 78 |
| WASP-121 | 07:10:24 | -39:05:51 | 10.4 | $1.184^{+0.065}_{-0.064}$ | 1.865 ± 0.044 | 1.27 | 181 |
| KELT-17 | 08:22:28 | +13:44:07 | 9.6 | 1.31 ± 0.29 | $1.525^{+0.065}_{-0.06}$ | 3.08 | 131 |
| HAT-P-69 | 08:42:01 | +03:42:38 | 9.8 | 3.58 ± 0.58 | $1.676^{+0.051}_{-0.033}$ | 4.79 | 309 |
| TOI-2669 | 08:58:53 | -13:18:45 | 9.5 | 0.61 ± 0.19 | 1.76 ± 0.16 | 6.20 | 60 |
| HD85628A | 09:50:19 | -66:06:50 | 8.6 | 3.1 ± 0.9 | $1.53^{+0.07}_{-0.04}$ | 2.82 | 307 |
| WASP-15 | 13:55:43 | -32:09:35 | 10.9 | 0.542 ± 0.05 | 1.428 ± 0.077 | 3.75 | 63 |
| NGTS-2 | 14:20:30 | -31:12:07 | 11.0 | 0.67 ± 0.089 | 1.536 ± 0.062 | 4.51 | 69 |
| WASP-189 | 15:02:44 | -03:01:53 | 6.6 | $1.99^{+0.16}_{-0.14}$ | 1.619 ± 0.021 | 2.72 | 182 |
| WASP-88 | 20:38:03 | -47:32:17 | 10.4 | 0.56 ± 0.08 | $1.7^{+0.13}_{-0.07}$ | 4.95 | 57 |
| MASCARA-1 | 21:10:12 | +10:44:20 | 8.3 | 3.7 ± 0.9 | 1.5 ± 0.3 | 2.15 | 405 |
| HD202772A | 21:18:48 | -26:36:59 | 8.3 | $1.008^{+0.074}_{-0.079}$ | $1.562^{+0.053}_{-0.069}$ | 3.31 | 97 |
| WASP-11 | 21:55:04 | -22:36:45 | 10.3 | 1.85 ± 0.16 | 1.442 ± 0.094 | 2.31 | 212 |

Acknowledgements. This work was generously supported by the Thüringer Ministerium für Wirtschaft, Wissenschaft und Digitale Gesellschaft. This work has made use of the <https://exoplanet.eu>. We are very grateful to the *exoplanet team* that is providing this service. This research has made use of the SIMBAD database, operated at CDS, Strasbourg, France.

References

- Bell, T.J., Zhang, M., Cubillos, P.E., 2019, *MNRAS* **489**, 1995.
- Bourrier, V., Lecavelier des Etangs, A., Ehrenreich, D. et al. 2018, *A&A* **620**, 147
- Collins, K.A., Kielkopf, J.F., Stassun, Keivan G., 2017, *AJ* **153**, 78
- Dwivedi, N.K., Khodachenko, M.L., Shaikhislamov, I., 2019, *MNRAS* **487**, 4208
- Fossati, L., Ayres T.R., Haswell C.A., Bohlender D., et al. 2013, *ApJL* **766**, L20
- Fridlund et al., 2020, *MNRAS* **498**, 4503
- Fulton, B.J. , Petigura, E.A, 2018, *AJ* **156**, 265
- García Muñoz, A., et al. 2007, *P&SS* **55**, 1426
- García Muñoz, A., et al. 2021, *ApJ* **907**, 36
- Haswell, C.A., Fossati, L., Ayres, T. et al. 2012, *ApJ* **760**, 79
- Izidoro , A., Schlichting, H.E., Isella, A. et al. 2022, *ApJL* **939**, 19
- Jin, H., Miyoshi, Y., Fujiwara, H., Shinagawa, H., 2014, *ApJ* **795**, 65
- Ketzer, L., Poppenheger, K., 2023, *MNRAS* **518**, 1683
- Kubyskhina, D., Lendl, M., Fossati, L., et al. 2018, *A&A* **612**, 10
- Lammer, H., Stökl, A., Erkaev, N. V. et al., 2014, *MNRAS* **439**, 3225
- Lecavelier Des Etangs, A., Ehrenreich, D., Vidal-Madjar, A. et al. 2010, *A&A* **514**, 72
- Lee, E.J, Karalis, A., Thorngren, D.P., 2022, *ApJ* **941**, 186
- Lopez, E.D., Fortney, J.J., 2014, *ApJ* **792**, 1
- Luque, R., Pallé, E., 2022, , *Science* **377**, 1211
- Owen, J.E., Wu, Y., 2013, *ApJ* **775**, 105
- Perez-Becker, D., Chiang, E. , 2013, *MNRAS* **433**, 2294
- Poppenhaeger, K., Ketzer, L., Mallon, M., 2021, *MNRAS* **500**, 4560
- Rauer, H. et al. 2021, *Experimental Astronomy* **Vol. 38**, Issue 1-2, pp. 249
- Rauet, H., et al. 2014, *15th Europlanet Science Congress 2021*, id. EPSC2021-90
- Shkolnik, E., Walker, G.A.H., Bohlender, D.A. , 2003, *ApJ* **597**, 1092
- Shkolnik, E., Walker, G.A.H., Bohlender, D.A. , et al. 2005, *ApJ* **622**, 1075
- Shkolnik, E., Walker, G.A.H., Bohlender, D.A. , et al. 2008, *ApJ* **676**, 628
- Tian, M., Heng, K., 2023, arXiv:2301.10217
- Vidal-Madjar, A., Lecavelier des Etangs, A., Désert J.-M., et al., 2003, *Nature* **422**, 143
- Venturini, J., Guilera, O. M., Haldemann, J., 2020 , *A&A* **643**, L1
- Zhang, Z. et al. 2023, *Science Advances* **Vol. 9**, issue 23, id eadf8736

First determination of the system parameters in five contact binaries

B. Dębski^{1,2}, L. Kulczycka², W. Skrobacz², J. Pęgiel² and M. Jacak²

¹ *Astronomical Observatory of the Jagiellonian University, Orla 171, 30-244 Kraków, Poland (E-mail: b.debski@oa.uj.edu.pl)*

² *Krakowskie Młodzieżowe Towarzystwo Przyjaciół Nauk i Sztuk, H. Jordan Youth Center in Kraków, Krupnicza 38, 31-123 Kraków, Poland*

Received: November 13, 2023; Accepted: January 23, 2024

Abstract. We present solutions of the BVRI-light curve numerical modeling for five low-mass ratio totally eclipsing contact binary stars. One object required the introduction of a cool star spot to the best-fitting model. Only one object returned a solution with a hotter secondary component. None of the objects required the introduction of a third component.

Key words: stars – binaries: close – binaries: eclipsing

1. Introduction

The W UMa-type contact binary stars are canonically described as binary systems consisting of two main-sequence stars that share a common convective envelope. A consequence of such a configuration is an equalized surface temperature and, in the case of eclipsing systems, a light curve with brightness minima of nearly equal depths (Lucy, 1968). This feature allowed us to compose a catalog of suspected contact binaries (Debski & Walczak, 2022), which subsequently are observed and studied in the Krakow Observatory.

The common outer envelope in contact binaries is very well described with the Roche geometry (Kopal, 1959), which makes these systems good targets for the light curve numerical modeling studies (Debski, 2022). On the other hand, the degeneracy between the system inclination, effective temperature, and the mass ratio poses a serious problem for the modeling process. The surface temperature can be derived from the color of the system, but the search for the latter two parameters must be done under very specific circumstances. One of such is that the mass ratio could be obtained from radial velocity studies and then put into the photometric modeling. The other way is to study the totally eclipsing systems only. Pribulla et al. (2003) and Terrell & Wilson (2005) have shown that the inclination-mass ratio entanglement breaks when the Roche model is constrained with total eclipses. Since most of our targets are faint and lack spectroscopical data, we, therefore, decided to focus on totally eclipsing systems in our photometric studies.

Table 1. The parameters of the observed objects: coordinates and brightness (top row); best-fitting model results (middle rows) and the calculated physical parameters (bottom rows).

| Parameter | KR 00017 | KR 00036 | KR 00059 | KR 00085 | KR 00225 |
|---------------------|------------|------------|------------|------------|------------|
| RA [h m s] | 06 29 57.7 | 15 58 54.2 | 02 34 25.0 | 06 50 47.2 | 20 40 03.6 |
| DEC [° ' ″] | 76 42 59.7 | 46 35 49.0 | 79 37 39.4 | 73 21 32.7 | 63 59 34.5 |
| P_{orb} [d] | 0.314556 | 0.272030 | 0.346980 | 0.338555 | 0.352281 |
| Max. mag, V | 13.04(1) | 13.37(1) | 13.19(1) | 13.10(3) | 10.70(2) |
| i [°] | 77(2) | 77(3) | 86(2) | 80(1) | 88(1) |
| T_1 [K] | 5628 | 5673 | 6184 | 5808 | 6618 |
| T_2 [K] | 5554(11) | 5712(9) | 5796(11) | 5543(12) | 6435(11) |
| Ω [K] | 2.004(39) | 2.075(52) | 2.080(48) | 1.986(11) | 1.985(41) |
| q [M_2/M_1] | 0.117(21) | 0.154(19) | 0.161(11) | 0.132(2) | 0.125(9) |
| Dist. [pc] | 517(3) | 602(4) | 756(6) | 627(4) | 271(1) |
| M_V | 4.26(4) | 4.41(3) | 3.47(4) | 3.78(4) | 3.18(4) |
| M_1 [M_\odot] | 1.36(25) | 1.33(26) | 1.84(37) | 1.75(33) | 1.74(29) |
| M_2 [M_\odot] | 0.16(5) | 0.20(6) | 0.30(8) | 0.23(7) | 0.22(6) |

2. The objects

The sample of objects studied in this work is a result of the individual tutoring program commenced by the Jagiellonian University at the Jordan Youth Center in Krakow. The objects selected for this study come from the precompiled list of suspected contact binaries¹. The temperatures of the primary components were adopted from the TESS Input Catalogue (TIC), v8.2 (Paegert et al., 2021). The distances to the objects were calculated using the Gaia DR3 (Gaia Collaboration et al., 2023) parallaxes. The absolute magnitudes, M_V , were derived from the distances, D , and observed brightness m_V (collected by us), corrected by the interstellar extinction adopted from TIC.

3. Observations and Analysis

The photometric data used for this study were taken with the Apogee Alta U42 camera in the D9 casing mounted on the Cassegrain telescope (aperture 500 mm, effective focal length 6650 mm) at the Astronomical Observatory of the Jagiellonian University in Krakow. The light curves of all objects were taken in the Bessel B, V, R and I filters. The light curve numerical modeling was conducted using a modified Wilson-Devinney code (Wilson & Devinney, 1971; Zola et al., 1997; Debski, 2022). The physical parameters were calculated by incorporating the total brightness and the modeling result to the Stefan-Boltzman Law

¹<http://bade.space/ew/>

and then using the derived orbital separation to the Third Kepler's Law. The individual masses were then calculated with the use of the mass ratio obtained from numerical modeling.

4. Results

This study presents first-time obtained physical parameters for five low-mass ratio contact binaries. The observational parameters, as well as the best-fitting model parameters and the calculated physical parameters for all objects, are compiled in the Table 1. One system (KR 00017) needed the introduction of a cool ($T_{spot} = 0.75 T_1$) spot on the back of the primary component. The spot was fixed at the stellar equator.

References

- Debski, B., The light-curve intrinsic variability in 47 Kepler contact binary stars. 2022, *Monthly Notices of the RAS*, **516**, 5003, DOI: 10.1093/mnras/stac2190
- Debski, B. & Walczak, K., A study of a contact binary system NSVS 2983201. 2022, *arXiv e-prints*, arXiv:2212.14085, DOI: 10.48550/arXiv.2212.14085
- Gaia Collaboration, Vallenari, A., Brown, A. G. A., et al., Gaia Data Release 3. Summary of the content and survey properties. 2023, *Astronomy and Astrophysics*, **674**, A1, DOI: 10.1051/0004-6361/202243940
- Kopal, Z. 1959, *Close binary systems*
- Lucy, L. B., The Structure of Contact Binaries. 1968, *Astrophysical Journal*, **151**, 1123, DOI: 10.1086/149510
- Paegert, M., Stassun, K. G., Collins, K. A., et al., TESS Input Catalog versions 8.1 and 8.2: Phantoms in the 8.0 Catalog and How to Handle Them. 2021, *arXiv e-prints*, arXiv:2108.04778, DOI: 10.48550/arXiv.2108.04778
- Pribulla, T., Kreiner, J. M., & Tremko, J., Catalogue of the field contact binary stars. 2003, *Contributions of the Astronomical Observatory Skalnaté Pleso*, **33**, 38
- Terrell, D. & Wilson, R. E., Photometric Mass Ratios of Eclipsing Binary Stars. 2005, *Astrophysics and Space Science*, **296**, 221, DOI: 10.1007/s10509-005-4449-4
- Wilson, R. E. & Devinney, E. J., Realization of Accurate Close-Binary Light Curves: Application to MR Cygni. 1971, *Astrophysical Journal*, **166**, 605, DOI: 10.1086/150986
- Zola, S., Kolonko, M., & Szczech, M., Analysis of a photoelectric light curve of the W UMa-type binary ST Ind. 1997, *Astronomy and Astrophysics*, **324**, 1010

Deep-learning classification of eclipsing binaries

Š. Parimucha¹, P. Gajdoš^{1,2}, Y. Markus^{1,3} and V. Kudak⁴

¹ *Institute of Physics, Faculty of Science, Pavol Jozef Šafárik University,
040 01 Košice, Slovakia*

² *Astronomical Institute of the Czech Academy of Sciences
251 65 Ondřejov, The Czech Republic*

³ *International Center of Astronomical, Medical, and Ecological Research,
NASU, Kyiv, Ukraine*

⁴ *Laboratory of Space Researches, Uzhhorod National University, Uzhhorod,
Ukraine*

Received: October 31, 2023; Accepted: December 18, 2023

Abstract. We present a deep-learning model for the classification of eclipsing binaries. Our classifier provides a tool for the categorization of light curves of eclipsing binaries into four classes: detached systems with and without spots, and over-contact systems with and without spots. The classifier was trained on 200 000 synthetic light curves created using ELISa code. We randomly selected 100 light curves from the GAIA catalogue, which were fitted for evaluation purposes, and their morphologies were determined. We tested several classifiers and found that the best-performing classifier combined a Long Short-Term Memory (LSTM) layer and two one-dimensional convolutional neural networks. The precision from the evaluation set was 97% compared with the predicted precision of 94 % for the validation of synthetic data. Our classifier is more likely to successfully process data from subsequent large observational surveys.

Key words: Stars: binaries: eclipsing – deep-learning

1. Introduction

Eclipsing binaries (EBs) are a well-known group of variable stars in which light variations are caused by the mutual obscuration of stars with respect to the observer. It produces typical light curves where valuable information about the physical properties of the stars within the system is coded, like the sizes and shapes of the stars, mass ratio, relative temperatures, and the inclination of the orbital plane. Moreover, the light curves of many EBs show irregularities caused by spot(s) on one or both components (Hilditch, 2001; Prša, 2018).

EBs can be classified in two different ways. The first is the morphological division into three classes (Algol, β Lyr, and W UMa) based only on the shape of the light curve. The second is based on the amount of Roche lobe filling in the binary systems (Wilson, 1994; Kallrath & Milone, 2009), where three classes are listed (detached, semi-detached, and over-contact).

From a geometrical point of view, the semi-detached system is, in principle, detached; both components can be described by a convex surface (Čokina et al., 2021). Moreover, to model such a system, we must know two potentials (Kallrath & Milone, 2009). Therefore, we divided the EBs for machine-learning purposes into four groups: 0 – over-contact without spots, 1 – over-contact with spots, 2 – detached without spots and 3 – detached with spots.

This approach will allow us to classify possibly all EBs, which were found in large surveys e.g. GAIA or KEPLER will also be found in prepared surveys, such as Vera Rubin (LSST). Sorting into these groups will enable the use of different approaches to determine other parameters (physical and geometrical) of EBs using machine-learning approaches.

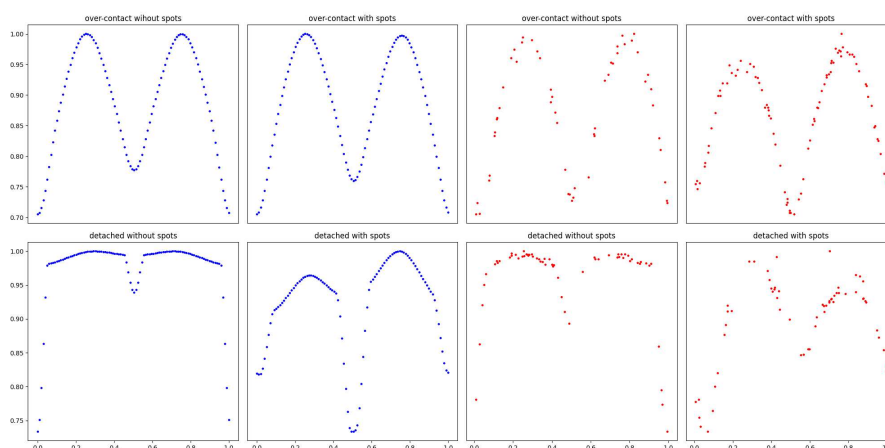


Figure 1. Examples of synthetic (blue) and GAIA (red) light curves from different groups.

2. Training and evaluation dataset

Deep-learning classification requires a large labelled training dataset, where all groups of objects have equal representations. In the analysis of EBs, we can create such datasets using software packages dedicated to EB modelling. In our study, the training dataset was created using the ELISa code (Čokina et al., 2021). For each group, we simulated 50 000 light curves created from the parameters covering a wide range of physically correct values for a specific group. Each light curve was represented by 100 data points of normalized flux phased to $< 0, 1 >$ interval.

To evaluate our model, we randomly selected 100 EB light curves published in the GAIA-DR3 catalogue (Mowlavi et al., 2023). All these light curves were

fitted using the ELISa code to determine the basic parameters of the systems and eventually spot(s) on the components, as well as to determine their morphology. Examples of synthetic and GAIA light curves are shown in Fig. 1.

3. Deep-learning model and its performance

We tested several classification models and found that the best performance was achieved by combining two one-dimensional convolutional neural networks (CNN) and a Long Short-Term Memory (LSTM) layer. We used Adam optimizer and sparse categorical cross-entropy loss function (Chollet et al., 2015).

The training of our model was performed for 10 epochs, during which the loss and accuracy were determined. We randomly selected 20% of the training light curves for the validation dataset. Using this, the predicted precision was calculated and a confusion matrix was created. The predicted precision of the validation data is 94%. A detailed inspection of the confusion matrix (Fig. 2) reveals that our model misclassified (on the level of approximately 10%) the spotted light curves for both the detached and contact systems. This is probably because small spots cause only small changes in the light curve, and the model is unable to recognize the changes. To solve this issue, a new, more complicated model should be trained on a much larger dataset with a better coverage of spot parameters.

We used an evaluation dataset with GAIA light curves to test our model using real data. The precision of the model is 97%. One overcontact system without spots was misclassified as a detached system with spots and two detached systems without spots were misclassified as detached systems with spots. This is probably because of the relatively poor data quality of the GAIA light curves (outliers and noise).

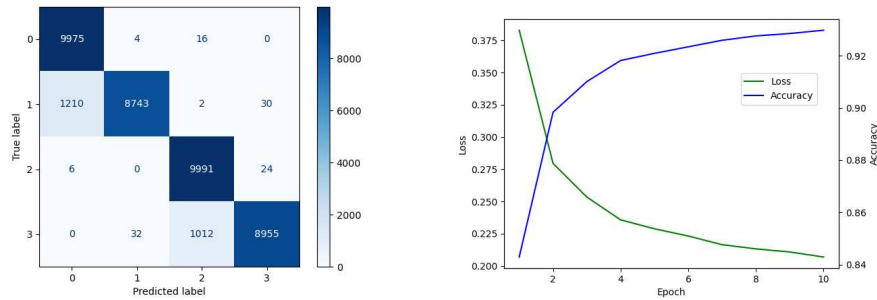


Figure 2. Confusion matrix (left) and performance of the model depending on epoch (right).

To achieve better results, it is necessary to process observational data better and train the model on more diverse synthetic data (wider range of system parameters and spots, different levels of noise, and/or adding outliers to synthetic data). Nevertheless, our classifier is now more likely to be applicable to GAIA data and promising for data analysis from large observational surveys, such as the Vera Rubin Telescope (LSST).

Acknowledgements. This research was supported by the Slovak Research and Development Agency under Contract No. APVV-20-0148. Y.M. was funded by the EU NextGenerationEU through the Recovery and Resilience Plan for Slovakia under project No. 09I03-03-V01-00011. V.K. was supported by Ukrainian National Grant 0122U000937.

References

- Chollet, F. et al. 2015, Keras, <https://github.com/fchollet/keras>
- Hilditch, R. W. 2001, *An Introduction to Close Binary Stars* (Cambridge University Press)
- Kallrath, J. & Milone, E. 2009, *Eclipsing Binary Stars: Modeling and Analysis* (New York: Springer-Verlag)
- Mowlavi, N., Holl, B., Lecoœur-Taïbi, I., et al., Gaia Data Release 3. The first Gaia catalogue of eclipsing-binary candidates. 2023, *Astronomy and Astrophysics*, **674**, A16, DOI: 10.1051/0004-6361/202245330
- Prša, A. 2018, *Modeling and Analysis of Eclipsing Binary Stars; The theory and design principles of PHOEBE* (IOP Publishing)
- Čokina, M., Fedurco, M., & Parimucha, Š., ELISa: A new tool for fast modelling of eclipsing binaries. 2021, *Astronomy and Astrophysics*, **652**, A156, DOI: 10.1051/0004-6361/202039171
- Wilson, R. E., Binary Star Light-Curve Models. 1994, *Publications of the ASP*, **106**, 921, DOI: 10.1086/133464

FM CMa: hot and massive eclipsing binary with a pulsating component

M. Vaňko¹ , T. Pribulla¹ , N. Shagatova¹ , R. Komžík¹  and
P. Dubovský² 

¹ *Astronomical Institute of the Slovak Academy of Sciences
059 60 Tatranská Lomnica, The Slovak Republic, (E-mail: vanko@ta3.sk)*

² *Vihorlat Astronomical Observatory, Mierová 4, 066 01 Humenné,
The Slovak Republic*

Received: November 2, 2023; Accepted: January 9, 2024

Abstract. Long-term spectroscopic monitoring of the eclipsing system FM CMa obtained between 2017–2023 at the Skalnaté Pleso (SPO, Slovakia) and Cerro-Tololo Interamerican observatories (CTIO, Chile) is presented. Preliminary analysis of the TESS high-precision satellite photometry (sectors 7 and 33, only FFI – Full Frame Image) shows that the eclipses in the system are total, and there is a slow apsidal motion. The light-curve solution requires a substantial amount of third light. In addition, the TESS light curve exhibits low-amplitude variability (in the out-of-eclipse parts), probably caused by radial pulsations with a frequency of about 5.5 cycles/day (4.3 hours). Line profiles show strong asymmetries corresponding to the photometric ephemeris but the possible third component is not visible. The nature of the system is discussed.

Key words: binary stars – eclipses – pulsations

1. Introduction

FM CMa ($V_{\max} = 8.73$, $\alpha_{2000} = 07^{\text{h}} 05^{\text{m}} 42.1^{\text{s}}$, $\delta_{2000} = -12^{\circ} 48' 43''$, HD 53756, TIC 148502346, TYC 5389-2875-1) is a hot eclipsing binary composed of a B2 primary and a colder secondary orbiting in $P = 2.78945$ days. Although the system is rather bright, it is neglected. Detailed information about the system is available in the literature (e.g. Hill 1967; van Hoof 1973; Eggen 1978; Kaltcheva & Hilditch 2000).

2. Observations

Our spectroscopic observations of FM CMa were obtained at the SPO with a MUSICOS-clone spectrograph fiber-fed from a 1.3m Nasmyth-Cassegrain telescope. In total, 19 high-resolution ($R = 35\,000$) spectra were obtained from

Table 1. The best photometric elements of the system, P – orbital period, T_0 – time of the periastron passage, i – inclination angle, r_{pri} – fractional radius of the primary component, $r_{\text{sec}}/r_{\text{pri}}$ – ratio of the component radii, e – orbital eccentricity, l_3 – third light expressed in the out-of-eclipse brightness of the eclipsing pair, T_{pri} , T_{sec} – effective temperatures of the components

| Parameter | Value | σ |
|---------------------------------|--------------|----------|
| P [d] | 2.78928 | 0.00012 |
| T_0 BJD [TDB] | 2459202.9041 | 0.0034 |
| i [deg] | 86.7 | 0.6 |
| r_{pri} | 0.2640 | 0.0025 |
| $r_{\text{sec}}/r_{\text{pri}}$ | 0.596 | 0.009 |
| e | 0.067 | 0.005 |
| ω [deg] | 274.4 | 0.4 |
| l_3 | 0.95 | 0.15 |
| T_{pri} [K] | 17368 | – |
| T_{sec} [K] | 14700 | 450 |

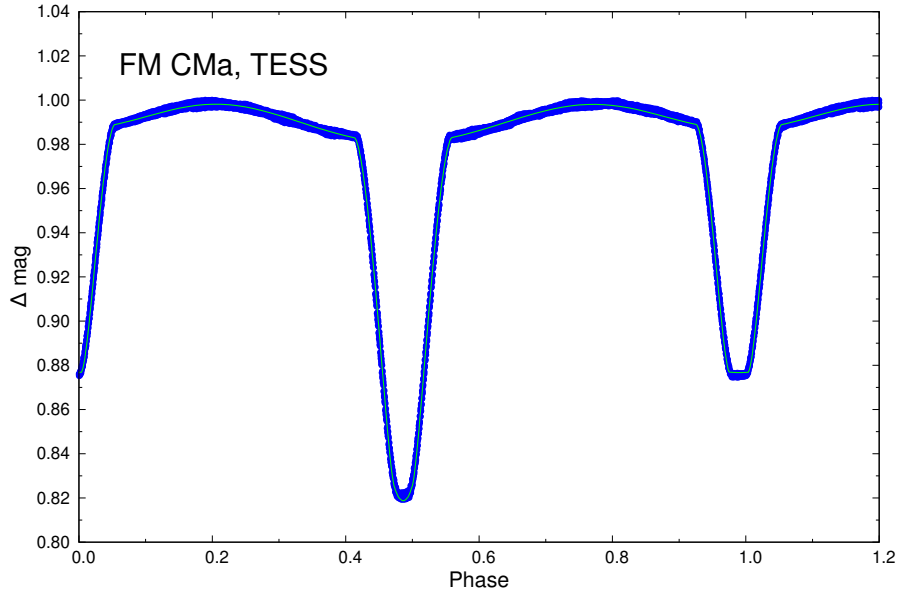


Figure 1. The best fit to the TESS photometry (sector 33) obtained with RMF. The fit corresponds to the parameters listed in Table 1.

January 2017 to March 2023. Because of its low declination, FM CMa was also observed with the CHIRON spectrograph (with an image slicer and $R = 70\,000$) fiber-fed from a 1.5m telescope at the CTIO. In total 7 spectra were obtained from October till December 2022. The spectra confirm the early B spectral type manifested by the dominant hydrogen Balmer and neutral helium lines. Only the strongest metallic lines are visible (e.g., Mg II 4481 Å, C II 4267 Å, the silicon triplet, Si III 4552 Å, 4567 Å, 4574 Å). The paucity of metallic lines complicates the determination of the radial velocity and spectra disentangling. The hydrogen-line profiles are asymmetric indicating a blend of two (or more) components. The light-curve solution indicates, the bolometric flux ratio of the primary and secondary component to be about 0.18.

In addition to the total eclipses, ellipsoidal variation and reflection effect, the TESS light curve exhibits additional low-amplitude variability, well visible in the out-of-eclipse parts of the light curve. This variability is very probably caused by radial pulsations. The dominant pulsational frequency is about 5.5 cycles/day (4.3 hours). The TESS light curve has been analysed using code RMF (Roche Modified code) (Garai et al., 2022). The light-curve model required a significant contribution of third light amounting to about 0.95 of the out-of-eclipse brightness of the eclipsing pair. Preliminary elements are listed in Table 1 and the corresponding fit to the TESS data is shown in Fig. 1. A comparison of the data from the two TESS sectors (almost two years apart) clearly shows that there is a slow apsidal motion with the apsidal motion cycle about $U = 92$ years long.

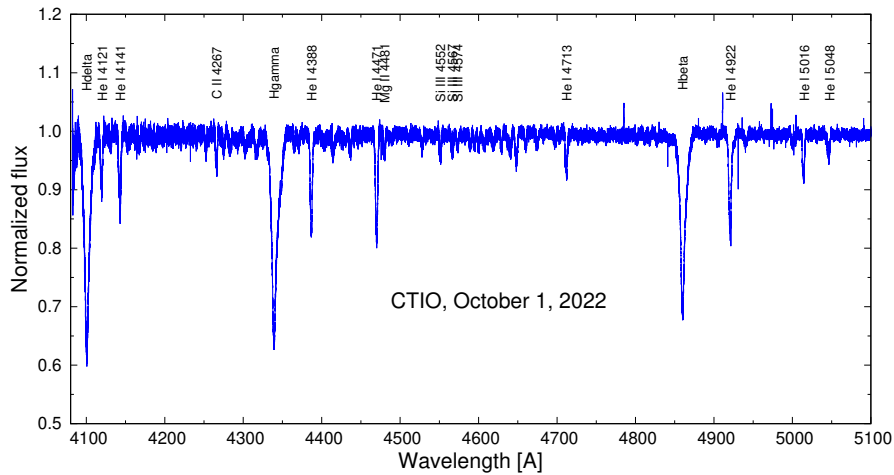


Figure 2. Blue spectrum of FM CMa with an identification of the most prominent spectral lines. A slight asymmetry best visible in the red wing of the hydrogen lines is very probably caused by the fainter and colder secondary component.

3. Conclusion

A preliminary analysis of the spectra indicates that the secondary component is possibly a rapidly rotating star which further complicates its detection and modelling, similar to the case of e.g., HD183986 (Vaňko et al., 2022). No traces of the possible tertiary component indicated by the photometric solution were found. Further spectroscopy will be focused on the total eclipses in the system which could help in disentangling the component's spectra.

Figure 2 shows that some lines in the blue part of the spectrum are slightly asymmetric. The variable asymmetric shapes of the absorption lines in this eclipsing system can be caused by the complex and non-uniform wind flows from the two components in the orbital plane. A similar system with an orbital period of 1.8 days with two massive B-type components AH Cep was detected in X-rays by Chandra observatory (Ignace et al., 2017). Its X-ray luminosity can originate from the wind collision between the two stars, supporting the complexity of the circum-stellar matter distribution in such systems.

Acknowledgements. This work was supported by the Slovak Research and Development Agency under contract No. APVV-20-0148 and by the VEGA grant (Scientific Grant Agency of Slovakia) of the Slovak Academy of Sciences No. 2/0031/22.

References

- Eggen, O. J., Canis Major OB1, Canis Major R1, NGC 2353, and W Canis Majoris. 1978, *Publications of the ASP*, **90**, 436, DOI: 10.1086/130354
- Garai, Z., Pribulla, T., Kovács, J., et al., Rapidly rotating stars and their transiting planets: KELT-17b, KELT-19Ab, and KELT-21b in the CHEOPS and TESS era. 2022, *Monthly Notices of the RAS*, **513**, 2822, DOI: 10.1093/mnras/stac1095
- Hill, G., On Beta Cephei Stars: a Search for Beta Cephei Stars. 1967, *Astrophysical Journal, Supplement*, **14**, 263, DOI: 10.1086/190156
- Ignace, R., Hole, K. T., Oskinova, L. M., & Rotter, J. P., An X-Ray Study of Two B+B Binaries: AH Cep and CW Cep. 2017, *Astrophysical Journal*, **850**, 82, DOI: 10.3847/1538-4357/aa93ea
- Kaltcheva, N. T. & Hilditch, R. W., The distribution of bright OB stars in the Canis Major-Puppis-Vela region of the Milky Way. 2000, *Monthly Notices of the RAS*, **312**, 753, DOI: 10.1046/j.1365-8711.2000.03170.x
- van Hoof, A., Note on Three of G. Hill's Stars. 1973, *Information Bulletin on Variable Stars*, **808**, 1
- Vaňko, M., Pribulla, T., Gajdoš, P., et al., HD 183986: A High-contrast SB2 System with a Pulsating Component. 2022, *Astronomical Journal*, **163**, 245, DOI: 10.3847/1538-3881/ac617b

The uniqueness of determination of the photometric mass ratio of contact binary stars with applications to selected binaries

E. Hambálek  and T. Pribulla 

*Astronomical Institute of the Slovak Academy of Sciences
059 60 Tatranská Lomnica, The Slovak Republic (E-mail: lhambalek@ta3.sk)*

Received: October 30, 2023; Accepted: December 14, 2023

Abstract. We have used a Roche-geometry code to pre-generate light curves of contact binary stars using only mass ratio q , fill out f of the Roche lobes, and the inclination i of the orbital plane. We have parametrized *TESS* light curves of several binaries with a trigonometric polynomial. We used our code **UNIQUE** to find the best fit of the overall shape of the observed light curve and its associated parameters (q , f , i). We compared these parameters to those from a rigorous modelling of our selected objects with known mass ratio q_{sp} inferred from spectra. The method is useful to find a close solution before the full modelling. We also got an indication of possible third light present in a system.

Key words: Stars: binaries: eclipsing – Techniques: photometric

1. Introduction

The shape of components of a binary star is dictated by the surface equipotential Ω and the mass ratio $q = M_2/M_1$. A direct way to find q is by measuring the radial velocities of both components and finding the ratio of their semi-amplitudes $q_{\text{sp}} = K_1/K_2$. Contact binaries are a special case, where the surface potential $\Omega(q)$ is a function of the mass ratio and is the same for both components. This allows us to connect it to the stellar radii. The system of parameters is more constrained, since the separation of both stars is also connected to their radii. We may define the so-called fill-out factor $f \in \langle 0.0, 1.0 \rangle$ as:

$$f = \frac{\Omega_{\text{inn}} - \Omega}{\Omega_{\text{inn}} - \Omega_{\text{out}}} \quad (1)$$

where $\Omega_{\text{inn}}(q)$ and $\Omega_{\text{out}}(q)$ pass through the Lagrange points corresponding to the inner (L_1) and outer (L_2) critical surfaces, respectively. Since for contact binaries, we have a monotonous function $q = M_2/M_1 \propto (r_2/r_1)^2$ (see Fig.1 in [Hambálek & Pribulla, 2013](#)), for any given f we can estimate the mass ratio from the shape of the light curve (LC).

Another important parameter is the inclination i of the orbital plane of companions from the line of sight of the observer. For contact binary stars, the separation of components is bound to their size, i.e. to their surface potential Ω . Because of this, the minimal inclination angle i_{tot} when a total eclipse is observed is a function of only the mass ratio q .

The amplitude of a light curve, or the difference in depths of primary and secondary minima, is larger for higher inclinations i (and saturated for total eclipses). However, the presence of another body in the system (that may or may not be visible in radial velocities) affects the LC with an added constant flux that results in shallower depths of minima. This leads to smaller apparent inclination values i and further underestimating the photometric mass ratio q_{ph} . We can add a new dimensionless parameter - the third light l_3 that can be defined as a ratio of the parasitic flux (F_3) to the overall flux of the contact binary: $l_3 = F_3 / (F_1 + F_2)$.

We can describe the overall shape of LC of contact binaries by an orthogonal trigonometric polynomial:

$$I(\varphi) = a_0 + \sum_{k=1}^n a_k \cos(2\pi k\varphi) + \sum_{k=1}^n b_k \sin(2\pi k\varphi) \quad (2)$$

In this study, we assume only LCs symmetrical around the orbital phase $\varphi = 0.5$ (secondary minimum), i.e. circular orbits and no O'Connell effect of starspots. This allows us to put $b_k = 0$. We have found that for our purpose a polynomial order $n = 10$ is sufficient to represent the most LCs. However, a totally eclipsing system might require the order $n = 20$ (see Rucinski, 1993). If we instead use only polynomial of the order $n = 10$, the residuals in the LC minima of a totally eclipsing system are ~ 5 -times larger than those of a partially eclipsing system and are still sufficient for the data noise present in the LC (Hambálek & Pribulla, 2013). We found by comparison that the mass ratio q of such a curve is not sensitive to the higher polynomial solution and opted for the minimum case of $n = 10$.

2. Finding close solutions from *TESS* light curves

We have used the code `ROCHE` (Pribulla, 2012) to generate LCs of contact binaries with mass ratios $q \in \langle 0.05, 1.00 \rangle$, step $\Delta q = 0.025$, fill-out factors $f \in \langle 0.0, 1.0 \rangle$, step $\Delta f = 0.25$, and inclinations $i \in \langle 30, 90 \rangle$ deg, step $\Delta i = 1$ deg. The Roche potential was used for the shape of the stellar surface. Fluxes were integrated over visible surface elements. This synthetic LC was parametrized by a_k coefficients of eq. 2 ($k = 0..10$). We have generated a library of total 11 895 LCs (see Hambálek & Pribulla, 2013).

For our purpose, the most notable coefficients are: a_1 which affects the difference of depths of primary and secondary minimum, a_2 which (for contact systems) is almost equal to the amplitude of LC, and a_4 which is tied to the

Table 1. Comparison of parameters q , f , i , and l_3 determined from modelling with available spectroscopy and model in literature (subscript L) to those found by **UNI**QUE as the best approximation of the *TESS* light-curve (subscript B). Note: the fill-out factor for EB-type binaries is not applicable.

| star | q_L | f_L | i_L [deg] | $l_{3,L}$ | q_B | f_B | i_B [deg] | $l_{3,B}$ | type |
|-----------|--------------------|-------------------|--------------------|--------------------|--------|----------|----------------|-----------|------|
| AG Vir | 0.341 ^a | 0.17 ^b | 84 ^b | 0.05 ^a | 0.325 | 0.00 | 78 | <0.20 | EW A |
| AW UMa | 0.108 ^c | 0.30 ^c | 78 ^d | 0.00 ^c | 0.075 | 0.25 | 84 | 0.00 | EW |
| DU Boo | 0.206 ^b | 0.56 ^b | 81 ^b | 0.00 ^b | >0.125 | 0.50 | 81 | 0.00 | EW A |
| EL Boo | 0.248 ^d | 0.00 ^e | 74 ^e | 1.00 ^f | >0.100 | 0.00 | 64 | 1.00 | EW |
| EQ Tau | 0.442 ^g | 0.09 ^e | 82 ^e | 0.00 ^g | 0.475 | 0.00 | 79 | 0.00 | EW A |
| FI Boo | 0.372 ^h | 0.50 ⁱ | 38 ⁱ | 0.30 ^h | 0.850 | 0.75(25) | 31 | 0.30(10) | EW W |
| FT UMa | 0.984 ^f | N/A | 60(3) ^j | 1.01 ^f | 1.000 | 0.00 | 61 | 0.80 | EB |
| SW Lac | 0.776 ^k | ? | ? | <0.05 ^k | 0.600 | 0.25 | 81 | <0.20 | EW W |
| SX Crv | 0.066 ^g | ? | 65(5) ^g | 0.00 ^g | 0.100 | 0.25 | 60 | 0.00 | EW A |
| V1191 Cyg | 0.107 ^l | 0.30 ^m | 83(2) ^m | 0.00 ^l | 0.075 | 0.25 | 74 | 0.00 | EW W |
| V523 Cas | 0.516 ⁿ | 0.00 ^o | 84(1) ^o | 0.00 ⁿ | 0.500 | 0.00 | 85(3) | 0.00 | EW W |
| V753 Mon | 0.970 ^p | N/A | 75 ^q | 0.00 ^p | 1.000 | 0.00 | 75 | 0.00 | EB |
| VW LMi | 0.423 ^a | 0.47 ^r | 79 ^s | 0.42 ^a | 0.325 | 0.25 | 71 | 0.20 | EW W |
| W UMa | 0.484 ^t | 0.10 ^u | 86 ^u | 0.00 ^t | 0.450 | 0.00 | 86(2) | 0.00 | EW |

Source: ^aPribulla et al. (2006), ^bPribulla et al. (2011), ^cPribulla & Rucinski (2008), ^dPribulla & Rucinski (2006), ^eDeb & Singh (2011), ^fPribulla et al. (2009), ^gRucinski et al. (2001), ^hLu et al. (2001), ⁱChristopoulou & Papageorgiou (2013), ^jYuan (2011), ^kRucinski et al. (2005), ^lRucinski et al. (2008), ^mEkmekçi et al. (2012), ⁿRucinski et al. (2003), ^oMohammadi et al. (2016), ^pRucinski et al. (2000), ^qQian et al. (2013), ^rSánchez-Bajo et al. (2007), ^sPribulla et al. (2008), ^tPribulla et al. (2007), ^uLinnell (1991).

fill-out factor (if component stars are not in contact) and affects the width of minima.

We have written a simple Python code **UNI**QUE to get an arbitrary LC and compare it with those in the pre-generated library. The input LC can be expressed in magnitudes or fluxes. First, it is reduced to a normalized flux (using zero magnitudes of common filters). A Python package `lightkurve` is used to re-bin and phase the LC by the orbital period. We apply a sigma clipping to remove any outliers. If the LC is too sparse, we can run a Savitzky-Golay filter (from `scipy.signal`) on the data to compute a smoothed average curve.

Then the code runs a least-square fitting model (from `lmfit.Model`) to determine the coefficients a_k . Finally, we can compare the set of coefficients to those (a'_k) from pre-computed LCs by computing a difference $D = \sqrt{\sum_k^{10} (a_k - a'_k)^2}$. The code produces a list of similar solutions (i.e. $D <$ an arbitrary value) with parameters q , f , i , and l_3 which were used in their generation. The limiting

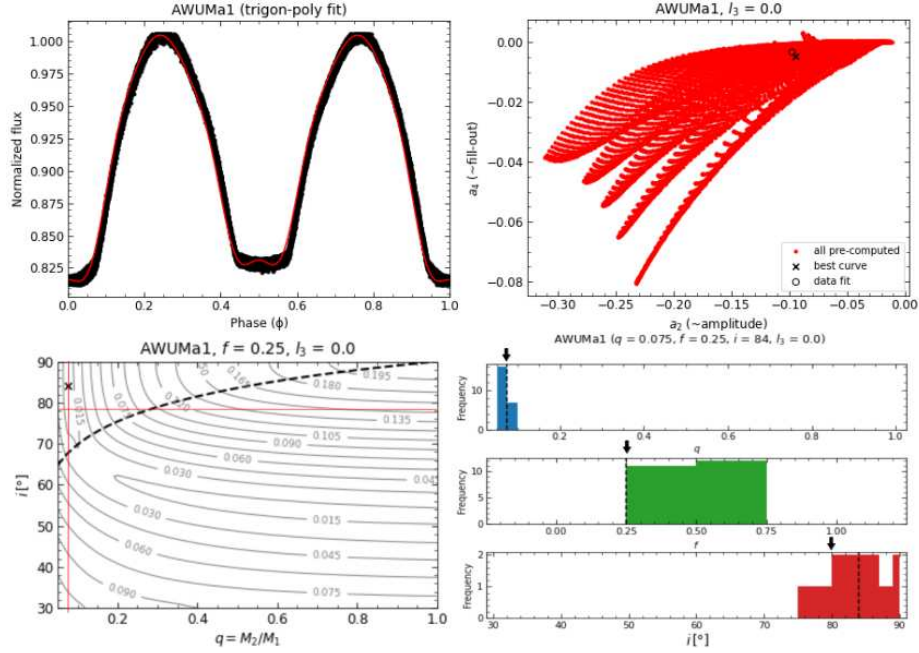


Figure 1. The result for star AW UMa (*TESS* cadence 120 s). Top left: trigonometric fit (red line) of observed LC (black). Top right: the best solution (\times) with $l_{3,B} = 0.0$ (even if unknown was assumed) is close to a pre-computed LC (\circ). Bottom left: Best solution (\times) in difference plot q vs. i corresponds to total eclipses (above the dashed line). Bottom right: Colour histograms (q - blue, f - green, i - red) of similar values with the smallest differences. The solution from rigorous modelling is marked with arrows, while the best result of **UNIQUE** is represented by a vertical dashed line.

value of D is selected based on the minimum value of D_{min} and a fraction of the standard deviation. The number of contours (Fig. 1 bottom left) depends on the total span of all D values. A statistical distribution is also generated to see the most probable result (Fig. 1 bottom right).

If the third light l_3 is known, the user can compute the LC coefficients for this specific value only. Otherwise a default set of typical values of $l_3 \in \{0.0, 0.2, 0.4, 0.6, 0.8, 1.0\}$ is used as a proxy for an unknown amount of the third light. In general, this increases the uncertainty of mass ratio q , which can be then treated only as a lower limit.

We have selected 14 eclipsing binaries with known q_{sp} and found photometric Roche-model parameters f , i , and possible l_3 in literature. In Table 1, we compare them to the best results from the **UNIQUE** library of LCs. All *TESS* LCs were analyzed by individual sectors. Sometimes, the results found a range of

“best” parameters caused mainly by uneven maxima brightness - the so-called O’Connell effect (see e.g. [Wilsey & Beaky, 2009](#)). This leads to higher values of i and lower values of q . Totally eclipsing systems (e.g. V523 Cas, AW UMa, etc.) have a small uncertainty of q , but virtually all values of i above the dashed line like in Figure 1 bottom left are indistinguishable. We note that the close binary AW UMa is accompanied by a third component on a ~ 17 -year orbit ([Pribulla & Rucinski, 2006](#)) that is not affecting the LC and thus the estimation of close binary parameters q , i , f . Also, systems FI Boo, SW LAc, V753 Mon, and W UMa have wider third components ([Pribulla & Rucinski, 2006](#)) on longer orbits than ~ 20 years. Furthermore, VW LMi is a quadruple system ([Pribulla et al., 2006](#)) with the second close binary being non-eclipsing, thus affecting only l_3 . EB-type systems (FT UMa and V753 Mon) are not in contact and our UNiQUE solutions are strictly favouring only LCs with $f = 0$. In general, l_3 was kept a free parameter and in our test cases, it still was sensitive to values as small as $l_3 \sim 0.05$ (e.g. SW Lac) when it selected an LC with the nearest non-zero l_3 .

Acknowledgements. This work was supported by the Slovak Research and Development Agency under the contract No. APVV-20-0148. This work has also been supported by the VEGA grant of the Slovak Academy of Sciences No. 2/0031/22.

References

- Christopoulou, P. E. & Papageorgiou, A., An Extensive Analysis of the Triple W UMa Type Binary FI Boo. 2013, *Astronomical Journal*, **146**, 157, DOI: 10.1088/0004-6256/146/6/157
- Deb, S. & Singh, H. P., Physical parameters of 62 eclipsing binary stars using the All Sky Automated Survey-3 data - I. 2011, *Monthly Notices of the RAS*, **412**, 1787, DOI: 10.1111/j.1365-2966.2010.18016.x
- Ekmekçi, F., Elmaslı, A., Yılmaz, M., et al., Physical parameters of some close binaries: ET Boo, V1123 Tau, V1191 Cyg, V1073 Cyg and V357 Peg. 2012, *New Astronomy*, **17**, 603, DOI: 10.1016/j.newast.2012.03.001
- Hambálek, E. & Pribulla, T., The reliability of mass-ratio determination from light curves of contact binary stars. 2013, *Contributions of the Astronomical Observatory Skalnaté Pleso*, **43**, 27
- Linnell, A. P., A Light Synthesis Study of W Ursae Majoris. 1991, *Astrophysical Journal*, **374**, 307, DOI: 10.1086/170120
- Lu, W., Rucinski, S. M., & Ogłóza, W., Radial Velocity Studies of Close Binary Stars. IV. 2001, *Astronomical Journal*, **122**, 402, DOI: 10.1086/321131
- Mohammadi, M., Abedi, A., & Riazi, N., Period and light-curve study of the contact eclipsing binary V523 Cas. 2016, *New Astronomy*, **44**, 78, DOI: 10.1016/j.newast.2015.10.001

- Pribulla, T., ROCHE: Analysis of Eclipsing Binary Multi-Dataset Observables. 2012, in *From Interacting Binaries to Exoplanets: Essential Modeling Tools*, ed. M. T. Richards & I. Hubeny (Cambridge University Press (CUP)), 279–282
- Pribulla, T., Baluďanský, D., Dubovský, P., et al., VW LMi: tightest quadruple system known. Light-time effect and possible secular changes of orbits. 2008, *Monthly Notices of the RAS*, **390**, 798, DOI: 10.1111/j.1365-2966.2008.13781.x
- Pribulla, T. & Rucinski, S. M., Contact Binaries with Additional Components. I. The Extant Data. 2006, *Astronomical Journal*, **131**, 2986, DOI: 10.1086/503871
- Pribulla, T. & Rucinski, S. M., Radial velocity mapping of Paczyński’s star AW UMa: not a contact binary. 2008, *Monthly Notices of the RAS*, **386**, 377, DOI: 10.1111/j.1365-2966.2008.13033.x
- Pribulla, T., Rucinski, S. M., Conidis, G., et al., Radial Velocity Studies of Close Binary Stars. XII. 2007, *Astronomical Journal*, **133**, 1977, DOI: 10.1086/512772
- Pribulla, T., Rucinski, S. M., DeBond, H., et al., Radial Velocity Studies of Close Binary Stars. XIV. 2009, *Astronomical Journal*, **137**, 3646, DOI: 10.1088/0004-6256/137/3/3646
- Pribulla, T., Rucinski, S. M., Lu, W., et al., Radial Velocity Studies of Close Binary Stars. XI. 2006, *Astronomical Journal*, **132**, 769, DOI: 10.1086/505536
- Pribulla, T., Vaňko, M., Chochol, D., Hambálek, Ľ., & Parimucha, Š., O’Connell effect in early-type contact binaries: du Boo and AG Vir. 2011, *Astronomische Nachrichten*, **332**, 607, DOI: 10.1002/asna.201111569
- Qian, S. B., Zhang, J., Wang, J. J., et al., V753 Mon: A Unique Close Binary Just after the Evolutionary Stage with the Shortest Period during Mass Transfer. 2013, *Astrophysical Journal, Supplement*, **207**, 22, DOI: 10.1088/0067-0049/207/2/22
- Rucinski, S. M., A Simple Description of Light Curves of W UMa Systems. 1993, *Publications of the ASP*, **105**, 1433, DOI: 10.1086/133326
- Rucinski, S. M., Capobianco, C. C., Lu, W., et al., Radial Velocity Studies of Close Binary Stars. VIII. 2003, *Astronomical Journal*, **125**, 3258, DOI: 10.1086/374949
- Rucinski, S. M., Lu, W., & Mochnacki, S. W., Radial Velocity Studies of Close Binary Stars. III. 2000, *Astronomical Journal*, **120**, 1133, DOI: 10.1086/301458
- Rucinski, S. M., Lu, W., Mochnacki, S. W., Ogłóza, W., & Stachowski, G., Radial Velocity Studies of Close Binary Stars. V. 2001, *Astronomical Journal*, **122**, 1974, DOI: 10.1086/323106
- Rucinski, S. M., Pribulla, T., Mochnacki, S. W., et al., Radial Velocity Studies of Close Binary Stars. XIII. 2008, *Astronomical Journal*, **136**, 586, DOI: 10.1088/0004-6256/136/2/586
- Rucinski, S. M., Pych, W., Ogłóza, W., et al., Radial Velocity Studies of Close Binary Stars. X. 2005, *Astronomical Journal*, **130**, 767, DOI: 10.1086/431226
- Sánchez-Bajo, F., García-Melendo, E., & Gómez-Forrellad, J. M., Photometric study of the W UMa eclipsing binaries VW LMi and BX Dra. 2007, *Astrophysics and Space Science*, **312**, 151, DOI: 10.1007/s10509-007-9668-4

- Wilsey, N. J. & Beaky, M. M., Revisiting the O'Connell Effect in Eclipsing Binary Systems. 2009, *Society for Astronomical Sciences Annual Symposium*, **28**, 107
- Yuan, J.-Z., A multicolor photometric study of the neglected eclipsing binary FT Ursae Majoris. 2011, *Research in Astronomy and Astrophysics*, **11**, 1158, DOI: 10.1088/1674-4527/11/10/004

TYC 1083-12-1 – an SB2 binary mimicking an exoplanetary candidate

M. Skarka^{1,2,4}, J. Lipták^{1,3}, D. Stoklásek², P. Cagaš⁴ and
P. Kabáth^{1,4}

¹ *Astronomical Institute of the Czech Academy of Sciences
251 65 Ondřejov, The Czech Republic, (E-mail: skarka@asu.cas.cz)*

² *Department of Theoretical Physics and Astrophysics, Faculty of Science,
Masaryk University, Kotlářská 267/2, 611 37 Brno, Czech Republic*

³ *Astronomical Institute, Faculty of Mathematics and Physics, Charles
University, V Holešovičkách 2, 180 00 Praha 8, Czech Republic*

⁴ *Variable Star and Exoplanet Section, Czech Astronomical Society, Fričova
298, 251 65 Ondřejov, Czech Republic*

Received: November 3, 2023; Accepted: December 20, 2023

Abstract. TYC 1083-12-1 (sp. type F8V) was identified as a potential exoplanetary candidate in the data from a photometric survey with a 30-cm telescope. From the radial velocity observations of the star, we found that it is a double-lined binary with very similar components. We present the basic parameters of this system.

Key words: Stars: binaries – Techniques: photometric – Techniques: spectroscopic – Methods: analysis

1. Introduction

Many new exoplanetary candidates are being discovered through large-sky surveys such as *TESS* (Ricker et al., 2015). However, to confirm these candidates, spectroscopic follow-up observations are necessary to identify false positives. In 2013, a star TYC 1083-12-1 (RAJ2000=19:55:24.32, DEJ2000=+13:11:05.9, $V = 12.52$ mag, $B - V = 0.53$ mag, Zacharias et al., 2013) was identified as a variable star of EA type and designated as CzeV3837 in the catalogue of variable stars discovered by Czech astronomers (Skarka et al., 2017). Due to the shallow eclipses with the same depth, we suspected CzeV3837 to be an exoplanetary candidate.

2. Observations

We collected 3,238 clear-filter observations with a mean photometric error of 4 mmag between September 2011 and July 2020. During the observing seasons

between 2011 and 2020, we used telescopes of 25cm and 30cm (after 2015) that were equipped with Kodak KAF-16803 CCD-based G4-16000 camera. Since 2015, we have used a C4-16000 camera with a GSENSE4040 CMOS chip. For the binary model, we utilized *TESS* data processed with the SPOC pipeline (Jenkins et al., 2016). We then downloaded and detrended this data using the LIGHTKURVE package (Lightkurve Collaboration et al., 2018). Both data sets are displayed in the top left panel of Fig. 1. We phase-folded them with the orbital period of 3.23647(1) days and zero epoch BJD= 2456204.3435(13). We estimated zero epoch using our observations.

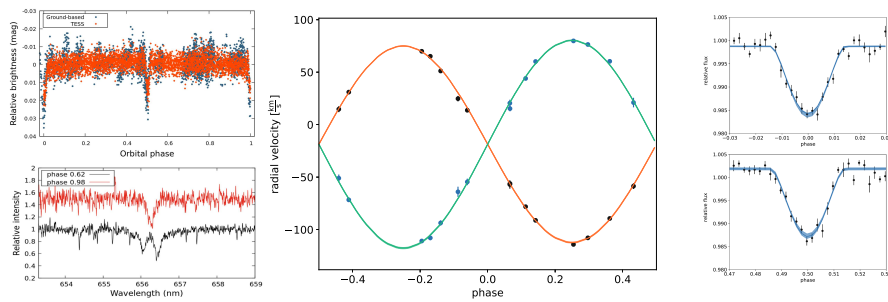


Figure 1. Photometric data (top left), spectra in different orbital phases (bottom left), radial-velocity curve showing both model and observations (middle panel) and models of primary (top right) and secondary eclipses (bottom right). Photometric data were binned for better readability.

We used the OES spectrograph ($R \approx 50000$, Koubský et al., 2004; Kabáth et al., 2020) mounted on the 2m telescope located in Ondřejov, Czech Republic to collect spectroscopic observations. From July to September 2020, we obtained 17 spectra with signal-to-noise ratios ranging from 5 to 21. The examples of spectra in different orbital phases are shown in the bottom left panel of Fig. 1 giving a clear picture of the binary nature of the radial-velocity variations.

3. Analysis

We used ELLC (Maxted, 2016) to model the system based on the radial velocity observations (determined with fxcor task in IRAF package, middle panel of Fig. 1) and *TESS* photometry (right-hand panels of Fig. 1). We fixed the temperature of the primary star T_1 at 6200 K (from the B-V based on relations from Ballesteros (2012)). This value is consistent with 6251 K from Gaia DR3 catalogue (Gaia Collaboration, 2022) which is based on *BP/RP* spectra and includes stellar extinction. We used logarithmic prescription for the limb darkening

Table 1. System parameters from the modeling.

| | | | | | | | |
|-----|----------|-------------------|----------|-----------|----------|-----------------|------------|
| q | 0.945(5) | i (deg) | 79.69(3) | T_2/T_1 | 1.02(2) | $(R_1 + R_2)/a$ | 0.200(5) |
| e | < 0.02 | a (R_\odot) | 12.54(4) | R_2/R_1 | 0.92(12) | γ (km/s) | -18.58(20) |

with coefficients for a given temperature from the atmospheric tables by [Husser et al. \(2013\)](#) and values of albedo $A = 0.6$, gravity darkening $\beta = 0.32$. From system parameters in Table 1 we derived radii and masses of the components as $R_1 = 1.31(9) R_\odot$, $R_2 = 1.2(1) R_\odot$, $M_1 = 1.301(17) M_\odot$, $M_2 = 1.229(18) M_\odot$.

4. Conclusions

We used spectroscopic observations to demonstrate that TYC 1083-12-1 is an SB2 eclipsing binary star, rather than an exoplanet. The stellar parameters of both components match those of F8 and F6 spectral type stars listed in the recent version¹ of the table by [Pecaut et al. \(2012\)](#) within uncertainties. According to [Raghavan et al. \(2010\)](#), TYC 1083-12-1 belongs to the 20% of FGK stars that have a semi-major axis less than 10 au.

Acknowledgements. MS and PK acknowledge the financial support of the Inter-transfer grant no LTT-20015, and JL acknowledges the financial support of the GAČR grant no 22-30516K. We acknowledge the usage of the data taken with the Perek telescope at the Astronomical Institute of CAS. We thank the anonymous referee for the comments.

References

- Ballesteros, F. J. 2012, *EPL (Europhysics Letters)*, **97**, 34008, DOI: 10.1209/0295-5075/97/34008
- Gaia Collaboration, VizieR Online Data Catalog: Gaia DR3 Part 1. Main source (Gaia Collaboration, 2022). 2022, *VizieR Online Data Catalog*, I/355, DOI: 10.26093/cds/vizier.1355
- Husser, T. O., Wende-von Berg, S., Dreizler, S., et al. 2013, *Astronomy and Astrophysics*, **553**, A6, DOI: 10.1051/0004-6361/201219058
- Jenkins, J. M., Twicken, J. D., McCauliff, S., et al., The TESS science processing operations center. 2016, in Society of Photo-Optical Instrumentation Engineers (SPIE) Conference Series, Vol. **9913**, *Software and Cyberinfrastructure for Astronomy IV*, ed. G. Chiozzi & J. C. Guzman, 99133E
- Kabáth, P., Skarka, M., Sabotta, S., et al. 2020, *Publications of the ASP*, **132**, 035002, DOI: 10.1088/1538-3873/ab6752

¹https://www.pas.rochester.edu/~emamajek/EEM_dwarf_UBVIJHK_colors_Teff.txt

- Koubský, P., Mayer, P., Čáp, J., et al. 2004, *Publications of the Astronomical Institute of the Czechoslovak Academy of Sciences*, **92**, 37
- Lightkurve Collaboration, Cardoso, J. V. d. M., Hedges, C., et al. 2018, Lightkurve: Kepler and TESS time series analysis in Python, Astrophysics Source Code Library
- Maxted, P. F. L. 2016, *Astronomy and Astrophysics*, **591**, A111, DOI: 10.1051/0004-6361/201628579
- Pecaut, M. J., Mamajek, E. E., & Bubar, E. J., A Revised Age for Upper Scorpius and the Star Formation History among the F-type Members of the Scorpius-Centaurus OB Association. 2012, *Astrophysical Journal*, **746**, 154, DOI: 10.1088/0004-637X/746/2/154
- Raghavan, D., McAlister, H. A., Henry, T. J., et al., A Survey of Stellar Families: Multiplicity of Solar-type Stars. 2010, *Astrophysical Journal, Supplement*, **190**, 1, DOI: 10.1088/0067-0049/190/1/1
- Ricker, G. R., Winn, J. N., Vanderspek, R., et al., Transiting Exoplanet Survey Satellite (TESS). 2015, *Journal of Astronomical Telescopes, Instruments, and Systems*, **1**, 014003, DOI: 10.1117/1.JATIS.1.1.014003
- Skarka, M., Mašek, M., Brát, L., et al. 2017, *Open European Journal on Variable Stars*, **185**, 1, DOI: 10.48550/arXiv.1709.08851
- Zacharias, N., Finch, C. T., Girard, T. M., et al. 2013, *Astronomical Journal*, **145**, 44, DOI: 10.1088/0004-6256/145/2/44

Optical observations of RS Oph after its 2021 outburst

M. Tomova¹, K. Stoyanov¹, Y. Nikolov¹ and P. Kaygorodov²

¹ *Institute of Astronomy and NAO, Bulgarian Academy of Sciences,
72 Tsarigradsko Chausse Blvd., BG-1784 Sofia, Bulgaria*

² *Institute of Astronomy of the Russian Academy of Sciences, 48 Pyatnitskaya
Str., 119017 Moscow, Russia*

Received: November 2, 2023; Accepted: January 11, 2024

Abstract. RS Oph is a recurrent symbiotic novae which underwent its last optical eruption in August 2021. The early H α spectroscopy of the system (at days 11–15 of the outburst) reveals satellite line components at the velocity position of about $\pm 2400 \text{ km s}^{-1}$ which are an indication of bipolar collimated outflow. We derived some parameters of the outflows and system's components and their evolution during our observation.

Key words: binaries: symbiotic – stars: mass-loss – stars: individual: RS Oph

1. Introduction

RS Oph consists of a red giant and a massive white dwarf with a heavy mass loss during activity. Its last 2021 outburst began on August 8.93¹ and was observed over the whole electromagnetic domain. Here we report high-resolution H α spectroscopy of the system, obtained at days 11–15 (August, 19–23) of the outburst with the Coudé spectrograph of the 2m RCC telescope at Rozhen NAO, Bulgaria. We present low-resolution observations (the resolving power is $R \sim 1100$) secured with the 2-Channel-Focal-Reducer Rozhen, attached to the Cassegrain focus of the 2m RCC telescope as well.

2. Spectral Energy Distribution (SED)

To examine the outflow structure of the outbursting compact object, we built the SED of the system for the first and last day of the observations. We used average U , B , V , R_C , and I_C photometric estimates from the light curves of the AAVSO database² taken during our observations from August 19 to 23. The approximation of the $UBVR_CI_C$ fluxes showed that for this period T_{eff} of the pseudophotosphere and T_e of the nebula have not changed: $T_{\text{eff}} = 15\,000 \pm 1\,000 \text{ K}$

¹Geary, K., 2021, AAVSO Alert Notice 752 (20210809)

²International Database contributed by observers worldwide.

and $T_e = 17\,000 \pm 3\,000$ K. We obtained $R_{\text{eff}} = (13.3 \pm 2.0)(d/1.6\text{kpc}) R_{\odot}$ and $EM = (9.50 \pm 0.59) 10^{61} (d/1.6\text{kpc})^2 \text{cm}^{-3}$ for August 19 and $R_{\text{eff}} = (10.3 \pm 1.6)(d/1.6\text{kpc}) R_{\odot}$ and $EM = (5.60 \pm 0.35) 10^{61} (d/1.6\text{kpc})^2 \text{cm}^{-3}$ for August 23. The SED is presented in Fig. 1 (Tomov et al., 2023).

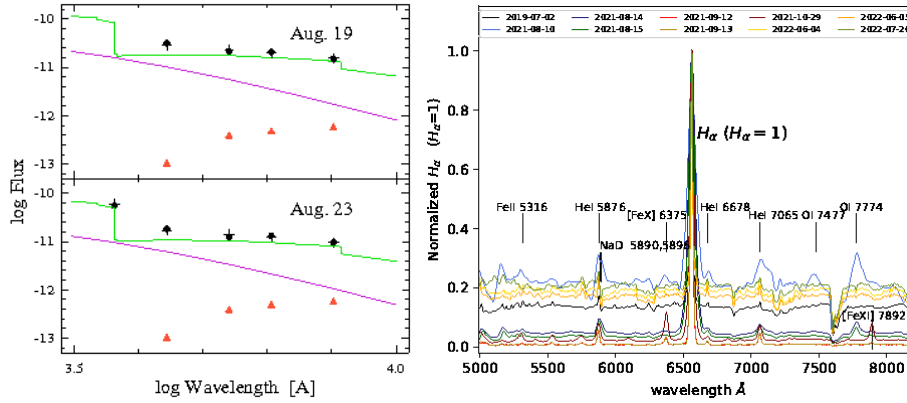


Figure 1. *Left panel:* SED for days 11 and 15 (see Tomov et al., 2023). *Right panel:* Spectral evolution based on low-resolution spectra (see Nikolov et al., 2023).

3. $H\alpha$ profile, spectral evolution and mass-loss rate

Our spectral observations reveal a typical behaviour of a nova with a complex structure dominated by broad Balmer, He, O and Fe lines with some P Cyg profiles, evolved towards a supersoft source phase (see Fig. 1). The most prominent feature on the spectra is the $H\alpha$ emission line. A P Cyg profile with velocity up to $\sim -4260 \text{ km s}^{-1}$ (Nikolov, 2023) is detected on day 2 (Aug. 10).

The complex structure of $H\alpha$ line is better seen in our high-resolution spectra, obtained at days 11–15 of the outburst (Tomov et al., 2023). The $H\alpha$ profile has strongly changed – the very sharp emission and absorption spikes, which were observed at day 2.3 (Munari et al., 2022) on top of the much wider and stronger emission line, were very weak. The very intensive broad component had an appreciable asymmetry and very broad low-intensity wings reaching $\pm 3500 \text{ km s}^{-1}$ (Fig. 2). We assume this velocity to be related to nebular material ejected by the outbursting component. $H\alpha$ had very weak satellite components at a velocity position of about $\pm 2400 \text{ km s}^{-1}$ as well. We suppose that the satellite components are an indication of bipolar outflow from the outbursting component as during the 2006 eruption. It is worth noting that satellite components were also present in 2006 (Skopal et al., 2008) and they were much more intense relative to the central emission of the line than during the 2021 eruption. To obtain the parameters of the stellar wind and bipolar outflow, we analysed the $H\alpha$ profile by means of approximation with different functions, which are

shown in Fig. 2. The parameters of the satellite components determined by this approximation are listed in Tab. 1 (Tomov et al., 2023).

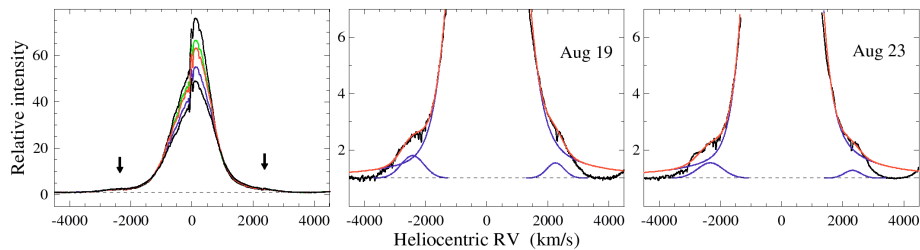


Figure 2. H α line. The spectrum of lowest intensity relates to August 19.

Table 1. Parameters of the satellite components. The flux is in units of 10^{-10} erg cm $^{-2}$ s $^{-1}$, velocity and FWHM in km s $^{-1}$, linear angle θ in deg, and mass-loss rate in $10^{-6}(\text{d}/1.6\text{kpc})^{3/2} M_{\odot} \text{yr}^{-1}$.

| Date | Blue | | | | | Red | | | | |
|--------|-------|------|------------|----------|-----------|-------|------|------------|----------|-----------|
| | F | FWHM | $v/\cos i$ | θ | \dot{M} | F | FWHM | $v/\cos i$ | θ | \dot{M} |
| Aug 19 | 3.320 | 880 | 3780 | 35.6 | 1.2 | 1.706 | 670 | 3500 | 29.0 | 0.6 |
| Aug 20 | 2.846 | 1000 | 3720 | 41.2 | 1.2 | 1.608 | 850 | 3460 | 37.5 | 0.8 |
| Aug 21 | 2.699 | 1040 | 3640 | 43.8 | 1.2 | 1.352 | 780 | 3540 | 33.5 | 0.6 |
| Aug 22 | 2.243 | 1030 | 3620 | 43.7 | 1.0 | 1.145 | 840 | 3500 | 36.7 | 0.6 |
| Aug 23 | 1.559 | 970 | 3620 | 40.9 | 0.8 | 0.519 | 640 | 3610 | 26.7 | 0.3 |

4. Conclusions

We analysed the H α profile with the aim being to study the structure of the outflowing material. We observed a disc-shaped warm shell occulting the central hot object and bipolar outflow. We find that during the 2021 eruption, about 30%–50% of the nebular emission belongs to the high-velocity wind, the H α luminosity of which was less than $2700 L_{\odot}$. The mass-loss rate of the outbursting object through its wind is much greater than through its streams. The total rate (from wind + streams) was less than $(4 - 5) 10^{-5} (\text{d}/1.6\text{kpc})^{3/2} M_{\odot} \text{yr}^{-1}$.

Acknowledgements. This work was supported by Bulgarian National Science Fund under grant KP-06-Russia/2-2020 and RFBR grant 20-52-18015.

References

- Munari, U., Giroletti, M., Marcote, B., O'Brien, T.J., Veres, P., Yang, J., Williams, D. R. A., Woudt, P.: 2022, *A&A*, **666**, L6
- Nikolov, Y., Luna, G.J.M., Stoyanov, K.A., et al.: 2023, *A&A*, **679**, A150
- Skopal, A., Pribulla, T., Buil, Ch., Vittone, A., Errico, L.: 2008, in *ASP Conf. Ser.*, Vol. **401**, 227
- Tomov, N.A., Tomova, M.T., Stoyanov, K.A., et al.: 2023, *A&A*, **671**, A49

Spectroscopic characterization of superflares on solar-type stars – a joint observing campaign

M. Leitzinger¹, P. Kabáth², M. Vaňko³, T. Pribulla³,
R. Komžík³, Z. Garai^{3,4,5}, R. Karjalainen², P. Odert¹,
J. Lipták^{2,6}, P. Heinzel^{2,7}, J. Wollmann², R. Greimel³ and
E.W. Guenther⁸

¹ *Institute of Physics/Department of Astrophysics and Geophysics, University of Graz, Universitätsplatz 5, 8010 Graz, Austria (E-mail: martin.leitzinger@uni-graz.at)*

² *Astronomical Institute, The Czech Academy of Sciences, 25165 Ondřejov, Czech Republic*

³ *Astronomical Institute, Slovak Academy of Sciences, 059 60 Tatranská Lomnica, Slovakia*

⁴ *HUN-REN-ELTE Exoplanet Research Group, 9700 Szombathely, Szent Imre h. u. 112, Hungary*

⁵ *ELTE Gothard Astrophysical Observatory, 9700 Szombathely, Szent Imre h.u. 112, Hungary*

⁶ *Charles University - Astronomický ústav UK, V Holešovičkách 2, 180 00 Praha, Czech Republic*

⁷ *University of Wrocław, Center of Scientific Excellence – Solar and Stellar Activity, Kopernika 11, 51-622 Wrocław, Poland*

⁸ *Thüringer Landessternwarte Tautenburg, Sternwarte 5, 07778 Tautenburg, Germany*

Received: October 26, 2023; Accepted: January 15, 2024

Abstract. During the last decade numerous superflares have been detected on solar-type stars using broadband photometry from the Kepler and TESS satellites. Still the spectroscopic exploration of this high-energy phenomenon is lacking. This exploration would reveal what makes normal flares different from superflares. The spectroscopic detection of superflares requires dedicated observational efforts, as this phenomenon is sporadic. We present here one step of joint observational efforts to spectroscopically characterize superflares. We focus on the solar-type stars EK Dra, V833 Tau, and BY Dra, as those are relatively bright and active, and especially V833 Tau shows a high superflare rate in TESS data. The spectroscopic observations have been done at the Skalnaté Pleso observatory operated by the Slovak Academy of Sciences and the Ondřejov observatory operated by the Czech Academy of Sciences. Coordinated photometry in two filters has been done at Stará Lesná/Skalnaté Pleso

observatory run by the Slovak Academy of Sciences, ELTE Gothard Astrophysical Observatory, Szombathely, Hungary, and Lustbühel Observatory run by the University of Graz, Austria. In total around 24 hours were spent on EK Dra, 12 hours on BY Dra, and 20 hours on V833 Tau. However, no superflares have been detected. We discuss detection probabilities and the importance of studying superflares spectroscopically.

Key words: stars – solar-type – stellar activity – superflares

1. Introduction

Superflares are highly energetic ($>10^{33}$ erg) outbreaks of stellar radiation (see e.g. [Maehara et al., 2012](#)). Still, their origin and the origin of their emission is debated. Spectroscopic characterization is one tool to evaluate what makes superflares different from normal flares. Especially what spectral lines are affected and how the continuum enhancement in the blue spectral range is evolving, are still open questions.

2. Target stars, results and conclusions

We select three solar-type stars as targets which are relatively bright and show numerous flares in TESS data (see Table 1).

Table 1. Characteristics of the target stars of the campaign. XUV flare rates have been determined based on the flare power law from [Audard et al. \(2000\)](#), the $H\alpha$ flare rates have been estimated based on [Leitzinger et al. \(2020\)](#), and the TESS flare rates have been determined by eye from the light curves. The logarithmic X-ray luminosities have been taken from [Güdel \(2007\)](#) and [Hinkel et al. \(2017\)](#).

| | spectral type | Age [Gyr] | $\log L_x$ [erg s $^{-1}$] | XUV/ $H\alpha$ /TESS flare rate [day $^{-1}$] | V [mag] |
|----------|---------------|--------------|--------------------------------|---|------------|
| EK Dra | dG0 | 0.1 | 29.93 | 50/3/0.5 | 7.6 |
| BY Dra | dK5e+dK7e | - | 29.92 | 50/3/1.4 | 8.2 |
| V833 Tau | dK2e | 0.65 | 29.92 | 50/3/2.8 | 8.2 |

In total four observatories contributed to the joint observing campaign: Ondřejov Observatory, Czech Republic (spectroscopy/photometry) and Skalnaté Pleso Observatory, Slovakia (spectroscopy/photometry), ELTE Gothard Astrophysical Observatory, Hungary (photometry), and Lustbühel Observatory, Austria (photometry). In total three nights were spent on EK Dra, half a night on BY Dra, and nearly one night on V833 Tau. Comparing these observing times to Table 1, one can see that regarding the TESS flare rates we should have detected at least one flare on BY Dra and V833 Tau. But the observations were

not taken in a row, therefore the probability of observing the star in non-flaring state is higher.

Flares in optical spectra are identified via an increase in flux of e.g. Balmer lines (see e.g. [Wollmann et al., 2023](#)) and the sudden formation of temperature sensitive spectral lines. As the involved spectrographs are Echelle spectrographs ([Kabáth et al., 2020](#)) yielding resolving powers of 50000 (Ondřejov) and 38000 (Skalnate Pleso), we binned the spectra in spectral direction, but even that did not reveal flaring signatures (for sample spectra see Fig. 1). Also the coordinated photometry (g-, and r-band) did not reveal any flares.

Certainly the total observing time was too short to see flares. However we probed with few hours on each target the potential of detecting flares on active solar analogues, and a follow-up campaign is already planned for 2023/2024 with an improved observing strategy involving consecutive nights. Due to the high flaring state and brightness of V833 Tau this target will be a promising candidate for detecting superflares spectroscopically.

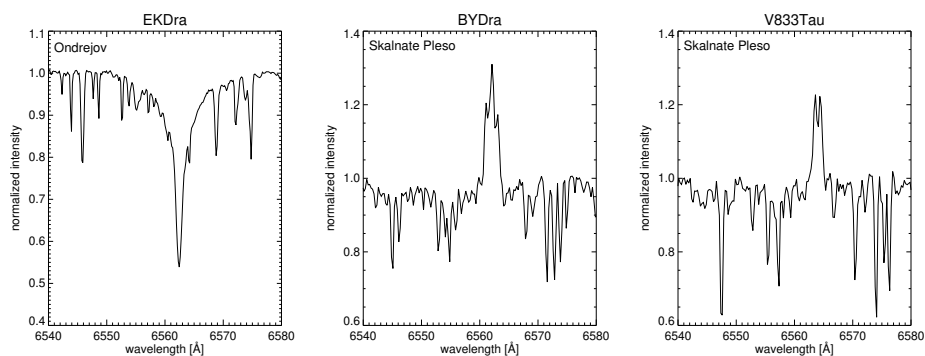


Figure 1. $H\alpha$ spectra of EK Dra, BY Dra, and V833 Tau, obtained from Ondřejov and Skalnate Pleso observatories. The spectra have been binned in spectral direction and are temporally averaged.

Acknowledgements. ML and PO acknowledge the Austrian Science Fund (FWF): 10.55776/15711 for supporting this project. PK, RKa, JL and JW acknowledge GAČR grant 22-30516K. MV, TP and RKo thank to the Slovak Research and Development Agency grant number APVV-20-0148. PH was supported by the program Excellence Initiative -Research University for years 2020–2026 at University of Wrocław, project No. BPIDUB.4610.96.2021.KG. ZG acknowledges the support of the Hungarian National Research, Development and Innovation Office (NKFIH) grant K-125015, the PRODEX Experiment Agreement No. 4000137122 between the ELTE University and the European Space Agency (ESA-D/SCI- LE-2021-0025), the VEGA grant of the Slovak Academy of Sciences No. 2/0031/22, and the support of the city of Szombathely.

References

- Audard, M., Güdel, M., Drake, J. J., & Kashyap, V. L., Extreme-Ultraviolet Flare Activity in Late-Type Stars. 2000, *Astrophysical Journal*, **541**, 396, DOI: 10.1086/309426
- Güdel, M., The Sun in Time: Activity and Environment. 2007, *Living Reviews in Solar Physics*, **4**, 3, DOI: 10.12942/lrsp-2007-3
- Hinkel, N. R., Mamajek, E. E., Turnbull, M. C., et al., A Catalog of Stellar Unified Properties (CATSUP) for 951 FGK-Stars within 30 pc. 2017, *Astrophysical Journal*, **848**, 34, DOI: 10.3847/1538-4357/aa8b0f
- Kabáth, P., Skarka, M., Sabotta, S., et al., Ondřejov Echelle Spectrograph, Ground Based Support Facility for Exoplanet Missions. 2020, *Publications of the ASP*, **132**, 035002, DOI: 10.1088/1538-3873/ab6752
- Leitzinger, M., Odert, P., Greimel, R., et al., A census of coronal mass ejections on solar-like stars. 2020, *Monthly Notices of the RAS*, **493**, 4570, DOI: 10.1093/mnras/staa504
- Maehara, H., Shibayama, T., Notsu, S., et al., Superflares on solar-type stars. 2012, *Nature*, **485**, 478, DOI: 10.1038/nature11063
- Wollmann, J., Heinzel, P., & Kabáth, P., Observations and modeling of spectral line asymmetries in stellar flares. 2023, *Astronomy and Astrophysics*, **669**, A118, DOI: 10.1051/0004-6361/202244544

Spotted eclipsing binary KIC 7023917 with δ -Scuti pulsations

P. Gajdoš^{1,2}, Š. Parimucha¹ and M. Kameneč¹

¹ *Institute of Physics, Faculty of Science, Pavol Jozef Šafárik University, 040 01 Košice, Slovakia*

² *Astronomical Institute of the Czech Academy of Sciences 251 65 Ondřejov, The Czech Republic*

Received: October 26, 2023; Accepted: December 20, 2023

Abstract. Eclipsing binary KIC 7023917 is one of nearly three thousand other binaries in the well-known Kepler Eclipsing Binary Catalog. However, it has some uncommon features. We focused on this system because we detected fast anti-correlated changes on the O-C diagram which could suggest the presence of apsidal motion. However, these changes are very fast for apsidal motion and the orbit of this binary is circular. Detailed analysis of the Kepler and TESS light curves reveals deformation of the light curve by short-periodic pulsations and the O’Connell effect caused by stellar spot(s). Here, we present our initial study of this system and a possible explanation of the observed O-C diagram.

Key words: eclipsing binaries – pulsations – starspots

1. Introduction

KIC 7023917 is a short-period eclipsing binary (EB) discovered by mission *Kepler*. Its orbital period is only about 18 hours (0.7728 days). *V* magnitude is 10.1 and parallax measured by *Gaia* mission is 2.337 mas what gives distance ~ 428 pc. *Gaia* also estimated temperature the whole system to 7460 K (spectral type A7; [Gaia Collaboration, 2023](#)). However, the temperature of the primary star should be nearly the same because of the big determined temperature and luminosity ratio between components.

This EB was observed by *Kepler* mission in long-cadence mode (30 minutes) and also by *TESS* in short-cadence mode (2 minutes) during sectors 14, 40, 41 and 54. In this paper, we use all available data collected by these two missions and analyse the light-curve (LC) of this EB and changes on it.

2. Light curve: analysing & modelling

The LC is significantly affected by stellar spots and also by the pulsations (see Fig. 1). The LCs covering about five orbital periods were phased and stacked together. After that the running mean and binning with a size in phase of

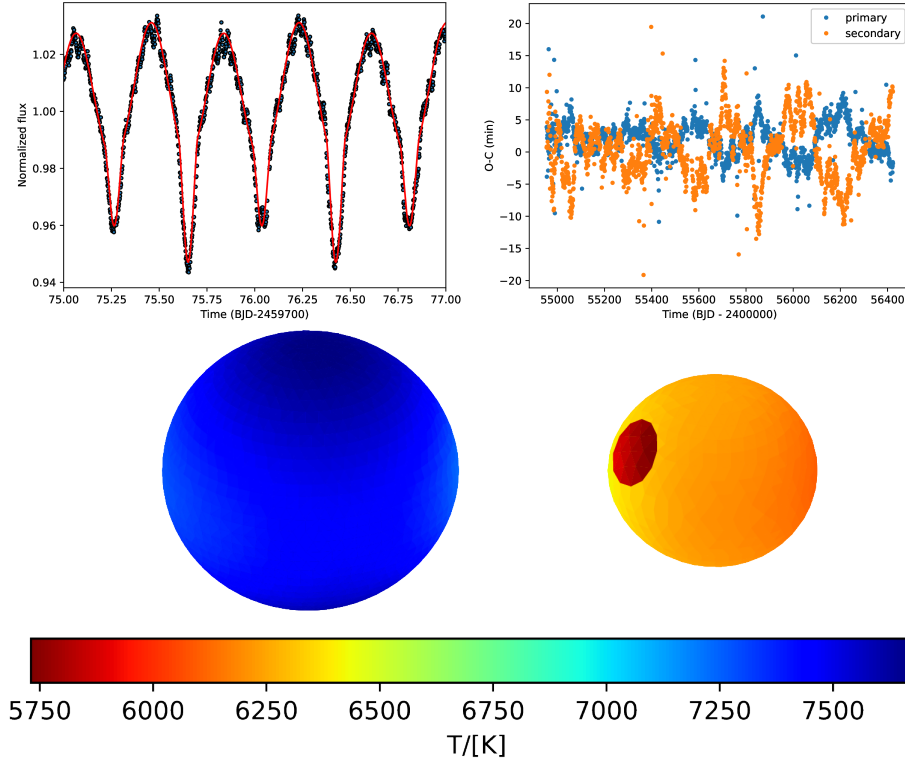


Figure 1. Part of LC obtained by *TESS* mission (*left*) and O-C diagram from *Kepler* data (*right*). Model of studied EB obtained by fitting in ELISa code (*bottom*).

0.01 were used. Because the pulsations were stacked in different phases, this procedure cleared their effect on the LC. Using a longer observing period could also clear out the stellar spots (see Sec. 3) which is undesirable at this step. We modelled the LC in the software package ELISa (Čokina et al., 2021) while assuming a cold spot on a secondary component.

From the model, the temperature of the secondary component is 6500 K (spectral type F6 - F7), the mass ratio is about 0.45 and the orbital inclination is 60° . The angular size of the spot is $\sim 20^\circ$.

3. O-C diagram & O’Connell effect

O-C diagram based on data from *Kepler* (Fig. 1) shows anti-correlated changes which look very similar to that caused by apsidal motion (AM; e.g. Wolf et al., 2013). However, these changes are very fast (with a period of 200–300 days) for considered AM. Data from *TESS* shows similar behaviour.

We focused on the O’Connell effect caused by starspots which was already partially studied by [Balaji et al. \(2015\)](#). We determined the heights of maxima and the difference between them. We found a very strong correlation between heights of maxima and values of O-Cs which suggests that the observed O-C diagram is only the result of the present starspot.

4. Pulsations

Short-period pulsations were detected in the data from *TESS*. Their periods (~ 50 – 100 minutes) are too short to be clearly visible also on *Kepler* data. Our hypothesis is that the primary component is a δ -Scuti pulsator as was already noted by different authors ([Murphy et al., 2018](#); [Shi et al., 2022](#)).

5. Preliminary results and future plans

We have used *Kepler* and *TESS* data to study short-period EB KIC 7023917. This EB is a detached or semi-detached system consisting of the primary star of spectral type A7 and colder secondary one of spectral type F6 or F7.

The primary component is a δ -Scuti pulsator with pulsation in a period range of 50–100 minutes. The secondary one contains extensive cold starspot that deforms LC by the O’Connell effect and probably also caused observed changes on the O-C diagram. Both effects require further analysis.

In addition, we are performing ground-based spectroscopic and photometric follow-up observations. We use the OES spectrograph on Perek’s 2-meter telescope in Ondřejov ([Kabáth et al., 2020](#)) to measure precise radial velocity caused by an orbital motion and to determine basic stellar parameters from spectra. We observe with the 15-cm Maksutov-Newton telescope at the Astronomical Observatory on the Kolonica saddle to obtain multicolour photometry (Sloan’s filters g' , r' and i' are used) for better characterization of this EB (mainly temperature ratio).

Acknowledgements. This paper has been supported by the grant of the Slovak Research and Development Agency with number APVV-20-0148. PG acknowledges the support by Inter-transfer grant No. LTT-20015.

References

- Balaji, B., Croll, B., Levine, A. M., & Rappaport, S., Tracking the stellar longitudes of starspots in short-period Kepler binaries. 2015, *Monthly Notices of the RAS*, **448**, 429, DOI: 10.1093/mnras/stv031
- Gaia Collaboration, Gaia Data Release 3. Summary of the content and survey properties. 2023, *Astronomy and Astrophysics*, **674**, A1, DOI: 10.1051/0004-6361/202243940

- Kabáth, P., Skarka, M., Sabotta, S., et al., Ondřejov Echelle Spectrograph, Ground Based Support Facility for Exoplanet Missions. 2020, *Publications of the ASP*, **132**, 035002, DOI: 10.1088/1538-3873/ab6752
- Murphy, S. J., Moe, M., Kurtz, D. W., et al., Finding binaries from phase modulation of pulsating stars with Kepler: V. Orbital parameters, with eccentricity and mass-ratio distributions of 341 new binaries. 2018, *Monthly Notices of the RAS*, **474**, 4322, DOI: 10.1093/mnras/stx3049
- Shi, X.-d., Qian, S.-b., & Li, L.-J., New Pulsating Stars Detected in EA-type Eclipsing-binary Systems Based on TESS Data. 2022, *Astrophysical Journal, Supplement*, **259**, 50, DOI: 10.3847/1538-4365/ac59b9
- Čokina, M., Fedurco, M., & Parimucha, Š., ELISa: A new tool for fast modelling of eclipsing binaries. 2021, *Astronomy and Astrophysics*, **652**, A156, DOI: 10.1051/0004-6361/202039171
- Wolf, M., Zasche, P., Kučáková, H., et al., Apsidal motion in five eccentric eclipsing binaries. 2013, *Astronomy and Astrophysics*, **549**, A108, DOI: 10.1051/0004-6361/201220505

Photometric study of the Delta Scuti variable 2MASS J13122513+5443409 in UMa

A. Maliuk¹, V. Krushevska^{1,2}, S. Shugarov¹, Z. Garai^{1,3,4},
Ya. Romanyuk², Yu. Kuznyetsova² and M. Andreev²

¹ *Astronomical Institute of the Slovak Academy of Sciences, 059 60 Tatranská
Lomnica, Slovakia*

² *Main Astronomical Observatory of National Academy of Sciences of
Ukraine, 27 Akademika Zabolotnoho St., 03143, Kyiv, Ukraine*

³ *HUN-REN-ELTE Exoplanet Research Group, 9700 Szombathely, Szent Imre
h. u. 112, Hungary*

⁴ *ELTE Gothard Astrophysical Observatory, 9700 Szombathely, Szent Imre h.
u. 112, Hungary*

Received: November 8, 2023; Accepted: February 2, 2024

Abstract. We keep investigating the new variable of Delta Scuti type 2MASS J13122513+5443409 discovered by our group previously. We have analyzed the data obtained not only from the relatively small telescopes of Slovakia and Ukraine, but also from the TESS mission. We calculated the pulsation period and amplitude using the Lomb-Scargle periodogram. We found that the dominant period is about 0.079 days. However, the oscillations displayed beating, indicating the presence of several pulsation frequencies.

Key words: δ Scuti – pulsating stars – variable stars

1. Introduction

Our team has discovered a variable star (Table 1) in the white dwarf SDSS J131156.70 + 544455.8 field (Figure 1) during photometric observations.

Subsequent observations yielded a variation period P of 0.079075 ± 0.000003 days. The brightness amplitude varied, reaching a peak of 0.1 magnitudes and a minimum of 0.02 magnitudes. The period and amplitude of the variations suggest the star could belong to the Delta Scuti pulsating variables. This type usually includes giants or main sequence stars of spectral classes from A0 to F5 with a magnitude variation amplitude ranging from $0.^m003$ to $0.^m9$ and a period of several hours (Breger, 2000). The shape of the light curve, period, and amplitude typically undergo significant changes. We keep studying the star with additional photometric data obtained from Stará Lesná Observatory (Slovakia), Lisnyky (Ukraine), MAO (Ukraine), and the TESS mission. The basic properties of the star, taken from the Simbad database (Wenger et al., 2000), are shown in Table 1.

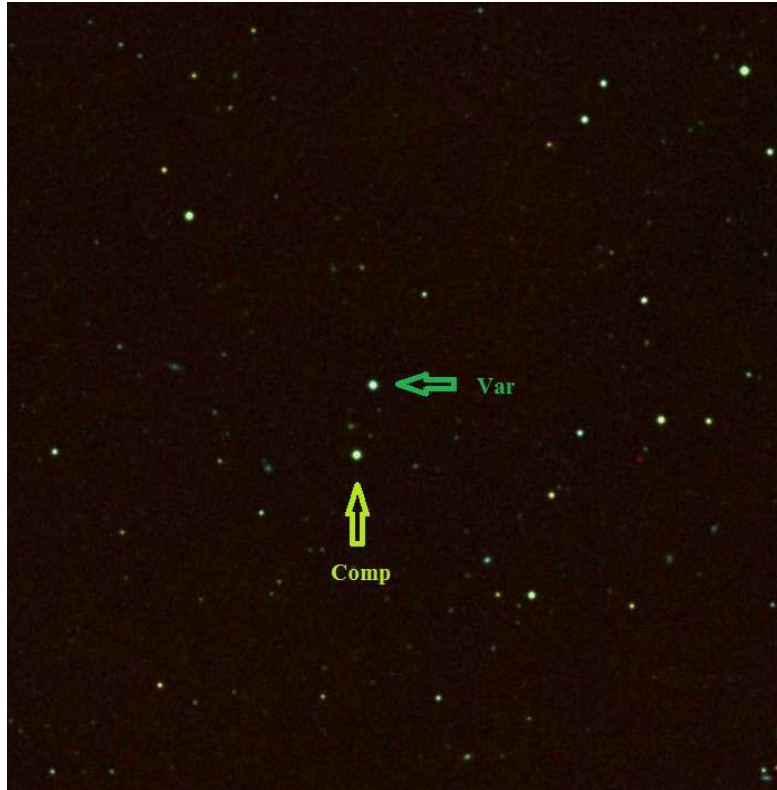


Figure 1. Color frame of variable star field created from the SDSS-frames obtained in different filters. The arrows indicate a new variable star and a comparison star

2. Observations

Ground-based photometry was made using telescopes in Slovakia (Stara Lesna) and Ukraine (MAO, Lisnyky station, Mayaky station). Their main characteristics are given in Table 2. There were 22 observation nights in total. Mainly we have observed in integral light, but Johnson filters BVRI were also applied later. Exposure time ranged from 30 to 120 seconds depending on the filter, telescope, and weather conditions.

The Transiting Exoplanet Survey Satellite (TESS), a NASA space telescope designed for discovering exoplanets through the transit method, offers high-precision photometry (Ricker, 2015). In 2019, TESS performed observations in the 15th sector over 26 days with an exposure time of 30 minutes. The data was downloaded via package Lightkurve (Lightkurve Collaboration et al., 2018). It was automatically processed and detrended with TASOC pipeline (Handberg et al., 2021; Lund et al., 2021) and contains 1197 data points.

Table 1. Basic properties of the star 2MASS J13122513 + 5443409

| | |
|------------------------|----------------------------|
| ICRS coord. (ep=J2000) | 13 12 25.138 +54 43 40.944 |
| Parallax (mas): | 0.2960 [0.0239] |
| Spectral type | A7.8 D |
| Magnitudes (mag) | G 14.3485 [0.0008] |
| | J 13.730 [0.025] |
| | H 13.739 [0.037] |
| | K 13.693 [0.053] |

Table 2. The main characteristics of available telescopes

| Observatory | Telescope | Number of nights | Aperture [cm] | FOV [arcmin] |
|---------------------------|-------------------------------------|---------------------|------------------|-----------------|
| Lisnyky (Ukraine) | Schmidt-Cassegrain Celestron-14" | 6 | 35 | 7×7 |
| Stará Lesná (Slovakia) | Cassegrain | 13 | 60 | 14×14 |
| MAO (Ukraine) | Schmidt-Cassegrain Celestron-14" | 1 | 35 | 18×14 |
| Mayaky (Ukraine) | Ritchey–Chrétien OMT-800 | 2 | 80 | 59×59 |
| TESS | NA | 26 | 10.5 | 1440×1440 |

3. Results

Because of various exposure times and precision, we conducted separate analyses of the photometric data obtained from TESS and ground-based telescopes. In the primary instances, we employed the Lomb-Scargle periodogram technique to identify periodicities within our dataset (Scargle, 1982).

Our periodogram derived from the TESS data is displayed in Figure 2. We clearly can see three prominent periods of 113.85 ± 0.12 (I), 120.86 ± 0.13 (II), and 122.39 ± 0.12 (III) minutes. Almost the same periods were found in the combined data from ground-based telescopes (Figure 3) listed in Tab. 2: 113.86 ± 0.12 (I), 121.73 ± 0.12 (II) and 122.38 ± 0.12 (III) minutes. Full periodograms of both ground-based and TESS data are displayed in Figure 4. For better comparison, the results are listed in Table 3.

It is worth noticing that the combination of two or more close frequencies results in beating which means that the amplitude of the combined signal changes periodically. Such a pattern is demonstrated in Figures 5 and 6.

To check our results, we fitted the TESS lightcurve with the combination of 3 harmonic oscillations (Figure 5). The obtained periods are in good agreement with the ones we got from the periodogram - 113.85 (I), 120.86 (II), and

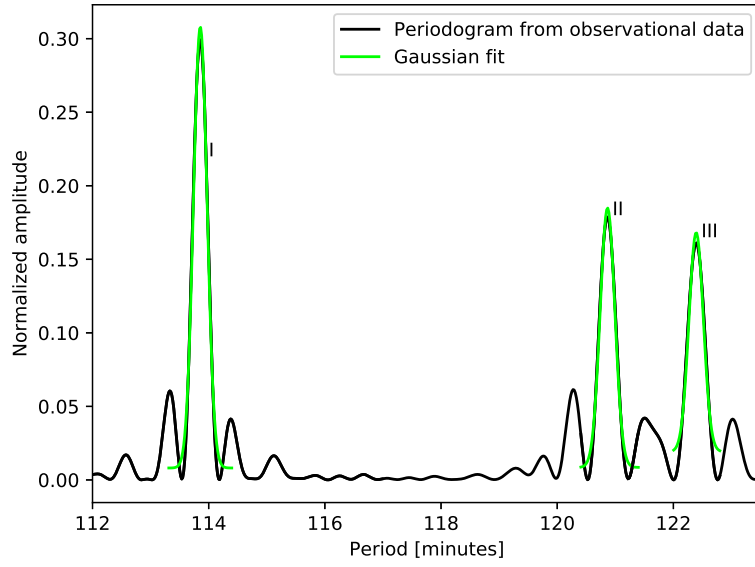


Figure 2. Periodogram based on the TESS data.

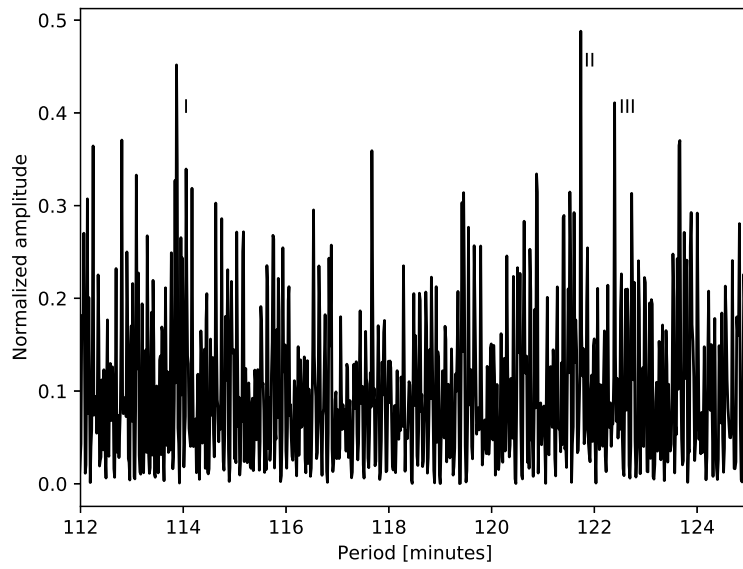


Figure 3. Periodogram from ground-based telescopes.

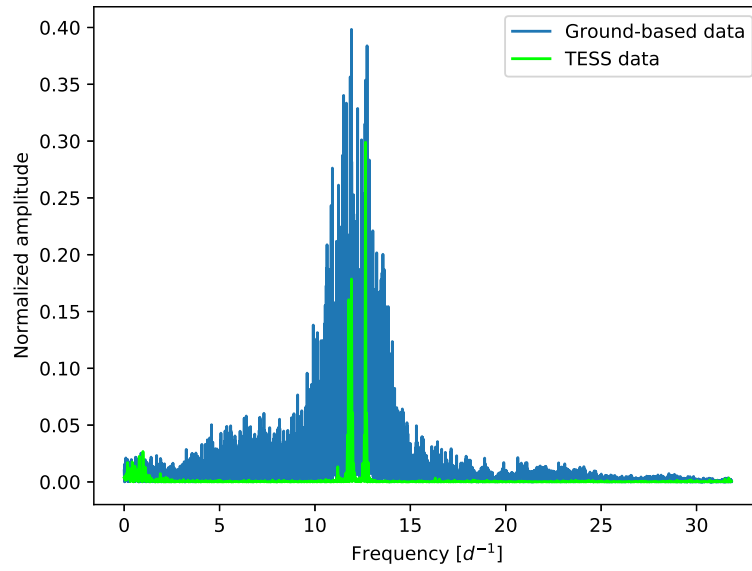


Figure 4. Full periodogram.

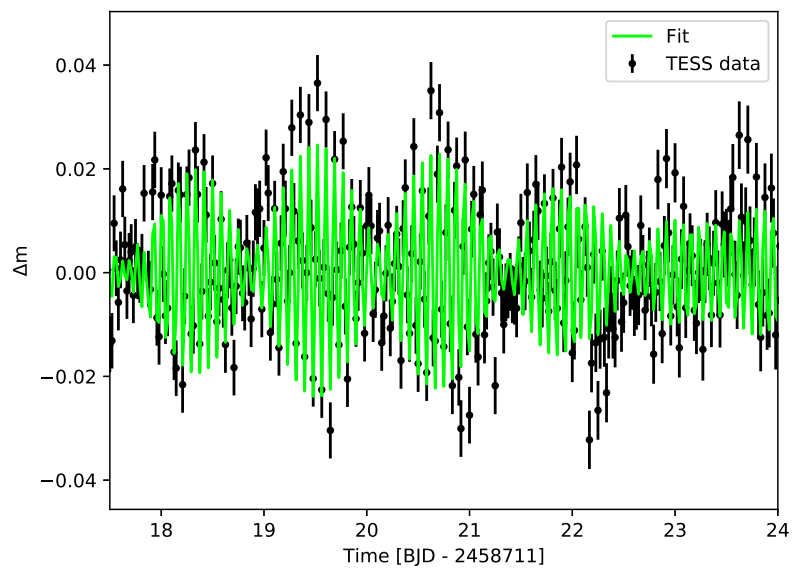


Figure 5. TESS lightcurve(black) with our model(green).

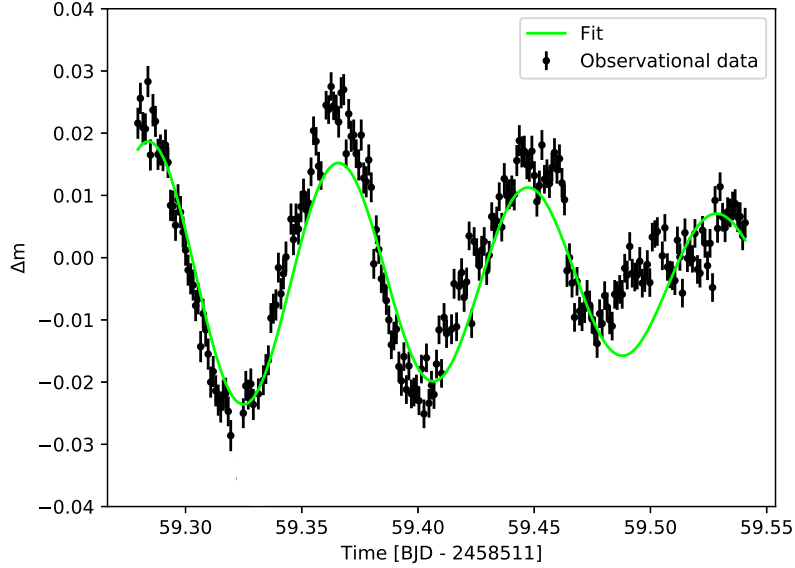


Figure 6. Lightcurve from the ground-based telescope in Stara Lesna (black) with our model (green). The amplitude is decaying at this part of observations

122.39(III) minutes. Amplitudes are estimated as $0^m.009$, $0^m.008$, $0^m.0075$ respectively. The same periods within the error we obtained from data collected with small telescopes (Figure 6), despite the light curve and periodogram being noisy. Both fits are good but not perfect, leaving the root mean square residual of $0^m.007$. At least three significant frequencies are present in the periodic oscillations of our star. This phenomenon is not particularly rare.

Table 3. Values of the periods in minutes based on TESS and ground-based data

| | | | |
|--------------|-------------------|-------------------|-------------------|
| Ground-based | 113.86 ± 0.12 | 121.73 ± 0.12 | 122.38 ± 0.12 |
| TESS | 113.85 ± 0.12 | 120.86 ± 0.13 | 122.39 ± 0.12 |

Freyhammer et al. (2001) reports findings of 13 δ Scuti stars with ten of them exhibiting oscillations in two or more frequencies.

4. Conclusions

We found at least three significant frequencies in the oscillation spectra of 2MASS J13122513+5443409. The combination of these frequencies results in

beating with a dominant period of about 32 hours. Multiperiodic Delta Scuti stars are of great interest to astroseismology as they offer a unique opportunity to probe the complex physical processes occurring within the stellar interiors. By analyzing their pulsation frequencies and modes, researchers can gain insights into properties such as stellar ages, masses, and evolutionary stages.

Acknowledgements. This work is supported by project APVV-20-0148 and VEGA 02/0031/22. V.K. acknowledges the support from the Government Office of the Slovak Republic within NextGenerationEU program under project no. 09I03-03-V01-00002. We would like to express our profound gratitude to Veles O., Kashuba V., Budaj J., Kundra E., Pribulla T., Dolinský P., Hambálek L., Vaňko M. , Komžík R. for their meticulous observations. ZG acknowledges the support of the Hungarian National Research, Development and Innovation Office (NKFIH) grant K-125015, the PRODEX Experiment Agreement No. 4000137122 between the ELTE University and the European Space Agency (ESA-D/SCI-LE-2021-0025) and the support of the city of Szombathely.

References

- Breger, M., δ Scuti stars (Review). 2000, in *Astronomical Society of the Pacific Conference Series*, Vol. **210**, *Delta Scuti and Related Stars*, ed. M. Breger & M. Montgomery, 3
- Freyhammer, L. M., Arentoft, T., & Sterken, C., Multimode delta Scuti stars in the open cluster <ASTROBJ>NGC 7062</ASTROBJ>. 2001, *Astronomy and Astrophysics*, **368**, 580, DOI: 10.1051/0004-6361:20010020
- Handberg, R., Lund, M. N., White, T. R., et al., TESS Data for Asteroseismology: Photometry. 2021, *Astronomical Journal*, **162**, 170, DOI: 10.3847/1538-3881/ac09f1
- Lightkurve Collaboration, Cardoso, J. V. d. M., Hedges, C., et al. 2018, Lightkurve: Kepler and TESS time series analysis in Python, *Astrophysics Source Code Library*
- Lund, M. N., Handberg, R., Buzasi, D. L., et al., TESS Data for Asteroseismology: Light-curve Systematics Correction. 2021, *Astrophysical Journal, Supplement*, **257**, 53, DOI: 10.3847/1538-4365/ac214a
- Ricker, G. R., The Transiting Exoplanet Survey Satellite (TESS): Discovering New Earths and Super-Earths in the Solar Neighborhood. 2015, in *AAS/Division for Extreme Solar Systems Abstracts*, Vol. **47**, *AAS/Division for Extreme Solar Systems Abstracts*, 503.01
- Scargle, J. D., Studies in astronomical time series analysis. II. Statistical aspects of spectral analysis of unevenly spaced data. 1982, *Astrophysical Journal*, **263**, 835, DOI: 10.1086/160554
- Wenger, M., Ochsenbein, F., Egret, D., et al., The SIMBAD astronomical database. The CDS reference database for astronomical objects. 2000, *Astronomy and Astrophysics, Supplement*, **143**, 9, DOI: 10.1051/aas:2000332

Photometric and colorimetric studies of target objects using small and medium-size telescopes

V.G. Godunova¹, A.O. Simon^{2,3}, Y.S. Markus^{1,4},
S.Yu. Shugarov⁵, V.V. Troianskyi^{6,7}, V.M. Reshetnyk²,
I.O. Izviekova^{1,8}, B.E. Zhilyaev⁸, A.V. Shchurova⁵,
M. Husárik⁵, S. Geier^{9,10}, D. Oszkiewicz¹¹ and D. Tomko⁵

¹ ICAMER Observatory of NASU, 27 Acad. Zabolotnoho str., Kyiv, 03143, Ukraine, (E-mail: vira.nova7@gmail.com)

² Astronomy and Space Physics Department, Taras Shevchenko National University of Kyiv, Glushkova Ave., 4, Kyiv, 03022, Ukraine

³ National Center "Junior academy of sciences of Ukraine", 38-44, Dehtiarivska St., Kyiv, 04119, Ukraine

⁴ Institute of Physics, Faculty of Science, Pavol Jozef Šafárik University, 04001 Košice, Slovakia

⁵ Astronomical Institute of the Slovak Academy of Sciences, SK-05960 Tatranská Lomnica, Slovakia

⁶ Department of Physics and Astronomy FMPIT of Odesa I. I. Mechnikov National University, Pastera Street 42, 65082 Odesa, Ukraine

⁷ Department of Physics and Methods of Teaching, Faculty of Physics and Technology, Vasyl Stefanyk Precarpathian National University, Shevchenko Street 57, 76000 Ivano-Frankivsk, Ukraine

⁸ Main Astronomical Observatory of the National Academy of Sciences of Ukraine, 27 Acad. Zabolotnoho Str., 03143 Kyiv, Ukraine

⁹ Gran Telescopio Canarias (GRANTECAN), Cuesta de San José s/n, E-38712, Breña Baja, La Palma, Spain

¹⁰ Instituto de Astrofísica de Canarias, Vía Láctea s/n, E38200, La Laguna, Tenerife, Spain

¹¹ Astronomical Observatory Institute, Faculty of Physics, Adam Mickiewicz University, Stoleczna 36, 60-286 Poznań, Poland

Received: November 12, 2023; Accepted: January 31, 2024

Abstract. We report on follow-up studies of transient events and objects, which have been conducted in recent years using ground-based optical observations. BVRI photometry has been performed with small and medium-sized telescopes located in Europe and North America. The purpose of these studies, which are mainly focused on objects of unknown nature, is to reveal features of

their variability that are critical for classifying the transients and understanding their evolution.

We present here some results obtained from long-term monitoring of transients Gaia18aes, Gaia19bpg, as well as the quasar 4C +21.35.

Key words: Stars: variables: individual: Gaia18aes, Gaia19bpg – Galaxies: quasars: individual: 4C +21.35 – Techniques: photometric

1. Introduction

Follow-up photometry is an important component of astrophysical studies, helping to reveal the nature and characteristics of stellar objects and transient events. Ground-based small- and medium-aperture telescopes, equipped with additional instruments and sensitive CCD cameras, are still able to provide good enough opportunities for short- and long-term observation programs, especially in response to survey alerts.

Today, these telescopes are actively involved in monitoring objects from the Gaia Science Alerts program, ASAS-SN, GRANDMA, and other projects.

2. Observations and results

Our research activities are focused on follow-up studies of recently detected transients and variable sources (CVs, QSO, etc.). A lot of objects have been continuously observed over the years in collaboration with research groups at other observatories. In our work, we used mainly photometric data gathered at the Terskol Observatory (Tarady *et al.*, 2010) in 2018-2021 and supplemented them with observations, which have been performed at other observatories (Table 1). Most of the datasets were obtained using filters close to the Johnson-Cousins B , V , R_c , and I_c system. Standard processing was applied to reduce data (i.e., debiasing, dark subtracting, flat-fielding); for details, see Oszkiewicz *et al.* (2020) and Troianskyi *et al.* (2023). Measurements were done using MaxIm DL¹ and MPO Canopus² software. Magnitudes of comparison stars were usually taken from the Gaia and Pan-STARR catalogs. Additionally, we used information and datasets available at the Cambridge Photometric Calibration Server³.

Here we provide some findings for the three objects, which have been observed over the last five years.

2.1. Gaia18aes

The bright blue declining transient on faint blue SDSS source Gaia18aes / AT2018ik was discovered on 2018-01-17 and reported on 2018-01-19 by the

¹ <https://diffractionlimited.com/product/maxim-dl/>

² <http://www.bdwpublishing.com>

³ <http://gsaweb.ast.cam.ac.uk/followup>

Table 1. Telescopes and detectors used for the BVRI photometric observations.

| Telescope | Observatory | Detector | Aperture [m] | IAU code | Object | Date of observations |
|------------|-----------------------|---------------|-----------------|-------------|-----------|-------------------------|
| Zeiss-2000 | Terskol | FLI PL4301 | 2.0 | B18 | Gaia18aes | 2018-2020 |
| | | | | | Gaia19bpg | 2019-2021 |
| Zeiss-600 | Terskol | SBIG STL-1001 | 0.6 | B18 | Gaia18aes | 2018-2019 |
| | | | | | Gaia19bpg | 2019-2021 |
| | | | | | 4C +21.35 | 2020 |
| B&C | Kitt Peak | ARC Camera | 0.96 | G82 | 4C +21.35 | 2023 |
| IAC80 | Teide | CAMELOT2 | 0.82 | 954 | 4C +21.35 | 2023 |
| AZT-8 | Kyiv Comet Station | FLI PL4710 | 0.7 | 585 | Gaia18aes | 2018-2023 |
| | | | | | Gaia19bpg | 2019 |
| | | | | | 4C +21.35 | 2018, 2023 |
| 0.61-m | Skalnáté Pleso | SBIG ST-10XME | 0.61 | 056 | Gaia19bpg | 2023 |
| | | | | | 4C +21.35 | 2023 |
| 0.6-m G2 | Stará Lesná | FLI ML3041 | 0.6 | - | Gaia18aes | 2019-2020 |

Gaia Photometric Science Alerts team at magnitude $G = 15.77^4$. On the Gaia images from 2017-12-30, the object was fainter than the limiting magnitude $G = 21.5$; therefore, at the time of its discovery by Gaia, the object became brighter by more than 5.7 mag. Two previous brightenings of this source were recorded by Catalina Real-Time Transient Survey on 2014-02-27 and 2015-02-26 with the unfiltered GSS magnitudes of 16.78 and 17.36, respectively (as CSS140227:111652+011436; Drake et al. (2009)). Most recently, on 2022-06-25, Gaia detected another outburst of Gaia18aes at magnitude $G = 16.59$.

We had begun to observe Gaia18aes using the astronomical facilities of the Kyiv Comet Station (Lisnyky) and the Terskol Observatory, just after the Gaia alert was published. On the images obtained on 2018-01-26 at Lisnyky, the object was detected at magnitude $R \sim 17$ indicating a fading trend in the brightness of the source. The light curve revealed a variability with a period of 0.056(3) h and amplitude of 0.65 mag (see Fig. 1 (the inset)). Further observations in March-April 2019 at Terskol and Stará Lesná revealed a new flare (Fig. 1).

We calculated the color indices for the object and compared them with those for black bodies of various temperatures. Based on the results obtained (Fig. 2), we can conclude that the object's color temperature is typical for dwarf novae during an outburst. Generally, the photometric behavior of Gaia18aes over a 5-year observation period allows us to suggest that this object could be a cataclysmic variable of U Gem type, by subtypes UGSS or UGSU; further observations are needed to clarify this.

⁴ <http://gsaweb.ast.cam.ac.uk/alerts>

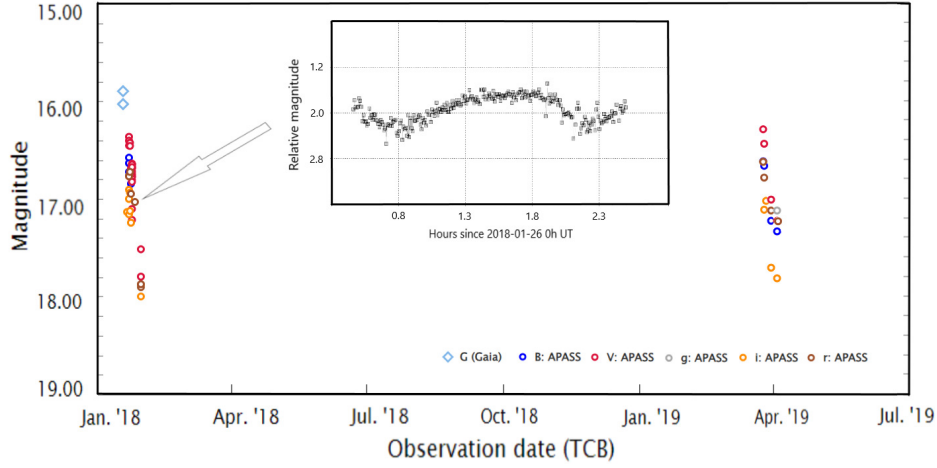


Figure 1. Multi-band photometric measurements of Gaia18aes in 2018-2019. (Image from <http://gsaweb.ast.cam.ac.uk/alerts/alert/Gaia18aes/> supplemented with measurements at Stará Lesná). The inset: Light curve of Gaia18aes from R-band observations on 2018-01-26 at Lisnyky.

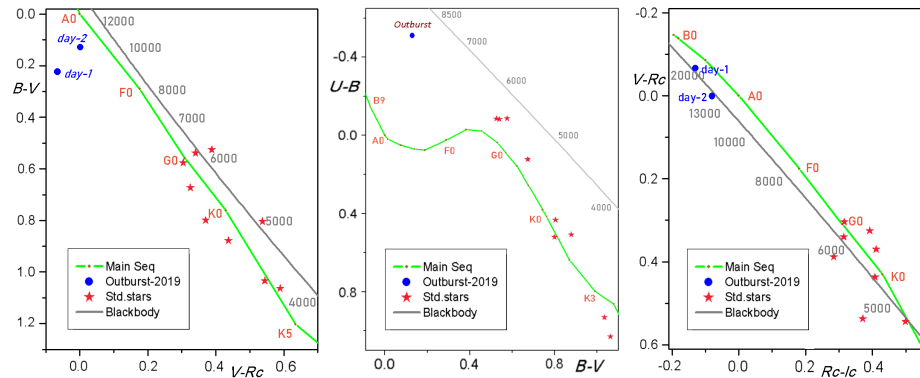


Figure 2. Two-color diagrams of Gaia18aes. The Main Sequence and blackbody lines with temperatures are plotted in green and gray, respectively. The blue dots show the position of Gaia18aes on the first and second days of observations at Stará Lesná in 2019. The positions of neighboring field stars are marked by red asterisks.

2.2. Gaia19bpg

On 2019-04-29, the Gaia Photometric Science Alerts Team⁵ reported activity from a red Galactic plane source at coordinates R.A. = 325.46012 deg, Dec. = +51.92930 deg: its brightness increased by 1.5 mag over 8 months and reached a magnitude $G = 14.62$. We have observed this transient Gaia19bpg in 2019-2023 in the BVRI bands (Fig. 3). The light curves show an upward trend in brightness, which continued over 20 months up to the magnitude of about $G \sim 12.7$. By the turning point in April 2021, the brightness began to decline, although a short-term re-brightening was observed in November 2021-January 2022 when the magnitude changed from $G \sim 14.04$ to $G \sim 13.48$. The multi-band photometric monitoring revealed a color evolution of the object; significant changes in colors were detected especially after the brightness peak. In particular, for the observed period of 4.5 years, V-R color shifted to red from 1.1 mag to 1.6 mag indicating a decrease in the temperature of the object. Generally, the photometric behavior of Gaia19bpg is similar to that of a symbiotic nova in outburst (Merc et al., 2023). The current spectroscopic observations are expected to help classify this object.

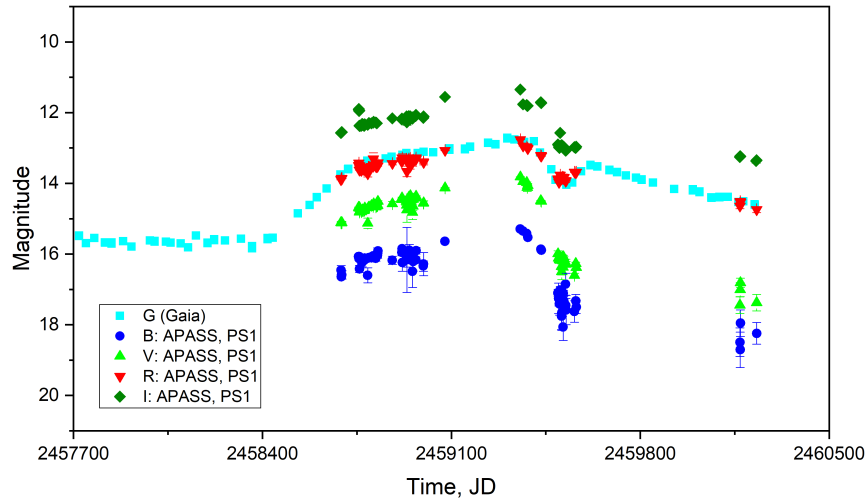


Figure 3. Multi-band follow-up observations of Gaia19bpg. The Gaia light curve is combined with photometric measurements provided by the observatories listed in Table 1 (Gaia data from <http://gsaweb.ast.cam.ac.uk/alerts/alert/Gaia19bpg/>).

⁵ <http://gsaweb.ast.cam.ac.uk/alerts>

2.3. Quasar 4C +21.35

The quasar 4C +21.35 (often termed PKS 1222+216) is a Seyfert 1 Galaxy at redshift $z = 0.435$, which was discovered in the 1960s as a radio source. Since the 1990s, it has also been known as a variable X- and gamma-ray source.

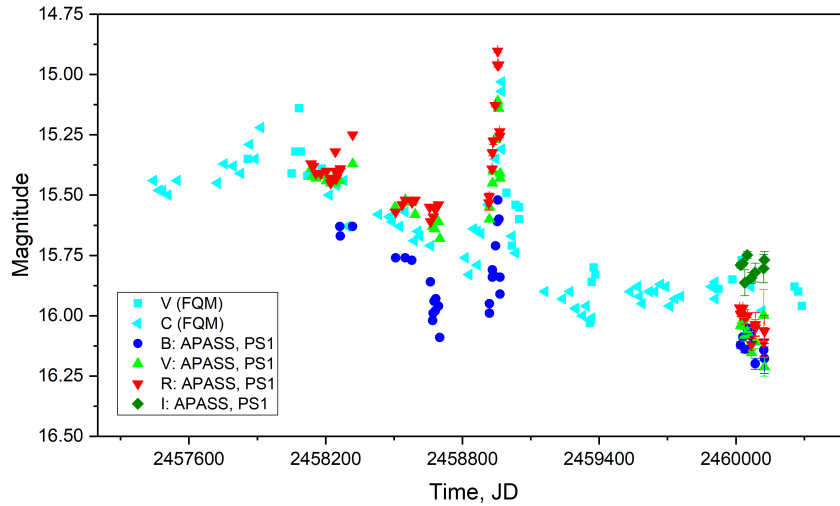


Figure 4. The photometric behaviour of 4C +21.35 in 2016–2023. Our observations are superimposed on the light curve provided by the Frankfurt Quasar Monitoring Project (<http://quasar.square7.ch/fqm/1222+216.html>).

Our photometric observations of this object started in 2016 (Ponomarenko *et al.* (2019); Fig. 4). In this paper, we focus on an outburst, which was observed in March–April 2020 at the Terskol Observatory. Observations were carried out through BVRI filters that allowed us to investigate the color variability of the source during the outburst. The results of our analysis are as follows: (i) the object reached a minimum brightness before the outburst; (ii) during the outburst, the colors ($B-V$) and ($V-R$) showed a reddening with increasing brightness (Fig. 5) that indicates the thermal emission from the accretion disc; (iii) in a quasi-quiet state, $B-V$ and $V-R$ colors of the object remain constant within ± 0.1 mag. It should be noted that during the 2020 outburst no noticeable increase in the activity of the quasar 4C +21.35 in the X-ray or gamma-ray wavelength range was detected (for instance, see Fermi-LAT Data⁶).

⁶ https://fermi.gsfc.nasa.gov/ssc/data/access/lat/msl_lc/index.php

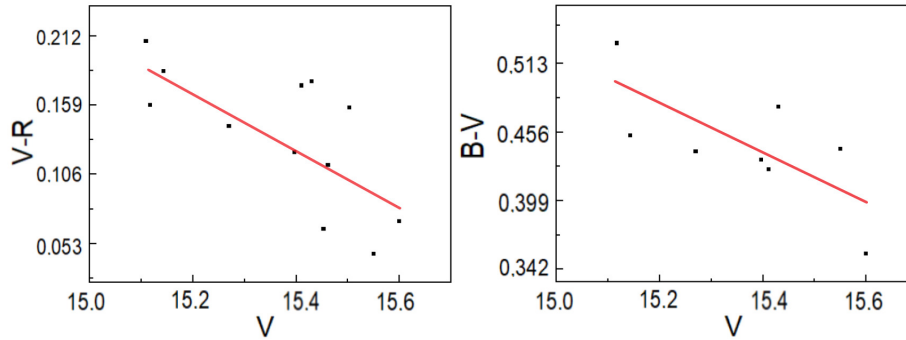


Figure 5. $(B-V)$ and $(V-R)$ color indices as a function of V magnitude during the outburst of 4C +21.35 in 2020.

3. Conclusions

Follow-up observations with small and medium-sized telescopes provide useful information, especially on the photometric short- and long-term variability of transient events.

Systematic, integrated use of these telescopes leads to the early detection of changes in the behavior of objects and better information about their evolution.

Acknowledgements. We acknowledge ESA Gaia, DPAC, and the Photometric Science Alerts Team⁷. SS was supported by the Slovak Academy Grants VEGA 2/0030/21 and APVV-20-0148. VT was supported by the National Scholarship Programme of the Slovak Republic - academic year 2023/2024. MH thanks the Slovak Academy of Sciences under the contract VEGA 2/0059/22. DO was supported by grant No. 2022/B/ST9/00267 from the National Science Center, Poland.

References

- Drake, A. J., Djorgovski, S. G., Mahabal, A., et al., First Results from the Catalina Real-Time Transient Survey. 2009, *Astrophysical Journal*, **696**, 870, DOI: 10.1088/0004-637X/696/1/870
- Merc, J., Gális, R., Velez, P., et al., V618 Sgr: galactic eclipsing symbiotic nova detected in repeated outbursts. 2023, *Monthly Notices of the RAS*, **523**, 163, DOI: 10.1093/mnras/stad1434
- Oszkiewicz, D., Troianskyi, V., Föhring, D., et al., Spin rates of V-type asteroids. 2020, *Astronomy and Astrophysics*, **643**, A117, DOI: 10.1051/0004-6361/202038062

⁷ <http://gsaweb.ast.cam.ac.uk/alerts>

- Ponomarenko, V., Simon, A., Vasylenko, A., Izvekova, I., & Baransky, O., The results of the photometric optical monitoring of four active galaxies in 2018-2019. 2019, *Bulletin of Taras Shevchenko National University of Kyiv Astronomy*, **59**, 48
- Tarady, V., Sergeev, O., Karpov, M., Zhilyaev, B., & Godunova, V., Observations with small and medium-sized telescopes at the Terskol Observatory. 2010, *400 Years of Astronomical Telescopes*, DOI: 10.48550/arXiv.1003.4875
- Troianskyi, V., Kashuba, V., Bazyey, O., et al., First reported observation of asteroids 2017 AB8, 2017 QX33, and 2017 RV12. 2023, *Contributions of the Astronomical Observatory Skalnat Pleso*, **53**, 5, DOI: 10.31577/caosp.2023.53.2.5

Multiwavelength research of the cyclic variability of symbiotic nova RT Ser

V. Marsakova¹ , S. Shugarov² and I. Andronov³

¹ *Odesa Richelieu Science lyceum, 65082, Odesa, Ukraine (E-mail: vlada.marsakova@gmail.com)*

² *Astronomical Institute of the Slovak Academy of Sciences
059 60 Tatranská Lomnica, The Slovak Republic*

³ *Odesa National Maritime University, 65029 Odesa, Ukraine*

Received: November 12, 2023; Accepted: January 9, 2024

Abstract. For symbiotic nova RT Ser, we corrected the orbital period by using the analysis of long-term wave-like variability in B passband, the new value is 4431(± 22) days. When analyzing the observations in the V-band, the cycles of the variability of about 93-107 and 159 days were found, which are probably caused by the multiperiodic pulsation variability of a red giant.

Key words: stars – symbiotic – photometry

1. Introduction

RT Ser showed a symbiotic nova outburst that started in 1909 with maximal brightness in 1920 and followed by a decline in brightness and its wave-like variations after about 1970 (Payne-Gaposhkin & Gaposhkin (1938), Shugarov et al. (2003)). For the first time, the existence of an orbital period of about 10 years in this system was suspected by Pavlenko et al. (1996). Then, as the result of the analysis of photographic observations over a 40-year interval (Shugarov et al. (1997), Shugarov et al. (2003)), it was possible not only to confirm the binarity of the system but also to correct the orbital period, which was determined to be about 4500 d. In the cited paper, a preliminary model of this broad binary system was proposed.

The main parameters of the system were estimated by Murset & Nussbaumer (1994): spectral class A8 (1919-21, in outburst), with the temperature of white dwarf rising from 7500 K to over 120000 after 1980, and by Rudy et al. (1999): spectral class of the red component M5.5, distance about 5.8 kpc, $E(B-V)=0.64(\pm 0.1)$.

2. Observations

The photometric observations were made using the telescopes of the Astronomical Institute of Slovak Academy of Science. Observations from August 2002 to

May 2012 were performed at the 50/225 cm Newton telescope (G1) with the CCD camera SBIG ST-10XME in BVRI passbands. Then (up to October 2023) at telescopes G1 and G2, but both Zeiss 60/750 cm, using cameras G4 Moravia Instrument (BVRI) or FLI-ML3041 (UBVRI). The magnitudes of comparison stars were taken from [Henden & Munari \(2006\)](#). The old observations in the B_{pg} and B passbands were described by [Shugarov et al. \(2003\)](#). In this article we will denote these close photometric systems as "B".

We used B-observations for analyzing the long-term wave-like brightness variations and our V-observations together with ones made by AAVSO observer Shawn Dvorak (DKS) for search of possible pulsation periods.

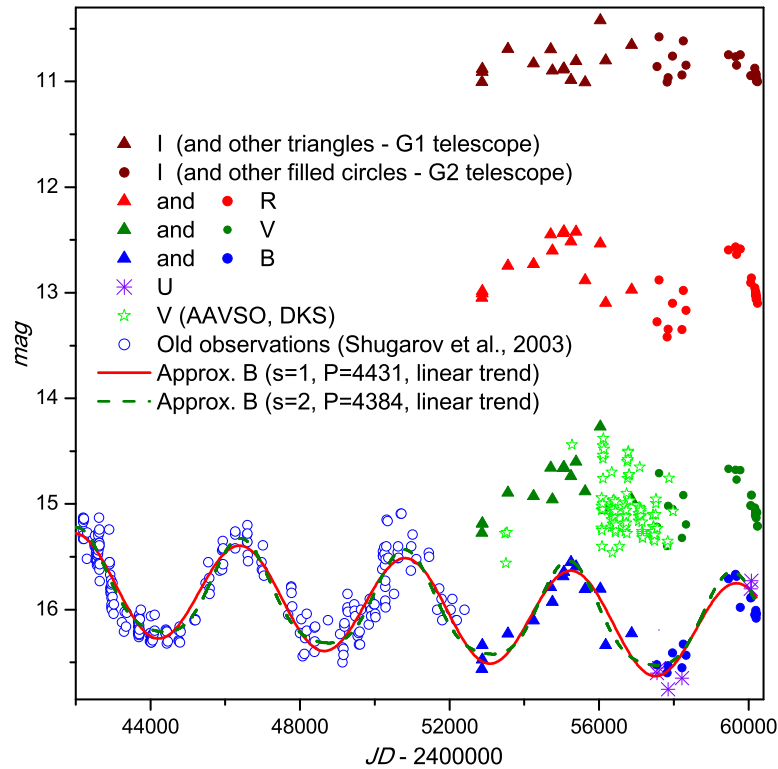


Figure 1. Observations and long-term wave-like brightness variations

3. Long-term wave-like brightness variations

Figure 1 shows wave-like brightness variations in the B passband. Similar brightness variations were observed in some symbiotic variables during the gradual decline after the symbiotic nova outburst and transition to the quiescent phase. Such effect was observed in AG Peg, V1329 Cyg, V426 Sge ([Skopal](#)

Table 1. Extrema and cycles of Long-term wave-like brightness variations

| Momemts | error | cycle lengths | error |
|---------|-------|---------------|-------|
| Minima | | | |
| 44267 | 33 | | |
| 48779 | 72 | 4512 | 79 |
| 53187 | 114 | 4408 | 135 |
| 57595 | 139 | 4408 | 180 |
| Maxima | | | |
| 46351 | 60 | | |
| 50856 | 44 | 4505 | 74 |
| 55150 | 170 | 4294 | 176 |
| 59592 | 209 | 4442 | 270 |

et al. (2020)), PU Vul (Cúneo et al. (2018)) and other variables. According to Skopal (2001), this type of variability is caused by the optically thick part of the symbiotic nebula (ionized by the hard radiation from the white dwarf), whose contributions are different at different orbital phases. Shugarov et al. (2003) studied wave-like brightness variations of RT Ser and found the ephemeris $JD_{max} = 2446550(\pm 50) + 4520(\pm 80) \cdot E$ with a slightly asymmetrical light curve. We analyzed the observations in B passband from JD 2437846 to 2460215, totaling 288 magnitudes (one per night). Approximation with the trigonometrical polynomial of the first degree with a linear trend (Andronov (1994); Andronov (2020), realized in code of Andronov & Baklanov (2004)), gives the ephemeris

$$JD_{max,B} = 2446406(\pm 21) + 4431(\pm 22) \cdot E \quad (1)$$

We have tested hypotheses of statistical significance of higher degrees s of the trigonometrical polynomial. The false alarm probabilities (FAP), according to Fischers distributions are $15 \cdot 10^{-8}$ and 0.185 for $s = 2$ and $s = 3$, respectively. So this criterion allows us to accept $s = 2$. The trigonometrical polynomial of the second degree with linear trend gives $JD_{max,B} = 2446434(\pm 20) + 4384(\pm 19) \cdot E$.

However, the best r.m.s. accuracy of the approximation at the times of observations 0^m:020 corresponds to the sinusoidal shape ($s = 1$), and increases by 12% for $s = 2$. The trend is linear during the interval of observations, the parabolic and higher degrees of the polynomial are not statistically significant. Thus we accept $s = 1$, which corresponds to the best accuracy of the approximation.

We also calculated moments of extrema during this variability in the B passband using the Asymptotic parabola method (Marsakova & Andronov (1996); Andrych et al. (2020)). Moments and cycle lengths between them are listed in Table 1. We suppose that this cycle becomes shorter with time (our value of the mean period is also shorter than one obtained by Shugarov et al. (2003))

4. Search for pulsation periods

Pavlenko (1997) suspected two periods (213 and 94 days) connected with red

giant pulsations by using the observations on TV-complex, including a 50-cm telescope in BVR (1983-96). We built the periodogram (Andronov (1994); Andronov (2020)) using the joint set of our and AAVSO V-observations and also the periodogram for these series with subtracted sinusoidal 4431.4-days wave. These periodograms are shown in Fig 2. One can see the high peaks near 94, 107, and 160-day values, which could represent the pulsation cycles of the red giant. However the periodogram for our R-observations (not so numerous, but also not showing the long near orbital wave) shows the highest peaks near 170 and 156 days.

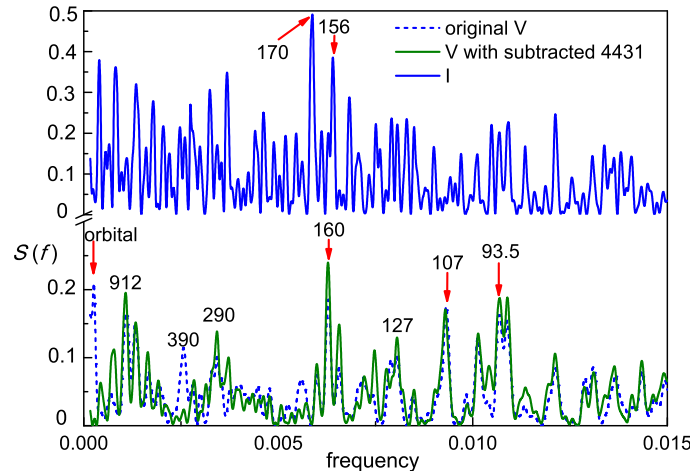


Figure 2. Periodogram for I and V-observations (initial and detrended)

We built two-periodic approximations of V-series with 93.5, 107, and 160-day secondary periods (the first period always was 4431 days). After differential corrections in these models, we obtain the more precise values 93.6 ± 0.2 , 107.9 ± 0.2 , 159.3 ± 0.4 . The same fragment of the light curve is shown in Fig.3 with different two-periodic approximations. As one can see, 159.3^d fits well cycle near JD 2456770, but looks too long in some other time intervals. 93.6^d represents the best approximation near JD 2456300-500 but shows at least a significant phase shift in the interval after JD 2456770. The period value of 107.9^d fits well cycle near JD 2457100, but also shows phase shifts and is bad for last year's oscillations. So we can conclude that there are cyclic oscillations but they are not strictly periodic.

5. Conclusion

We corrected the ephemerid of the long-term wave and suspected that the cycle was getting shorter. We found the cyclicity from about 90 to 170 days and supposed that the pulsating variability of the red giant is not strictly periodic.

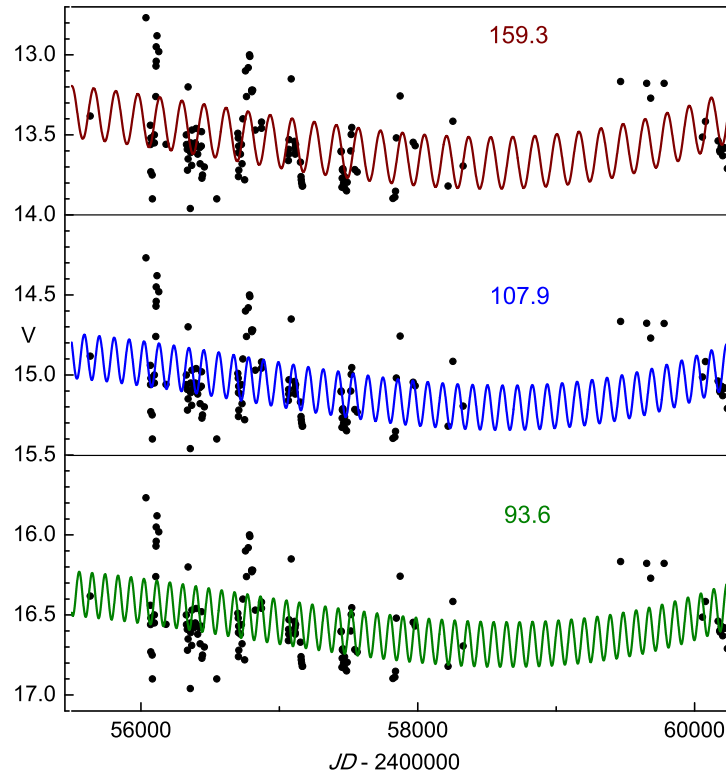


Figure 3. Two-periodic approximations of V-series with 93.6^d (shifted by 1.5^m , 107.9^d , 159.3^d (shifted by -1.5^m) secondary periods (the first period always was 4431 days)

Acknowledgements. We are grateful to AAVSO observer Shawn Dvorak for his observations. The research by V. Marsakova was funded by the National Scholarship Programme of the Slovak Republic. The research by S. Shugarov was supported by the Slovak Research and Development Agency under contract No. APVV-15-0458, APVV-20-0148, and by the Slovak Academy of Sciences grant VEGA No. 2/0030/21.

References

- Andronov, I. L., (Multi-) Frequency Variations of Stars. Some Methods and Results. 1994, *Odessa Astronomical Publications*, **7**, 49
- Andronov, I. L., Advanced Time Series Analysis of Generally Irregularly Spaced Signals: Beyond the Oversimplified Methods. 2020, in *Knowledge Discovery in Big Data from Astronomy and Earth Observation*, ed. P. Škoda & F. Adam, DOI: 10.1016/B978-0-12-819154-5.00022-9, 191–224

- Andronov, I. L. & Baklanov, A. V., Algorithm of the artificial comparison star for the CCD photometry. 2004, *Astronomical School's Report*, **5**, 264, DOI: 10.18372/2411-6602.05.1264
- Andrych, K. D., Andronov, I. L., & Chinarova, L. L., MAVKA: Program of Statistically Optimal Determination of Phenomenological Parameters of Extrema. Parabolic Spline Algorithm And Analysis of Variability of The Semi-Regular Star Z UMa. 2020, *Journal of Physical Studies*, **24**, 1902, DOI: 10.30970/jps.24.1902
- Cúneo, V. A., Kenyon, S. J., Gómez, M. N., et al., An illumination effect and an eccentric orbit for the symbiotic binary PU Vul revealed by 32 yr of optical spectroscopy. 2018, *Monthly Notices of the RAS*, **479**, 2728, DOI: 10.1093/mnras/sty1686
- Henden, A. & Munari, U., UBV(RI)C photometric sequences for symbiotic stars. III. 2006, *Astronomy and Astrophysics*, **458**, 339, DOI: 10.1051/0004-6361:20065662
- Marsakova, V. I. & Andronov, I. L., Local Fits of Signals with Asymptotic Branches. 1996, *Odessa Astronomical Publications*, **9**, 127
- Murset, U. & Nussbaumer, H., Temperatures and luminosities of symbiotic novae. 1994, *Astronomy and Astrophysics*, **282**, 586
- Pavlenko, E., The short-term light variations of RT Serpentis. 1997, in *Physical Processes in Symbiotic Binaries and Related Systems*, ed. J. Mikołajewska, 205–206
- Pavlenko, E. P., Bochkov, V. V., & Vasil'Yanovskaya, O. P., 9,6-Year periodicity of symbiotic nova RT Ser (1909) during the outburst decay from 1940 to 1994. 1996, *Astrophysics*, **39**, 15, DOI: 10.1007/BF02044949
- Payne-Gaposhkin, C. & Gaposhkin, S. 1938, *Variable Stars (Harvard Obs. Monograph, N5, New York: McGraw-Hill)*
- Rudy, R. J., Meier, S. R., Rossano, G. S., et al., Near-Infrared and Ultraviolet Spectrophotometry of Symbiotic Novae. 1999, *Astrophysical Journal, Supplement*, **121**, 533, DOI: 10.1086/313197
- Shugarov, S., Pavlenko, E., & Malanushenko, V., The Nature of a Twelve-Year Periodicity in the Symbiotic Nova RT Ser. 2003, in *Astronomical Society of the Pacific Conference Series, Vol. 303, Symbiotic Stars Probing Stellar Evolution*, ed. R. L. M. Corradi, J. Mikołajewska, & T. J. Mahoney, 87–91
- Shugarov, S. Y., Pavlenko, E. P., & Boczkov, V. V., The Appearance of Strong Reflection Effect in RT Serpentis - the Wide Orbit Binary. 1997, in *Physical Processes in Symbiotic Binaries and Related Systems*, ed. J. Mikołajewska, 207–208
- Skopal, A., What mimics the reflection effect in symbiotic binaries? 2001, *Astronomy and Astrophysics*, **366**, 157, DOI: 10.1051/0004-6361:20000217
- Skopal, A., Shugarov, S. Y., Munari, U., et al., The path to Z And-type outbursts: The case of V426 Sagittae (HBHA 1704-05). 2020, *Astronomy and Astrophysics*, **636**, A77, DOI: 10.1051/0004-6361/201937199

Validation of selected *TESS* exoplanetary candidates

M. Mesarč¹  and L. Hambálek² 

¹ *Department of Theoretical Physics and Astrophysics, Faculty of Science
Masaryk University, Kotlářská 267/2, 611 37 Brno, Czech Republic*

² *Astronomical Institute of the Slovak Academy of Sciences
059 60 Tatranská Lomnica, The Slovak Republic, (E-mail: lhambalek@ta3.sk)*

Received: October 30, 2023; Accepted: December 12, 2023

Abstract. We have selected suitable 6 exoplanetary candidates from the *TESS* database which were observable using a network of small ground-based telescopes to collect photometric transits during follow-up observation. We have made a new reduction of *TESS* photometry using a custom aperture, as well as reducing the ground-based aperture photometry. We have refined the period of transits and constructed $O - C$ diagrams. Mean transit was fitted in all observed photometric filters and we derived individual candidate's physical parameters. Using the colour indices during transit, we hint at the exoplanetary nature of candidates. Three targets TOI-1518b, TOI-2046b, and TOI-2109b were confirmed as exoplanets by other authors during the writing of this thesis. Here, we have provided an independent evaluation and analysis, without any knowledge of their results. TOI-3856.01 is among the targets more likely a substellar object based on my results, but it has not been confirmed yet. In the case of TOI-1834.01, we have proposed another scenario incompatible with the original assumption that it was an exoplanetary candidate and we assume that it is a hierarchical triple system. TOI-3604.01 was also modelled concerning parasitic light in the aperture. Individual models suggest a body too large for an exoplanet.

Key words: Planetary systems – Binaries: eclipsing – Techniques: photometric

1. Introduction

The Transiting Exoplanet Survey Satellite (*TESS*, Ricker et al., 2015) is a NASA space all-sky survey that continuously monitors strips of the sky for ~ 27 continuous days (i.e. sectors) alternating between the north and south hemispheres. The cadence of observation was at first 30 min, 2 min and later 20 s for selected targets. The detector bandpass spans from 600 – 1040 nm and is centred on the traditional Cousins I-band ($\lambda_{\text{eff}} = 786.5$ nm). The red part is preferred for increased sensitivity to small planets transiting in front of cool, red stars, but lacks the colour information of standard photometric filters.

We have selected six *TESS* objects of interest (TOIs) that were still considered candidates for exoplanets (see Tab. 1) in 2021. The selection criteria had

Table 1. Preliminary transit properties of target TOIs at the start of the campaign: host star magnitudes in *TESS* and *V* bands, normalized depth of transit ΔF , transit duration t_T , and period P .

| TOI | 1518.01 | 1834.01 | 2046.01 | 2109.01 | 3604.01 | 3856.01 |
|-------------------|---------|---------|---------|---------|---------|---------|
| <i>TESS</i> [mag] | 8.75 | 11.50 | 11.00 | 9.79 | 11.73 | 11.66 |
| <i>V</i> [mag] | 8.95 | 12.15 | 11.55 | 10.22 | 12.51 | 12.29 |
| ΔF [%] | 0.98 | 2.11 | 1.47 | 0.67 | 1.49 | 1.29 |
| t_T [h] | 2.35 | 1.85 | 2.41 | 1.80 | 1.64 | 1.51 |
| P [d] | 1.90261 | 1.21681 | 1.49718 | 0.67249 | 1.06669 | 2.04345 |

to ensure observability in Central Europe (Dec > -10 deg), a higher occurrence of transits per night ($P < 2.2$ d, $t_T < 3$ h), and bright host stars ($V \leq 12.5$ mag) with deep transits ($\Delta F \geq 0.65$ %) enough for sub-metre telescopes. We planned the observation with TransitFinder (Jensen, 2013) and coordinated observers who were part of ETD (Poddaný et al., 2010), ExoClock (Kokori et al., 2022), and MuSCAT2 (Narita et al., 2019) projects (see Acknowledgements). This article is based on results of the master thesis by Mesarč (2023).

2. Reduction

The available *TESS* data of our targets covered 2–5 sectors per object during the September 2019 – December 2022 time frame. In total, 316 individual transits were identified. *TESS* data were reduced independently of the pipeline first by TPF (Target Pixel File) identification using Python package `lightkurve` (Lightkurve Collaboration et al., 2018) with custom pixel aperture for each TOI using `tpfplotter` (Aller et al., 2020). Each FOV was individually visually inspected for nearby transit-like variable signals in each pixel of the selected aperture and close vicinity. Individual sectors (with 20 s, 2 min, and 30 min cadence) were treated separately. Outliers were removed by Sigma clipping, transits were identified and incomplete ones were omitted for further analysis. For TOI-3856.01 we also had to correct for momentum dumps. Afterwards, our custom-mask flux was de-trended using `exoplanet` package (Foreman-Mackey et al., 2021).

Follow-up observations took part from May 2021 to April 2022. In total, 136 transits were observed at 27 sites with the help of 33 observers in the campaign. Telescopes with diameters 150-1520 mm were used. Various observers had different photometric passbands at their disposal: Johnson *BVRI*, Sloan *g'r'i'z'*, or filter-less clear or luminance band.

For the basic photometric reduction, the HOPS software (Tsiaras, 2019) was used. This allowed for the use of multiple check stars with a circular aperture automatically determined by the stellar FWHM. In each field, we have selected

Table 2. Comparison of our results to those models from papers published during the preparation of the master thesis. Individual papers are: C21 = Cabot et al. (2021), K22 = Kabáth et al. (2022), and W21 = Wong et al. (2021).

| Parameter | TOI-1518b | | TOI-2046b | | TOI-2109b | |
|--------------------------------|-----------|-----------|------------|------------|------------|------------|
| | This work | C21 | This work | K22 | This work | W21 |
| R_P/R_S | 0.0819(6) | 0.0816(2) | 0.1173(8) | 0.1213(19) | 0.1022(20) | 0.0988(13) |
| a/R_S | 2.14(1) | 2.27(2) | 4.53(5) | 4.75(18) | 4.13(1) | 4.29(1) |
| b | 0.785(6) | 0.748(7) | 0.60(2) | 0.51(6) | 0.882(6) | 0.904(6) |
| i [deg] | 68.9(3) | 70.7(4) | 81.8(3) | 83.6(9) | 77.7(2) | 77.8(2) |
| t_T [h] | 2.070(12) | 1.801(13) | 2.591(10) | 2.410(31) | 2.395(18) | 2.347(8) |
| ρ_* [g cm ⁻³] | 0.417(50) | 0.417(55) | 0.859(101) | 0.890(98) | 0.341(56) | – |
| ΔF [%] | 0.667(6) | 0.665(4) | 1.476(18) | 1.627(9) | 1.044(16) | 0.976(8) |

4–7 check stars so that they show no signs of variability. A standard dark and flat calibration of all frames was performed. From the check stars available in each FOV, an artificial star was constructed to do the relative aperture photometry.

3. Modelling of transits

The total de-trended *TESS* light curve (LC) was analysed with a box-fitting least-square algorithm by Kovács et al. (2002) to find period P and starting epoch T_0 for the transit ephemeris. This was used to predict follow-up ground-based observations. We have constructed the phased *TESS* LC and selected the region ± 4 hours around the mid-transit.

Using the mean transit shape, we were able to find more precise times of mid-transit for 30-minute *TESS* cadence even when each transit was covered by only a handful of points. The data was used to construct an $O - C$ diagram.

TESS transit model was calculated using the `pyaneti` code by Barragán et al. (2019). The code utilises the MCMC method to compute transit parameters: the planet-star radius ratio R_P/R_S , the ratio of the semi-major axis to the stellar radius a/R_S , inclination i of the orbital plane (or the impact parameter b), duration t_T . The limb-darkening coefficients were adopted using a parametrization proposed by Kipping (2013).

The ground-based transits were modelled by the HOPS package (Tsiaras et al., 2016). The necessary stellar limb-darkening coefficients were calculated with the ExoTETHys package (Morello et al., 2020) for each passband using the non-linear law by Claret (2000) and the stellar parameters were taken from NASA Exoplanet Archive.

Table 3. Our results of assumed exoplanet transit models of TOIs without known paper published before May 2023. Note: for TOI-3604.01, model A treats all light as a single star in *TESS* pixel, while model B assumes half of the observed flux as contamination.

| Parameter | TOI-1834.01 | TOI-3604.01 | | TOI-3856.01 |
|--------------------------------|-------------|-------------|------------|-------------|
| | | A | B | |
| R_P/R_S | 0.1485(59) | 0.1219(20) | 0.1599(7) | 0.1135(24) |
| a/R_S | 3.25(6) | 4.38(8) | 5.50(3) | 6.13(22) |
| b | | 0.891(9) | 0.724(49) | 0.818(26) |
| i [deg] | 74.1(4) | 81.0(5) | 86.5(9) | 82.3(5) |
| t_T [h] | 2.178(27) | 1.689(15) | 1.715(9) | 1.942(40) |
| ρ_* [g cm ⁻³] | 1.332(162) | 1.407(360) | 1.407(360) | 0.957(201) |
| ΔF [%] | 2.206(37) | 1.585(40) | 2.556(28) | 1.289(13) |

4. Results

Since the *TESS* detector has 21-arcsec pixel scale (see [Ricker et al., 2015](#)), we had to check if there are more light sources at the target TOIs position below this resolution. We have used publicly available speckle polarimetry from SAI 2.5-m telescope ([Safonov et al., 2017](#)), Alopeke Speckle Instrument at Gemini-North telescope ([Howell et al., 2016](#); [Howell & Furlan, 2022](#)), and PHARO instrument at Palomar 5-m telescope ([Hayward et al., 2001](#)) of angular resolution in range of 20-89 mas. Only in the case of TOI 3604.01, there was a visible detection of another source within 0.3 arcsec off the target.

Some transit parameters from independent modelling of confirmed exoplanets during this work are listed in Tab. 2 and as of date non-confirmed candidates are in Tab. 3. We have additionally revised the linear ephemerides (Tab. 4) by incorporating every observed minimum.

Ground-based observations taken in different filters were analyzed separately. Parameters R_P/R_S , a/R_S , and i were found for each passband. The relation between R_P/R_S and λ_{eff} of filter shows “jumps” similar to rigorous models (see e.g. [Fortney et al., 2010](#)). TOI-1834.01 is an exception to this, which seems to have a monotonous function $R_P/R_S \propto \lambda_{\text{eff}}$ but only from $VR + r'i'$ passbands. It is also the only system with a periodic $O-C$ signal, with ~ 10 -min amplitude and a period of 80.3501 ± 0.3149 days.

Our multi-colour ground-based photometry allowed us to construct a differential colour transit LC. While no sufficiently precise spectroscopy was available for us, we still wanted to limit the possibility of false detection by investigating the limb-darkening profile of the transiting body. If the second component is a star on an inclined orbit, it would produce shallow grazing eclipses. However, a star has a different limb-darkening profile than an exoplanet with a night side facing the observer. According to [Tingley \(2004\)](#), exoplanetary transits produce

a double-horned profile in differential colour transit LC while a close binary shows no such feature.

Only a handful of our ground-based transits were observed in two or more filters during a single night. We have constructed a model LC for each colour. Then, by subtracting any two models we created an artificial colour LC in arbitrary phases to cover the full transit. The more distant the effective wavelength of bands, the higher the signal.

Table 4. Updated periods (P) and reference time of primary transit (T_0).

| Object | T_0 [BJD _{TDB}] | P [d] |
|-------------|-----------------------------|-----------------|
| TOI-1518b | 2459854.414430(41) | 1.90261125(9) |
| TOI-1834.01 | 2458928.271637(210) | 1.21644035(28) |
| TOI-2046b | 2459883.844897(58) | 1.49718679(15) |
| TOI-2109b | 2459718.730971(82) | 0.67247386(17) |
| TOI-3604.01 | 2459825.953340(850) | 1.0666837(427) |
| TOI-3856.01 | 2459609.405178(2180) | 2.04360450(119) |

We have used all identified transits from *TESS* as well as ground-based follow-up to construct the $O - C$ diagram. Except for TOI-1834.01 (Fig. 1), no other target shows a meaningful signal. The most notable part of $O - C$ is taken during *TESS* sector 49 (February 26 – March 26, 2022). We have modelled this part and the whole $O - C$ using the code `OCFit` by Gajdoš & Parimucha (2019). We have fitted a simple 3-body scenario with MCMC resulting in $P_3 = 80.35013 \pm 0.31488$ d on a short ($a_3 \sin i_3 = 1.161 \pm 0.157$ au) eccentric ($e_3 = 0.265 \pm 0.135$) orbit. It is a similar solution to that of Czavalinga et al. (2023) which was published shortly before submitting the thesis. The problem is that considering the total $O - C$ amplitude is caused solely by LITE leads to unrealistic large mass function $f(m) = 32.33 M_\odot$.

We have also tried to model the transit of TOI-1834.01 as a grazing binary with the code `RMF` by Garai et al. (2020). The simplest case was to assume $M_2/M_1 = R_2/R_1$ and fit a model spectrum to the spectral energy distribution fixed around VizieR photometry. The best-fitting temperature was 5200 K corresponding to K0 spectral type or $\sim 0.79 M_\odot$, $\sim 0.85 R_\odot$ (based on tables by Cox (2000)). We can use equations 8 and 12 from Borkovits et al. (2016) to estimate amplitudes of LTTE and dynamical effects (for $M_1 = M_2 = M_3$) as $\mathcal{A}_{LTTE} = 78.68$ s and $\mathcal{A}_{dyn} = 567.38$ s, respectively. This is already enough to explain the observed 10-minute amplitude of $O - C$.

TOI-3604.01 is the only target resolved by speckle interferometry in near-IR into two sources of similar apparent luminosity separated by 0.3 arcsec. We have thus removed a constant 50% of total *TESS* out-of-transit flux and constructed a new model (B in Tab. 3) from the normalized treated flux. In this case, the supposed exoplanet orbiting one of the two stars had to be $\sim 30\%$ larger than

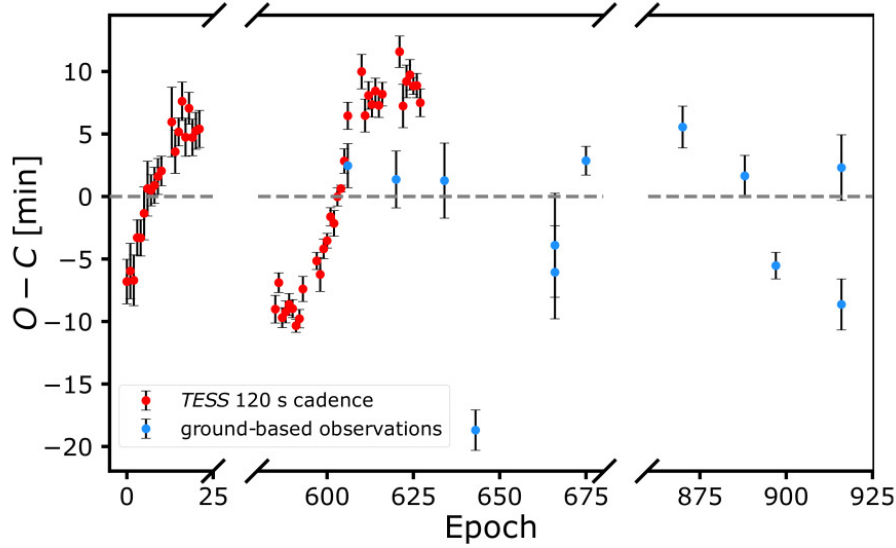


Figure 1. The $O - C$ diagram for TOI-1834.01 constructed with the updated ephemeris $T_0 = 2458925.271637 + 1.21644035 \times E$.

initially assumed, making it more likely to be a low-mass star. The parent object is also a very active red dwarf. Lambert et al. (2023) found maybe a similar (by R_P/R_S) object TOI-5375.01 which hosts a brown dwarf/low-mass star at hydrogen-burning limit with $\sim 83.8 \pm 2.1 M_J$.

TOI-3856.01 was at the time of this work not independently analyzed. The transit model based on ground photometry gives $R_P/R_S \in [0.112, 0.128]$ in seven different passbands (c.f. with Tab. 3). With stellar radius $R_\star = 1.12864 R_\odot$ (taken from the EXOFOP page), this gives the candidate radius as $R_P \in [1.26, 1.44] R_J$. The U-shaped single colour transits and double-horned differential colour transit suggest this object may be a hot Jupiter on ~ 0.034 au orbit.

5. Conclusion

We have selected six exoplanetary candidates as indicated by the *TESS* pipeline. From *TESS* photometry, we modelled their transits and got independent solutions for TOIs 1518b, 2046b, and 2109b. The TOI-1834.01 was independently found to be most probably a hierarchical triple star system of late K-type stars. Based on the corrected flux in *TESS* aperture, we found TOI-3604.01 to be probably a very low-mass star close to the hydrogen-burning limit. Based on our analysis, TOI-3856.01 appears to be a sub-stellar object.

Acknowledgements. This work was supported by the Slovak Research and Development Agency under the contract No. APVV-20-0148. This work has also been supported by the VEGA grant of the Slovak Academy of Sciences No. 2/0031/22. Thanks to all observers: Reinhold Friedrich Auer, Paul Benni, Giorgio Bianciardi, Matteo Cataneo, Giuseppe Conzo, Yannic Delisle, Vojtěch Dienstbier, Tommaso Dittadi, Frank Dubois, Gareb Enoc Fernández, Zoltán Garai, Snævarr Gudmundson, Veli-Pekka Hentunen, Yves Jongen, Taiki Kageyama, Peter Klagyivik, Felipe Murgas, Andre Kovacs, Hana Kučáková, Jean Claude Mario, Zlatko Orbanic, Ivo Peretto, Karol Petrik, Theodor Pribulla, Manfred Raetz, Roy René, Mark Salisbury, Sergei Shugarov, Pieter Vuylsteke, Noriharu Watanabe, Anaël Wünsche, and Miloslav Zejda.

References

- Aller, A., Lillo-Box, J., Jones, D., Miranda, L. F., & Barceló Forteza, S., Planetary nebulae seen with TESS: Discovery of new binary central star candidates from Cycle 1. 2020, *Astronomy and Astrophysics*, **635**, A128, DOI: 10.1051/0004-6361/201937118
- Barragán, O., Gandolfi, D., & Antoniciello, G., PYANETI: a fast and powerful software suite for multiplanet radial velocity and transit fitting. 2019, *Monthly Notices of the RAS*, **482**, 1017, DOI: 10.1093/mnras/sty2472
- Borkovits, T., Hajdu, T., Sztakovics, J., et al., A comprehensive study of the Kepler triples via eclipse timing. 2016, *Monthly Notices of the RAS*, **455**, 4136, DOI: 10.1093/mnras/stv2530
- Cabot, S. H. C., Bello-Arufe, A., Mendonça, J. M., et al., TOI-1518b: A Misaligned Ultra-hot Jupiter with Iron in Its Atmosphere. 2021, *Astronomical Journal*, **162**, 218, DOI: 10.3847/1538-3881/ac1ba3
- Claret, A., A new non-linear limb-darkening law for LTE stellar atmosphere models. Calculations for $-5.0 \leq \log[M/H] \leq +1$, $2000 \text{ K} \leq T_{\text{eff}} \leq 50000 \text{ K}$ at several surface gravities. 2000, *Astronomy and Astrophysics*, **363**, 1081
- Cox, A. N. 2000, *Allen's astrophysical quantities* (Springer New York, NY)
- Czavalinga, D. R., Borkovits, T., Mitnyan, T., Rappaport, S. A., & Pál, A., "Four new compact triply eclipsing triples found with Gaia and TESS. 2023, *Monthly Notices of the RAS*, **526**, 2830, DOI: 10.1093/mnras/stad2759
- Foreman-Mackey, D., Luger, R., Agol, E., et al., exoplanet: Gradient-based probabilistic inference for exoplanet data & other astronomical time series. 2021, *The Journal of Open Source Software*, **6**, 3285, DOI: 10.21105/joss.03285
- Fortney, J. J., Shabram, M., Showman, A. P., et al., Transmission Spectra of Three-Dimensional Hot Jupiter Model Atmospheres. 2010, *Astrophysical Journal*, **709**, 1396, DOI: 10.1088/0004-637X/709/2/1396
- Gajdoš, P. & Parimucha, Š., New tool with GUI for fitting O-C diagrams. 2019, *Open European Journal on Variable Stars*, **197**, 71
- Garai, Z., Pribulla, T., Komžík, R., et al., Periodic transit timing variations and refined system parameters of the exoplanet XO-6b. 2020, *Monthly Notices of the RAS*, **491**, 2760, DOI: 10.1093/mnras/stz3235

- Hayward, T. L., Brandl, B., Pirger, B., et al., PHARO: A Near-Infrared Camera for the Palomar Adaptive Optics System. 2001, *Publications of the ASP*, **113**, 105, DOI: 10.1086/317969
- Howell, S. B., Everett, M. E., Horch, E. P., et al., Speckle Imaging Excludes Low-mass Companions Orbiting the Exoplanet Host Star TRAPPIST-1. 2016, *Astrophysical Journal, Letters*, **829**, L2, DOI: 10.3847/2041-8205/829/1/L2
- Howell, S. B. & Furlan, E., Speckle Interferometric Observations With the Gemini 8-m Telescopes: Signal-to-Noise Calculations and Observational Results. 2022, *Frontiers in Astronomy and Space Sciences*, **9**, DOI: 10.3389/fspas.2022.871163
- Jensen, E. 2013, Tapir: A web interface for transit/eclipse observability, Astrophysics Source Code Library, record ascl:1306.007
- Kabáth, P., Chaturvedi, P., MacQueen, P. J., et al., TOI-2046b, TOI-1181b, and TOI-1516b, three new hot Jupiters from TESS: planets orbiting a young star, a subgiant, and a normal star. 2022, *Monthly Notices of the RAS*, **513**, 5955, DOI: 10.1093/mnras/stac1254
- Kipping, D. M., Efficient, uninformative sampling of limb darkening coefficients for two-parameter laws. 2013, *Monthly Notices of the RAS*, **435**, 2152, DOI: 10.1093/mnras/stt1435
- Kokori, A., Tsiaras, A., Edwards, B., et al., ExoClock project: an open platform for monitoring the ephemerides of Ariel targets with contributions from the public. 2022, *Experimental Astronomy*, **53**, 547, DOI: 10.1007/s10686-020-09696-3
- Kovács, G., Zucker, S., & Mazeh, T., A box-fitting algorithm in the search for periodic transits. 2002, *Astronomy and Astrophysics*, **391**, 369, DOI: 10.1051/0004-6361:20020802
- Lambert, M., Bender, C. F., Kanodia, S., et al., TOI-5375 B: A Very Low Mass Star at the Hydrogen-burning Limit Orbiting an Early M-type Star. 2023, *Astronomical Journal*, **165**, 218, DOI: 10.3847/1538-3881/acc651
- Lightkurve Collaboration, Cardoso, J. V. d. M., Hedges, C., et al. 2018, Lightkurve: Kepler and TESS time series analysis in Python, Astrophysics Source Code Library, record ascl:1812.013
- Mesarč, M. 2023, Validation of selected *TESS* exoplanetary candidate
- Morello, G., Claret, A., Martin-Lagarde, M., et al., The ExoTETHyS Package: Tools for Exoplanetary Transits around Host Stars. 2020, *Astronomical Journal*, **159**, 75, DOI: 10.3847/1538-3881/ab63dc
- Narita, N., Fukui, A., Kusakabe, N., et al., MuSCAT2: four-color simultaneous camera for the 1.52-m Telescopio Carlos Sánchez. 2019, *Journal of Astronomical Telescopes, Instruments, and Systems*, **5**, 015001, DOI: 10.1117/1.JATIS.5.1.015001
- Poddaný, S., Brát, L., & Pejcha, O., Exoplanet Transit Database. Reduction and processing of the photometric data of exoplanet transits. 2010, *New Astronomy*, **15**, 297, DOI: 10.1016/j.newast.2009.09.001

- Ricker, G. R., Winn, J. N., Vanderspek, R., et al., Transiting Exoplanet Survey Satellite (TESS). 2015, *Journal of Astronomical Telescopes, Instruments, and Systems*, **1**, 014003, DOI: 10.1117/1.JATIS.1.1.014003
- Safonov, B. S., Lysenko, P. A., & Dodin, A. V., The speckle polarimeter of the 2.5-m telescope: Design and calibration. 2017, *Astronomy Letters*, **43**, 344, DOI: 10.1134/S1063773717050036
- Tingley, B., Using color photometry to separate transiting exoplanets from false positives. 2004, *Astronomy and Astrophysics*, **425**, 1125, DOI: 10.1051/0004-6361:20035792
- Tsiaras, A., HOPS: the photometric software of the HOlonom Astronomical Station. in , *EPSC-DPS joint Meeting - Exoplanet exploration*, Vol. **13**, EPSC-DPS2019-1594
- Tsiaras, A., Waldmann, I. P., Rocchetto, M., et al. 2016, pylightcurve: Exoplanet lightcurve model, Astrophysics Source Code Library, record ascl:1612.018
- Wong, I., Shporer, A., Zhou, G., et al., TOI-2109: An Ultrahot Gas Giant on a 16 hr Orbit. 2021, *Astronomical Journal*, **162**, 256, DOI: 10.3847/1538-3881/ac26bd

Eclipse timing variations of evolved eclipsing binaries: potential targets for meter-sized telescopes in the light of TESS observations

E.M. Esmer^{}, Ö. Baştürk^{}, S. O. Selam^{}, F. Akar^{}, E. Sertkan^{},
B. Güler^{} and S. Yalçinkaya^{}

Department of Astronomy & Space Sciences, Faculty of Science, Ankara University, TR-06100, Ankara, Türkiye (E-mail: esmer@ankara.edu.tr)

Received: November 6, 2023; Accepted: December 8, 2023

Abstract. Evolved eclipsing binaries, featuring a white dwarf or a subdwarf companion on relatively short orbital periods of a few hours, exhibit interesting characteristics in their eclipse timing variations (ETV), analysis of which brings several advantages. Firstly, their small total masses enable us to detect substellar mass objects by observing the light-time effect, due to a subtle wobbling of the binary system around the barycenter. Additionally, the short orbital periods of these binaries allow for the accumulation of a large dataset comprising numerous observations, facilitating rigorous analysis and enhancing statistical significance. Moreover, their minima profiles have symmetric V-shapes in most cases, which decrease the uncertainties in the measurements of minima timings. In this study, we collect and analyze all available photometric data from the Transiting Exoplanet Survey Satellite (TESS), using observation cadences of both 20 and 120 seconds for such systems identified by various surveys. Our sample includes more than 60 evolved eclipsing binaries, whose primaries are either white dwarf or subdwarf companions. By calculating mid-eclipse timings, we construct detailed ETV diagrams and apply the Lomb-Scargle period analysis to determine the amplitudes and periods of their ETVs.

Key words: binaries: eclipsing – methods: data analysis – planetary systems

1. Introduction

The Eclipse Timing Variation (ETV) method is a well-known and useful tool for detecting additional objects within a binary system. This method relies on analyzing the cyclic variations in eclipse times, which are caused by the radial component of the binary's orbit around the barycenter, influenced by the presence of one or more additional objects.

The emergence of the eclipse signal with varying distances to observers induces the light-time effect (LiTE), also known as the Roemer delay. In many cases, the precision of timing data and the relatively simple system complexity, such as a small number of bodies and large orbital separations, allow for the

use of elliptical orbit models (Keplerian orbits) to sufficiently model ETVs with LiTE. However, as photometric precision increases, perturbations between the bodies necessitate the use of Newtonian approaches to precisely determine the orbital properties of such systems. It's important to note that other cyclic ETV-causing mechanisms, like the magnetic activity cycles of late-type companions, can produce signals that mimic those of additional objects.

The ETV method has detected numerous substellar mass circumbinary objects (Baştürk et al., 2023). However, the history of ETV searches for substellar objects includes both successful detections and rejections. The lack of independent confirmation methods has contributed to the variability in these ETV analyses. Long-period ETV modulations make comprehensive radial velocity follow-ups challenging and significantly reduce transit probabilities. Orbital stability tests for systems with multiple circumbinary candidate objects are currently the most practical tools for confirmation purposes.

Eclipsing binaries with circumbinary substellar mass objects detected using the ETV method share common characteristics. They typically fall into two categories: HW Virginis-like binaries with a subdwarf OB (sdOB) primary star and a low-mass main sequence companion, or cataclysmic binaries with a white dwarf primary and a main sequence companion. These systems generally have a total mass of less than one solar mass, which is crucial for detecting the wobbling induced by substellar mass objects. Their short orbital periods enable frequent eclipse observations, while their eclipse light curves often feature prominent V-shaped eclipses, facilitating precise determination of eclipse mid-times. The presence of a common envelope in previous evolutionary stages may be a key factor in these binaries hosting circumbinary planets (Zorotovic & Schreiber, 2013).

Baştürk et al. (2023) revealed that many multiplanet ETV systems lack stable orbital configurations. Several potential reasons for this issue include: i) The cyclic ETV modulations have long periods spanning years or decades, requiring extended observations and thorough analysis, which are often lacking. ii) Modeling of the ETV tends to result in positive eccentricity parameters, increasing the likelihood of close encounters or even orbit crossings. iii) In some cases, other ETV mechanisms may not have been correctly implemented.

This research undertakes an initial exploration of a thorough ETV search to identify potential timing modulations of eclipsing binaries. We introduce our research project and present preliminary results based on TESS observations. Our main objective in this study is to detect potential short-period ETV modulations within the TESS data. Following this, we aim to amalgamate timing data from TESS with existing ground and space-based timings, creating a comprehensive ETV dataset. This dataset will serve as a valuable resource for conducting timing analyses on a variety of eclipsing binary systems.

Table 1. Gaia G brightness values, number of TESS sectors with 120-second and 20-second exposures, number of mid-eclipse timings calculated for each exposure, and their corresponding uncertainties. The first group is HW Vir-like systems and the second one is cataclysmic variables. ¹Full identifier is ATO J294.7689+11.1822

| System | G Mag | Sectors | | Timings | | σ_{120s} (s) | σ_{20s} (s) |
|------------------------------|-------|---------|------|--------------|------|------------------------|-----------------------|
| | | 120 s | 20 s | 120 s - 20 s | | | |
| DD CrB | 12.9 | 3 | 2 | 580 | 366 | 2.61 | 2.65 |
| HW Vir | 10.6 | 1 | 1 | 380 | 374 | 6.57 | 0.72 |
| NY Vir | 13.4 | 3 | 2 | 1116 | 749 | 2.91 | 1.72 |
| AA Dor | 11.1 | 29 | 17 | 4727 | 2985 | 4.44 | 2.26 |
| V1828 Aql | 13.2 | 1 | 1 | 223 | 190 | 8.59 | 4.74 |
| CHSS 3072 | 14.3 | 1 | 0 | 101 | 0 | 5.55 | - |
| HS 0705+6700 | 14.6 | 3 | 2 | 1252 | 714 | 5.01 | 11.63 |
| Kepler-451 | 12.1 | 4 | 0 | 1166 | 0 | 10.18 | - |
| HS 2231+2441 | 14.2 | 1 | 1 | 342 | 249 | 25.61 | 7.98 |
| PN A66 46 | 15.0 | 3 | 2 | 251 | 196 | 22.68 | 6.04 |
| UCAC4 489-038954 | 15.2 | 1 | 0 | 495 | 0 | 26.37 | - |
| TIC 455206965 | 15.2 | 3 | 2 | 1093 | 721 | 35.56 | 25.63 |
| ATO J294.7+11.1 ¹ | 14.9 | 1 | 1 | 97 | 133 | 94.17 | 19.05 |
| TIC 467187065 | 15.8 | 8 | 6 | 4318 | 3370 | 43.39 | 17.41 |
| V588 Vir | 13.8 | 1 | 0 | 51 | 0 | 97.65 | - |
| RW Tri | 13.2 | 1 | 0 | 248 | 0 | 8.07 | - |
| V1315 Aql | 14.3 | 1 | 0 | 231 | 0 | 7.16 | - |
| TIC 240872692 | 15.1 | 3 | 1 | 461 | 236 | 16.22 | 13.34 |
| V363 Aur | 14.1 | 2 | 0 | 272 | 0 | 17.96 | - |
| UZ For | 16.6 | 1 | 0 | 411 | 0 | 43.53 | - |
| TIC 271137877 | 16.9 | 1 | 0 | 217 | 0 | 24.48 | - |
| V870 Lyr | 15.9 | 4 | 0 | 744 | 0 | 25.06 | - |
| V1776 Cyg | 16.5 | 5 | 0 | 1276 | 0 | 55.73 | - |

2. ETV analysis of evolved eclipsing binaries

We selected a subgroup of evolved eclipsing binaries from a larger pool of 68 similar systems (see Table 1) for which TESS data was available. Our objective was to construct ETV diagrams and identify periodic patterns within their TESS data. To achieve this, we obtained both 120-second and 20-second exposure TESS data for each system through the Space Telescope Science Institute’s (STScI) Mikulski Archive for Space Telescopes (MAST)¹. The data underwent quality flag filtering, and any evident outliers were removed. We applied second-degree polynomial detrending to continuous observation sections within each sector and normalized the data to their respective median flux levels.

¹<https://archive.stsci.edu>

To generate ETV diagrams, we initially computed mid-eclipse times using the well-established Kwee & van Woerden method (Kwee & van Woerden, 1956), focusing solely on the primary eclipses. We concurrently updated the linear ephemeris for each system while also eliminating outliers from the ETV diagrams. By combining timings from all available sectors, we produced the final ETV diagrams for each evolved eclipsing binary. The ETV scatter is generally smaller for HW Virginis-like binaries in comparison to cataclysmic variables, primarily due to the symmetrical eclipse features of HW Virginis-like systems. Notably, we observed that the scatter tends to be smaller for systems with 120-second exposures and brighter systems, aligning with our expectations.

To identify periodic patterns in the ETV diagrams, we employed the Lomb-Scargle periodogram (Lomb, 1976; Scargle, 1982) on the ETVs from 120-second exposures using our custom Python script. The script is based on relevant functions from the `ASTROPY` package (Astropy Collaboration et al., 2013, 2018, 2022). For each periodogram, we determined the periods corresponding to the highest Lomb-Scargle power and calculated their associated amplitude and false alarm probability (FAP), which are listed in Table 2.

We identified two distinct groups within our results. The first group comprises three systems: HW Virginis, NY Virginis, and V1776 Cyg. Their associated false alarm probability (FAP) values are effectively zero, suggesting potential periodic variations in the ETV diagrams based on TESS data. For HW Virginis and NY Virginis, we compared the ETV diagrams between 120-second and 20-second exposures. The periodic variation observed in 120-second exposures disappears in the 20-second ETV diagram of HW Virginis, indicating that the periodicity is a result of the 120-second TESS exposure times. Conversely, for NY Virginis, the periodicity remains consistent in the 20-second exposures, which we attribute to pulsations of the primary sdB component within the eclipsing binary. These pulsations have detectable amplitudes, even in ground-based observations, as demonstrated in a prior study by Vučković et al. (2007). We have deferred assessing the source of periodicity in V1776 Cyg due to the absence of 20-second exposures, leaving it for further investigation.

The second group exhibits periodicities extending beyond a single TESS sector, and the associated false alarm probability (FAP) values for these periodicities are notably high ($\text{FAP} > 0.2$). These systems include HS 0705+6700 and Kepler-451. We phase-folded the ETV diagrams for these systems using the periods with the highest Lomb-Scargle power. In the case of HS 0705+6700, the phase-folded ETV lacks coverage for almost half of the phase. For Kepler-451, although the period we found is somewhat close to that of the innermost planet ($P_d = 43$ d) detected by Esmer et al. (2022), however, the amplitude is significantly higher than expected for such an object. The periodicities observed in these cases may result from jitter caused by pulsations of the primary star or stellar spots on the secondary star, phenomena expected in these types of eclipsing binaries. Additionally, the sampling of TESS may introduce jitter at a detectable level in their ETVs. However, a comprehensive explanation for these

Table 2. Periods, amplitudes, and false alarm probabilities (FAP) of the ETV data calculated by Lomb-Scargle periodograms for our target subgroup.

| System | LS Period (d) | Amplitude (sec) | FAP |
|------------------|---------------|-----------------|------------|
| DD CrB | 6.408 | 1.30 | 0.94 |
| HW Vir | 3.884 | 4.85 | 10^{-38} |
| NY Vir | 4.309 | 1.93 | 10^{-7} |
| AA Dor | 3.146 | 0.52 | 1.00 |
| V1828 Aql | 2.005 | 3.73 | 1.00 |
| CHSS 3072 | 2.311 | 6.30 | 0.31 |
| HS 0705+6700 | 61.345 | 7.81 | 0.49 |
| Kepler-451 | 33.671 | 8.68 | 0.21 |
| HS 2231+2441 | 2.200 | 10.11 | 1.00 |
| PN A66 46 | 2.112 | 15.73 | 0.89 |
| UCAC4 489-038954 | 2.351 | 10.85 | 1.00 |
| TIC 455206965 | 5.294 | 10.88 | 1.00 |
| ATO J294.7+11.1 | 5.767 | 61.34 | 1.00 |
| TIC 467187065 | 4.562 | 22.25 | 1.00 |
| V588 Vir | 2.751 | 3749.80 | 0.38 |
| RW Tri | 5.607 | 12.84 | 1.00 |
| V1315 Aql | 6.96 | 13.94 | 1.00 |
| TIC 240872692 | 3.203 | 12.47 | 1.00 |
| V363 Aur | 7.175 | 30.15 | 0.96 |
| UZ For | 2.382 | 16.37 | 1.00 |
| TIC 271137877 | 8.651 | 26.69 | 1.00 |
| V870 Lyr | 4.092 | 24.66 | 0.76 |
| V1776 Cyg | 6.520 | 87.33 | 10^{-8} |

periodicities in their ETVs is yet to be provided and remains a subject for future studies.

3. Summary

With this study, our primary goal is to search for potential short-period ETV modulations within the TESS data. We intend to expand our ETV datasets for these systems by incorporating both ground-based and space-based timing calculations. The TESS photometry, in particular, will play a crucial role in binary modeling, which we aim to apply to a majority of the evolved eclipsing binaries on our target list.

This study serves as a preliminary ETV search for our list of evolved eclipsing binaries. We have compiled this list as part of a comprehensive ETV research project, where we aim to detect circumbinary substellar mass objects around evolved binaries. Our objectives include testing the validity of previous ETV solutions, updating them as necessary, building population statistics for hosts and

substellar companions, creating a comprehensive ETV catalog, and contributing to the research field by developing the required software tools.

Acknowledgements. We gratefully acknowledge the support by The Scientific and Technological Research Council of Türkiye (TÜBİTAK) under Project 122F358. We also extend our gratitude to the SOC and LOC of the conference, *Observing techniques, instrumentation and science for metre-class telescopes III* for their financial support. We appreciate the valuable discussions with fellow conference attendees.

References

- Astropy Collaboration, Price-Whelan, A. M., Lim, P. L., et al., The Astropy Project: Sustaining and Growing a Community-oriented Open-source Project and the Latest Major Release (v5.0) of the Core Package. 2022, *Astrophysical Journal*, **935**, 167, DOI: 10.3847/1538-4357/ac7c74
- Astropy Collaboration, Price-Whelan, A. M., Sipőcz, B. M., et al., The Astropy Project: Building an Open-science Project and Status of the v2.0 Core Package. 2018, *Astronomical Journal*, **156**, 123, DOI: 10.3847/1538-3881/aabc4f
- Astropy Collaboration, Robitaille, T. P., Tollerud, E. J., et al., Astropy: A community Python package for astronomy. 2013, *Astronomy and Astrophysics*, **558**, A33, DOI: 10.1051/0004-6361/201322068
- Baştürk, Ö., Esmer, E. M., Demir, E., & Selam, S. O., Eclipse Timing Variations Observed in PCEB Systems. 2023, *Bulletin de la Societ Royale des Sciences de Lige*, DOI: 10.255118/0037-9565.11197
- Esmer, E. M., Baştürk, Ö., Selam, S. O., & Aliş, S., Detection of two additional circumbinary planets around Kepler-451. 2022, *Monthly Notices of the RAS*, **511**, 5207, DOI: 10.1093/mnras/stac357
- Kwee, K. K. & van Woerden, H., A method for computing accurately the epoch of minimum of an eclipsing variable. 1956, *Bulletin Astronomical Institute of the Netherlands*, **12**, 327
- Lomb, N. R., Least-Squares Frequency Analysis of Unequally Spaced Data. 1976, *Astrophysics and Space Science*, **39**, 447, DOI: 10.1007/BF00648343
- Scargle, J. D., Studies in astronomical time series analysis. II. Statistical aspects of spectral analysis of unevenly spaced data. 1982, *Astrophysical Journal*, **263**, 835, DOI: 10.1086/160554
- Vučković, M., Aerts, C., Östensen, R., et al., The binary properties of the pulsating subdwarf B eclipsing binary ι ASTROBJ₂PG 1336-018/ ι ASTROBJ₂ (NY Virginis). 2007, *Astronomy and Astrophysics*, **471**, 605, DOI: 10.1051/0004-6361:20077179
- Zorotovic, M. & Schreiber, M. R., Origin of apparent period variations in eclipsing post-common-envelope binaries. 2013, *Astronomy and Astrophysics*, **549**, A95, DOI: 10.1051/0004-6361/201220321

Three decades of the OGLE survey

I. Soszyński 

*Astronomical Observatory, University of Warsaw, Al. Ujazdowskie 4,
00-478 Warszawa, Poland (E-mail: soszynsk@astrouw.edu.pl)*

Received: November 9, 2023; Accepted: December 17, 2023

Abstract. The Optical Gravitational Lensing Experiment (OGLE) is one of the most extensive sky surveys on a global scale. It focuses on optical astrophysical variability and is carried out using the dedicated 1.3-meter Warsaw Telescope located at Las Campanas Observatory in Chile. Since 1992, the OGLE project has been continuously observing the densest regions of the southern sky, namely, the Galactic bulge, Galactic disk, and Magellanic Clouds. To date, the survey has collected over a trillion individual photometric observations for approximately two billion stars. Throughout its long history, the OGLE project has yielded significant contributions to various fields of astrophysics, including gravitational lensing and microlensing, dark matter, exoplanets, variable stars, the structure of the Milky Way and other galaxies, and more. This article presents the most significant achievements of OGLE over the past 30 years.

Key words: Surveys – Gravitational microlensing – Planetary systems – Variable stars – Cepheids – Galaxy: structure – Catalogs

1. Introduction

The name of the Optical Gravitational Lensing Experiment (OGLE) project reflects its initial objective: the search for gravitational microlensing phenomena. However, over the course of its long history, the project has evolved, and presently, OGLE is a large-scale photometric survey aimed at identifying and studying all forms of variability in the sky. The OGLE project was initiated in 1992 in response to the seminal paper by Paczyński (1986), who introduced the theory of gravitational microlensing and suggested arranging an observational program aimed at monitoring the brightness of at least a few million stars with the goal of detecting the first microlensing events. Such a sky survey was designed to shed light on the nature of dark matter and to serve as a potential source of a substantial number of newly discovered variable stars.

Historically, the OGLE project has been divided into four phases. The initial phase of the survey (OGLE-I; Udalski *et al.*, 1992) was carried out from 1992 to 1995, using the 1-meter Swope telescope at Las Campanas Observatory in Chile. In 1996, a dedicated 1.3-meter Warsaw Telescope was constructed at the same observatory, marking the beginning of the second phase of the OGLE project (OGLE-II; Udalski *et al.*, 1997). The next milestone occurred in 2001,

Table 1. Four phases of the OGLE project

| Phase of the project | Camera size [pixels] | Observed area [deg ²] | Number of stars [$\times 10^6$] | Data flow [TB/year] | Main targets |
|----------------------|----------------------|-----------------------------------|-----------------------------------|---------------------|--|
| OGLE-I (1992–1995) | 4M | 1.5 | 6 | 0.09 | Galactic bulge |
| OGLE-II (1997–2000) | 4M | 27 | 44 | 0.4 | Galactic bulge Magellanic Clouds |
| OGLE-III (2001–2009) | 64M | 170 | 389 | 3.8 | Galactic bulge Magellanic Clouds |
| OGLE-IV (2010–now) | 256M | 3600 | 2000 | 40 | Galactic bulge Galactic disk Magellanic Clouds |

when the Warsaw Telescope was equipped with an 8-chip mosaic CCD camera, which initiated the OGLE-III project (Udalski, 2003). Finally, in 2010, Andrzej Udalski, the leader of the OGLE project, designed and constructed a camera consisting of 32 CCD chips. Since then, the fourth phase of the OGLE project (OGLE-IV; Udalski *et al.*, 2015) has been conducted. Tab. 1 shows the progress that has been made between the successive phases of the OGLE project. The initiation of each new stage of the survey was associated with a tenfold enhancement of its observational capabilities. Over the past three decades, the number of monitored stars, the volume of collected data, and the area of the surveyed sky have been expanded by three orders of magnitude. Currently, OGLE ranks among the world’s largest sky surveys dedicated to the exploration of celestial variability.

The OGLE-IV project monitors approximately two billion point sources across an area of about 3600 square degrees, encompassing the most densely populated stellar regions of the southern sky, including the central regions of the Milky Way, the Galactic disk, and the Large and Small Magellanic Clouds (LMC and SMC). The OGLE database presently contains approximately $1.2 \cdot 10^{12}$ individual photometric measurements, making it one of the largest photometric database in the history of astronomy. This huge dataset has served as the basis for numerous pioneering discoveries, some of which will be discussed in the following sections of this proceedings contribution.

2. Dark matter

The primary goal of the OGLE survey was to detect gravitational microlensing events in order to validate the hypothesis that dark matter is composed of

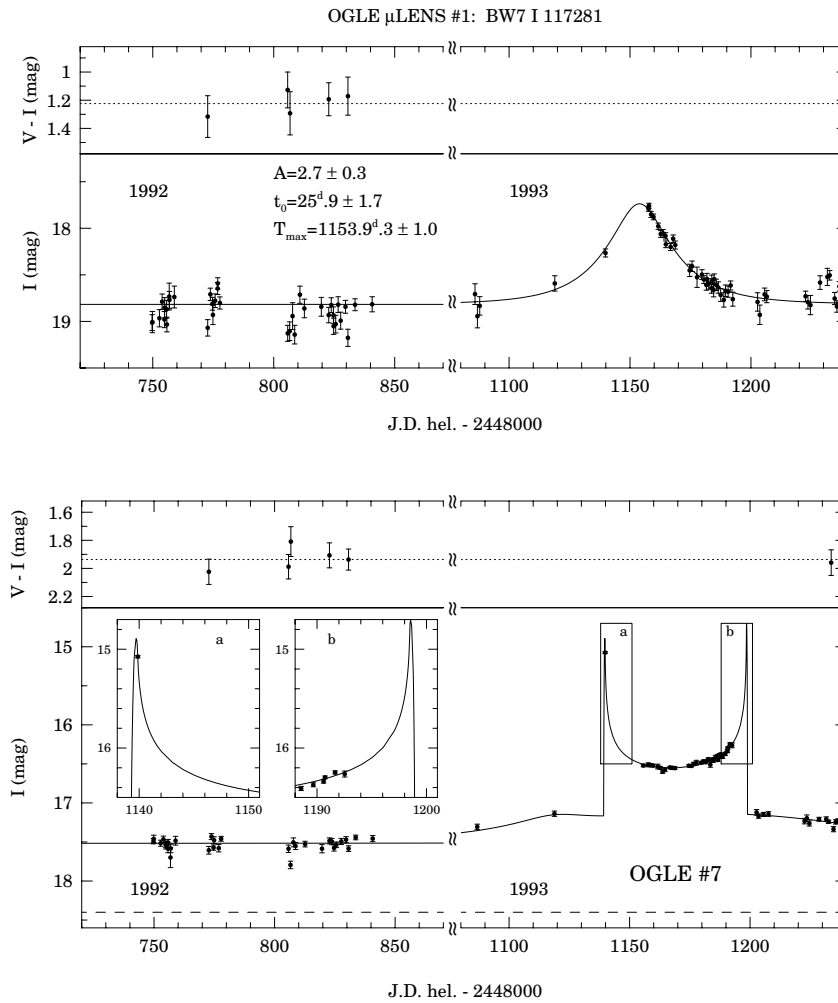


Figure 1. Upper panel: light curve of the first microlensing event detected by OGLE (Udalski *et al.*, 1993). Lower panel: light curve the first known binary microlensing event (Udalski *et al.*, 1994).

MASSIVE Compact Halo Objects (MACHOs). This term refers to hypothetical non-emitting or extremely faint objects, such as primordial black holes, brown dwarfs, or even free-floating planets, located in galactic halos and contributing to the observed mass of galaxies. A gravitational microlensing event occurs when the light of a background source star is temporarily magnified due to its alignment with a foreground lens object (Einstein 1936). When Paczyński

(1986) proposed using this phenomenon to assess the contribution of MACHOs to dark matter, not a single microlensing event had been observed until then.

The OGLE team announced the discovery of its first microlensing event in September 1993 (Udalski *et al.*, 1993), almost simultaneously with the first-ever gravitational microlens toward the LMC recorded by the MACHO group (Alcock *et al.*, 1993). The upper panel of Fig. 1 displays the light curve of the OGLE's microlensing event number 1. Today, such characteristic light curves are commonly referred to as Paczyński curves. The first OGLE microlensing event was found toward the center of the Milky Way. Currently, the OGLE project routinely detects between 1000 and 2000 gravitational microlensing events per year (depending on the adopted observational strategy), and the overwhelming majority of the lensed stars also reside in the Galactic bulge.

The limited number of gravitational microlensing events detected by OGLE in the direction of the Magellanic Clouds imposes strong constraints on possible explanations for the nature of dark matter. Wyrzykowski *et al.* (2011) analyzed 13 years of the OGLE-II and OGLE-III observations of the LMC and SMC and found only eight candidates for microlensing events, which demonstrated that MACHOs with masses in the range $10^{-2} M_{\odot} \lesssim M \lesssim 1 M_{\odot}$ cannot constitute more than 10% of dark matter. Much stronger limits have recently been obtained by Mróz *et al.* (2023, in preparation) based on the analysis of light curves of over 78 million stars in the LMC monitored for 20 years by the OGLE-III and OGLE-IV surveys. It was found that MACHOs in the mass range $1.8 \cdot 10^{-4} M_{\odot} \lesssim M \lesssim 6.3 M_{\odot}$ cannot contribute more than 1% to the dark matter in the Galactic halo, while MACHOs with masses in the range of $1.3 \cdot 10^{-5} M_{\odot} \lesssim M \lesssim 860 M_{\odot}$ cannot compose more than 10% of dark matter. In fact, all thirteen microlensing events detected by Mróz *et al.* (2023) in the direction of the LMC can be explained by astrophysical objects located in the LMC itself or in the Milky Way disk.

3. Exoplanets

The significance of the OGLE's contribution to exoplanetary research cannot be overestimated. The OGLE observations have been used to the first successful applications of two new techniques for detecting extrasolar planets: gravitational microlensing and transit methods.

Mao & Paczyński (1991) originally proposed the idea that binary stars and planetary systems could be detected through the microlensing phenomena. Binary lenses may produce significantly different light curves than the Paczyński curve, and this effect can be easily detectable even if the companion is a planet. This characteristic is the foundation of the microlensing technique for identifying planetary systems.

In 1994, the OGLE group discovered the first-ever binary microlensing event (Udalski *et al.*, 1994; the lower panel of Fig. 1). This was an important step to-

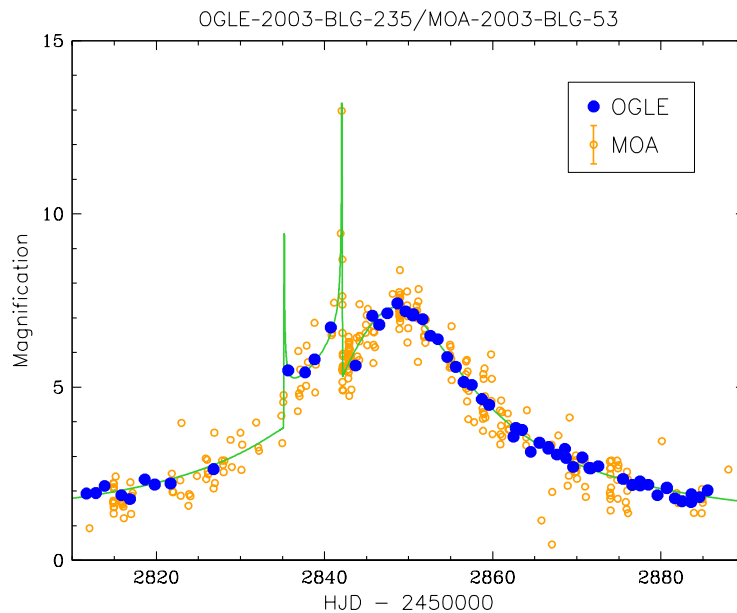


Figure 2. Light curve of OGLE 2003-BLG-235/MOA 2003-BLG-53 – the first planetary microlensing event (Bond *et al.* 2004). The OGLE and MOA measurements are shown as blue and yellow symbols, respectively.

ward detecting the microlensing exoplanets. OGLE-2003-BLG-235/MOA-2003-BLG-53 was the first gravitational microlensing event that yielded a definitive planet identification (Bond *et al.* 2004). This breakthrough discovery was possible thanks to the collaboration between the OGLE survey and the Microlensing Observations in Astrophysics (MOA) project. Fig. 2 presents the light curve of this microlensing event, where the characteristic shape of the Paczyński curve is distorted by an anomaly attributed by the presence of a Jupiter-like planet. Since then, OGLE has participated in the discovery of over a hundred microlensing exoplanets, including the first known cold super-Earth, a scaled analog of the Solar System, planets orbiting brown dwarfs, and planets in binary star systems.

Gravitational microlensing is an effective method for detecting free-floating planets, i.e. worlds that have been ejected from their parent planetary systems and are no longer gravitationally bound to any star. Microlensing events caused by Jupiter-mass planets typically last from 1 to 2 days, whereas Earth-mass lenses last merely a few hours. An in-depth analysis of the OGLE photometric database conducted by Mróz *et al.* (2017) unveiled a notable surplus of very short microlensing events, indicating the presence of a substantial population of Earth-to-Neptune-mass planets that appear to have no host stars. Mróz *et*

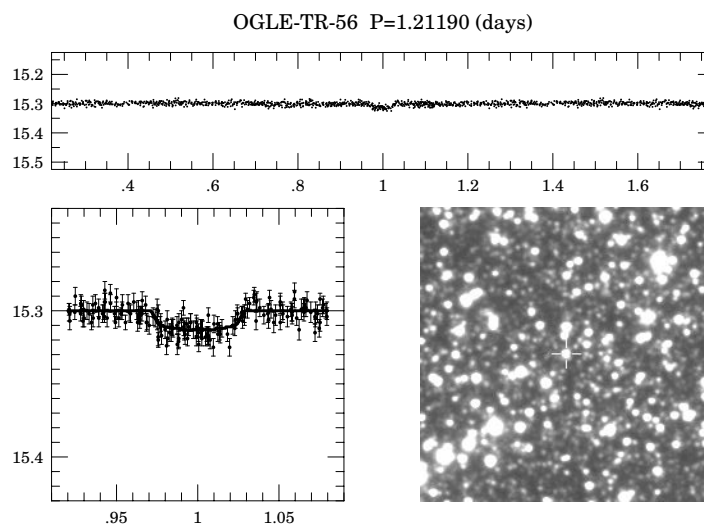


Figure 3. Light curve and finding chart of OGLE-TR-56 – the first exoplanet discovered with the transit method.

al. (2017) estimated that free-floating planets far outnumber stars in the Milky Way.

Finally, the OGLE survey pioneered another technique of detecting extrasolar planets: the transit method. In 2002, the OGLE team published its first list of candidates for planetary transits (Udalski *et al.*, 2002). It was the result of a special observing campaign conducted at the onset of the OGLE-III project. At that time, only one transiting exoplanet was known – HD 209458 b (Charbonneau *et al.*, 2000; Henry *et al.*, 2000) – but this object had been discovered using the spectroscopic method, while the observations of its transits followed afterward.

OGLE-TR-56 b was the first spectroscopically confirmed exoplanet discovered with the transit method (Konacki *et al.*, 2003). Fig. 3 displays the light curve of this system folded with its orbital period of 1.2119 days. In the next several years, seven more OGLE planets were positively verified through spectroscopy. At that time, HD 209458 b and the OGLE planets were the only known transiting planets. Then, dedicated wide-field sky surveys, such as WASP, HAT, and TrES, began to discover transiting planets around much brighter stars, which led to the discontinuation of the OGLE's observing campaigns aimed at searching for transiting planet candidates.

Table 2. OGLE Collection of Variable Stars

| Type of variable stars | Number of stars |
|--------------------------|------------------|
| Classical Cepheids | 11 707 |
| Type II Cepheids | 2 010 |
| Anomalous Cepheids | 390 |
| RR Lyrae stars | 128 472 |
| δ Scuti stars | 42 672 |
| Long-Period Variables | 403 636 |
| Eclipsing binaries | 510 782 |
| Dwarf novae | 1 091 |
| R Coronae Borealis stars | 23 |
| TOTAL | 1 100 783 |

4. The OGLE Collection of Variable Stars

The light curves of two billion sources observed for decades by the OGLE survey constitute an ideal dataset for detecting and studying variable stars of all types. The OGLE Collection of Variable Stars (OCVS) is a continuously growing catalog of variable stars identified in the OGLE database. Tab. 2 shows a list of different types of variables included in the already published parts of the OCVS. At present, the OGLE catalog contains over 1.1 million variable stars in the Milky Way and Magellanic Clouds. The OCVS is accessible through the WWW and FTP sites:

*<https://ogle.astrouw.edu.pl> → OGLE Collection of Variable Stars
<https://www.astrouw.edu.pl/ogle/ogle4/OCVS/>*

The catalog data include observational parameters of the variable stars, such as coordinates, periods, mean magnitudes, amplitudes, etc. Additionally, time-series OGLE photometry in the I and V bands is made available to the astronomical community.

It is worth emphasizing that the OCVS is characterized by exceptionally high levels of completeness and purity because we still employ the traditional method of variable star classification, namely, the visual inspection of their light curves. Each of the over one million variables included in the OCVS has been carefully reviewed by experienced astronomers. This rigorous procedure has not only resulted in an extraordinarily low contamination rate of our collection but has also led to the discovery of new types of variable stars (see Section 6). Therefore, the OGLE catalog is widely used as a training set for machine learning variable star classification algorithms.

5. Classical Cepheids

Due to the limited space of this contribution, I cannot present the full variety of studies on different types of variable stars included in the OCVS. Therefore, for illustrative purposes, I will concentrate on the latest investigations related to only one type of pulsating stars – classical Cepheids – which are relatively young ($\lesssim 400$ My) and luminous (10^2 – $10^5 L_{\odot}$) standard candles, 4–20 times more massive than the Sun. Classical Cepheids play a key role as primary distance indicators thanks to the famous relationship between their pulsation periods and intrinsic luminosities, the period–luminosity relation.

Most of the Cepheid pulsators in the Magellanic Clouds (Soszyński *et al.*, 2017), and approximately half of the classical Cepheids currently known in the Milky Way (Pietrukowicz *et al.*, 2021), were identified in the OGLE photometric databases. At present, the OGLE collection comprises a virtually complete census of Cepheids in the LMC and SMC, thus our group concluded the task of cataloging these variable stars initiated by Henrietta Leavitt in the early 20th century.

The OCVS contains 4713 and 4954 classical Cepheids in the LMC and SMC, respectively. These are the largest known samples of such variables detected in any galaxy, including the Milky Way, so classical Cepheids in the Magellanic Clouds have been the subject of extensive studies in recent decades. These two satellite galaxies are close enough to us that individual stars are easily distinguishable for ground-based telescopes, but they are far enough that their stellar populations can be considered to be located at the same distance from us. Moreover, the distance to the LMC is known with unprecedented accuracy of about 1% (Pietrzyński *et al.*, 2019). Consequently, the Magellanic Clouds, particularly the LMC, serve as anchors for the cosmic distance scale.

Fig. 4 shows the period–Wesenheit index¹ diagram for classical Cepheids in the LMC. The four ridges visible in this diagram are attributed to the stellar pulsations in the fundamental, first-, second-, and third-overtone modes. Cepheids in the Magellanic Clouds play a crucial role in the calibration of the period–luminosity, period–luminosity–color and period–Wesenheit index relations across a wide range of wavelengths, spanning from optical to mid-infrared domains (e.g., Macri *et al.*, 2015; Riess *et al.*, 2019; Chown *et al.*, 2021). In addition, a thorough exploration of the non-linearities of the period–luminosity relations (e.g., García-Varela *et al.*, 2013; Bhardwaj *et al.*, 2016) and the correlation of the zero-points of these relations with the metallicity of Cepheids (e.g., Wielgórski *et al.*, 2017; Gieren *et al.*, 2018; Breuval *et al.*, 2022) has been conducted to assess their influence on the cosmic distance scale, particularly in the context of the Hubble constant measurements.

¹The Wesenheit index is an extinction-free quantity, defined as $W_I = I - 1.55(V - I)$, where I and V are apparent mean magnitudes of the stars.

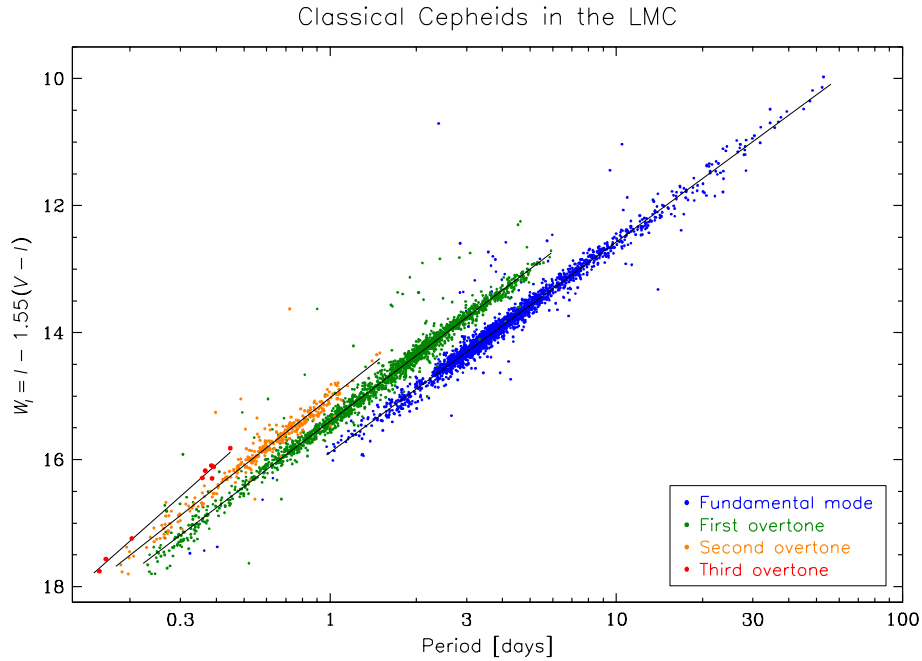


Figure 4. Period–Wesenheit index diagram for classical Cepheids in the LMC. Blue, green, orange, and red dots mark the fundamental, first-, second-, and third-overtone pulsation modes, respectively.

The complete samples of classical Cepheids have been employed to investigate the three-dimensional geometry of the LMC and SMC (e.g. Jacyszyn-Dobrzniecka *et al.*, 2016; Ripepi *et al.*, 2022). These studies are vital for gaining insights into past interactions between the Magellanic Clouds and between the Magellanic System and the Milky Way.

An analogous analysis of the structure of the Milky Way’s disk was performed by Skowron *et al.* (2019) using the sample of about 2500 Galactic classical Cepheids, significantly expanded thanks to the observations carried out by the OGLE survey (Udalski *et al.*, 2018). In particular, OGLE was the first survey that identified a significant number of Cepheids in the outskirts of the Milky Way, which was used to construct of a three-dimensional map of the Galactic disk. This map unambiguously revealed that the disk is not flat but exhibits a warp, beginning at galactocentric distances of about than 8 kpc, and extending to the edge of the Milky Way, approximately 20 kpc from the center. Moreover, the spatial distribution of Cepheids was utilized to assess the disk’s flaring, its scale height, and pinpoint the Sun’s location within the disk. Additionally, the relationship between periods and ages for classical Cepheids was employed to

obtain an age tomography of the young stellar population in the Milky Way. Finally, this analysis was supplemented by Mróz *et al.* (2019) who used the OGLE Cepheids with their proper motions and radial velocities from the Gaia database to construct the most precise rotation curve for the outer regions of our Galaxy.

6. New types of variable stars

The huge OGLE photometric database contains light curves of variable stars belonging to all categories, including types that have remained entirely unknown. Thanks to our individualized approach to the analysis of observational data, the OGLE team discovered several new classes and subclasses of variable stars, for example the so-called peculiar W Virginis stars (Soszyński *et al.*, 2008), anomalous double-mode RR Lyrae stars (Soszyński *et al.*, 2016), type II Cepheids pulsating in the first overtone (Soszyński *et al.*, 2019), and the first known multimode anomalous Cepheid (Soszyński *et al.*, 2020).

A completely new class of pulsating stars was extracted from the OGLE database by Pietrukowicz *et al.* (2017). These stars, known as Blue Large Amplitude Pulsators (BLAPs), are hot subdwarfs with temperatures around 30 000 K, pulsating in the fundamental mode with periods ranging from 3 to 75 minutes. The light curves of BLAPs (Fig. 5) resemble those of Cepheids or RR Lyrae stars. The uniqueness of BLAPs lies in the fact that they are the only known type of fundamental-mode pulsating stars situated on the blue side of the Hertzsprung-Russell diagram. Recently, the total number of known BLAPs has been significantly increased, reaching 80 objects at present (Borowicz *et al.*, 2023). However, the evolutionary status of these stars still remains a mystery.

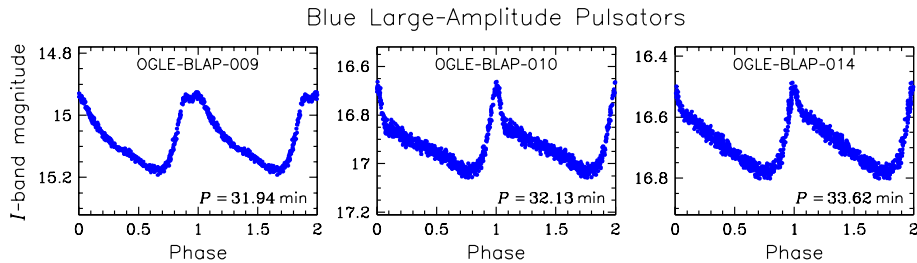


Figure 5. *I*-band light curves of three example Blue Large Amplitude Pulsators (Pietrukowicz *et al.*, 2017).

Another new type of pulsating stars was discovered in the OGLE database by chance. OGLE-BLG-RRLYR-02792, as its name suggests, was initially classified in the OCVS as an RR Lyrae star due to its short period ($P \approx 0.6275$ days) and characteristic light curve morphology (Fig. 6). This pulsating star stood out as

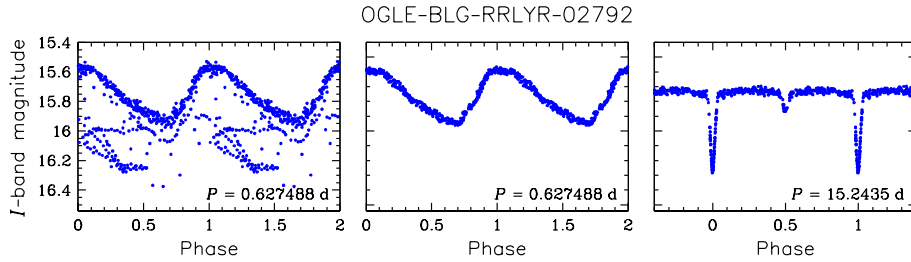


Figure 6. Light curves of the Binary Evolution Pulsator OGLE-BLG-RRLYR-02792 (Pietrzyński *et al.*, 2012). The left panel displays the original light curve folded with the pulsation periods, while the middle and right panels show the disentangled pulsation and eclipsing light curves of the same object.

it is a component of an eclipsing binary system, providing an opportunity for the first direct determination of the RR Lyrae’s mass. Pietrzyński *et al.* (2012) obtained highly precise spectroscopic observations for this system and measured the mass of the pulsating component, which turned out to be surprisingly small – only $0.26 M_{\odot}$. Such low mass indicates that OGLE-BLG-RRLYR-02792 is not an RR Lyrae variable but rather a representative of a new category of pulsating stars that mimic RR Lyrae stars. Because these stars pulsate as a consequence of their evolution in binary systems, they have been named Binary Evolution Pulsators.

7. V1309 Scorpii – a “Rosetta stone” for stellar mergers

V1309 Scorpii (Nova Scorpii 2008) was discovered in September 2008 when it underwent an outburst, increasing its brightness by about 10 mag. This event represented a rare case of a so-called “red nova” – a class of variable stars for which there was no definitive explanation at that time. Fortunately, V1309 Scorpii had been observed by the OGLE-III project for seven years prior to the eruption. Using the OGLE time-series photometry, Tylenda *et al.* (2011) demonstrated that the progenitor of V1309 Sco was a contact binary with an orbital period decreasing at an accelerating rate.

Fig. 7 displays the light curve of V1309 Scorpii, obtained within 20 years of the OGLE monitoring. After the outburst, there are no signs of binarity, proving that Nova Scorpii 2008 and, consequently, other red novae were stellar-merger events. Because of the pivotal role played by V1309 Scorpii in clarifying the process of star mergers, this object has been dubbed a “Rosetta stone” for the interpretation of red novae.

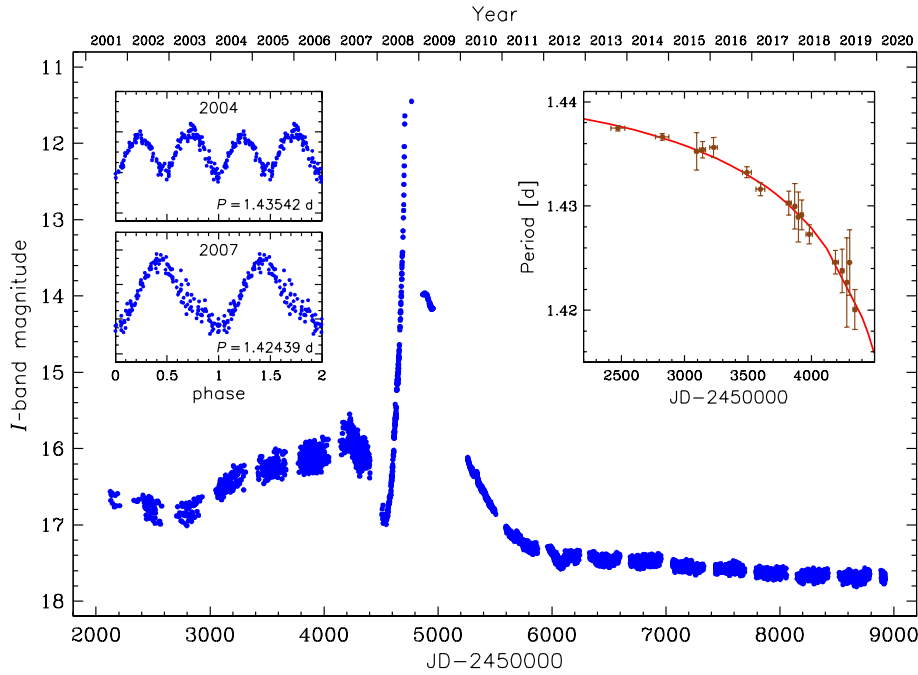


Figure 7. OGLE light curve of V1309 Scorpii (Tyłenda *et al.*, 2011). The insets on the left side display detrended and phased light curves observed four years and one year prior to the outburst, respectively. The inset on the right side shows the evolution of the orbital period of the V1309 Scorpii progenitor.

8. Summary

In this proceeding, I have presented a subjective overview of the most fascinating achievements of the OGLE project. I have outlined OGLE's research in the area of gravitational microlensing, dark matter, extrasolar planets, variable stars, and the structure of galaxies. Nevertheless, over the last three decades, the OGLE survey has made a substantial contribution to many other fields of astrophysics. OGLE observations have been widely used to establish cosmic distance scale, analyze star clusters, investigate both old and young stellar populations, identify unique modes of stellar oscillations, and produce maps of interstellar extinction. The OGLE team has been involved in the discovery of free-floating black holes, thousands of novae and supernovae, hundreds of quasars, Cepheids in eclipsing binary systems, as well as transneptunian objects in the Solar System.

Acknowledgements. This work has been funded by the National Science Centre, Poland, grant no. 2022/45/B/ST9/00243. For the purpose of Open Access, the author

has applied a CC-BY public copyright license to any Author Accepted Manuscript (AAM) version arising from this submission.

References

- Alcock, C., Akerlof, C.W., Allsman, R.A., Axelrod, T.S., Bennett, D.P., Chan, S., Cook, K.H., Freeman, K.C., Griest, K., Marshall, S.L., Park, H.-S., Perlmutter, S., Peterson, B.A., Pratt, M.R., Quinn, P.J., Rodgers, A.W., Stubbs, C.W., Sutherland, W.: 1993, *Nature* **365**, 621, DOI: 10.1038/365621a0
- Bhardwaj, A., Kanbur, S.M., Macri, L.M., Singh, H.P., Ngeow, C.-C., Ishida, E.E.O.: 2016, *Monthly Notices of the RAS* **457**, 1644, DOI: 10.1093/mnras/stw040
- Bond, I.A., Udalski, A., Jaroszyński, M., Rattenbury, N.J., Paczyński, B., Soszyński, I., Wyrzykowski, L., Szymański, M.K., Kubiak, M., Szewczyk, O., Żebruń, K., Pietrzyński, G., Abe, F., Bennett, D.P., Eguchi, S., Furuta, Y., Hearnshaw, J.B., Kamiya, K., Kilmartin, P.M., Kurata, Y., Masuda, K., Matsubara, Y., Muraki, Y., Noda, S., Okajima, K., Sako, T., Sekiguchi, T., Sullivan, D.J., Sumi, T., Tristram, P.J., Yanagisawa, T., Yock, P.C.M.: 2004, *Astrophysical Journal, Letters* **606**, L155, DOI: 10.1086/420928
- Borowicz, J., Pietrukowicz, P., Mróz, P., Soszyński, I., Udalski, A., Szymański, M.K., Ulaczyk, K., Poleski, R., Kozłowski, S., Skowron, J., Skowron, D.M., Rybicki, K., Iwanek, P., Wrona, M., Gromadzki, M.: 2023, *Acta Astron.* **73**, 1, DOI: 10.32023/0001-5237/73.1.1
- Breival, L., Riess, A.G., Kervella, P., Anderson, R.I., Romaniello, M.: 2022, *Astrophysical Journal* **939**, 89, DOI: 10.3847/1538-4357/ac97e2
- Charbonneau, D., Brown, T.M., Latham, D.W., Mayor, M.: 2000, *Astrophysical Journal, Letters* **529**, L45, DOI: 10.1086/312457
- Chown, A.H., Scowcroft, V., Wuyts, S.: 2021, *Monthly Notices of the RAS* **500**, 817, DOI: 10.1093/mnras/staa3186
- Einstein, A.: 1936, *Science* **84**, 506, DOI: 10.1126/science.84.2188.506
- García-Varela, A., Sabogal, B.E., Ramírez-Tannus, M.C.: 2013, *Monthly Notices of the RAS* **431**, 2278, DOI: 10.1093/mnras/stt325
- Gieren, W., Storm, J., Konorski, P., Górski, M., Pilecki, B., Thompson, I., Pietrzyński, G., Graczyk, D., Barnes, T.G., Fouqué, P., Nardetto, N., Gallenne, A., Karczmarek, P., Suchomska, K., Wielgórski, P., Taormina, M., Zgirski, B.: 2018, *Astronomy and Astrophysics* **620**, A99, DOI: 10.1051/0004-6361/201833263
- Henry, G.W., Marcy, G.W., Butler, R.P., Vogt, S.S.: 2000, *Astrophysical Journal, Letters* **529**, L41, DOI: 10.1086/312458
- Jacyszyn-Dobrzeńska, A.M., Skowron, D.M., Mróz, P., Skowron, J., Soszyński, I., Udalski, A., Pietrukowicz, P., Kozłowski, S., Wyrzykowski, L., Poleski, R., Pawlak, M., Szymański, M.K., Ulaczyk, K.: 2016, *Acta Astron.* **66**, 149, DOI: 10.48550/arXiv.1602.09141
- Konacki, M., Torres, G., Jha, S., Sasselov, D.D.: 2003, *Nature* **421**, 507, DOI: 10.1038/nature01379

- Macri, L.M., Ngeow, C.-C., Kanbur, S.M., Mahzooni, S., Smitka, M.T.: 2015, *Astronomical Journal* **149**, 117, DOI: 10.1088/0004-6256/149/4/117
- Mao, S., Paczyński, B.: 1991, *Astrophysical Journal, Letters* **374**, L37, DOI: 10.1086/186066
- Mróz, P., Udalski, A., Skowron, J., Poleski, R., Kozłowski, S., Szymański, M.K., Soszyński, I., Wyrzykowski, L., Pietrukowicz, P., Ulaczyk, K., Skowron, D., Pawlak, M.: 2017, *Nature* **548**, 183, DOI: 10.1038/nature23276
- Mróz, P., Udalski, A., Skowron, D.M., Skowron, J., Soszyński, I., Pietrukowicz, P., Szymański, M.K., Poleski, R., Kozłowski, S., Ulaczyk, K.: 2019, *Astrophysical Journal, Letters* **870**, L10, DOI: 10.3847/2041-8213/aaf73f
- Paczyński, B.: 1986, *Astrophysical Journal* **304**, 1, DOI: 10.1086/164140
- Pietrukowicz, P., Dziembowski, W.A., Latour, M., Angeloni, R., Poleski, R., di Mille, F., Soszyński, I., Udalski, A., Szymański, M.K., Wyrzykowski, L., Kozłowski, S., Skowron, J., Skowron, D., Mróz, P., Pawlak, M., Ulaczyk, K.: 2017, *Nature Astronomy* **1**, 0166, DOI: 10.1038/s41550-017-0166
- Pietrukowicz, P., Soszyński, I., Udalski, A.: 2021, *Acta Astron.* **71**, 205, DOI: 10.32023/0001-5237/71.3.2
- Pietrzyński, G., Thompson, I.B., Gieren, W., Graczyk, D., Stępień, K., Bono, G., Moroni, P.G.P., Pilecki, B., Udalski, A., Soszyński, I., Preston, G.W., Nardetto, N., McWilliam, A., Roederer, I.U., Górski, M., Konorski, P., Storm, J.: 2012, *Nature* **484**, 75, DOI: 10.1038/nature10966
- Pietrzyński, G., Graczyk, D., Gallenne, A., Gieren, W., Thompson, I. B., Pilecki, B., Karczmarek, P., Górski, M., Suchomska, K., Taormina, M., Zgirski, B., Wielgórski, P., Kołaczkowski, Z., Konorski, P., Villanova, S., Nardetto, N., Kervella, P., Bresolin, F., Kudritzki, R. P., Storm, J., Smolec, R., Narloch, W.: 2019, *Nature* **567**, 200, DOI: 10.1038/s41586-019-0999-4
- Riess, A.G., Casertano, S., Yuan, W., Macri, L.M., Scolnic, D.: 2019, *Astrophysical Journal* **876**, 85, DOI: 10.3847/1538-4357/ab1422
- Ripepi, V., Chemin, L., Molinaro, R., Cioni, M.-R.L., Bekki, K., Clementini, G., de Grijs, R., De Somma, G., El Youssoufi, D., Girardi, L., Groenewegen, M.A.T., Ivanov, V., Marconi, M., McMillan, P.J., van Loon, J.T.: 2022, *Monthly Notices of the RAS* **512**, 563, DOI: 10.1093/mnras/stac595
- Skowron, D.M., Skowron, J., Mróz, P., Udalski, A., Pietrukowicz, P., Soszyński, I., Szymański, M.K., Poleski, R., Kozłowski, S., Ulaczyk, K., Rybicki, K., Iwanek, P.: 2019, *Science* **365**, 478, DOI: 10.1126/science.aau3181
- Soszyński, I., Udalski, A., Szymański, M.K., Kubiak, M., Pietrzyński, G., Wyrzykowski, L., Szewczyk, O., Ulaczyk, K., Poleski, R.: 2008, *Acta Astron.* **58**, 293
- Soszyński, I., Smolec, R., Dziembowski, W.A., Udalski, A., Szymański, M.K., Wyrzykowski, L., Ulaczyk, K., Poleski, R., Pietrukowicz, P., Kozłowski, S., Skowron, D., Skowron, J., Mróz, P., Pawlak, M.: 2016, *Monthly Notices of the RAS* **463**, 1332, DOI: 10.1093/mnras/stw1933

- Soszyński, I., Udalski, A., Szymański, M.K., Wyrzykowski, L., Ulaczyk, K., Poleski, R., Pietrukowicz, P., Kozłowski, S., Skowron, D.M., Skowron, J., Mróz, P., Pawlak, M.: 2017, *Acta Astron.* **67**, 103, DOI: 10.32023/0001-5237/67.2.1
- Soszyński, I., Smolec, R., Udalski, A., Pietrukowicz, P.: 2019, *Astrophysical Journal* **873**, 43, DOI: 10.3847/1538-4357/ab04ab
- Soszyński, I., Smolec, R., Udalski, A., Szymański, M.K., Pietrukowicz, P., Skowron, D.M., Skowron, J., Mróz, P., Poleski, R., Kozłowski, S., Iwanek, P., Wrona, M., Gromadzki, M., Ulaczyk, K., Rybicki, K.: 2020, *Astrophysical Journal, Letters* **901**, L25, DOI: 10.3847/2041-8213/abb817
- Tylenda, R., Hajduk, M., Kamiński, T., Udalski, A., Soszyński, I., Szymański, M.K., Kubiak, M., Pietrzyński, G., Poleski, R., Wyrzykowski, L., Ulaczyk, K.: 2011, *Astronomy and Astrophysics* **528**, A114, DOI: 10.1051/0004-6361/201016221
- Udalski, A., Szymański, M., Kałużny, J., Kubiak, M., Mateo, M.: 1992, *Acta Astron.* **42**, 253
- Udalski, A., Szymański, M., Kałużny, J., Kubiak, M., Krzemiński, W., Mateo, M., Preston, G.W., Paczyński, B.: 1993, *Acta Astron.* **43**, 289
- Udalski, A., Szymański, M., Mao, S., Di Stefano, R., Kałużny, J., Kubiak, M., Mateo, M., Krzemiński, W.: 1994, *Astrophysical Journal, Letters* **436**, L103, DOI: 10.1086/187643
- Udalski, A., Kubiak, M., Szymański, M.: 1997, *Acta Astron.* **47**, 319
- Udalski, A., Paczyński, B., Żebruń, K., Szymański, M., Kubiak, M., Soszyński, I., Szewczyk, O., Wyrzykowski, L., Pietrzyński, G.: 2002, *Acta Astron.* **52**, 1
- Udalski, A.: 2003, *Acta Astron.* **53**, 291
- Udalski, A., Szymański, M.K., Szymański, G.: 2015, *Acta Astron.* **65**, 1
- Udalski, A., Soszyński, I., Pietrukowicz, P., Szymański, M.K., Skowron, D.M., Skowron, J., Mróz, P., Poleski, R., Kozłowski, S., Ulaczyk, K., Rybicki, K., Iwanek, P., Wrona, M.: 2018, *Acta Astron.* **68**, 315, DOI: 10.32023/0001-5237/68.4.1
- Wielgórski, P., Pietrzyński, G., Gieren, W., Górski, M., Kudritzki, R.-P., Zgirski, B., Bresolin, F., Storm, J., Matsunaga, N., Graczyk, D., Soszyński, I.: 2017, *Astrophysical Journal* **842**, 116, DOI: 10.3847/1538-4357/aa7565
- Wyrzykowski, L., Skowron, J., Kozłowski, S., Udalski, A., Szymański, M.K., Kubiak, M., Pietrzyński, G., Soszyński, I., Szewczyk, O., Ulaczyk, K., Poleski, R., Tisserand, P.: 2011, *Monthly Notices of the RAS* **416**, 2949, DOI: 10.1111/j.1365-2966.2011.19243.x

Discovery of star systems at the merger limit by large astronomical surveys

P.-E. Christopoulou¹ , E. Lalounta¹, A. Papageorgiou¹,
C.E. Ferreira Lopes², M. Catelan^{3,4,5} and A.J. Drake⁶

¹ *Department of Physics, University of Patras, 26500, Patra, Greece,
(E-mail: pechris@upatras.gr)*

² *Instituto de Astronomía y Ciencias Planetarias, Universidad de Atacama,
Copayapu 485, Copiapó, Chile*

³ *Instituto de Astrofísica, Facultad de Física, Pontificia Universidad Católica
de Chile, Av. Vicuña Mackenna 4860, 7820436 Macul, Santiago, Chile*

⁴ *Millennium Institute of Astrophysics, Nuncio Monseñor Sotero Sanz 100,
Of. 104, 7500000 Providencia, Santiago, Chile*

⁵ *Centro de Astroingeniería, Facultad de Física, Pontificia Universidad
Católica de Chile, Av. Vicuña Mackenna 4860, 7820436 Macul, Santiago,
Chile*

⁶ *California Institute of Technology, 1200 East California Boulevard,
Pasadena, CA 91225, USA*

Received: November 9, 2023; Accepted: December 12, 2023

Abstract. This study presents the identification and the best photometric solution of 92 low mass ratio (LMR) totally eclipsing contact binaries in Catalina Sky Survey data, among which 37 are new discoveries, six are candidates for mergers, and a unique ultra-short period LMR.

Key words: contact binaries- eclipsing binaries – fundamental parameters– data analysis

1. Introduction

A low mass ratio contact binary (LMRCB) is a type of binary star system where the two stars have a significant difference in mass. They are believed to exhibit a low mass ratio cut-off and will merge into fast-rotating single stars due to Darwin’s instability (Darwin & Glaisher, 1879). The research on LMRCBs is essential to our understanding of the merging process and the theoretical low mass ratio limit that is still debated around 0.070.1 (Rasio, 1995; Arbutina, 2009). Recently Pešta & Pejcha (2023) found a dependence of the minimum mass ratio on the structure of the components. The confirmation by Tylenda et al. (2011) that Nova 2008 Sco (V1390 Sco) is a red nova formed by the merger of eclipsing cool contact binary components has also increased interest in the

different ways leading to stellar mergers. Although the observed period of the premerger of V1309 Sco was long for the observed population of contact binaries (1.4 days), and the primary was more evolved in the suggested model of [Stępień \(2011\)](#), the low mass ratio (0.1-0.15) of the progenitor triggered the investigation of the orbital stability of LMRCBs in search of pre-mergers.

To study LMRCBs at the merger limit, large astronomical surveys such as ASAS-SN (in the V filter; [Shappee et al., 2014](#); [Jayasinghe et al., 2018](#)), Catalina Sky Surveys (CSS; [Drake et al., 2014b](#)), Zwicky Transient Facility (ZTF¹, in g and r ; [Masci et al., 2019](#)), and the Asteroid Terrestrial-impact Last Alert System (ATLAS², o and c bands; [Heinze et al., 2018](#)) play a crucial role as they discover a large number of contact binaries. Although without spectroscopy the automated methods of classification can result in erroneous samples, we can take advantage of the totality in eclipses to search for the most reliable mass ratio ([Terrell & Wilson, 2005](#); [Hambálek & Pribulla, 2013](#))

1.1. Methodology

The sample used focuses on the initial sample of 30 743 eclipsing binaries ([Drake et al., 2014a](#)), classified as eclipsing contact binaries from the Catalina Real-Time Survey Data Release 2 (CRTS DR2), and includes observations from 2004-2013. The data was obtained unfiltered to maximize throughput and transformed to an approximate V magnitude. After excluding systems with less than 150 observations and periods longer than 0.8 days, we removed outliers and poor measurements, cleaned the light curves (LCs), and determined the initial epoch values. LMRCBs with total eclipses have LCs with flat bottoms of long duration, unlike common contact systems. We compiled LCs from 42 well-studied LMRCBs based on mass ratios, eclipse totality, and V -band LC availability and performed a high order (20 terms) Fourier decomposition (FD) of the phase-folded, normalized flux LCs of both samples. The performance of FD of the phase-folded, normalized flux LCs of both samples revealed that higher order coefficients can separate LMRCBs from the common contact systems. After visually examining 2100 discoveries, we recognized 92 LMRCBs, including 37 that are newly identified (the remaining 55 systems are common to [Sun et al. \(2020\)](#)).

In addition, new multicolor photometric observations for three of them (CSS J210228.3-031048, CSS J231513.3+34533, and CRTS J163819.6+03485) were carried out using the Ritchey-Chrétien 2.3 m Aristarchos telescope at Helmos Observatory, Greece in 2018-2021.

¹<https://irsa.ipac.caltech.edu/>

²<https://atlas.fallingstar.com/>

2. Light-curve modeling and results

The photometric properties of the binaries were analyzed by light curve modeling with PHOEBE-0.31a scripter (Prsa & Zwitter, 2005; Papageorgiou et al., 2019), to explore the parameter space through a detailed scan in the mass ratio–inclination plane, using also in some cases the PIKAIA ³ genetic algorithm optimizer. The uncertainties in the derived physical parameters were estimated by performing Monte Carlo simulations (Papageorgiou & Christopoulou, 2015; Papageorgiou et al., 2023). In the absence of spectroscopic data, given the photometric mass ratio of contact binaries with total eclipses, we use our semi-empirical mass-luminosity relation for the primary component (Christopoulou et al., 2022) to estimate the absolute parameters

$$\log L_1 = \log(0.63 \pm 0.04) + (4.8 \pm 0.2) \log M_1. \quad (1)$$

using the systems temperature by Stassun et al. (2019), the distance by *Gaia* Early Data Release 3 (EDR3; Bailer-Jones et al., 2021) or *Gaia* Data release 3 (DR3; Gaia Collaboration, 2022), and the total line-of-sight Galactic extinction from the 3D dust reddening map of Green et al. (2019). The physical parameters of the 37 new LMRCBs are presented in Christopoulou et al. (2022) and Lalounta et al. (in prep) and of the 92 systems in Lalounta (PhD 2023)⁴. The main results from our study shown in Fig. 1 are as follows:

- The distribution of the mass ratio of the 92 CSS LMRCBs systems has a peak of 0.12 although a significant number has $q=0.17$. 10% systems have $q < 0.10$ whereas the lower value is 0.07 ± 0.02 (CSS_J075839+131355).
- Primary masses M_1 are $1.0 - 1.4M_\odot$ whereas there are a lot of systems with $M_1 > 1.4M_\odot$ which is unusual for contact binaries (e.g 22% of systems have $M_1 > 1.5M_\odot$).
- The distribution of T_1 shows that the majority has $T_1 > 6000K$ and 13% has $T_1 > 7000K$ larger than the mean primary temperature 5758 ± 928 K of contact binaries (Latković & Čeki, 2021).
- The 92 CSS LMRCBs present deep, medium, and shallow degrees of contact although 50% of them have $f > 45\%$. By including all previously known LMRCBs from literature (updated Table A1; Christopoulou et al., 2022) together with contact binaries with spectroscopic mass ratio (EW_{sp}), we confirm their conclusion that the smaller the q value, the larger the fill-out factor distribution range.

We compared our parameters of the 55 common systems to those of Sun et al. (2020) using CRTS DR1 data, different analysis, and relations for the absolute parameters and found that the mass ratios are similar within the reported

³<http://n2t.net/ark:/85065/d70r9ntr>

⁴<https://hdl.handle.net/10889/26132>

errors. We observe the largest deviation in the ratio of the temperatures of the components when their difference is increasing.

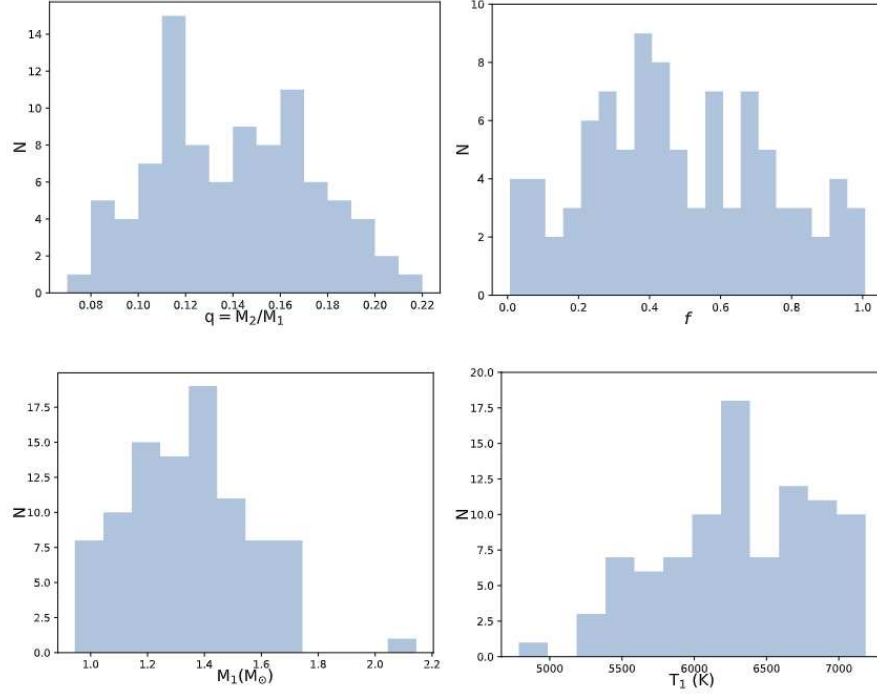


Figure 1. The distributions of q , f , M_1 and T_1 of the 92 CSS LMRCBs

2.1. Orbital stability

To investigate the dynamical stability we apply

- Darwins criterion by adopting the gyration radius $k_2^2=0.205$ for convective secondary because of its very low mass and k_1 from the derived linear relationships (Christopoulou et al., 2022) as $k_1 = -0.250 M + 0.539$ for stars with $M = 0.5 - 1.4 M_\odot$ and $k_1 = 0.014 M + 0.152$ for stars with $M > 1.4 M_\odot$.
- the instability mass ratio criterion of (Wadhwa et al., 2021) that involves the mass of the primary and the degree of contact.

Systems that fulfill both criteria $(J_s/J_o)_k \sim 0.3$ and $q/q_{inst} \sim 1$ are considered candidates for merging. These are

- CSS_J075839.9+131355

- CSS_J090748.9+375447
- CSS_J093010.1-021624
- CSS_J095733.5+151606
- CSS_J224450.0+071816
- CSS_J231513.3+345335.

2.2. The unique low mass ratio and ultra short period contact binary

We have discovered the first LMRCB binary system CRTS_J163819.6+034852 ($q = 0.16 \pm 0.02$) with a period ($P = 0.2053321$ d) under the contact binary period limit (Fig 2 left). It appears to be an A subtype, in deep contact ($72 \pm 15\%$), in which a primary of $F5/F4$ spectral type is eclipsed during the deeper minimum. Based on the analysis of the dedicated BVRI LCs and LCs from CSS, ASAS-SN, ZTF, ATLAS and the distance of Gaia DR3, the physical parameters are estimated as $M_1 = 1.19 \pm 0.02 M_\odot$, $M_2 = 0.19 \pm 0.02 M_\odot$, $R_1 = 0.93 \pm 0.02 R_\odot$, $R_2 = 0.44 \pm 0.01 R_\odot$, $L_1 = 1.45 \pm 0.07 L_\odot$ and $L_2 = 0.31 \pm 0.05 R_\odot$ (Papageorgiou et al., 2023).

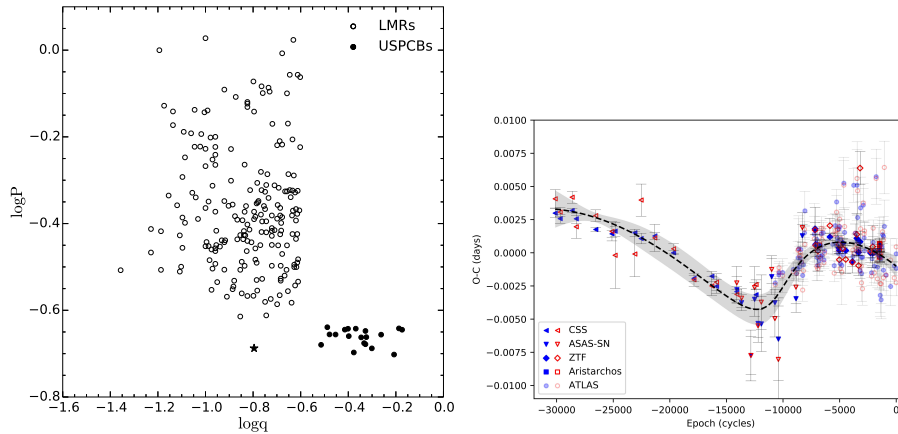


Figure 2. (left) Distribution of LMRCBs (open circles, from Christopoulou et al., 2022) and Ultra Short Period Contact Binaries (USPCBs) (filled circles, from Papageorgiou et al., 2023) in the $\log q - \log P$ plane. The star symbol represents CRTS_J163819. (right) $O - C$ diagram of CRTS_J163819. The dashed line represents the full contribution of the quadratic plus LTTE ephemeris.

In the time span of 15 yr (2004–2021), the orbital period of this unique object decreases at a rate of -7.11×10^{-8} days yr^{-1} implying mass transfer at

the rate of $dM_1/dt = -2.61 \times 10^{-8} M_{\odot} \text{ yr}^{-1}$ in addition to a periodic variation, interpreted by the light travel time effect (Figure 2 right). The latter may be due to the presence of a circumbinary companion of minimum mass $M_3 = 0.18 M_{\odot}$ at a separation from the binary $\sim 11.0 \text{ AU}$. Through the analysis of stability criteria, CRTS_J163819.6+03485 is currently in a stable contact stage. According to [Stepien \(2006\)](#) and [Stepień & Kiraga \(2015\)](#), and references therein) the formation and evolution investigation of the progenitors of CRTS J163819.6+03485 indicate that it may have evolved from a detached binary with masses $0.89 + 0.46 M_{\odot}$ and an initial period of 2.2 days or from a detached binary with masses $1.01 + 0.35 M_{\odot}$ and 2.5 days that required around 10.7 and 7.2 Gyr, respectively, to match the current properties of the system.

Acknowledgements. This research is co-financed by Greece and the European Union (European Social Fund- ESF) through the Operational Programme “Human Resources Development, Education and Lifelong Learning” in the context of the project “Reinforcement of Postdoctoral Researchers - 2nd Cycle” (MIS-5033021), implemented by the State Scholarships Foundation (IKY). EL gratefully acknowledges the support provided by IKY “Scholarship Programme for PhD candidates in the Greek Universities”.

References

- Arbutina, B., The Minimum Mass Ratio for Contact Close Binary Systems of W Ursae Majoris-type. 2009, *Publications of the ASP*, **121**, 1036, DOI: 10.1086/605616
- Bailer-Jones, C. A. L., Rybizki, J., Fouesneau, M., Demleitner, M., & Andrae, R., VizieR Online Data Catalog: Distances to 1.47 billion stars in Gaia EDR3 (Bailer-Jones+, 2021). 2021, *VizieR Online Data Catalog*, I/352
- Christopoulou, P.-E., Lalounta, E., Papageorgiou, A., et al., New low mass ratio contact binaries in the Catalina Sky Survey. 2022, *Monthly Notices of the RAS*, **512**, 1244, DOI: 10.1093/mnras/stac534
- Darwin, G. H. & Glaisher, J. W. L., I. On the bodily tides of viscous and semi-elastic spheroids, and on the ocean tides upon a yielding nucleus. 1879, *Philosophical Transactions of the Royal Society of London*, **170**, 1, DOI: 10.1098/rstl.1879.0061
- Drake, A. J., Graham, M. J., Djorgovski, S. G., et al., The Catalina Surveys Periodic Variable Star Catalog. 2014a, *Astrophysical Journal, Supplement*, **213**, 9, DOI: 10.1088/0067-0049/213/1/9
- Drake, A. J., Graham, M. J., Djorgovski, S. G., et al., VizieR Online Data Catalog: Catalina Surveys periodic variable stars (Drake+, 2014). 2014b, *VizieR Online Data Catalog*, J/ApJS/213/9
- Gaia Collaboration, VizieR Online Data Catalog: Gaia DR3 Part 1. Main source (Gaia Collaboration, 2022). 2022, *VizieR Online Data Catalog*, I/355

- Green, G. M., Schlafly, E., Zucker, C., Speagle, J. S., & Finkbeiner, D., A 3D Dust Map Based on Gaia, Pan-STARRS 1, and 2MASS. 2019, *Astrophysical Journal*, **887**, 93, DOI: 10.3847/1538-4357/ab5362
- Hambálek, Ľ. & Pribulla, T., The reliability of mass-ratio determination from light curves of contact binary stars. 2013, *Contributions of the Astronomical Observatory Skalnaté Pleso*, **43**, 27
- Heinze, A. N., Tonry, J. L., Denneau, L., et al., A First Catalog of Variable Stars Measured by the Asteroid Terrestrial-impact Last Alert System (ATLAS). 2018, *Astronomical Journal*, **156**, 241, DOI: 10.3847/1538-3881/aae47f
- Jayasinghe, T., Kochanek, C. S., Stanek, K. Z., et al., The ASAS-SN catalogue of variable stars I: The Serendipitous Survey. 2018, *Monthly Notices of the RAS*, **477**, 3145, DOI: 10.1093/mnras/sty838
- Latković, O. & Čeki, A., Light curve analysis of six totally eclipsing W UMa binaries. 2021, *Publications of the ASJ*, **73**, 132, DOI: 10.1093/pasj/psaa109
- Masci, F. J., Laher, R. R., Rusholme, B., et al., The Zwicky Transient Facility: Data Processing, Products, and Archive. 2019, *Publications of the ASP*, **131**, 018003, DOI: 10.1088/1538-3873/aae8ac
- Papageorgiou, A., Catelan, M., Christopoulou, P.-E., Drake, A. J., & Djorgovski, S. G., Physical Parameters of Northern Eclipsing Binaries in the Catalina Sky Survey. 2019, *Astrophysical Journal, Supplement*, **242**, 6, DOI: 10.3847/1538-4365/ab13b8
- Papageorgiou, A. & Christopoulou, P. E., Absolute Parameters and Physical Nature of the Low-amplitude Contact Binary HI Draconis. 2015, *Astronomical Journal*, **149**, 168, DOI: 10.1088/0004-6256/149/5/168
- Papageorgiou, A., Christopoulou, P.-E., Ferreira Lopes, C. E., et al., Three Ultra-short-period Contact Eclipsing Binary Systems Mined from Massive Astronomical Surveys. 2023, *Astronomical Journal*, **165**, 80, DOI: 10.3847/1538-3881/aca65a
- Pešta, M. & Pejcha, O., Mass-ratio distribution of contact binary stars. 2023, *Astronomy and Astrophysics*, **672**, A176, DOI: 10.1051/0004-6361/202245613
- Prsa, A. & Zwitter, T., Introducing Adapted Nelder & Mead's Downhill Simplex Method to a Fully Automated Analysis of Eclipsing Binaries. 2005, in ESA Special Publication, Vol. **576**, *The Three-Dimensional Universe with Gaia*, ed. C. Turon, K. S. O'Flaherty, & M. A. C. Perryman, 611
- Rasio, F. A., The Minimum Mass Ratio of W Ursae Majoris Binaries. 1995, *Astrophysical Journal, Letters*, **444**, L41, DOI: 10.1086/187855
- Shappee, B. J., Prieto, J. L., Grupe, D., et al., The Man behind the Curtain: X-Rays Drive the UV through NIR Variability in the 2013 Active Galactic Nucleus Outburst in NGC 2617. 2014, *Astrophysical Journal*, **788**, 48, DOI: 10.1088/0004-637X/788/1/48
- Stassun, K. G., Oelkers, R. J., Paegert, M., et al., The Revised TESS Input Catalog and Candidate Target List. 2019, *Astronomical Journal*, **158**, 138, DOI: 10.3847/1538-3881/ab3467

- Stepień, K., Evolution of the progenitor binary of V1309 Scorpii before merger. 2011, *Astronomy and Astrophysics*, **531**, A18, DOI: 10.1051/0004-6361/201116689
- Stepień, K. & Kiraga, M., Model computations of blue stragglers and W UMa-type stars in globular clusters. 2015, *Astronomy and Astrophysics*, **577**, A117, DOI: 10.1051/0004-6361/201425550
- Stepien, K., The Low-Mass Limit for Total Mass of W UMa-type Binaries. 2006, *Acta Astronomica*, **56**, 347
- Sun, W., Chen, X., Deng, L., & de Grijs, R. 2020, *Astrophysical Journal, Supplement*, **247**, 50, DOI: 10.3847/1538-4365/ab7894
- Terrell, D. & Wilson, R. E., Photometric Mass Ratios of Eclipsing Binary Stars. 2005, *Astrophysics and Space Science*, **296**, 221, DOI: 10.1007/s10509-005-4449-4
- Tylenda, R., Hajduk, M., Kamiński, T., et al., V1309 Scorpii: merger of a contact binary. 2011, *Astronomy and Astrophysics*, **528**, A114, DOI: 10.1051/0004-6361/201016221
- Wadhwa, S. S., De Horta, A., Filipović, M. D., et al., ZZ Piscis Austrinus (ZZ PsA): a bright red nova progenitor and the instability mass ratio of contact binary stars. 2021, *Monthly Notices of the RAS*, **501**, 229, DOI: 10.1093/mnras/staa3637

PRÁCE ASTRONOMICKÉHO OBSERVATÓRIA
NA SKALNATOM PLESE
LIV, číslo 2

| | |
|------------------------|---|
| Zostavovatelia: | RNDr. Theodor Pribulla, CSc. RNDr. Ján Budaj, CSc. RNDr. Augustín Skopal, DrSc. RNDr. Martin Vaňko, CSc. |
| Výkonný redaktor: | RNDr. Richard Komžík, CSc. |
| Vedecký redaktor: | RNDr. Augustín Skopal, DrSc. |
| Vydal: | Astronomický ústav SAV, Tatranská Lomnica |
| IČO vydavateľa: | 00 166 529 |
| Periodicita: | 3-krát ročne |
| ISSN (on-line verzia): | 1336-0337 |
| CODEN: | CAOPF8 |
| Rok vydania: | 2024 |
| Počet strán: | 258 |

Contributions of the Astronomical Observatory Skalnaté Pleso are processed using
L^AT_EX 2_ε CAOSP DocumentClass file 3.09 ver. 2021.